HAL
open science

Optimization of coupled driving-and-charging strategies for electric vehicles in an urban environment

Benoit Sohet

To cite this version:

Benoit Sohet. Optimization of coupled driving-and-charging strategies for electric vehicles in an urban environment. Modeling and Simulation. Université d'Avignon, 2021. English. NNT : 2021AVIG0290 . tel-03662438

HAL Id: tel-03662438

https://theses.hal.science/tel-03662438v1

Submitted on 9 May 2022

HAL is a multi-disciplinary open access archive for the deposit and dissemination of scientific research documents, whether they are published or not. The documents may come from teaching and research institutions in France or abroad, or from public or private research centers.

L'archive ouverte pluridisciplinaire **HAL**, est destinée au dépôt et à la diffusion de documents scientifiques de niveau recherche, publiés ou non, émanant des établissements d'enseignement et de recherche français ou étrangers, des laboratoires publics ou privés.

THÈSE DE DOCTORAT D'AVIGNON UNIVERSITÉ

École Doctorale n°536
Agrosciences et Sciences

Mention de doctorat :
Informatique

Laboratoire d'Informatique d'Avignon

Présentée par
Benoît SOHET

Optimization of coupled driving-and-charging strategies for electric vehicles in an urban environment

Soutenue publiquement le 08/11/2021 devant le jury composé de :

Mahnoosh ALIZADEH	Professeure Associée	UC Santa Barbara	Rapporteuse
Jakob PUCHINGER	Professeur	CentraleSupélec	Rapporteur
Samson LASAULCE	Directeur de Recherche	Université de Lorraine	Examinateur
Luce BROTCORNE	Directrice de Recherche	INRIA	Examinatrice
Dominique QUADRI	Professeure	Université Paris-Saclay	Examinatrice
Samir PERLAZA	Chargé de Recherche	INRIA	Examinateur
Didier DERUY	Ingénieur	Renault R&D	Examinateur
Yezekael HAYEL	Professeur Associé	Avignon Université	Directeur de thèse
Olivier BEAUDE	Ingénieur-chercheur	EDF R&D	Co-dir. (invité)
Alban JEANDIN	Ingénieur-chercheur	IZIVIA groupe EDF	Co-dir. (invité)

Remerciements

Mahnoosh Alizadeh, Jakob Puchinger, I am profoundly grateful for all the time you dedicated to reading this manuscript. Mahnoosh, I wish I could have visited you as planned, but I am glad you took part in my thesis in another way. To all the members of the jury, with Samson Lasaulce, Luce Brotcorne, Dominique Quadri, Samir Perlaza and Didier Duruy, I am honored to discuss my work with you.

À mes encadrants: Yezekael, merci d'avoir su me motiver à tout instant. Mon séjour à Avignon fut un des meilleurs moments de ma thèse, à travailler avec toi pendant des heures d'affilée. Je regrette que nous n'ayons pas pu réitérer l'expérience. Olivier, contre vents et marées, tu as été d'un soutien sans faille. La justesse de tes mots et de tes remarques m'impressionnera toujours. Je m'estime chanceux de pouvoir rester encore un peu dans ton sillage. Alban, tu as toujours su trouver du temps pour moi, même après avoir changé d'activités. Merci pour ta ténacité à me rapprocher des problématiques "métier". Jean-Baptiste, je suis heureux que tu aies rejoint l'aventure. Merci d'avoir su accrocher en cours de route, tu mériterais une place en page de garde de ce manuscrit ! Nos chemins se recroiseront assurément à "éDF".

À mes collègues d'EDF, un immense merci à toutes les personnes qui ont permis à cette thèse de voir le jour, à celles qui m'ont aidé pendant ces trois années, notamment lors du sprint final. J'ai une pensée particulière pour mes co-équipiers, anciens et nouveaux, avec qui j'ai tant discuté, et pour les doctorants de MIRE, OSIRIS et EFESE avec qui j'ai partagé toutes ces activités sportives et moins sportives. Une mention spéciale pour ma très chère collègue Arbia : merci d'avoir égayé notre bureau en toute occasion, je suis de tout cœur avec toi pour la suite. À mes collègues d'Avignon, je vous remercie de m'avoir recueilli durant ces périodes, malheureusement trop courtes.

Je pense aussi à tous mes amis que j'ai pu côtoyer durant ces trois années. Un merci particulier à ceux qui m'ont tenu compagnie en thèse, qui se reconnaîtront. Hugo, j'espère que je ne te fais pas trop culpabiliser de ne pas nous avoir fait de remerciements. Cette période a également été marquée par de riches expériences, comme ces mardis soirs avec vous, Aude, Bruno et les autres, sans oublier ma courte carrière d'acteur. Enfin, Romain, merci pour cette assistance téléphonique inébranlable, et surtout d'avoir été là pour tous mes problèmes de traduction.

À mes parents, je vous dédie ce travail. Merci d'avoir toujours été là pour moi, et pour votre soutien indéfectible tout au long de mes études, enfin terminées ! Je pense à toi aussi bichette, ainsi qu'à mes grands-parents et ma petite famille de Montrouge. Je n'oublie pas non plus ma belle-famille, qui m'a accueilli ô combien de fois pendant ces trois années.

Perrine, je vais tâcher de ne pas être gênant, bien que la tentation soit grande ! Ce fut les trois meilleures années de ma vie, et c'est grâce à toi. Tu as toujours su m'aider et me soutenir quand j'en avais besoin, merci. Tu m'as montré dans les moments difficiles de la thèse que la vie sera toujours douce avec toi.

Enfin, à toi, Jean-Pierre, qui m'a accompagné durant cette année de confinement plus que quiconque.

Contents

List of Figures vii

Résumé xi

Abstract xii

Chapter 1
Introduction 1

1.1 Electric Vehicles definition and figures 1
1.2 Present and future challenges for electric mobility 2
1.2.1 Environmental comparison of electric and non-electric vehicles 3
1.2.2 Impact of Electric Vehicles on power system 5
1.3 The coupled electrical-transportation system 7
1.4 Thesis approach: commuting, long-term incentives and game theory 8
1.5 Contents of the manuscript 10
1.6 Publications related to this thesis 11

I Driving-and-charging behavior of vehicle users 13

Chapter 2
A non-separable routing game to model vehicle user behavior 15

2.1 Introduction 16
2.2 The driving-and-charging routing game 17
2.2.1 Non-atomic and rational players 17
2.2.2 Routing game: choices modeled as fictitious graph arcs 19
2.2.3 Standard driving and charging cost functions 23
2.3 The charging unit price: a particular congestion cost function 26
2.3.1 General non-separable congestion cost functions 26
2.3.2 Linearly non-separable congestion cost functions 27

2.4 Equilibrium of linearly non-separable games using Beckmann's function . . . 28
2.4.1 Wardrop equilibrium: solution concept of non-atomic games 28
2.4.2 The equilibrium as a minimum of Beckmann's function 30
2.4.3 Wardrop Equilibrium properties 31
2.5 Conclusion 33

Chapter 3
Learning Nash equilibrium in linearly non-separable congestion games 35

3.1 Introduction 36
3.1.1 Motivation 36
3.1.2 Atomic game notations 37
3.2 Standard reinforcement learning algorithm 39
3.2.1 Principle of the reinforcement learning process 39
3.2.2 Theoretical results: existence of potentials and learning convergence . 41
3.2.3 Application to a non-separable smart charging game 46
3.3 Stochastic reinforcement learning algorithm 49
3.3.1 Principle of the stochastic reinforcement learning process 49
3.3.2 Theoretical results from literature 51
3.3.3 Application to a non-separable smart charging game 53
3.4 Conclusion 56

II Smart charging and pricing mechanisms 59

Chapter 4
Smart charging scheduling at charging stations 61

4.1 Introduction 62
4.2 Smart charging of aggregated charging need at a charging station 64
4.2.1 Basic water-filling scheduling 64
4.2.2 Extensions of the water-filling scheduling 69
4.3 Online smart charging of asynchronous charging needs 73
4.3.1 Asynchronous charging scheduling framework 73
4.3.2 Offline charging scheduling 74
4.3.3 Online charging scheduling 74
4.3.4 Illustration and comparison of online and offline schedulings on asynchronous commuting. 78
4.4 Smart charging at several charging stations of a grid 81

4.4.1 Model of grid costs related to EV charging 81
4.4.2 Three different possible operators for the charging scheduling 82
4.4.3 Three charging scheduling methods depending on available information 83
4.4.4 Numerical comparison between the three charging schedulings 85
4.5 Conclusion 87

Chapter 5
Smart charging pricing methods at charging stations 89

5.1 Introduction 90
5.1.1 State of the art 90
5.1.2 Iterative locational marginal pricing method 92
5.2 Average water-filling pricing method 93
5.2.1 Definition based on the water-filling scheduling cost 93
5.2.2 Properties of the charging unit price functions 94
5.2.3 Illustration of the increasing property with real data 96
5.3 Locational marginal pricing method based on water-filling charging scheduling 99
5.3.1 Definition based on the marginal water-filling scheduling cost 99
5.3.2 Properties of the charging unit price functions 99
5.3.3 Online and offline pricing methods for asynchronous charging needs . 100
5.4 Numerical comparisons of the pricing methods 102
5.4.1 Illustration of the pricing methods 102
5.4.2 Impact of the pricing methods on a transportation-electrical system . 106
5.5 Conclusion 111

III Incentive design in coupled electrical-transportation system 113

Chapter 6
Use cases for numerical incentive design 115

6.1 Reducing local air pollution with traffic tolls 116
6.1.1 Introduction of use case and game between vehicle users 116
6.1.2 Sensitivity of Wardrop equilibrium to fuel price 119
6.1.3 Numerical complexity of Wardrop equilibrium computations 120
6.1.4 Definition and numerical study of local air pollution 120
6.2 Solar panel sizing at a multimodal e-Park & Ride hub 123
6.2.1 Introduction of use case and game between vehicle users 124
6.2.2 Numerical study of solar panel sizing 128

6.3 Conclusion 133

Chapter 7
Hierarchical coupled driving-and-charging model of electric vehicles, stations and grid operators **135**

7.1 Introduction 136
7.2 A smart coupled driving-and-charging model with three types of actors . . . 138
7.2.1 Vehicle users: a coupled driving-and-charging decision 138
7.2.2 Charging Service Operator: sets charging price 140
7.2.3 Electrical Network Operator: designs CSO electricity supply contract 141
7.3 The trilevel optimization problem 142
7.3.1 Vehicle users at Wardrop equilibrium 143
7.3.2 The trilevel problem formulation 144
7.4 Resolution of trilevel optimization problem 145
7.4.1 An iterative method for upper and middle levels optimization 145
7.4.2 CSO and ENO optimization problems: a simulated annealing approach 147
7.5 Case studies 148
7.5.1 Sensitivity to electric vehicles penetration level 150
7.5.2 Sensitivity to public transport fare 151
7.5.3 Comparison with the standard bilevel framework 152
7.6 Conclusion 153

Conclusion and perspectives **155**

List of Acronyms **159**

Bibliography **161**

List of Figures

1.1 Global vehicle stock of BEVs and PHEVs from year 2010 to 2020 for different regions in the world. . . . 2
1.2 Global EV sales for two IEA scenarios, in 2025 and 2030 compared to 2020. . . . 3
1.3 Climate change impacts: example comparison of BEVs with ICEVs, considering life cycle GreenHouse Gas emissions. . . . 4
1.4 Total electricity demand in France and residual demand in different EV smart charging configurations for an average weekday in 2035. . . . 6
1.5 Schematic view of the electric mobility ecosystem. . . . 7

2.2 Sioux falls transportation network modeled as a directed graph. . . . 20
2.3 Illustration of a graph modeling several kinds of choices for vehicle users. . . . 22
2.4 Schematic representation of the charging hub scenario: commuters can either choose to leave their vehicle at the hub and take public transport, or drive all the way to their destination. . . . 22
2.5 Travel duration normalized by the free-flow reference time, in function of the total vehicle flow normalized by the road capacity. . . . 25
2.6 EV users costs in function of the proportion of EV users choosing public transport. 29

3.2 Summary of contributions. . . . 46
3.3 Electrical grid containing three EVCS, all managed by the Electrical Network Operator. . . . 47
3.4 Evolution of mixed strategiesthroughout iterations of Algorithm 3.1. . . . 48
3.5 Evolution of mixed strategies throughout iterations of asynchronous version of Algorithm 3.1. . . . 49
3.6 Electrical grid containing three EVCS all managed by the Electrical Network Operator. . . . 53
3.7 Perceptions of a given player associated with the three EVCSs, throughout the iterations of the stochastic RLA and for different rationality values. . . . 54
3.8 Evolution of mixed strategies of all players and the corresponding mean throughout the iterations of the stochastic RLA. . . . 55
3.9 Comparison of the perturbed NE obtained with Algorithm 3.3 and the limit of the stochastic learning Algorithm 3.2, in function of the rationality parameter. . . . 56

4.2 Illustration of the water-filling charging profile solution. . . . 68
4.3 Load cost in function of EV charging and PV generation in the case of no remuneration for unused PV. . . . 71
4.4 Water-filling optimal scheduling of the charging operation considering PV electricity generation, for two different aggregated charging needs. . . . 71

4.5 Load cost in function of EV charging and PV generation in case of convex remuneration. 72
4.7 Example of the optimal charging profiles for five EV classes, computed with the online scheduling charging problem in function of a non-flexible consumption profile. 77
4.8 Arrival and departure discretized distributions, both with ENTD data and in the case where both variances were multiplied by three. 78
4.9 Comparison of optimal per-class aggregated charging profiles obtained with online and offline charging problems. 79
4.10 Average power overload of the online charging profile over the offline one and number of overload time slots in a day, in function of the EVs distribution variance. 79
4.12 Electrical network considered in this work. ENO, FO and CSO respectively stand for Electrical Network, Flexibility and Charging Service Operators. 85
4.13 Example of the three scheduling algorithms. 86

5.2 Household electricity consumption during summer and winter, weekday and weekend, in France (a) and Texas (b). 97
5.3 Proportion of days per month when the CUP function is increasing, for different number of time slots (top: Recoflux; bottom: Pecan Street). 98
5.4 CUPs in function of the variance of EV classes' distribution, for each EV class and both online and offline scheduling problems. 101
5.5 Electrical network containing the three EVCS. 102
5.6 Comparison of the CUPs of AVG, WF, GA and α pricing methods at EVCS $i = 3$ in function of the aggregated charging need L_3, with $L_1 = L_2 = 0$. 105
5.7 Comparison of the CUPs of AVG, WF, GA and α pricing methods at EVCS 2, in function of the aggregated charging need L_3 at EVCS 3, with $L_1 = L_2 = 0$. . . . 106
5.8 Extension of the electrical network of Figure 5.5 by a transportation network. . . 107
5.9 Aggregated charging needs at the EVCSs in function of the path toll, for the pricing methods CST, GA, AVG and WF. 108
5.10 Charging Unit Prices at the EVCSs in function of the path toll, for GA, AVG and WF pricing methods. 109
5.11 Normalized grid cost in function of the path toll, for CST, GA, AVG and WF pricing methods. 110

6.2 Schematic representation of the transportation network considered. 117
6.3 Schematic representation of the operators considered in this use case. 118
6.4 Evolution of the vehicle flows at WE with respect to fuel price. 119
6.5 Average execution time of minimization algorithm in function of number of parallel arcs. 120
6.6 Evolution of the optimal toll and the environmental gain with respect to the EV penetration level, for different local pollution importance levels inside the city. . . 122
6.7 Distribution of EVs and GVs at WE corresponding to optimal toll (a) and no toll (b) scenarios, as the proportion of EV grows. 123
6.9 Schematic representation of the charging hub scenario. 124
6.10 Variable part of the Charging Unit Price at the hub, in function of the EV flow, for different energy amounts PV generated during the working hours of a day. . . 127
6.11 Variable part of the Charging Unit Price at the hub, in function of the PV electricity generation throughout the year 2014, for two different nominal powers. . . 129

6.12 Impact of the constant Charging Unit Price at the hub on the Wardrop Equilibrium and the CSO revenue function. 130
6.13 Daily CSO's payoff in function of the constant Charging Unit Price at the hub, for different daily PV productions. 131
6.14 CSO's payoff over 20 years in function of the PV installed at the hub. 132
6.15 Optimal CSO's variables to maximize in function of the PV nominal power installed at the hub. 133

7.2 Illustration of a transportation network. 139
7.3 Electricity supplying cost in function of the total load, for two values of power threshold. 142
7.4 Diagram of the different agents, their decision variables and their interactions. . . 143
7.5 Sioux falls transportation network. 148
7.6 IEEE 33-bus medium-voltage distribution network. 148
7.7 Aggregated charging profiles for each CSO's hub, for the water-filling method (*Trilevel*), the improved reference method (GA-GA) and the PC-GA method. . . 149
7.8 Optimal ENO and CSO's payoffs and normalized strategies depending on EV penetration level. 150
7.9 Normalized charging needs at all hubs depending on EV penetration level, for two different non-flexible consumption profiles. 151
7.10 Charging needs at all hubs depending on the unique PT fare. 152
7.11 ENO grid costs and CSO charging revenues, depending on EV penetration level, obtained with our Trilevel framework, the PC-GA one and GA-GA method for different normalizations of the LMP. 153

Résumé

Dans un futur proche, les Véhicules Electriques (VE) constitueront une part importante du parc automobile mondial. Cela représente une opportunité pour réduire les émissions de gaz à effet de serre et la pollution locale (qualité de l'air, bruit). En ce qui concerne le système électrique, la recharge intelligente pourrait atténuer l'impact des VE sur les infrastructures de réseau par exemple. Ainsi, les VE ont un effet à la fois sur le réseau électrique et sur le réseau de transport, ce qui rend les actions des différents acteurs (ou opérateurs) de ces systèmes interdépendantes. L'objectif de cette thèse est d'aider les opérateurs à prendre des décisions dans cet environnement couplé, en modélisant les réactions des usagers de véhicules, ainsi que des mécanismes tels que la planification de la recharge des VE, et une méthode de tarification basée sur celle-ci. Le cas d'usage considéré pour illustrer ce couplage est celui des déplacements urbains tels que les trajets domicile-travail, associés à une recharge dans des Infrastructures de Recharge (IRVE) publiques. Le comportement des usagers de véhicules sur la route et lors de la recharge est modélisé par un jeu de routage, prenant en compte des phénomènes de congestion à la fois sur le réseau de transport et sur le réseau électrique. La méthode de Beckmann pour trouver un équilibre de Wardrop du jeu est étendue aux fonctions de coût de *Congestion Linéairement non-Séparables* (LnSC), tel que le mécanisme de tarification de la recharge défini dans cette thèse. De plus, pour des fonctions de coût LnSC croissantes, il est prouvé que les combinaisons linéaires associées des flux de véhicules sont uniques à l'équilibre. Ce jeu de routage est ensuite lié à un algorithme d'apprentissage par renforcement dans lequel les usagers de véhicules n'ont aucune connaissance préalable de leurs coûts mais les observent seulement. La preuve de la convergence de cet algorithme vers un équilibre du jeu est étendue aux fonctions de coût LnSC croissantes. Cette thèse se concentre ensuite sur les Opérateurs de Services de Charge (CSO) des IRVE, et deux mécanismes de maîtrise de la demande en énergie sont ajoutés au jeu de routage. Premièrement, le choix des profils de charge est fait de manière centralisée par le CSO, qui utilise la méthode *water-filling* pour lisser le profil de puissance totale de tous les usages électriques à l'IRVE. Une expression analytique de cette planification de la recharge est trouvée dans différents cas d'usage, comme l'autoconsommation de la production renouvelable locale, des besoins de charge asynchrones, et plusieurs IRVE exploitées en parallèle. Deuxièmement, les tarifs de recharge sont définis comme l'impact approché des profils de recharge sur le réseau électrique, pour inciter les usagers de VE dans leur choix d'IRVE par exemple. Il est démontré que ces prix sont des fonctions de coût LnSC croissantes (sous certaines conditions), et que le besoin de charge à chaque IRVE est unique à l'équilibre du jeu de routage. La méthode standard de tarification marginale locale, fonction du coût marginal réel du réseau, est affinée et comparée au mécanisme de tarification de cette thèse. Ensuite, le jeu de routage accompagné de la planification de charge et du mécanisme de tarification de cette thèse sont testés sur deux exemples : la réduction de la pollution locale de l'air par des péages routiers, et le dimensionnement de panneaux solaires dans un Parc Relais multimodal. Enfin, un système à trois niveaux est proposé pour modéliser les interactions entre les usagers de véhicules, un CSO et l'opérateur du réseau de distribution, qui choisit la forme du contrat d'approvisionnement en électricité du CSO. Une méthode de résolution itérative est adaptée à ce cadre, et il est prouvé qu'elle converge vers la solution du problème d'optimisation à trois niveaux. Cette solution est illustrée sur des réseaux électrique et de transport concrets, et comparée à un système standard à deux niveaux avec un seul opérateur.

Mots-clés: théorie des jeux, véhicules électriques, réseaux intelligents.

Abstract

In the near future, Electric Vehicles (EVs) are going to constitute a significant share of the global vehicle stock. This represents an opportunity to reduce greenhouse gas emissions and local pollution (air quality, noise). Regarding the electrical system, smart charging could mitigate the impact of EVs on the grid infrastructures for example. Thus, EVs have an effect on both the electrical and the transportation networks, which makes the actions of the different stakeholders (or operators) of these systems interdependent. The aim of this thesis is to help operators to make decisions in this coupled environment, by modeling the reactions of vehicle users, and mechanisms like an EV charging scheduling and a pricing method based on it. The coupled use case considered for vehicles is urban trips such as commuting, associated with charging at public Charging Stations (EVCSs). The behavior of commuters while driving and charging is modeled by a routing game with congestion both on the transportation and electrical networks. Beckmann's method to find a Wardrop equilibrium of the game is extended to *Linearly non-Separable Congestion* (LnSC) cost functions such as the charging pricing mechanism specific to this work. In addition, for increasing LnSC cost functions, the associated linear combinations of vehicle flows are proved to be unique at equilibrium. This routing game is then linked to a reinforcement learning algorithm in which vehicle users have no prior knowledge but observe their driving and charging costs. The proof of convergence of this algorithm towards an equilibrium is extended to increasing LnSC cost functions. This thesis then focuses on the Charging Service Operators (CSOs) of EVCSs and two demand-side management mechanisms are added to the vehicle game framework. First, the choice of charging profiles is centralized at the level of the CSO, which uses the water-filling scheduling to smooth the total load profile of all electricity usages at the EVCS. An analytic expression of this scheduling is found in different cases, including self-consumption of local renewable generation, asynchronous charging needs and multiple operated EVCSs. Second, charging prices are defined as the approximate impact the water-filling profiles have on the grid, to incentivize EV users in their choice of an EVCS for example. These prices are shown to be increasing LnSC cost functions (under certain conditions), and the charging needs at EVCSs are unique at equilibrium of the routing game. The locational marginal pricing method, defined as the actual marginal grid cost, is refined and compared to the pricing mechanism of this thesis. Then, the routing game along with these CSO's charging scheduling and pricing mechanism are tested on two examples: reducing local air pollution with traffic tolls, and solar panel sizing at a multimodal e-Park & Ride hub. Finally, a trilevel framework is suggested to model the interactions between vehicle users, a CSO and an electrical network operator which designs the electricity supplying contract of the CSO. An iterative optimization method is adapted to this framework and is proved to converge towards its optimal solution. This solution is illustrated on realistic electrical and transportation networks and compared to a standard bilevel framework with a unique operator.

Keywords: game theory, electric vehicles, smart grids.

Chapter 1

Introduction

Contents

1.1 Electric Vehicles definition and figures 1
1.2 Present and future challenges for electric mobility 2
1.2.1 Environmental comparison of electric and non-electric vehicles . . . 3
1.2.2 Impact of Electric Vehicles on power system 5
1.3 The coupled electrical-transportation system 7
1.4 Thesis approach: commuting, long-term incentives and game theory 8
1.5 Contents of the manuscript 10
1.6 Publications related to this thesis 11

1.1 Electric Vehicles definition and figures

In the current literature, Electric Vehicles (EVs) usually correspond to all vehicles which may need external electrical charging and therefore have an impact on the electrical grid, such as:

- Battery Electric vehicles (BEVs) whose only mean of propulsion is an electric motor powered by a battery pack (unlike fuel cell electric vehicles – or FCEVs – which use a fuel cell instead of a battery);
- Plug-in Hybrid Electric Vehicles (PHEVs) which use a combination of an internal combustion engine with an electric propulsion system and whose battery can be recharged.

In the following, EVs will be considered mostly as a unique vehicle class sharing the same characteristics (see section 2.2.1.1 for the concept of vehicle class), characteristics which correspond to those of BEVs. For the consideration of PHEVs specifically, please refer to [Turker, 2012].

Remark 1.1. *The recent white paper [Plötz et al., 2020] from the International Council on Clean Transportation (ICCT) indicates that the portion of kilometers driven on electric motor versus kilometers driven on combustion engine is only 37 % for private cars and 20 % for company cars, based on real-world usage of 100,000 PHEVs. This suggests that PHEVs have a smaller coupling effect on the electrical grid and the transportation network, which is the focus of this thesis (see Section 1.3 for more details on this coupling concept).*

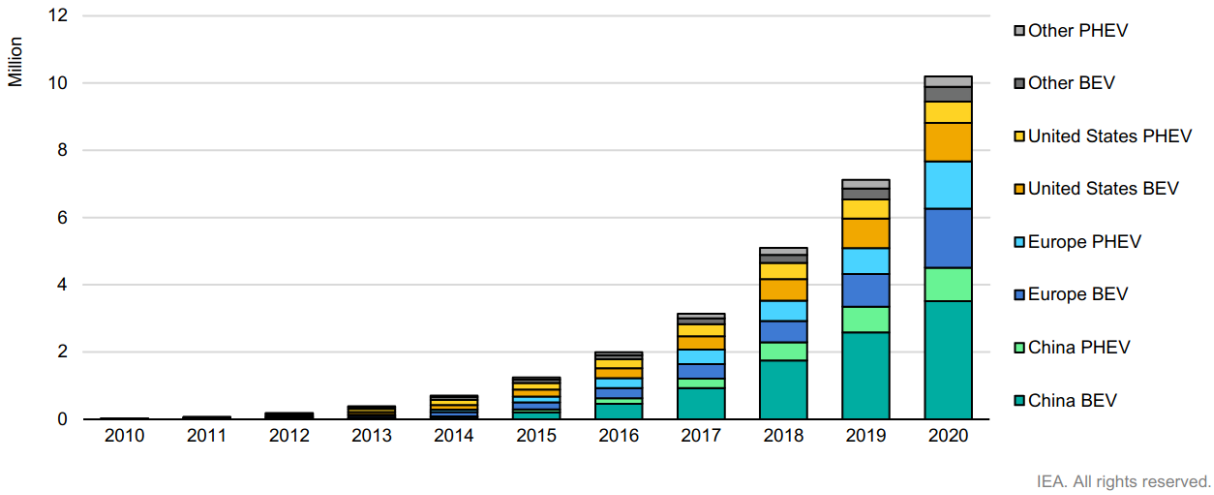

Figure 1.1: Global vehicle stock of BEVs and PHEVs from year 2010 to 2020 for different regions in the world. "Other" includes Australia, Brazil, Canada, Chile, India, Japan, Korea, Malaysia, Mexico, New Zealand, South Africa and Thailand. "Europe" includes countries of the European Union, Norway, Iceland, Switzerland and United Kingdom. Sources: International Energy Agency (IEA) analysis based on country submissions, complemented by ACEA (2021); CAAM (2021); EAFO (2021); EV Volumes (2021) and Marklines (2021).

Since the invention of the first EV in 1884 by Thomas Parker, the deployment of EVs has failed several times [Fréry, 2000]. For more details on the history of EVs, see [Burton, 2013]. Since the years 2010s and the launch of the first Nissan Leaf model, with a lithium battery, predictions of EV penetration level have rather been confirmed (see for example in USA predictions of [Block et al., 2015] compared to actual figures[1]). This could be explained first by battery technology development [Gaonac'h, 2015], followed by coercive public policies following societal expectations (see for example the technical report by the French electricity distribution company [Enedis, 2019]) and subsequent manufacturers commitments [IEA, 2021]. The global BEV and PHEV stocks from year 2010 to 2020 are shown in Figure 1.1.

The proportion of EVs in the global vehicle stocks are not significant yet. Figure 1.2 shows that the progression during year 2020 from around 7 to 10 millions of global EV stocks (see Figure 1.1) already represents almost 5 % of the global vehicle sales (red dot)[2]. In this figure are also given predictions made by the International Energy Agency (IEA) of EV sales in 2025 and 2030 in different regions of the world for two different scenarios (stated policies and sustainable development). The expected EV sales' share should range between around 10 and 17 % in 2025 and between 16 and 34 % in 2030. By 2030, EVs should account for respectively 7 % and 12 % of the road vehicle fleet, considering the two different IEA scenarios [IEA, 2021].

1.2 Present and future challenges for electric mobility

[1] The figures of sales up to year 2021 can be retrieved from the following website: https://www.energy.ca.gov/data-reports/energy-insights/zero-emission-vehicle-and-charger-statistics.

[2] The grey dots indicate that around 32 % of EV sales correspond to PHEVs, and therefore the remaining 68 % are BEVs.

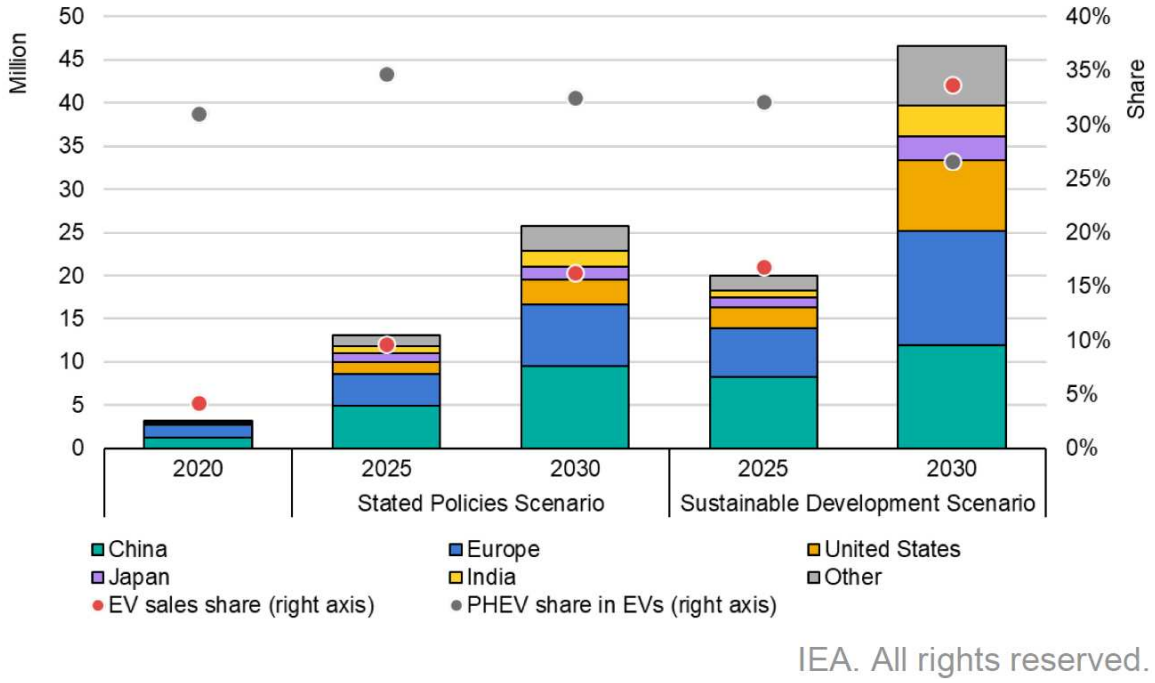

Figure 1.2: Global EV sales for two IEA scenarios (stated policies and sustainable development), in 2025 and 2030 compared to 2020. These sales in different regions of the world are shown in color bars (in millions of vehicles) while dots represent the global share of EVs. Source: IEA analysis developed with the Mobility Model.

1.2.1 Environmental comparison of electric and non-electric vehicles

This increasing EV penetration level represents an opportunity, but also challenges. The most discussed EV characteristic is its potential benefit for the environment. Indeed, the whole transport sector accounts for about a quarter (23 %) of global energy-related GreenHouse Gas (GHG) emissions [IEA, 2017] (in 2015). However, the environmental study is not limited to GHG emissions but also includes air and noise pollution as well as ecosystem impacts (or ecotoxicity), as summarized in [EEA, 2018]. These effects not only depend on vehicle use phase, but also on the production phase, hence the use of Life Cycle Assessment (LCA)[3].

Concerning the GHG emissions, first note that one of the most important factor is the size of the vehicle: from 21 tons of carbon dioxide equivalents for a mini BEV[4] (1,100 kg like Mitsubishi i-MiEV) during a life cycle, to 35 for a luxury BEV (2,100 kg, like Tesla model S) [Ellingsen et al., 2016] due to both the vehicle production and usage. Another major factor studied in [Ellingsen et al., 2016] is the electricity generation mix of the country where the EV is charged. Regarding the comparison with Internal Combustion Engine Vehicles (ICEVs[5]), BEVs emit 1.3 to 2 times more GHG when considering the production stage only [Kim et al., 2016] (which represents almost half of the life cycle GHG emissions), in part due to the carbon-intensive electricity mix of countries manufacturing EV batteries. Therefore, it is necessary to consider

[3]LCA is *a means of assessing the environmental impact associated with all stages of a product's life: from raw material extraction and processing, to its production, to its use in day-to-day life, and finally to its end of life and related opportunities for reuse, recycling and disposal* [EEA, 2018].

[4]The paragraph on GHG emissions consider Battery EVs and not Plug-in Hybrid EVs.

[5]Note that ICEVs are grouped under the name of Gasoline Vehicles (GVs) in the other chapters.

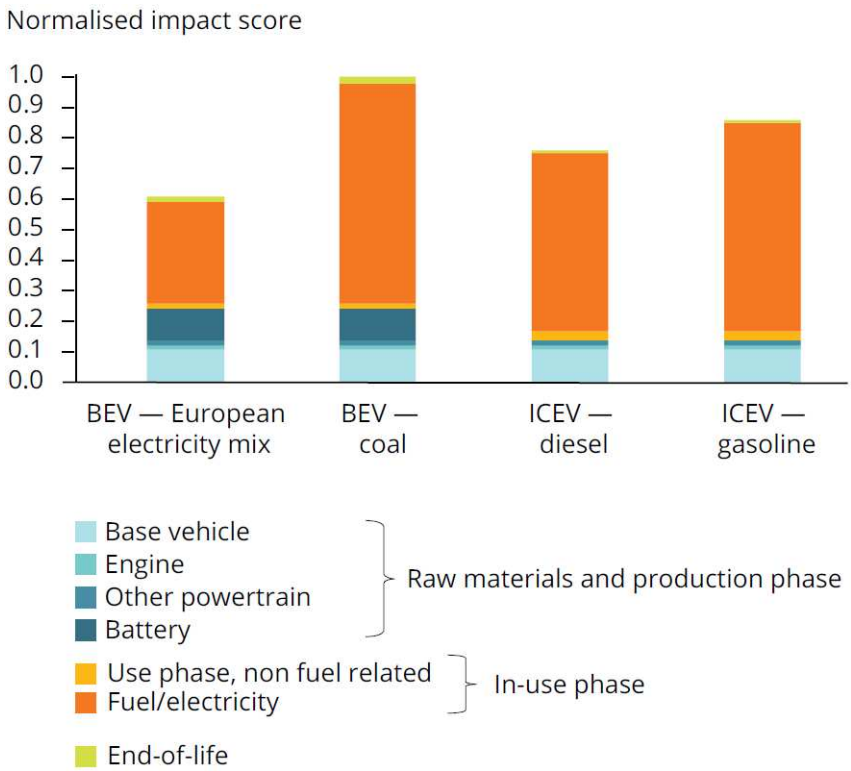

Figure 1.3: Climate change impacts: example comparison of BEVs with ICEVs, considering life cycle GreenHouse Gas emissions. The GHG emissions are normalized by the highest value, and then referred to as normalized impact scores. *The GHG benefit of BEVs compared to ICEVs highly depends on the electricity generation mix providing for EV charging. Life cycle GHG emissions are around 25 % lower for BEVs compared to ICEVs considering the European electricity mix, but higher if the mix is only composed of coal.* Source: [EEA, 2018] and [Hawkins et al., 2013].

a high enough lifetime mileage for vehicles in order to potentially offset these manufacturing GHG emissions. In [Hawkins et al., 2013], a lifetime mileage of 150,000 km is assumed[6], and the life cycle GHG emissions are lower for BEVs by 17-21 % compared to diesel ICEVs (26-30 % compared to petrol ICEVs), considering the European electricity mix for BEV charging. Note that in the case of a full coal electricity generation mix, BEVs have life cycle GHG emissions higher than ICEVs by 17 and 27 % respectively for petrol and diesel.

Concerning the other environmental criteria, the benefits of BEVs are mixed. Although having zero exhaust emissions, BEVs are associated with Particulate Matter (PM) emissions due to coal-generated electricity for the battery manufacture and the BEV charging (the latter being even higher than PM emissions from ICEV fuel combustion, when considering the European electricity mix [Hawkins et al., 2013]), as well as road, tire and brake wear while driving. Note however that replacing ICEVs with BEVs improves the urban air quality when generation stations are located away from population centers. It also reduces noise in urban areas with a lot of traffic [Campello Vicente et al., 2017][7]. On the contrary, BEVs are associated with a

[6]Note that BEV batteries are likely to last for such a mileage, in line with the insurance conditions in Renault company: https://www.renault.fr/vivre-en-electrique/batterie.html (in French).

[7]Note however that from 30 km/h, the noise of a vehicle is dominated by the interaction between the tires and

higher impact on human toxicity [Nordelöf et al., 2014] (due to toxic emissions during copper and nickel mining), on freshwater ecotoxicity [Hawkins et al., 2013] and on terrestrial acidification [Bauer et al., 2015]. Despite these mixed benefits, the electrification of the transport sector is definitely on the way (see previous section).

1.2.2 Impact of Electric Vehicles on power system

The growing number of EVs also brings changes to the electrical grid, as illustrated in the following in the case of France. In 2030, the number of personal EVs is expected to reach 7 millions, representing 20 % of personal vehicles (see report [RTE, 2021] by French electricity transportation network operator RTE). The corresponding electricity consumption in 2030 will be 17 TWh, i.e. around 3.5 % of the expected roved French electricity consumption[8]. This roved consumption is only 6 % higher than in 2019 in part thanks to housing isolation and energy efficiency of electrical appliances, and will remain below the expected capacity of nuclear and renewable generation sources, according to another RTE report [RTE, 2019].

A recent report [Enedis and RTE, 2019] predicts a 4 GW EV power demand during busy holiday periods in 2035. This should not represent a concern in terms of security of supply during summer week-ends, associated with high margins, as well as for Christmas, considering that the charging facilities are not sized for as much as 4 GW, and that two thirds of the charging need could be scheduled before or after [RTE, 2019]. The EV power demand associated with local mobility (representing 75 % of traveled distances) however is a challenge for the electrical system. The corresponding daily access to charging points is concentrated at the same time as the evening peak load and a lack of photovoltaic generation. In the case of uncontrolled charging, EVs are immediately charged at full power, and local mobility causes a charging peak load of 5 GW at 7 pm (in the *Crescendo* scenario of RTE). Moreover, the EV power load is temperature-sensitive (due to vehicle heating), which may add a 3 GW charging load [RTE, 2019]. Then, smart charging seems to be the natural solution to these power load challenges.

Smart charging is a Demand-Side Management mechanism [Palensky and Dietrich, 2011], which is an emerging field in "smart grids"[9]. It consists in controlling the electricity consumption profile by, e.g., postponing usages in time, or reducing the level of power consumed, and it has been largely studied [Wang et al., 2016b, Nimalsiri et al., 2019]. There are different objectives for the electrical system: local management of generation-consumption balance, mitigating the impact on the electricity network [Beaude et al., 2016], constituting a "Virtual Power Plant" by aggregating flexible usages (see, e.g., [Vasirani et al., 2013] in the case of EV), etc. It is revolutionizing the traditional paradigm of the electricity system, where almost only generation units were flexible to ensure its effective operation. EV charging is flexible in terms of compatibility with end users mobility needs and technical capabilities for load management. According to RTE report [RTE, 2019], private EVs are used only 4 % of the time, and are often charged during several consecutive hours: 85 % of annual EV consumption can be smartly charged, which in 2035 will amount to the energy consumed by hot water tanks (25 TWh, or 5 % of the French consumption in 2035). The flexibility of EV charging can also be used on a weekly basis. Indeed, the daily charging need is around[10] 6 kWh, compared to the 52 kWh battery of Renault Zoé

the road.

[8] Note that in *Crescendo* scenario of RTE, the EV electricity consumption could reach 40 TWh in 2035.

[9] This is particularly true in comparison to other typical electrical tasks, like heating, cooking, lighting, for which there is no potential to "smartly" schedule the associated electricity consumption profile.

[10] The average daily driving distance in France is 30 km [CGDD, 2010], at a 0.2 kWh/km average consumption

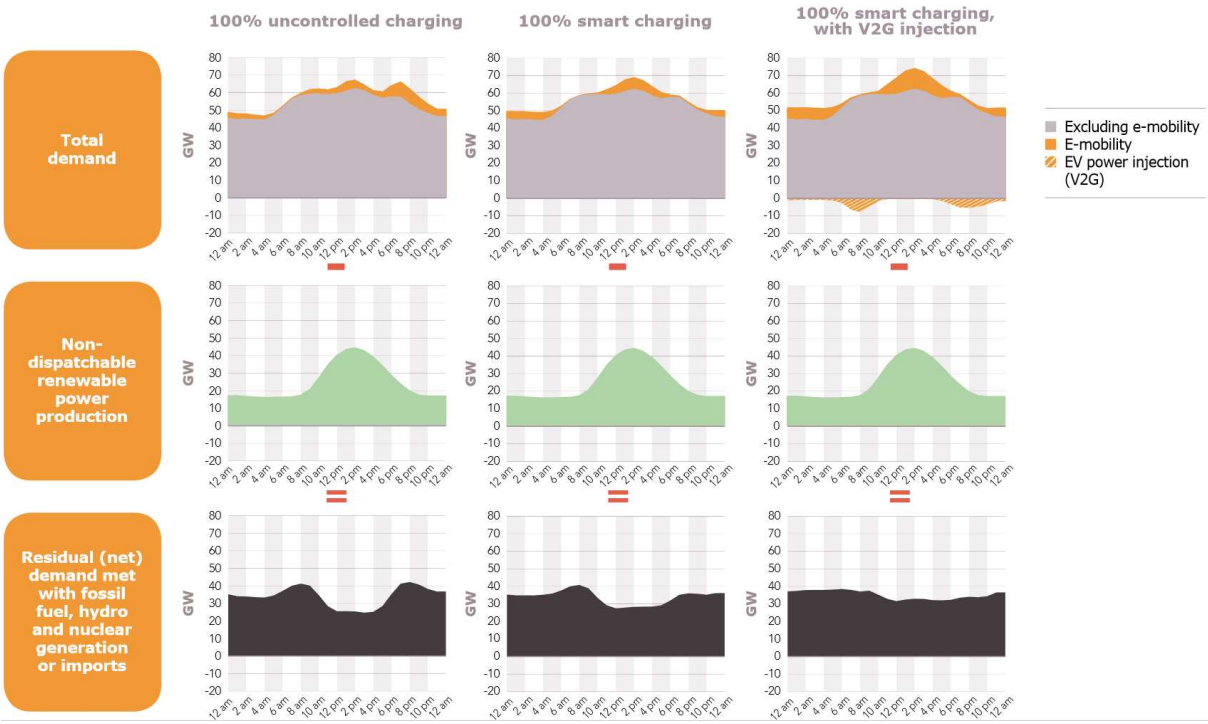

Figure 1.4: Total electricity demand in France and residual demand (total demand minus non-dispatchable renewable energy generation) in different EV smart charging configurations for an average weekday in 2035. Source: [RTE, 2019], Crescendo intermediate 2035 scenario.

E-Tech for example.

Smart charging can also limit the capping of renewable electricity generation by scheduling EV charging during such peaks. This is shown in Figure 1.4 from [RTE, 2019]: the residual demand – which is the total demand (including EV charging) minus the renewable generation – is smoother in the case of 100 % smart charging (second column of profiles) compared to the case of 100 % uncontrolled charging (first column). The remaining peaks of this residual demand can be smoothed by considering the Vehicle to Grid (V2G) technology, with which EVs can feed energy back to the electricity grid (see third column of Figure 1.4). In other words, thanks to V2G, EV charging can either be a load, or a distributed energy and power resource. Note that if in 2035, 20 % of EVs are V2G-compatible, the flexibility offered then by the EV fleet will be equivalent to the Pumped-Storage Hydroelectricity one in France both in terms of storage capacity and available power [RTE, 2019].

Smart charging can also help to reduce the distribution grid investment costs, with 75 % dedicated to connecting the EV Charging Stations (EVCSs) to the grid, and 25 % for reinforcing the grid [Enedis, 2019]. From now to year 2030, these investment costs are estimated to amount to almost 10 % of the total Enedis (the main French electricity distribution company) investments, according to the report [Enedis, 2019]. EV charging brings other distribution grid costs, such as transformer aging [Hilshey et al., 2012], thermal overloading of cables [Hu et al., 2013], power losses due to Joule heating [Sortomme et al., 2010], impact on grid voltage [Geth et al., 2012] and impact on power quality [Gómez and Morcos, 2003].

per distance unit [De Cauwer et al., 2015].

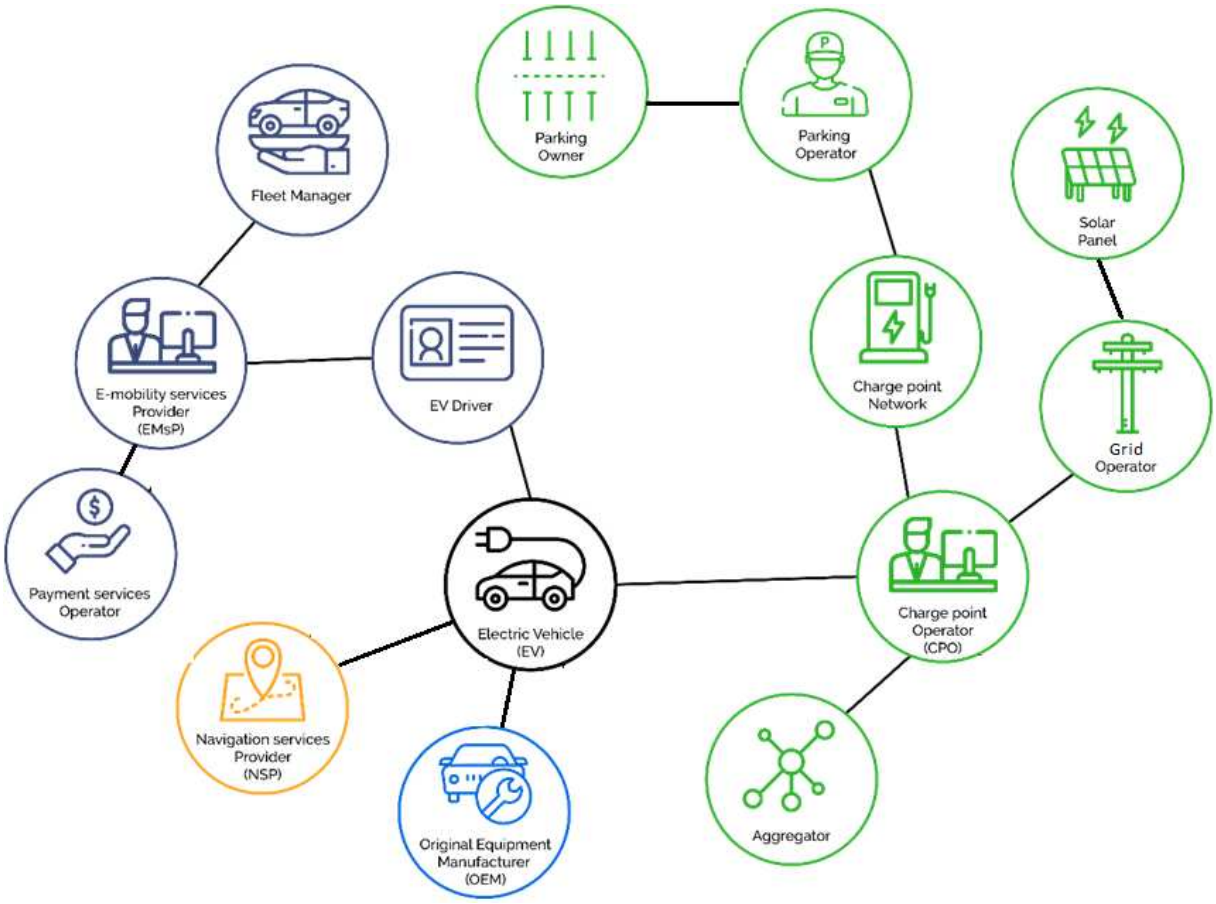

Figure 1.5: Schematic view of the electric mobility ecosystem. Source: E-motec

All these challenges associated with EV advent affect several stakeholders, also called operators in this work. Figure 1.5 from E-motec gives a non-exhaustive look at this operators' environment. These stakeholders may use various incentives to face these challenges, and the goal of this thesis is to help to design these incentives. To efficiently design their incentives, operators need an estimation of how vehicle users react to these incentives, which is given by a model of their decision-making process (Chapter 2). Note that in this thesis, the charge point operator, the aggregator, the e-mobility services provider, the solar panel operator and the parking operator are often assumed to be the same operator, called Charging Service Operator (CSO). Typically, the CSO uses smart charging to schedule EV charging profiles (Chapter 4) and smart pricings to incentivize EVs not to charge during peak loads (Chapter 5).

1.3 The coupled electrical-transportation system

In the following, the term "transportation system" or "electrical system" are often used, and include all relative infrastructures and stakeholders. The "transportation system" thus refers to the transportation network and its facilities (such as public transport), the concerned agents (vehicle users, public transport operator, local authorities, etc.) and potential externalities such as traffic congestion, local (air or noise) pollution, greenhouse gas emissions, etc. The "electrical system" refers to the distribution and transmission grids, the electricity generation facilities,

all the corresponding operators, the electricity consumers (as well as their suppliers), etc. EV users, the EVCSs and their operators can be considered as part of both systems, hence the interdependence (or coupling) between them.

This coupling means that a change in one system can also have an impact on the other, due to EVs. For example, traffic congestion can delay the time period during which an EV user wanted to charge, or make her charge at another EVCS than the one planned. This impact of the transportation system on the electrical one is clearly observable during widespread holidays departures or notable sport events: the majority of driving EV users need to charge at public EVCSs, where there could be a significant waiting time[11] and available power reduction (when allocated/shared between plugged EVs) due to simultaneous power demands. Inversely, the impact of the electrical system on the transportation one (via EVs) will be more pronounced in the near future and a higher EV penetration level. However, there are already examples, such as an electrical system maintenance in South China in may 2018 provoking the outage of 500 charging poles and the congestion of adjacent EVCSs by 2,700 EVs[12]. Voluntary changes in the electrical system such as charging pricing incentives may also impact the transportation system. Tesla EVCSs may adapt the charging prices in order to encourage EV users to charge in empty EVCSs rather than congested ones[13], which induces itinerary changes and potentially different congested roads. Another example of this impact worth mentioning comes from the project between the French companies CNR (*Compagnie Nationale du Rhône*) and Enalp (via its "Move In Pure" charging subscription) as well as Renault[14]: in order to guarantee that the source of electricity is renewable, EV users are incentivized to charge at some hours of the day and locations. In a more futuristic vision, the transportation and electrical systems can be coupled explicitly with a dynamic wireless inductive charging system (under the road) as suggested in [Wei et al., 2017] and already tested around the world, such as in London for some double-decked buses.

As a consequence, due to EVs, infrastructure and pricing strategies of an operator of the transportation or the electrical system not only have an impact on the corresponding system, but also on the operators and users of the other system. For example, Park & Ride hubs installed at a city's outskirt by local authorities to mitigate traffic congestion and pollution are also an opportunity for "smart charging" (see Section 6.2) – hence the emerging literature modeling the interdependence of the transportation and electrical systems, in part identified in review paper [Wei et al., 2019].

1.4 Thesis approach: commuting, long-term incentives and game theory

For long-range trips needing fast charging, such as holidays departures, the impact of the electrical system on the transportation one is limited: for example, EV users are unlikely to change their planned driving path in response to charging price signals (but may charge at an EVCS rather than at another one, both EVCSs being on the planned driving path). Therefore, we limit ourselves to intra-urban trips. Considering the driving distances of such trips (typically 30 km

[11] Gas stations on highways are sized relatively to the thirtieth most congested hour of the year [Enedis and RTE, 2019].

[12] This event was reported in the following press article http://news.sznews.com/content/2018-05/22/content_19164366.htm (in Chinese).

[13] https://www.tesla.com/support/supercharging.

[14] https://www.automobile-propre.com/move-in-pure-cnr-renault/ (in French).

a day in France), the EV driving range[15] (smaller than for ICEVs) is assumed never reached, and the range anxiety (studied in [Rauh et al., 2015]) is not taken into account. The typical use case considered in this thesis is commuting, which corresponds to the trips between home and work and which is the main type of local mobility. According to a French government study [CGDD, 2010] in 2008, among the local trips (confined in a 80 km-radius), 48 % of the total distance traveled with a personal vehicle (39 % of local trips) is done in commuting.

Similarly, charging EVs at home is not specifically considered, as changes in the electrical system would not impact EV users in their driving decisions. Instead, the EV charging during working hours is studied, in particular when EV users have several choices of EVCSs where to park and charge (and finish their commuting trip by public transport if needed[16], as in Section 6.2). As the charging period (working hours) is relatively long compared to the time needed to charge 6 kWh (the typical daily charging need), the charging profiles may be optimized (see Chapter 4).

The ultimate goal of this thesis is to model the coupled electrical-transportation system – in the commuting use case – in order to efficiently design incentives of operators of this coupled system. The type of mechanisms considered is long-term, such as sizing EVCSs (or even solar panels, as in Section 6.2), smart pricing (for EV charging, traffic tolls, public transport ticket fare, etc.), the electricity supplying contract of the CSO (see Section 7.2.3), etc. Note however that measures to increase EV adoption are not the object of this thesis. Short-term problems like queues at EVCSs or per-EV charging profiles (to be opposed with aggregated charging profiles studied in Chapter 4) are not studied in this work but constitute an interesting follow-up. Such short-term studies require real-time models of vehicle users' behavior, as in [Tan and Wang, 2017], in which the time period considered (typically the morning commuting period in the case of the present thesis) is discretized into several time slots. The different time slots are coupled: vehicle users leaving from home at different times which find themselves on the same road at the same time. For long-term incentives, a static behavior model may be sufficient: the morning commuting time period is modeled by a unique time slot, which remains relevant as this specific time period is particularly narrow (see Figure 4.8). Note that only the vehicle users' behavior model is assumed static: the charging time period (during working hours) is still discretized into several time slots which enables the smart scheduling of charging profiles of Chapter 4.

Although assumed static, this commuting use case may be repeated a certain number of days in order to see the evolution of vehicle users' behavior during this learning period, as shown in Chapter 3. For example, if at first all vehicle users choose the shortest path, this path becomes too congested and the next day most vehicle users choose the second shortest path, which also becomes congested, so that the third day some vehicle users come back to the first shortest path, and so on. For the long-term strategies studied in this thesis, the stationary behavior – also called equilibrium [Knight, 1924] – obtained after some time is sufficient. This traffic equilibrium is typically described and found using a game theoretical framework [Wardrop, 1952] (see Chapter 2). Game theory is the formal study of interactions between several decision-makers (here, vehicle users), each having their own interests. Because of these interactions, the situation of a decision-maker (and therefore her strategy) depends on the others' strategies, which is typical on the road with the congestion concept. The game framework is thus also suited to model the interactions between the operators of the coupled electrical-transportation system and their various incentives [Fudenberg and Tirole, 1991].

[15] The Renault Zoé E-Tech has a WLTP (Worldwide Harmonized Light vehicles Test Procedure) autonomy of 395 km.

[16] Note that this framework could be applied during night-time, where commuters would charge their vehicle at a public EVCS instead of at home, and go back home by public transport.

There already exists a scientific literature studying the coupled electrical-transportation system with game theory tools, as shown in review paper [Wei et al., 2019]. The specificity of this thesis lies in the particular EV charging pricing considered, which is the main incentive studied here (see Chapter 5). This pricing is function of the negative impact (on the electrical grid, the payoff of the EVCS operator, etc.) of EV charging, which is already reduced by scheduling the charging profile in Chapter 4. Chapter 2 extends results in game theory to this special pricing, which makes it possible to obtain in the final Chapter 7 an original global theoretical model of the interactions between different operators of the coupled electrical-transportation system and the reactions of vehicle users to their incentives.

1.5 Contents of the manuscript

The organization of the rest of this thesis is briefly summarized here. The present work is organized in three major parts, each containing two chapters.

Part I focuses on modeling how vehicle users behave while driving and charging in function of various parameters of the coupled electrical-transportation system, using game theory. Existing theoretical results related to the concept of game equilibrium are extended to the particular charging pricing considered in this work. This part is constituted of Chapters 2 and 3:

2 The non-atomic congestion game model [Rosenthal, 1973] of vehicle users (and the corresponding assumptions) used in the subsequent chapters (except Chapter 3) is detailed. Beckmann's method [Beckmann et al., 1956] to find a game equilibrium [Wardrop, 1952] is extended to *linearly non-separable* increasing congestion cost functions introduced in Definition 2.11 in order to apply to our particular charging pricing (detailed in Chapter 5).

3 The assumptions of Chapter 2 on vehicle users' rationality are relaxed by considering two different types of Reinforcement Learning Algorithms (RLAs) [Sutton and Barto, 2018]. The convergence of the first type of RLAs [Sastry et al., 1994, Bournez and Cohen, 2013] towards the game equilibrium – where vehicle users have no prior knowledge but observe their driving and charging costs – is extended to *linearly non-separable* cost functions (such as our charging pricing). The second type [Cominetti et al., 2010] – where vehicle users' observations are imperfect – is only illustrated on *linearly non-separable* cost functions.

This thesis focuses on two main incentives for Electric Vehicles, detailed in Part II: the smart charging of EVs charging profiles (Chapter 4) and how this charging is priced (Chapter 5). These two incentives are expressed in terms of the game theory tools introduced in Chapter 2 and are assumed to be controlled by the same operator, called Charging Service Operator.

4 In this work, the smart charging of EVs at a CSO's Charging Station follows the water-filling algorithm [Shinwari et al., 2012], which possesses an analytic solution. This algorithm is extended to the case where EVs may arrive at the EVCS and leave at different times, which are not communicated to the CSO in advance. Another extension results in an almost optimal algorithm in the case where a CSO owns several EVCSs.

5 The particular charging pricings considered in this thesis depend on the total load profile obtained with the water-filling algorithm of Chapter 4. This way, they form *linearly non-separable* congestion cost functions (see Definition 2.11) in a game framework. These pricings are studied (specifically their monotonicity) and compared to the Locational Marginal Pricing, common in the literature [Alizadeh et al., 2016].

In the last Part III, various operators' incentives are studied using the behavior model of vehicle users introduced in Chapter 2 with the charging pricings defined in Chapter 5;

6 The reaction of vehicle users to incentives are illustrated numerically on two examples. In the first example, a Transportation Network Operator reduces the local air pollution in a city by imposing a traffic toll on Internal Combustion Engine Vehicles downtown. In the other, an e-Park & Ride hub operator optimizes the size of solar panels with which the EVs are charged.

7 A trilevel framework between three stakeholders (including vehicle users) of the coupled electrical-transportation system is given. The lower level of the model corresponds to the congestion game between vehicle users defined in Chapter 2. At the middle level, a Charging Service Operator uses the water-filling charging scheduling algorithm and the corresponding pricings defined respectively in Chapters 4 and 5. At the upper level, the Electrical Network Operator chooses the electricity supplying contract of the CSO.

1.6 Publications related to this thesis

Each chapter is based on conference proceedings and journal articles reviewed and accepted for publication:

[Sohet et al., 2019a] **Sohet, B.**, Beaude, O., and Hayel, Y. (2019). Routing game with non-separable costs for EV driving and charging incentive design. *International Conference on NETwork Games COntrol and OPtimization: Proceedings of NETGCOOP 2018*, New York, NY, pages 233–248. Springer.

[Sohet et al., 2019b] **Sohet, B.**, Hayel, Y., Beaude, O., and Jeandin, A. (2019). Optimal incentives for electric vehicles at e-park & ride hub with renewable energy source. *World Electric Vehicle Journal*, 10(4):70.

[Sohet et al., 2019c] **Sohet, B.**, Hayel, Y., Beaude, O., and Jeandin, A. (2019). A model to evaluate coupled driving-and-charging incentives for electric vehicles. *In 32nd Electric Vehicle Symposium (EVS32).*

[Sohet et al., 2020a] **Sohet, B.**, Hayel, Y., Beaude, O., and Jeandin, A. (2020). Impact of strategic electric vehicles driving behavior on the grid. *In 2020 IEEE PES Innovative Smart Grid Technologies Europe (ISGT-Europe)*, pages 454-458.

[Sohet et al., 2020b] **Sohet, B.**, Hayel, Y., Beaude, O., and Jeandin, A. (2020). Learning pure nash equilibrium in smart charging games. *In 2020 59th IEEE Conference on Decision and Control (CDC)*, pages 3549-3554.

[Sohet et al., 2021a] **Sohet, B.**, Hayel, Y., Beaude, O., Breal, J., and Jeandin, A. (2021). Online smart charging algorithm with asynchronous electric vehicles demand. *In 2021 IEEE PES Innovative Smart Grid Technologies Europe (ISGT-Europe).*

[Sohet et al., 2021b] **Sohet, B.**, Hayel, Y., Beaude, O., and Jeandin, A. (2021). Coupled charging-and-driving incentives design for electric vehicles in urban networks. *IEEE Transactions on Intelligent Transportation Systems*, 22(10):6342-6352.

[Sohet et al., 2021c] **Sohet, B.**, Hayel, Y., Beaude, O., and Jeandin, A. (2021). Hierarchical coupled routing-charging model of electric vehicles, stations and grid operators. *IEEE Transactions on Smart Grid*, 12(6):5146-5157.

Part I

Driving-and-charging behavior of vehicle users

Chapter 2

A non-separable routing game to model vehicle user behavior

This chapter and the following one focus on the modeling of vehicle user behavior while driving and charging. The present chapter introduces the different choices vehicle users face – such as the driving path, the charging location, etc. – as well as cost functions which indicate the preferences of the vehicle users for each choice's option. More precisely, the different choices are modeled by fictitious arcs of a transportation graph, and the preferences are represented by linearly non-separable congestion cost functions in order to take into account the EV Charging Unit Price defined in Chapter 5. These characteristics, in addition to the assumptions made on vehicle users rationality in this chapter, form a routing game. Beckmann's method to find the equilibrium of this driving-and-charging routing game is extended to this type of cost functions. This allows the integration of the vehicle user behavior model in a larger model of the coupled transportation-electrical system (including its operators, see Part III).

This chapter is inspired mostly from the following papers:

[Sohet et al., 2019a] **Sohet, B.**, Beaude, O., and Hayel, Y. (2019). Routing game with non-separable costs for EV driving and charging incentive design. *International Conference on NETwork Games COntrol and OPtimization: Proceedings of NETGCOOP 2018*, New York, NY, pages 233–248. Springer.

[Sohet et al., 2021b] **Sohet, B.**, Hayel, Y., Beaude, O., and Jeandin, A. (2021). Coupled charging-and-driving incentives design for electric vehicles in urban networks. *IEEE Transactions on Intelligent Transportation Systems*, 22(10):6342-6352.

Contents

2.1 Introduction **16**

2.2 The driving-and-charging routing game **17**

2.2.1 Non-atomic and rational players 17

2.2.1.1 Vehicles grouped in non-atomic classes 17

2.2.1.2 Hyper-rational drivers with common knowledge 18

2.2.2 Routing game: choices modeled as fictitious graph arcs 19

2.2.2.1 The driving path choice 19

2.2.2.2 The charging choices 21

2.2.3 Standard driving and charging cost functions 23
2.2.3.1 Constant cost functions 23
2.2.3.2 Congestion cost function: travel duration 24
2.3 The charging unit price: a particular congestion cost function . 26
2.3.1 General non-separable congestion cost functions 26
2.3.2 Linearly non-separable congestion cost functions 27
2.4 Equilibrium of linearly non-separable games using Beckmann's function 28
2.4.1 Wardrop equilibrium: solution concept of non-atomic games 28
2.4.2 The equilibrium as a minimum of Beckmann's function 30
2.4.3 Wardrop Equilibrium properties 31
2.5 Conclusion 33

Table 2.1: Notations of Chapter 2

Symbols	Signification
$\mathbb{G}$	The common driving-and-charging routing game in this thesis
$\mathcal{S}$	Set of vehicle classes s
$\mathcal{V}$	Set of vertices v of the transportation graph
$\mathcal{A}$	Set of arcs a of the transportation graph
$\mathcal{R}$	Set of paths r of the transportation graph
$\mathcal{R}^{OD}$	Set of paths from $O \in \mathcal{V}$ to $D \in \mathcal{V}$
$\delta_{a,r}$	1 if arc $a \in \mathcal{A}$ belongs to path $r \in \mathcal{R}$, 0 otherwise
l_a	Length of arc $a \in \mathcal{A}$
$f_{s,r}$	Flow of vehicles of class $s \in \mathcal{S}$ choosing path $r \in \mathcal{R}$
$x_{s,a}$	Flow of vehicles of class $s \in \mathcal{S}$ on arc $a \in \mathcal{A}$
$d_a(x_a)$	Travel duration on arc a depending on total flow x_a
X_s^{OD}	Travel demand of vehicle class s from $O \in \mathcal{V}$ to $D \in \mathcal{V}$
$\mathcal{X}$	Set of feasible flow vectors $\boldsymbol{f}$ which satisfy the travel demand
m_s, λ_s	Resp. energy consumption and energy unit price for vehicle class s
$c_{s,r}$	Cost function for a vehicle of class $s \in \mathcal{S}$ choosing path $r \in \mathcal{R}$
$\alpha_{s,r}\lambda(\langle \boldsymbol{\alpha}, \boldsymbol{f} \rangle)$	Linearly non-Separable Congestion cost function
$\mathcal{B}$	Beckmann's function
$\boldsymbol{f}^*, \boldsymbol{x}^*$	Flow vectors at Wardrop Equilibrium

2.1 Introduction

As mentioned in Section 1.4, the behavior of vehicle users both while driving and charging is modeled using game theory because of the two following aspects:

- there are interactions between the different vehicle users on the roads and at charging stations, and also between users and station operators, etc.;

- the point of view is economical: all the choices of vehicle users are modeled as a rational decision between several alternatives, decision which is based on a unique financial metric (with a monetary conversion for non-financial choices).

In this chapter, additional assumptions are made in Section 2.2 relating to general properties of the driving-and-charging game, and in Section 2.3 for the specific EV Charging Unit Price. The goal is to use Beckmann's method (see Section 2.4) in order to have a tractable behavior model, which can be integrated into a global model of the coupled transportation-electrical system (i.e. including its operators in addition to the vehicle users, as in Chapter 7), and which can be solved efficiently. Some of these assumptions are relaxed in next Chapter 3 in order to model more realistic behaviors such as learning.

2.2 The driving-and-charging routing game

The most common way to describe a game is to give its strategic (also called normal) form, made of three parts [Osborne et al., 2004]:

- a set of players $\mathcal{N}$, and for each player $i \in \mathcal{N}$;
- the set $\mathcal{R}_i$ of choices available to player i
- the cost function c_i of player i defined on its set of choices $\mathcal{R}_i$.

Note that these three components may slightly differ in the games considered in the other chapters: the present chapter gives the common outline of these games, outline referred to as game $\mathbb{G}$ in this chapter. Game $\mathbb{G}$ is entirely defined by the three components $\mathbb{G} = \{\mathcal{N}, (\mathcal{R}_i)_{i\in\mathcal{N}}, (c_i)_{i\in\mathcal{N}}\}$, which are detailed in the three following sections. Note that in this thesis, games are non-cooperative, meaning that each player has its own objective and is selfish, compared to coalitional games [Aumann and Peleg, 1960].

2.2.1 Non-atomic and rational players

This section describes how the players of the game $\mathbb{G}$ introduced in this chapter are modeled. In the following, players can also be referred to as vehicle users or drivers. Note that the following theoretical framework and results can be applied to case studies other than driving-and-charging vehicles, like facilities in wireless networks [Lasaulce and Tembine, 2011]. In this game, two major assumptions on the players are made, and are developed in the two following sections: they are grouped into several vehicle classes sharing the same characteristics, and they are *hyper-rational*.

2.2.1.1 Vehicles grouped in non-atomic classes

Due to a potentially large number of vehicles, problems such as scheduling the EV charging profiles in Chapter 3 can be NP-hard [Sassi and Oulamara, 2017] (Non-deterministic Polynomial-time hard) and classical algorithms limited[1]. Therefore, assumptions have to be made, such as the classical *non-atomic* framework [Aumann and Shapley, 2015] used since the 1950s [Wardrop, 1952,

[1] Such problems could however be solved by quantum algorithms [Dalyac et al., 2021].

Beckmann et al., 1956] in Traffic Assignment Problems[2] (TAP) [Patriksson, 2015]. In this framework, vehicles are not considered individually but as a continuous mass. Such an assumption remains accurate enough for our long-term study of the coupled electrical-transportation system.

Example 2.1. *Consider EV users having the choice between two actions a and b (e.g., the choice to charge at two different EV Charging Stations a and b). The variables of interest in the non-atomic framework are the proportions*[3] *(written x_i) of the continuous mass of EV users choosing action i ($i = a$ or b). Note that by definition, these variables verify $x_i \in [0, 1]$ and $\sum_{i=a,b} x_i = 1$, for a normalized mass.*

A continuous mass is called *homogenous* if all vehicle users have the same cost functions (introduced in Section 2.2.3) upon which they base their choices. Basic homogenous TAPs are defined and studied in [Sheffi, 1985]. A continuous mass can be split into several classes (or types), each one having its own cost functions (which are the same only for the vehicle users of the same class) and is thus called *heterogenous*. For example in this thesis, there are two main vehicle classes considered in game $\mathbb{G}$, with different characteristics and thus different cost functions: the Electric Vehicles (mostly battery EVs, as mentioned in Section 1.1) associated with subscript e, and the vehicles working on Internal Combustion Engines and grouped under the name of "Gasoline Vehicles" (GVs, subscript g). Note that not all GVs work on gasoline: some use diesel[4], but the characteristics of this vehicle class (such as fuel consumption and price) are taken as an average between gasoline and diesel vehicles. Each one of these two vehicle classes can also be divided into smaller classes, as in Chapter 7 which distinguishes EVs with low State of Charges (SoCs) from those with high SoCs. In this thesis, it is assumed that the mass X_s of each vehicle class s is fixed[5]. The variables $x_{s,i}$ of game $\mathbb{G}$ (corresponding to the proportion of vehicles of class s choosing action i) verify $\sum_{i=a,b} x_{s,i} = X_s$.

In the recent years, there has been an increasing interest for mixed (or multiclass) TAP (MTAP) first introduced in [Dafermos, 1972] and where multiple classes of vehicles are considered [Jiang and Xie, 2014, Wang et al., 2019a, Pi et al., 2019]. There is also some research on infinitely many classes [Jacquot and Wan, 2018], each one having its own cost functions and possible choices. In this thesis, the (finite) set of classes is denoted $\mathcal{S}$.

Remark 2.2. *Note that in the non-atomic framework, it is only possible to know how many vehicle users (with the same cost functions) made each choice, not which vehicle user made which choice, which is accurate enough for our long-term study of the coupled electrical-transportation system.*

2.2.1.2 Hyper-rational drivers with common knowledge

A fundamental assumption in this work is the economic rationalism of vehicle users in game $\mathbb{G}$: they can sort their different choices by preference and select their favorite one. In this thesis (except for Chapter 3), additional rationality assumptions are taken.

(i) Firstly, game $\mathbb{G}$ is assumed to be with *complete information*, i.e. that everything is common knowledge. By "everything" is meant both the set of choices available $\mathcal{R}_i$ to every

[2] Traffic or route assignment corresponds to the selection of a path to fulfill a travel demand between an origin and a destination. TAP are usually solved using game theory, like in this work.

[3] Proportion and number of vehicles are equivalent in this thesis, as the total number of vehicles is always fixed.

[4] Diesel vehicles represent around 20 % of all vehicles in the world, a little less than 50 % in Europe and up to 59 % in France (https://www.statistiques.developpement-durable.gouv.fr/382-millions-de-voitures-en-circulation-en-france).

[5] For a normalized total vehicle mass, $X_s \in [0, 1]$ and $\sum_s X_s = 1$.

driver i (see Section 2.2.2), and their preferences modeled by cost functions c_i (see Section 2.2.3). The term "common knowledge" [Aumann, 1976] means that all vehicle users know everything, that they know the other users know, and so on. A realistic framework of common knowledge can be delivered by a smartphone application with an integrated model of congestion on the roads and at the charging stations (like the model suggested in this chapter) and an access on information such as the current travel demand for example (like an improved version of Waze). However, most often players have partial information, and the corresponding games are called Bayesian [Zamir, 2020]. For example, one way to introduce partial information is to consider a restricted common knowledge model, also called bounded rationality [Nagel, 1995]. In such models, players with so-called level-k rationality believe all the other players are level-$(k-1)$, and so on, with level-0 rationality players making random choices.

(ii) Secondly, in this work (except Chapter 3) players of game $\mathbb{G}$ are assumed *hyper-rational* [Lasaulce and Tembine, 2011], meaning that they are capable of finding their best option and effectively choose it. For example, in case of complex computations, a smartphone application could find the best option itself. Limited computation capacity and other types of limited rationality are identified in [Simon, 1972].

In Chapter 3, vehicle users do not know their exact cost functions as in assumption (i) but only observe them, and in Section 3.3, they do not systematically choose the action associated with the lowest observed cost, as in assumption (ii). In some cases, even without assumptions (i) and (ii), the same theoretical results – in particular the equilibrium (see Section 2.4) corresponding to game $\mathbb{G}$ – are obtained (see Section 3.2.2.3).

2.2.2 Routing game: choices modeled as fictitious graph arcs

This section describes how the different options available to the players of game $\mathbb{G}$ are modeled. In the following, a choice refers to a distinct decision vehicle users have to make, like the driving path, the place of charging, etc. Considering a given choice (e.g. the driving path), players have to decide between different options (the different possible paths), also called actions or strategies in the following[6]. In the commuting framework of this work, vehicle users face several choices like the path to get to their destination, the charging station where to park and charge, whether to park before arriving at the destination and take public transport, whether charging while at work or later at home, the charging quantity, the hour of departure from work, etc. As our work focuses on the coupling between the transportation and electrical systems, the behavior model introduced in this chapter always integrates the choice of the driving path, also called the Traffic Assignment Problem (TAP) [Patriksson, 2015]. This choice of the driving path necessitates graph theory [West et al., 2001] and is detailed in Section 2.2.2.1. In this thesis, the others choices mentioned above (e.g. the choice of the EV Charging Station, of the charging quantity) are also integrated in graphs, as explained in Section 2.2.2.2.

2.2.2.1 The driving path choice

The driving path choice in game $\mathbb{G}$ is modeled using a graph. Non-atomic games where players choose a path in a graph are called routing games [Roughgarden, 2007]. Figure 2.2 illustrates a

[6]Note that "actions" and "strategies" are not always synonyms, like in Chapter 3 when considering mixed strategies. Then, the mixed strategy of a player is to choose each option with different probabilities, and the action is the effective choice.

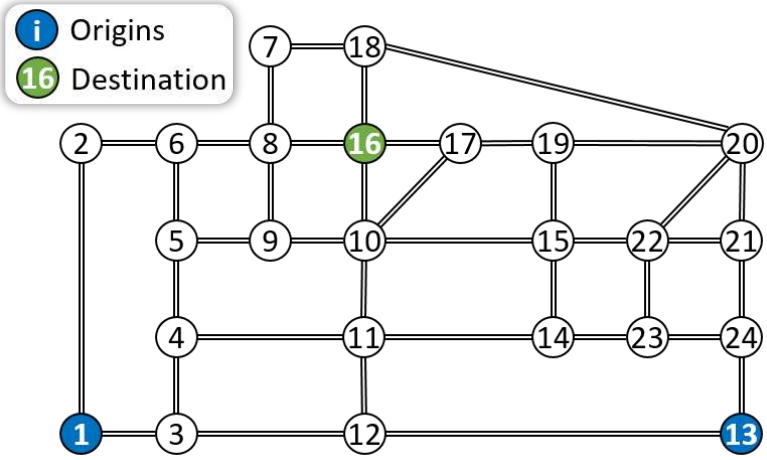

Figure 2.2: Sioux falls transportation network modeled as a directed graph (two directed arcs connecting pairs of vertices). In this example, there is travel demand from the origins 1 and 13 to the destination 16.

typical transportation network graph, used in our journal paper [Sohet et al., 2021c] (see Chapter 7). This figure shows the graph representing the simplified road network of Sioux falls, South Dakota (USA), which is widespread in the transport research community and first introduced in [Morlok, 1973]. The *directed* graph of Figure 2.2 is a pair $(\mathcal{V}, \mathcal{A})$ with $\mathcal{V}$ the set of nodes or vertices (from 1 to 24) and $\mathcal{A}$ the set of *ordered* pairs of vertices, called arcs. Each node represents an intersection between several roads, and each segment of a (two-way) road between two nodes is represented by two directed arcs. For example, the road between nodes 1 and 2 is made of both the (directed) arc going from 1 to 2 and the inversed arc going from 2 to 1[7]. Such graphs $(\mathcal{V}, \mathcal{A})$ where for all arc $a \in \mathcal{A}$, the corresponding inversed arc also belongs to $\mathcal{A}$ are called symmetric directed graph. Note that the transportation network is modeled by a directed graph and not an undirected one (where each couple of nodes is at most connected by one undirect link) because, among other reasons, traffic congestion might be higher for one way of a road than the other inversed way.

A driving path from any Origin node $O \in \mathcal{V}$ to any Destination node $D \in \mathcal{V}$ is represented in the graph by a (directed) path r, which is a finite sequence of arcs $(a_1, \ldots, a_{n-1}) \in \mathcal{A}^{n-1}$ for which there is a sequence of *distinct*[8] vertices $(v_1, \ldots, v_n) \in \mathcal{V}^n$ such that each arc a_k goes from node v_k to v_{k+1} and $v_1 = O, v_n = D$. The set of all paths is $\mathcal{R}$. The set of paths r going from O to D is denoted $\mathcal{R}^{OD}$. For example, the set $\mathcal{R}^{1,16}$ of paths going from origin 1 to destination 16 of Figure 2.2 contains $3,722$ different paths[9], found by an exhaustive recursive function. This number of paths is prohibitive, and in practice only a few (e.g. three in our paper [Sohet et al., 2021c]) paths are actually taken by vehicle users. This is why for each origin-destination couple, we limit the number of possible paths to the (e.g. five) shortest ones, using a shortest path algorithm[10].

In the rest of this Section 2.2.2.1, the subscript s corresponding the class s of the vehicles

[7] The direction arrows are not apparent in Figure 2.2 for a better readability.

[8] In this thesis, cycles (passing several times by a same node) are prohibited in the definition of paths.

[9] Note that there are infinitely many paths from 1 to 16 if cycles are accepted in the definition of a path.

[10] Note that the shortest paths are not necessarily the least expensive ones for the vehicle users, but in practice the vehicle users actually use the three shortest paths.

considered is omitted for a better readability. The input data of the Traffic Assignment Problem (TAP) modeled by game $\mathbb{G}$ is the travel demand, expressed as flows of vehicles per time unit [Wardrop, 1952] (or flow rates) which need to drive from $O \in \mathcal{V}$ to $D \in \mathcal{V}$, and denoted X^{OD}. We consider normalized travel demand flow rates, which thus verify $\sum_{O,D\in\mathcal{V}} X^{OD} = 1$ ($= X_s$ if different vehicle classes s are considered, with $\sum_s X_s = 1$)

Therefore, X^{OD} is the portion of the total flow rate which needs to travel from O to D. In the TAP, the choice vehicle users have to make is the path $r \in \mathcal{R}^{OD}$ to go from their origin O to their destination D. The aim of traffic assignment is to find, for each $O, D \in \mathcal{V}$ pair, the flow f_r of vehicle users choosing each path $r \in \mathcal{R}^{OD}$, verifying the following travel demand constraints.

Definition 2.3 (Travel demand constraints)**.**

$$\forall O, D \in \mathcal{V}\,, \quad \begin{cases} \sum_{r\in\mathcal{R}^{OD}} f_r = X^{OD}\,, \\ f_r \geq 0\,, \forall r \in \mathcal{R}^{OD}\,. \end{cases} \tag{2.1}$$

The set of vector flows $\boldsymbol{f}$ verifying these constraints, called the feasible set*, is denoted $\mathcal{X}$.*

Necessarily, $f_r \leq X^{OD}$ for all $r \in \mathcal{R}^{OD}$. Game $\mathbb{G}$ is then associated with these travel demand constraints (2.1). The routing game solving this TAP can be written $\{(\mathcal{V}, \mathcal{A})\,, (\mathcal{R}^{OD})_{O,D\in\mathcal{V}}\,, (c_{s,r})_{s,r}\}$.

Remark 2.4. *As detailed in next section, paths may be associated with EVCSs. These EVCSs may have a limited number of charging points and therefore a limited number $X_{e,r}$ of EV users can choose the associated paths r. This can be expressed by the following additional travel demand constraint, for each path r concerned:*

$$f_{e,r} \leq X_{e,r}\,. \tag{2.2}$$

The theoretical results in this thesis extend to any of these additional constraints.

Remark 2.5. *In Section 2.2.3, modeling traffic congestion requires the flow x_a of vehicles on each arc $a \in \mathcal{A}$:*

$$x_a = \sum_{O,D\in\mathcal{V}} \sum_{r\in\mathcal{R}^{OD}} \delta_{a,r} f_r\,, \tag{2.3}$$

with $\delta_{a,r}$ equal to 1 if arc $a \in \mathcal{A}$ belongs to path $r \in \mathcal{R}^{OD}$ and 0 otherwise[11].

2.2.2.2 The charging choices

In this thesis, the other possible choices vehicle users have to make in game $\mathbb{G}$ can also be modeled using a graph theory framework, following the idea of [Alizadeh et al., 2016]. This way, game $\mathbb{G} = \{(\mathcal{V}, \mathcal{A})\,, (\mathcal{R}^{OD})_{O,D\in\mathcal{V}}\,, (c_{s,r})_{s,r}\}$ is a routing game This idea is illustrated by the choices studied in our paper [Sohet et al., 2021c], which are simplified in Figure 2.3. In this paper, to get to their destination, vehicle users choose their driving path, the EVCS where they park and whether they charge there or rather later at home. Figure 2.3 is a schematic simplification of this problem: vehicle users have the choice between two driving arcs a_1 and a_2 in order to get to their destination, each driving arc a_i ($i = 1, 2$) passing by a different EVCS i. A way to take into account another choice (here whether EV users charge at the EVCS or later at home) is to create fictitious arcs a_i ($i = 3, 4, 5, 6$). Specifically, charging at EVCS 1 is represented by fictitious arc

[11] With normalized travel demand, $\sum_{O,D\in\mathcal{V}} \sum_{r\in\mathcal{R}^{OD}} f_r = \sum_{O,D\in\mathcal{V}} X^{OD} = 1$ while the sum $\sum_{a\in\mathcal{A}} x_a = \sum_{O,D\in\mathcal{V}} \sum_{r\in\mathcal{R}^{OD}} (f_r \sum_a \delta_{a,r})$ is likely to be greater than one as paths are likely to be composed of several arcs ($\sum_a \delta_{a,r} \geq 2$).

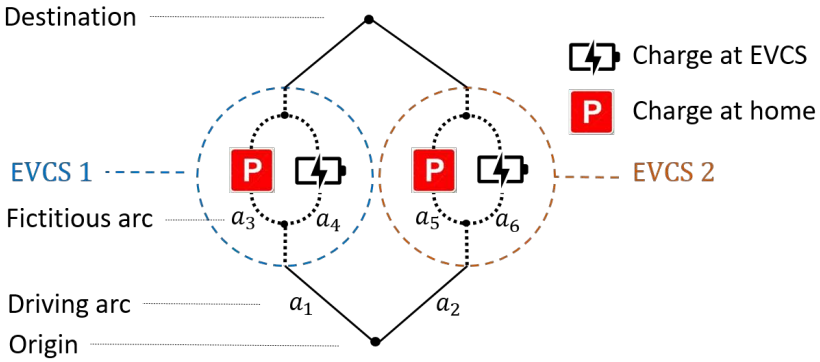

Figure 2.3: Illustration of a graph modeling several kinds of choices for vehicle users. *There are two driving arcs a_i ($i = 1, 2$) connecting the origin to the destination, each one passing by a different EVCS i. At EVCS i, it is possible to only park there and charge later at home (respectively fictitious arcs a_3 and a_5); or, it is possible to charge at the EVCS (a_4 and a_6).*

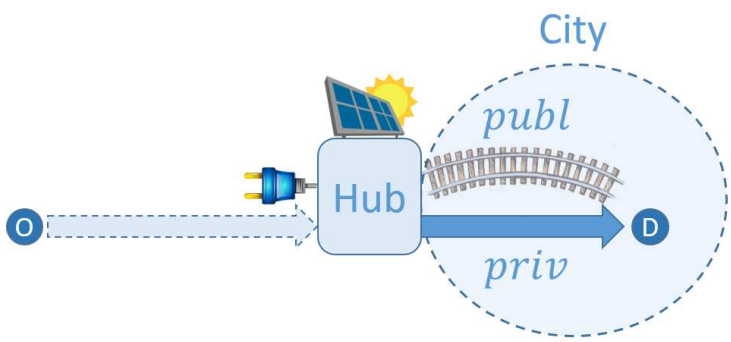

Figure 2.4: Schematic representation of the charging hub scenario: commuters can either choose to leave their vehicle at the hub and take public transport (*publ*), or drive all the way to their destination (*priv*). *Another example where driving-and-charging decisions of vehicle users can be cast as fictitious paths.*

a_4 while charging later at home after having chosen driving arc a_1 is represented by a_3. The same applies after driving arc a_2. Therefore in this simplified game, vehicle users have four different strategies, or paths: (a_1, a_3), (a_1, a_4), (a_2, a_5) and (a_2, a_6). By choosing between one of these four augmented paths, EV users actually make two simultaneous choices: the driving path and the charging location.

In paper [Alizadeh et al., 2016], the idea of fictitious arcs is originally used to model the choice of the charging quantity at the charging station. More precisely, the EVCS is modeled by a finite number of parallel fictitious arcs, each arc representing a different electricity amount the EV users might want to charge. Another example of fictitious arcs is used in our journal paper [Sohet et al., 2019b] (see Figure 2.4), where vehicle users can either drive through a congested city center to get to their destination (arc "*priv*", for private transport mode) or park their vehicle at a e-Park & Ride hub on the outskirt of the city and finish the trip by public transport (arc "*publ*", for public transport mode).

2.2.3 Standard driving and charging cost functions

The last characteristic of routing game $\mathbb{G}$ left to be specified is the cost functions, which indicate the preferences of each class s of vehicle users (which have commonly shared preferences, see Section 2.2.1) for each strategy r (see Section 2.2.2). The total cost function a vehicle user of class s associates to the augmented path r is denoted $c_{s,r}$ and can be composed of three types of cost functions: constant (Section 2.2.3.1), congestion (Section 2.2.3.2) and non-separable congestion cost functions (Section 2.3).

Remark 2.6. *In this thesis, a distinction is made between cost functions and costs. For example, a driving arc a is associated with a* cost function $x_a \mapsto d_a(x_a)$ *representing the travel duration d_a on this arc, which depends on the vehicle flow x_a on a (see Section 2.2.3.2 for more details on this function d_a). Except in next Chapter 3, the common knowledge assumption is made in this thesis, which means that players know the different cost functions (e.g., vehicle users know how the travel duration d_a on arc a depends on the vehicle flow x_a on it) and that they base their strategy on them. The* costs *is what players get once their strategy is chosen and that they take action*[12]*: it is the real value $d_a(x_a) \in \mathbb{R}$ obtained by the evaluation of the cost function d_a at vehicle flow x_a.*

2.2.3.1 Constant cost functions

The cost function $c_{s,r}$ of a vehicle user of class s choosing path r is said constant when it does not depend on the choices made by the other vehicle users. Note that these costs however can depend on the choices the vehicle user makes, and even depend on its vehicle class. For example, for a given vehicle, the following costs can be considered as constant functions:

- the public transport ticket fare in the use case illustrated by Figure 2.4, for vehicle users choosing to park their vehicle at the hub and then take public transport. This cost does not depend on the choices of the other vehicle users, but it can vary if the vehicle user under consideration chooses to travel a longer distance by public transport (corresponding to a higher ticket fare), for example;
- the toll when entering the highway, a parking, a city, etc., which in addition can depend on the vehicle class (e.g., toll reduction for low-emitting vehicles [Wang et al., 2019b]);
- the oil price for GVs, which depends on the gas station chosen by the GV user[13].

Note that in this work, the fueling cost – the oil price λ_g multiplied by the GV consumption – is also constant, due to the following assumption.

Assumption 2.7. *For all vehicle classes s, the common energy consumption m_s per distance unit is assumed constant, i.e. not to depend on the driving speed and acceleration profiles as well as exogenous weather conditions (for auxiliary consumption). Therefore, the fuel consumption cost function for GV users choosing driving path r is constant and equal to $l_r m_g \lambda_g$, with l_r the length of r.*

[12] The distinction between strategy and action is only relevant in next Chapter 3 when considering mixed strategies.

[13] On the contrary, the electricity price for EV users is not a constant function but a linearly non-separable increasing congestion cost function, introduced in Section 2.3.2.

A more realistic consumption model such as the one calibrated in [Fontana, 2013] for EVs, which not only depends on the traveled distance but also on the speed profile, leads to a complex energy consumption cost function (which does not have the symmetry property (2.7)) for which the theoretical results of Section 2.4 are not obtained yet.

Another example of a constant cost function comes from the utility for EVs of having a State of Charge (SoC) higher than necessary. When EV users face the choice of the charging quantity at the EVCS [Alizadeh et al., 2016], in classical models they tend to reach the minimal SoC requested because the objective is to minimize the charging cost. In reality, EV users charge more than that due to risk aversion[14] (among others) [Pan et al., 2019], and it is necessary to add a utility term in the model to compensate for the charging cost. A standard [Samadi et al., 2012, Deng et al., 2015] function for the utility associated with electricity consumption is:

$$u(s_f) = \begin{cases} w \times s_f - \frac{s_f^2}{2}\,, & \text{if } 0 \leq s_f < w\,, \\ \frac{w^2}{2}\,, & \text{if } s_f \geq w\,, \end{cases} \tag{2.4}$$

where, when considering EV charging, s_f is the final State of Charge (SoC) and $w > 0$ is a preference parameter (a higher w goes with a higher charging quantity) and can differ from one vehicle class to another. This utility function u is concave and increasing up to $s_f = w$ and is then constant equal to $\frac{w^2}{2}$, meaning that charging above w brings no additional benefit (but only additional charging costs). Then, such utility terms need to be subtracted in the total cost function $c_{s,r}$.

If in a game, players only face constant cost functions which do not depend on the choices made by others, then the game is equivalent to independent optimization problems for each player, as the choices of different players are independent.

2.2.3.2 Congestion cost function: travel duration

In the following definition, the concept of vehicle class is ignored in order to give a general definition (which can be extended to different classes s by replacing c_r by $c_{s,r}$, etc.).

Definition 2.8 (Non-atomic congestion cost functions [Rosenthal, 1973]). *The cost function c_r associated with strategy r is a congestion cost function if it is only a function of the number of players choosing r, i.e. the flow f_r of players choosing path r: $c_r(f_r)$.*

The class of games with congestion cost functions, called congestion games, possess strong theoretical properties [Rosenthal, 1973].

A classical example of a congestion cost function is traffic congestion. The cost function under consideration is the total travel duration d_r needed to drive from an origin to a destination, and which depends to the chosen driving path r. In order to study the total travel duration d_r, we need to consider the travel duration d_a on each arc a of the path r, since the total travel duration on path r is the sum of the travel duration on each arc of the path: $d_r = \sum_{a \in \mathcal{A}} \delta_{a,r} d_a$. In this thesis, we chose the following congestion function, called BPR (for Bureau of Public Roads) function [Spiess, 1990], to model the travel duration d_a on arc a:

$$d_a(x_a) = d_a^0 \left[1 + \alpha \left(x_a / C_a\right)^\beta\right], \tag{2.5}$$

[14] Risk aversion is the tendency of people to prefer outcomes with low uncertainty. In the commuting use case, risk aversion make EV users charge more than necessary in case of road diversions, consuming traffic congestion, etc.

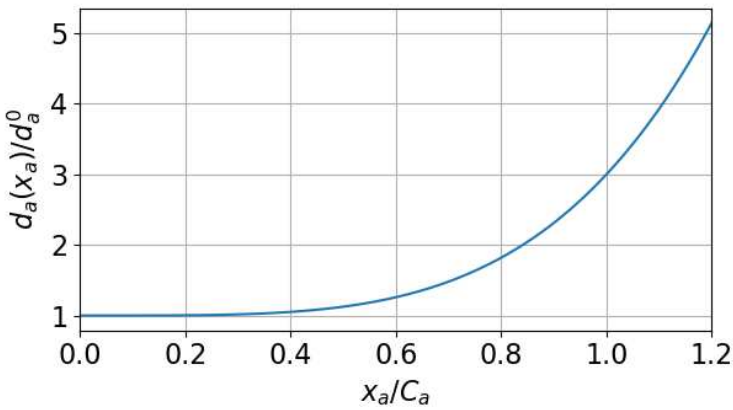

Figure 2.5: Travel duration d_a on arc a normalized by the free-flow reference time d_a^0, in function of the total vehicle flow x_a on arc a normalized by its capacity C_a. *If the vehicle flow reaches the arc capacity, the travel duration is three times the free-flow reference time.*

where x_a is the total flow of vehicle users which have chosen a driving path containing arc a, C_a is the capacity of the link in vehicles per unit of time and $d_a^0 = \frac{l_a}{v_a}$ is the *free flow* reference time, with l_a the length of the arc and v_a the maximum speed limit on the arc. The two remaining parameters $\alpha > 0$ and $\beta > 1$ are adjusted empirically. In this thesis, they are always chosen as $\alpha = 2$ and $\beta = 4$, in accordance with [Jeihani et al., 2006] for urban area congestion measures[15]. This means that if the vehicle flow reaches the arc capacity, the travel duration is three times the free-flow reference time (see Figure 2.5). As the driving congestion d_a is expressed in time units, it needs to be multiplied by a constant denoted τ, the value of time, to get a monetary cost.

Note that this congestion cost function is the same for all vehicle classes, and that it depends on the total vehicle flow $x_a = \sum_s x_{s,a}$ on the arc a, which is the sum of the flows of each vehicle class. The capacity of an arc a is not a mandatory upper bound of x_a [Wei et al., 2019], but congestion becomes prohibitive when $x_a > C_a$ (see Figure 2.5). Other travel duration cost functions can be considered, like the Davidson function [Davidson, 1966] or generalized cost functions [Nie et al., 2004], introducing a penalty whenever the road capacity (which is mandatory there) is reached.

In this thesis, the total cost function for a vehicle user of class s whose strategy is choosing path r, has the following general shape, using the last two Sections 2.2.3.1 and 2.2.3.2:

$$c_{s,r}(\boldsymbol{x}) = d_r(\boldsymbol{x}) + l_r m_s \lambda_s + t_{s,r} \,, \tag{2.6}$$

with $d_r(\boldsymbol{x}) = \sum_{a \in \mathcal{A}} \delta_{a,r} d_a(x_a)$ the total travel duration associated with path r, $l_r = \sum_{a \in \mathcal{A}} \delta_{a,r} l_a$ the total length of path r and $t_{s,r}$ a term gathering all constant cost functions other than the fuel consumption cost (e.g., traffic tolls or public transport ticket fare, as mentioned in Section 2.2.3.1). Regarding λ_s it is a constant function for $s = g$ (oil price), but a linearly non-separable increasing congestion cost function for $s = e$ (electricity price), as defined in next section.

To summarize Section 2.2, the common outline $\mathbb{G}$ of the games considered in this thesis can be characterized by the following properties: $\mathbb{G}$ is a multiclass non-atomic game, with linearly

[15] In this thesis, the notations α and β will then be used for other parameters.

non-separable congestion cost functions (defined in the following section).

2.3 The charging unit price: a particular congestion cost function

The particularity of game $\mathbb{G}$ of this thesis comes from the consideration of a specific class of *non-separable* congestion cost functions. Indeed the specific concept of congestion cost function is not totally adapted in order to model the Charging Unit Price (CUP) at the heart of this thesis, and detailed in Chapter 5. This particular CUP is based on the power load obtained after smart charging the EV charging profiles as in Chapter 4. Therefore, the charging cost for an EV user at an EVCS may depend on other users which did not make the same choices with different strategies (e.g., taking another path in order to get to the same EVCS). In the case a same operator manages several EVCSs and bases each CUP on the load profiles of all EVCSs, the charging cost even depends on EVs at other EVCSs. The general class of non-separable congestion cost functions is the topic of Section 2.3.1 and the particular subclass introduced in this work is defined in Section 2.3.2.

2.3.1 General non-separable congestion cost functions

In order to take into account the particular CUP defined in Chapter 5, a more general class of congestion cost functions must be introduced: the non-separable congestion cost functions [Dafermos, 1971].

Definition 2.9. *A cost function c_r corresponding to strategy r is said to be separable if it is only a function of the number (or flow) f_r of players having chosen this strategy: $c_r(f_r)$. Thus, cost function c_r is non-separable when there exists another strategy $r' \neq r$ such that: $c_r(f_{r'}, \dots)$.*

Studies of non-atomic games with non-separable cost functions are highly complicated and very few papers deal with this framework. In [Chau and Sim, 2003], the authors generalize the bound obtained by Roughgarden and Tardos [Roughgarden and Tardos, 2000] on the Price of Anarchy (PoA)[16] for non-separable, symmetric and affine costs functions. In [Perakis, 2004], the author considers a similar framework but with asymmetric and non-linear cost functions. The bounds obtained are tight and are based on a semi-definite optimization problem. In [Correa et al., 2008], the authors propose a new proof for the bound on the PoA in non-atomic congestion games, particularly with non-separable and non-linear cost functions. Their geometric approach leads to obtain in a simple manner the bounds found in [Chau and Sim, 2003] and [Perakis, 2004].

All these works focus on the PoA metric. In this thesis, we focus on the algorithmic part and techniques to obtain the equilibrium solution of game $\mathbb{G}$, based on potential functions and Beckmann's techniques (see Section 2.4.2). In fact, our framework induces particular cost functions which enables us to characterize a Wardrop Equilibrium as a minimum of a global function.

Remark 2.10. *Note that modeling traffic congestion by* separable *congestion functions (see Section 2.2.3) is a simplifying assumption taken in this thesis. Indeed, traffic congestion is better modeled by* non-separable *congestion functions, as the traffic on a given arc depends on the traffic on the reversed arc [Prager, 1954], on the intersections with other arcs [Dafermos, 1972, Dafermos, 1971], etc. However, these non-separable cost functions do not verify the property defined in next section and necessary to obtain the theoretical results of Section 2.4.*

[16] The PoA is the performance or cost function evaluation at the worst equilibrium situation, compared to the one at social optimum.

2.3.2 Linearly non-separable congestion cost functions

It should be noted that the non-separable congestion cost functions considered in game $\mathbb{G}$ verify the following symmetric property on the derivatives [Ortega and Rheinboldt, 2000], in order to simplify the theoretical treatment (i.e. use Beckmann's method presented in Section 2.4.2):

$$\forall s, s' \in \mathcal{S}, \forall r, r' \in \mathcal{R} \text{ with } (s,r) \neq (s',r'), \quad \frac{\partial c_{s,r}}{\partial f_{s',r'}} = \frac{\partial c_{s',r'}}{\partial f_{s,r}} . \tag{2.7}$$

In other words, a non-separable congestion cost function verifies the symmetric condition if and only if the impact any player class s choosing any strategy r has on any player class s' choosing any strategy r' is the same than the opposite impact. This symmetric assumption has been criticized in the literature [Sender et al., 1970] for being unrealistic. However, it is necessary for the Beckmann method used in Section 2.4.2 to obtain a WE (see Remark 2.20). With asymmetric cost functions, it is possible for example to extend the constant energy consumption Assumption 2.7 made in this thesis to a more realistic model taking into account the driving speed. Asymmetric cost functions require different techniques for characterizing the equilibrium, which are reviewed in [Florian and Hearn, 1995].

The vehicle user costs studied in this thesis – and in particular the smart Charging Unit Price considered – all belong to a specific class of symmetric non-separable congestion cost functions, which we called *Linearly non-Separable Congestion cost functions*.

Definition 2.11 (Linearly non-Separable Congestion (LnSC) cost functions)**.** *Let $c_{s,r}$ be a cost function associated with each player class s and strategy r. The corresponding cost functions vector $\boldsymbol{c} = (c_{s,r})_{s\in\mathcal{S},r\in\mathcal{R}}$ is a LnSC cost function (vector) if for all $s \in \mathcal{S}$ and $r \in \mathcal{R}$:*

$$c_{s,r}(\boldsymbol{f}) = \alpha_{s,r}\lambda\big(\langle \boldsymbol{\alpha}, \boldsymbol{f}\rangle\big) , \quad \textit{with:} \quad \begin{cases} \alpha_{s,r} \in \mathbb{R} , \ \textit{constant,} \\ \lambda : \mathbb{R} \to \mathbb{R} , \ \textit{a continuous function,} \end{cases} \tag{2.8}$$

where $f_{s,r}$ is the flow of players of class s choosing strategy r and $\langle \boldsymbol{\alpha}, \boldsymbol{f}\rangle = \sum_{s\in\mathcal{S},r\in\mathcal{R}} \alpha_{s,r} f_{s,r}$ is the scalar product between vectors $\boldsymbol{\alpha}$ and $\boldsymbol{f}$.

In other words, a LnSC cost function is the same for all player classes s and strategies r up to a multiplicative constant $\alpha_{s,r}$. This constant also corresponds to the impact the corresponding player flow $f_{s,r}$ has on the common part of the cost, function λ. This means that players pay proportionally to the impact they have on the LnSC cost function.

Example 2.12. *In the example of the Charging Unit Prices used in this thesis and defined as a LnSC cost function in Chapter 5, $\alpha_{e,r} = m_e l_r$ (up to an additive constant as in Chapter 7), which corresponds to the electricity consumed while traveling along the chosen path r and charged at an EV Charging Station. Note that $\alpha_{g,r} = 0$, as GV users neither pay this charging cost or have an impact on it.*

We chose the term "linearly" because λ is a function of the linear combination of player flows, while λ may be a non-linear function itself. This function λ is assumed continuous in order to be integrated when using Beckmann's method presented in Section 2.4.2.

Remark 2.13. *Separable congestion (continuous) cost functions are included in LnSC cost functions (providing that the Definition 2.9 is such that the class of non-separable congestion cost functions contains is a generalization of the separable class). For example, the travel duration d_a on arc a defined in (2.5) can be written $\alpha_{s,r}\lambda$ with $\lambda = d_a$ and $\alpha_{s,r} = 1$ for $r = a$ and 0 otherwise. Note that for each arc, the travel duration is defined by a different LnSC cost function.*

In the following, LnSC *increasing* cost functions refer to LnSC cost functions with non-negative parameters $\alpha_{s,r}$ and function λ increasing and with non-negative values. Note that even for increasing LnSC cost functions $c_{s,r}$, the corresponding cost functions vector $\boldsymbol{c}$ may be not strictly monotone, due to the linear combination term $\langle \boldsymbol{\alpha}, \boldsymbol{f} \rangle$ (e.g., in the case where there exist $s, s' \in \mathcal{S}$ and $r, r' \in \mathcal{R}$ such that $\alpha_{s,r} = \alpha_{s',r'}$). In the following, the name "LnSC game" refers to routing games with total cost functions possibly made of constant, separable, and Linearly non-Separable Congestion cost functions[17].

2.4 Equilibrium of linearly non-separable games using Beckmann's function

The class of LnSC games introduced in previous Section 2.2 has been theoretically treated in our paper [Sohet et al., 2021b]. This section presents the corresponding theoretical results in three parts, respectively the Wardrop Equilibrium solution concept for non-atomic games, the Beckmann method to find the WE, and the WE properties thereby obtained.

2.4.1 Wardrop equilibrium: solution concept of non-atomic games

The solution concept corresponding to non-atomic games is the Wardrop Equilibrium.

Definition 2.14 (Wardrop Equilibrium (WE) [Wardrop, 1952]). *A flow $\mathbf{f}^*$ is a Wardrop Equilibrium of game $\mathbb{G}$ if and only if for all player classes s:*

$$c_{s,r}(\mathbf{f}^*) \leq c_{s,r'}(\mathbf{f}^*), \tag{2.9}$$

for all paths r, r' with r such that $f^*_{s,r} > 0$.

Literally it means that at a WE, for any given player class, the costs on all the paths *actually used* ($\{r : f_{s,r} > 0\}$) are equal, and smaller than those on any *unused* path ($\{r' : f_{s,r'} = 0\}$). Therefore at a WE, no player has an interest to change its choice unilaterally – which is the definition of a Nash equilibrium [Nash et al., 1950] (see Section 3.1.2) – because the costs corresponding to the other actions are either of the same value or higher.

Notation. *A WE flow $\mathbf{f}^*$ (or equivalently $\mathbf{x}^*$ when considering flows on arcs rather than on paths) will be denoted with an asterisk thereafter.*

The WE is illustrated in Figure 2.6, based on the use case of an e-Park & Ride hub introduced earlier in Figure 2.4 and studied in Section 6.2. Figure 2.6 shows the total EV costs (made of the travel duration and the charging cost) in function of the proportion $x_{e,publ}$ of EV users choosing the public mode. When most users choose to drive downtown ($x_{e,publ}$ small), the total cost for EV users choosing the private mode (in blue) is higher than the one corresponding to the public mode (in red), due to traffic congestion downtown. The opposite is true when most players choose to park and charge at the hub, due to the congestion at the charging hub and an associated higher Charging Unit Price (see Section 6.2). The WE corresponds to the EV flow ($x^*_{e,publ} = 0.53$) such that the traffic congestion is compensated by the congestion at the charging hub and the total costs of the private and public mode are equal.

[17] LnSC games are not limited to a unique LnSC cost function as in the simplified Proposition 2.19 for example.

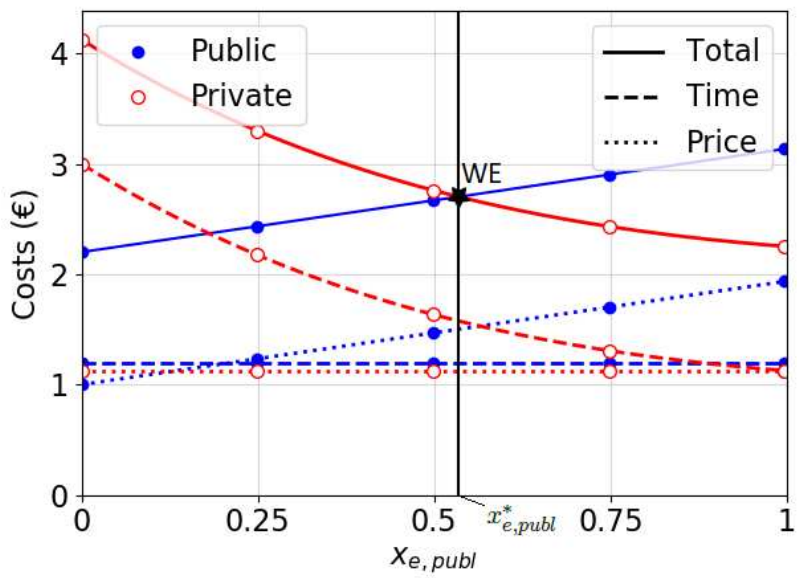

Figure 2.6: EV users costs in function of the variable $x_{e,publ}$ (proportion of EV users choosing public transport). In blue (respectively red) is the cost for EV users choosing public (respectively private) transport mode. The dotted lines refer to the monetary costs (consumption and ticket fare for public mode; only consumption for private mode) and the dashed lines refer to travel duration. *The WE (black star) happens when total costs are equal between the two transport modes, for* $x^*_{e,publ} = 0.53$.

Remark 2.15. *In practice, such an equilibrium is naturally reached by players in real life [Davis, 2009]: it corresponds to the stable stationary regime after a certain learning time*[18] *(see Chapter 3). In the current chapter, as vehicle users of game* $\mathbb{G}$ *are assumed hyper-rational with complete information (see Section 2.2.1.2), they directly choose strategies corresponding to the WE, without the need of a learning period of time. Operators of the coupled electrical-transportation system can therefore use the game model introduced in the present chapter instead of the learning model in Chapter 3 in order to visualize the reaction of vehicle users to various incentives.*

Remark 2.16. *Thanks to the use of fictitious arcs in a graph (see Section 2.2.2), the definition of WE can be applied even when players face multiple choices (driving path, charging station, etc.).*

The WE concept can thus be used to evaluate various incentive mechanisms numerically – in a planning stage or tool – in order to favor a particular equilibrium. This concept is now commonly used in many operational public transportation planning tools which estimate the travel demand[19] [Patriksson, 2015].

[18] In the commuting use case, vehicle users learn from one day to another.

[19] The transportation planning process usually follows a four-steps procedure: trip generation, distribution, modal split and traffic assignment. The WE concept may be used for this last step.

2.4.2 The equilibrium as a minimum of Beckmann's function

There exist different techniques and approaches in order to compute a WE of a game, like non-linear complementarity, variational inequality and fixed-point problems [Florian and Hearn, 1995]. Thanks to the properties of the LnSC cost functions considered in this thesis, the simple method of Beckmann [Beckmann et al., 1956] (first adapted to separable congestion cost functions) can be used for multiclass game $\mathbb{G}$. This method consists in finding a function, called Beckmann's function or potential function, whose minima verify the definition (2.9) of a WE of game $\mathbb{G}$, and in minimizing this function to obtain a WE. Intuitively, the derivatives of Beckmann's function correspond to the cost functions of game $\mathbb{G}$, so that the first order condition of the associated optimization problem corresponds to the definition (2.9) of a WE. More generally, finding a WE of a non-atomic game can be done by solving an optimization problem (referred to as Beckmann's problem) with a particular objective function.

This newly introduced characterization of a WE offers a simple way to show some WE properties, such as existence and uniqueness (in some cases). Such properties have been proved by [Patriksson, 2015] in the case of symmetric non-separable congestion cost functions defined in (2.7), using the Beckmann's method. However, there is no explicit Beckmann's function for general symmetric non-separable congestion cost functions. In this thesis, the definition of the particular class of Linearly non-Separable Congestion cost functions enables an explicit Beckmann's function. This is shown in next Proposition 2.19 in the case of a multiclass routing game with only one LnSC cost function[20].

Remark 2.17. *Note that Beckmann's method is linear (due to integration linearity) in the sense that if a game $\mathbb{G}_1$ associated with cost functions $\boldsymbol{c}_1$ possesses a Beckmann's function $\mathcal{B}_1$ and a similar game $\mathbb{G}_2$, whose only difference with $\mathbb{G}_1$ is the cost functions $\boldsymbol{c}_2$, also possesses a Beckmann's function $\mathcal{B}_2$, then game $\mathbb{G}$ with cost functions $\boldsymbol{c}_1 + a \times \boldsymbol{c}_2$ has a Beckmann's function equal to $\mathcal{B}_1 + a \times \mathcal{B}_2$. Therefore, the Beckmann's function of game $\mathbb{G}$ with multiple congestion cost functions (constant, separable and linearly non-separable) can be deduced from Proposition 2.19 and the original method given in [Beckmann et al., 1956] for separable congestion cost functions.*

Remark 2.18. *Note that the Beckmann function for LnSC cost functions was first introduced in our conference paper [Sohet et al., 2019a] for a driving-and-charging game with a transportation network made of only two parallel arcs, then extended to any transportation network in [Sohet et al., 2021b] and finally extended to any LnSC cost function in [Sohet et al., 2021c].*

Proposition 2.19 (Beckmann's method)**.** *The local minima of the following constrained optimization problem are Wardrop Equilibria of game $\mathbb{G}$ with travel demand constraints defined in (2.1) and a continuous Linearly non-Separable Congestion cost function vector $\boldsymbol{c} : \boldsymbol{f} \mapsto \boldsymbol{\alpha}\lambda(\langle \boldsymbol{\alpha}, \boldsymbol{f} \rangle)$:*

$$\min_{\boldsymbol{f}} \mathcal{B}(\boldsymbol{f}) \quad s.t. \quad (2.1) \tag{2.10}$$

with

$$\mathcal{B}(\boldsymbol{f}) \triangleq \int_0^{\langle \boldsymbol{\alpha}, \boldsymbol{f} \rangle} \lambda(t) \mathrm{d}t \,. \tag{2.11}$$

Proof. Let a path flow vector $\mathbf{f}$ be a solution of the minimization problem (2.10) of Beckmann's function $\mathcal{B}$ under travel demand constraints (2.1). Then there exist constants ν_s^{OD} and $\mu_{s,r}$ (for

[20] Note that for example a sum of any two LnSC cost functions is generally not a LnSC cost function.

all $s \in \mathcal{S}$, $O, D \in \mathcal{V}$ and $r \in \mathcal{R}^{OD}$) such that $\mathbf{f}$ is a solution of the corresponding Karush-Kuhn-Tucker (KKT) system of equations:

$$\begin{cases} \dfrac{\partial \mathcal{L}}{\partial f_{s,r}} = 0 \\ h_s^{OD} = 0 \\ \mu_{s,r} \times f_{s,r} = 0 \\ \mu_{s,r},\ f_{s,r} \geq 0 \end{cases} \quad \text{where} \quad \begin{cases} \mathcal{L} = \mathcal{B}(\mathbf{f}) - \sum\limits_{O,D \in \mathcal{V}, s \in \mathcal{S}} \nu_s^{OD} h_s^{OD} - \sum\limits_{s \in \mathcal{S}, r \in \mathcal{R}^{OD}} \mu_{s,r} f_{s,r}\,, \\ h_s^{OD} = \sum\limits_{r \in \mathcal{R}^{OD}} f_{s,r} - X_s^{OD}\,. \end{cases} \tag{2.12}$$

Using relation (2.3) ($x_{s,a} = \sum_{O,D \in \mathcal{V}} \sum_{r \in \mathcal{R}^{OD}} \delta_{a,r} f_{s,r}$) and differentiating $\mathcal{L}$ w.r.t. $f_{s,r}$ with $r \in \mathcal{R}^{OD}$ gives:

$$\frac{\partial \mathcal{L}}{\partial f_{s,r}} = c_{s,r} - \nu_s^{OD} - \mu_{s,r}\,, \tag{2.13}$$

so that using the KKT conditions: $\forall r \in \mathcal{R}^{OD}$, $c_{s,r} \geq \nu_s^{OD}$, with equality for r such that $f_{s,r} > 0$.

Hence, if for any $O, D \in \mathcal{V}$ there are two paths $r, r' \in \mathcal{R}^{OD}$ with different costs $c_{s,r} < c_{s,r'}$, then $f_{s,r'} = 0$. Otherwise, $f_{s,r'} > 0$ and $c_{s,r'} = \nu_s^{OD} \leq c_{s,r}$, which is contradictory. Thus, the KKT conditions correspond exactly to the Definition 2.14 of a WE. □

Remark 2.20. *As mentioned before and written in this proof, the derivatives of Beckmann's function $\mathcal{B}$ correspond to the cost functions of game $\mathbb{G}$. Therefore, due to the symmetry of second derivatives*[21] *(of $\mathcal{B}$, if they exist), a necessary condition on the costs for the existence of a Beckmann function is that the cost functions should verify the symmetry property defined in* (2.7).

2.4.3 Wardrop Equilibrium properties

Thanks to the existence of a Beckmann function associated with LnSC multiclass games, it is possible to find and specify some WE properties known for general non-separable congestion games [Patriksson, 2015], such as existence and pseudo-uniqueness of WE.

Corollary 2.21 (WE existence)**.** *There exists a Wardrop Equilibrium for Linearly non-Separable Congestion multiclass games.*

Proof. According to Proposition 2.19 and Remark 2.17, Linearly non-Separable Congestion multiclass games possess a Beckmann function $\mathcal{B}$, whose local minima are WE of the game. As $\mathcal{B}$ is continuous and the feasible set defined by constraints (2.1) is compact, function $\mathcal{B}$ has at least one local minimum and therefore the game has at least one WE. □

This proof of WE existence is general and applies to any game – including game $\mathbb{G}$ – with a Beckmann function.

Proposition 2.22 (Uniqueness of linear combination of WE)**.** *Any two different Wardrop Equilibria $\boldsymbol{f}^* \neq \boldsymbol{g}^*$ of a game with a* unique *Linearly non-Separable Congestion* increasing *cost function vector $\boldsymbol{c} : \boldsymbol{f} \mapsto \boldsymbol{\alpha}\lambda(\langle \boldsymbol{\alpha}, \boldsymbol{f} \rangle)$ verify:*

$$\langle \boldsymbol{\alpha}, \boldsymbol{f}^* \rangle = \langle \boldsymbol{\alpha}, \boldsymbol{g}^* \rangle\,. \tag{2.14}$$

[21] This property is also called Schwarz's theorem or Clairaut's theorem.

The proof of Proposition 2.22 requires the following definition.

Definition 2.23 (Variational Inequality). *Let $Y \subseteq \mathbb{R}^N$ be a non-empty, closed and convex set. A vector $\boldsymbol{x} \in Y$ is a solution of the Variational Inequality VI($\boldsymbol{c}$, Y) if, for any vector $\boldsymbol{y} \in Y$:*

$$\boldsymbol{c}(\boldsymbol{x})^T(\boldsymbol{y}-\boldsymbol{x}) \geq 0\,. \tag{2.15}$$

Proof of Proposition 2.22. Let $\boldsymbol{f}^* \neq \boldsymbol{g}^*$ be two WE of a game with unique LnSC increasing cost function. According to [Smith, 1979], WE $\boldsymbol{f}^*$ and $\boldsymbol{g}^*$ are solutions of $VI(\boldsymbol{c}, \mathcal{X})$. Equation (2.15) applied to $(\boldsymbol{f}^*, \boldsymbol{g}^*)$ and $(\boldsymbol{g}^*, \boldsymbol{f}^*)$ results in:

$$\big(\boldsymbol{c}(\boldsymbol{f}^*) - \boldsymbol{c}(\boldsymbol{g}^*)\big)^T(\boldsymbol{f}^* - \boldsymbol{g}^*) \quad \leq \quad 0\,, \tag{2.16}$$

or in other terms:

$$\big(\langle\boldsymbol{\alpha}, \boldsymbol{f}^*\rangle - \langle\boldsymbol{\alpha}, \boldsymbol{g}^*\rangle\big)\Big(\lambda\big(\langle\boldsymbol{\alpha}, \boldsymbol{f}^*\rangle\big) - \lambda\big(\langle\boldsymbol{\alpha}, \boldsymbol{g}^*\rangle\big)\Big) \quad \leq \quad 0\,. \tag{2.17}$$

As function λ is increasing by definition of Linearly non-Separable Congestion cost functions, we also have

$$\big(\boldsymbol{c}(\boldsymbol{f}^*) - \boldsymbol{c}(\boldsymbol{g}^*)\big)^T(\boldsymbol{f}^* - \boldsymbol{g}^*) = \big(\langle\boldsymbol{\alpha}, \boldsymbol{f}^*\rangle - \langle\boldsymbol{\alpha}, \boldsymbol{g}^*\rangle\big)\Big(\lambda\big(\langle\boldsymbol{\alpha}, \boldsymbol{f}^*\rangle\big) - \lambda\big(\langle\boldsymbol{\alpha}, \boldsymbol{g}^*\rangle\big)\Big) \quad \geq \quad 0 \tag{2.18}$$

and therefore:

$$\big(\boldsymbol{c}(\boldsymbol{f}^*) - \boldsymbol{c}(\boldsymbol{g}^*)\big)^T(\boldsymbol{f}^* - \boldsymbol{g}^*) \quad = \quad 0\,. \tag{2.19}$$

Using the increasing property of λ again, this is equivalent to:

$$\langle\boldsymbol{\alpha}, \boldsymbol{f}^*\rangle - \langle\boldsymbol{\alpha}, \boldsymbol{g}^*\rangle = 0\,. \tag{2.20}$$

□

Like for Proposition 2.19 (see Remark 2.17), Proposition 2.22 on games with a unique LnSC increasing cost function can be extended[22] to LnSC *increasing* games[23], including game $\mathbb{G}$: for each LnSC increasing cost function $\boldsymbol{c} : \boldsymbol{f} \mapsto \boldsymbol{\alpha}\lambda(\langle\boldsymbol{\alpha}, \boldsymbol{f}\rangle)$, (2.14) is verified for any two different WE $\boldsymbol{f}^* \neq \boldsymbol{g}^*$.

Remark 2.24. *Equation (2.18) is the definition of cost function vector $\boldsymbol{c}$ being monotone. Therefore, as $\boldsymbol{c}$ is the differential of $\mathcal{B}$ (see proof of Proposition 2.19), Beckmann's function is convex. Thus, the Beckmann optimization problem (2.10) is equivalent to its KKT conditions, which are equivalent to WE Definition 2.14 (see proof of Proposition 2.19). Finally, the WE correspond exactly to the local minima – which are global minima in a convex framework – of Beckmann's function $\mathcal{B}$. If $\mathcal{B}$ is not convex, some WE might not be one of its local minima.*

However, as mentioned in Section 2.3.2, cost function vector $\boldsymbol{c}$ may be not strictly monotone, due to the linear combination term $\langle\boldsymbol{\alpha}, \boldsymbol{f}\rangle$ (even if the common cost function λ is increasing). For example, in the commuting use case, if two paths have exactly the same characteristics

[22] For this extension, the left-hand term in (2.19) is developed in a sum over all cost functions constituting the total cost function $\boldsymbol{c}$. As each of these cost functions is assumed increasing, this sum is null if and only if each term (non-negative by definition of the increasing property of each cost) is null. Thus, (2.20) is obtained for each cost function.

[23] LnSC increasing games are LnSC games whose LnSC cost functions are said increasing (meaning that, in Definition 2.11, $\boldsymbol{\alpha} \geq 0$ and λ is increasing) and the separable congestion cost functions are increasing (constant cost functions are annihilated in (2.17)).

(driving range, speed limit, Charging Unit Price, etc.), the vehicle flows on those two paths are interchangeable and therefore there are an infinity of WE. In that case, $\mathcal{B}$ is not strictly convex, which means $\mathcal{B}$ can have several minima and in that case the WE is not unique. At WE, only the scalar product between the parameter vector $\boldsymbol{\alpha}$ and the flow vector at equilibrium is unique, according to Proposition 2.22.

In such cases, if necessary, a specific Wardrop Equilibrium $\boldsymbol{f}$ is selected, the "pro-rata" one, which verifies (for any WE $\boldsymbol{f}^*$):

$$\forall s \in \mathcal{S}, r \in \mathcal{R}, \quad f_{s,r} = \frac{\sum_s f^*_{s,r}}{\sum_{s,r} f^*_{s,r}} \sum_r f^*_{s,r} \,. \tag{2.21}$$

In other words, the proportions of a player class are the same for all paths $r \in \mathcal{R}$. Note that equilibrium selection is a theory in itself [Harsanyi et al., 1988] but is not studied in this thesis.

Remark 2.25. *Note that for games with a* unique *LnSC increasing cost function vector $\boldsymbol{c} : \boldsymbol{f} \mapsto \boldsymbol{\alpha}\lambda(\langle \boldsymbol{\alpha}, \boldsymbol{f} \rangle)$, the set of WE can be characterized. Let us define the set*[24] *$\mathcal{R}^+ = \{r \in \mathcal{R} \mid \alpha_r > \min_{s \in \mathcal{R}} (\alpha_s)\}$ of paths except the ones associated with the lowest α_r. Then, the Wardrop equilibria of such games are the vehicle flows verifying $\boldsymbol{f}_r = 0$ for all $r \in \mathcal{R}^+$. The proof is the same as for the atomic version of such games (see Proposition 3.10).*

This means that there is a unique minimal value α_r, then the WE is unique (stronger result than in Proposition 2.22) and corresponds to all vehicle flows on path r. If there are at least two minimal values α_r and α_s, then there are an infinity of WE, with the vehicle flows either on path r or s.

In practice, the uniqueness of the WE of game $\mathbb{G}$ allows the different operators of the coupled electrical-transportation system to predict accurately drivers' behavior and in turn, to design efficient incentives according to their own objectives. As mentioned in Remark 2.24, the WE of a Linearly non-Separable Congestion game might not be unique, due to the linear combination term $\langle \boldsymbol{\alpha}, \boldsymbol{f} \rangle$. However, the linear combination term $\langle \boldsymbol{\alpha}, \boldsymbol{f} \rangle$ is unique at WE, which can be sufficient for operators. For example, our paper [Sohet et al., 2021c] considers two LnSC increasing cost functions: travel duration and energy consumption. Proposition 2.22 extended to LnSC increasing games then ensures the uniqueness of respectively the total vehicle flow[25] x_a on each arc a, and the total charging need at each EV Charging Station[26] (see Chapter 7). Then, the various operators of the coupled system can design incentives or size infrastructures using these (unique) metrics.

2.5 Conclusion

The vehicle users behavior while driving and charging is modeled by a game with:

- non-atomic and rational players;
- driving-and-charging choices modeled as fictitious graph arcs (routing game);

[24] The underlying assumption is non-negative parameters α_r and function λ, but the definition of the set $\mathcal{R}^+$ can be adapted to the other cases.

[25] The uniqueness of x_a is equivalent to the uniqueness of $\langle \boldsymbol{\alpha}, \boldsymbol{f}^* \rangle$ at WE $\boldsymbol{f}^*$, with $\alpha_{s,r}$ corresponding to travel duration defined in Remark 2.13.

[26] In the case of the charging cost, the corresponding linear combination term $\langle \boldsymbol{\alpha}, \boldsymbol{f}^* \rangle$ is equivalent to the charging need (see 2.12).

- Linearly non-Separable Congestion increasing cost functions in order to take into account the particular EV Charging Unit Price (see Chapter 5).

A Beckmann function associated with this LnSC routing game is provided, whose minima are Wardrop Equilibria of the game. Using this Beckmann function with *increasing* LnSC cost functions, it is shown for example that the aggregated charging need at each EV Charging Station and the total vehicle flow on each driving arc are unique at WE. In conclusion, operators of electric mobility using this vehicle user behavior model can effectively design their incentives by only finding any minimum of a convex function with linear constraints.

Chapter 3

Learning Nash equilibrium in linearly non-separable congestion games

This chapter is the second about vehicle users' behavior. Compared to the previous chapter which focuses on the stationary behavior obtained with the common knowledge and the hyper-rationality assumptions, this chapter deals with the dynamic process of converging to this stationary behavior. Therefore, the common knowledge assumption is relaxed and drivers have no choice but to observe their current costs and update their strategies accordingly, in a reinforcement learning fashion. This chapter shows that for linearly non-separable increasing congestion games, the standard Reinforcement Learning Algorithm [Sastry et al., 1994] converges towards the unique Nash (similar to Wardrop) equilibrium of the game. A stochastic version of the reinforcement learning algorithm is also illustrated for such games.

This chapter is in part inspired from the following paper:

[Sohet et al., 2020b] **Sohet, B.**, Hayel, Y., Beaude, O., and Jeandin, A. (2020). Learning pure nash equilibrium in smart charging games. *In 2020 59th IEEE Conference on Decision and Control (CDC)*, pages 3549-3554.

Contents

3.1 Introduction **36**
3.1.1 Motivation 36
3.1.2 Atomic game notations 37
3.2 Standard reinforcement learning algorithm **39**
3.2.1 Principle of the reinforcement learning process 39
3.2.2 Theoretical results: existence of potentials and learning convergence 41
3.2.2.1 Potential function of pure strategies 41
3.2.2.2 Action-dependent continuous potential 43
3.2.2.3 Convergence of the reinforcement learning algorithm towards the Nash equilibrium 45
3.2.3 Application to a non-separable smart charging game 46
3.2.3.1 Choice of charging station in function of charging cost . . 46
3.2.3.2 Numerical illustration of convergence 48

3.3 Stochastic reinforcement learning algorithm **49**
3.3.1 Principle of the stochastic reinforcement learning process 49
3.3.2 Theoretical results from literature 51
3.3.2.1 Adaptive dynamics and perturbed Nash equilibrium . . . 51
3.3.2.2 Sufficient conditions for the convergence of the stochastic learning algorithm 52
3.3.3 Application to a non-separable smart charging game 53
3.3.3.1 Illustration of the stochastic reinforcement learning algorithm 53
3.3.3.2 Learning the perturbed Nash equilibrium 55
3.4 Conclusion **56**

Table 3.1: Notations of Chapter 3

Symbols	Signification
$\mathcal{N}$	Set of N players i
$\mathcal{R}$	Set of M resources a
$\boldsymbol{r} = (r_i, \boldsymbol{r_{-i}})$	Resources chosen by player i and all the other players $(-i)$
$n_a(\boldsymbol{r})$	Number of players choosing resource a for a strategy vector $\boldsymbol{r}$
$c_a(\boldsymbol{r})$	Cost observed by a player choosing resource a
α_a	Weight parameter associated with resource a
λ	Common increasing cost function
$\pi_{i,a}$	Probability with which player i chooses resource a
$\boldsymbol{\pi}_i$	Mixed strategy vector of player i
$\boldsymbol{e}_a$	Pure strategy vector corresponding to resource a
$\bar{c}_{i,a}$	Expected cost for player i choosing resource a
δ	Standard reinforcement learning parameter
P	Ordinal potential function
F	Action-dependent continuous potential function
$\boldsymbol{r}^*, \boldsymbol{\pi}^*$	Actions and strategies at Nash equilibrium
$z_{i,r}$	Player i's perception of cost associated with resource r
δ_k	Averaging factor of the stochastic RLA at iteration k
β	Rationality parameter

3.1 Introduction

3.1.1 Motivation

The previous Chapter 2 was dedicated to give the stable stationary behavior of vehicle users in a coupled transportation-electrical system and the methodology to find this behavior. The present chapter focuses on how each player will adapt her strategy through time and therefore learn to play her stationary strategy. Learning algorithms in game theoretical settings have been known

for several years [Fudenberg et al., 1998]. Many techniques are based on the well known *best response* principle like fictitious play [Brown, 1951], which assumes that players choose a best reply to the observed empirical distribution of past actions of the other players. The main drawback of such techniques is the computation of the best action, which can be computationally complex and also needs specific information (utility functions, set of actions, etc.). Other types of algorithms, based on reinforcement mechanisms [Sutton and Barto, 2018], have also been employed in game theoretical problems [Erev and Roth, 1998]. These types of decentralized learning techniques, based on trials as in repeated games, proved to be efficient in particular games such as congestion games and more generally potential games, which have convergence properties, as illustrated recently in machine learning community with different feedback information [Cohen et al., 2017]. This chapter deals with Reinforcement Learning Algorithms (RLA) [Sutton and Barto, 2018], which work on atomic games, i.e. games with a finite number of players instead of non-atomic games with their continuous mass of players. The differences in notations and concepts (congestion cost functions, linearly non-separable costs, equilibrium) are detailed in the following section.

3.1.2 Atomic game notations

In an atomic game, the number N of players is finite. Each player $i \in \mathcal{N} = \{1, \dots, N\}$ chooses her strategy r_i among the same set $\mathcal{R}$ of resources. For example, $\mathcal{R}$ can be the set of paths introduced in Section 2.2.2. The atomic game $\mathbb{G}$ considered in this chapter is also finite: the set $\mathcal{R}$ is made of $M < \infty$ resources. Here, the set $\mathcal{R}$ of resources is also called the set of pure (compared to mixed, see below) strategies. In a classical atomic congestion game [Rosenthal, 1973], a player chooses a resource $a \in \mathcal{R}$ depending on the number of players having chosen the same resource, $n_a(\boldsymbol{r})$, defined as:

$$n_a(\boldsymbol{r}) = \#\{i \in \mathcal{N} \mid r_i = a\} \ , \tag{3.1}$$

with $\boldsymbol{r} = (r_1, \dots, r_N) = (r_i, \boldsymbol{r}_{-i}) \in \mathcal{R}^N$ the vector of strategies and $\boldsymbol{r}_{-i} \in \mathcal{R}^{N-1}$ the vector of strategies of the players other than i. In other words, the cost function associated with resource a is written $c_a(n_a(\boldsymbol{r}))$ and called a congestion cost function. Note that a congestion cost in atomic games is a function of the number of players n_a choosing the resource a while in non-atomic games, it is a function of the proportion x_a of the non-atomic mass choosing a (see Section 2.2.3.2). A non-separable congestion cost function c_a of a resource a does not only depend on n_a, but also on the number of players n_b choosing other resources $b \in \mathcal{R} \setminus \{a\}$ [Chau and Sim, 2003]. Linearly non-Separable Increasing Congestion cost functions are defined as in Definition 2.11.

Definition 3.1 (Linearly non-Separable *Increasing* Congestion (LnSIC) cost functions)**.** *Linearly non-Separable Increasing Congestion cost functions are defined, for all resources $a \in \mathcal{R}$ and vectors of strategies $\boldsymbol{r} \in \mathcal{R}^N$, as:*

$$c_a(\boldsymbol{r}) = \alpha_a \lambda\big(L(\boldsymbol{r})\big) \ , \tag{3.2}$$

$$\textit{with:} \quad \begin{cases} \alpha_a \geq 0 \ , \ \textit{constant,} \\ \lambda : \mathbb{R}_+ \to \mathbb{R}_+ \ , \ \textit{an increasing function,} \\ L(\boldsymbol{r}) = \sum_{i=1}^N \alpha_{r_i} = \sum_{b \in \mathcal{R}} \alpha_b n_b(\boldsymbol{r}). \end{cases} \tag{3.3}$$

The term $L(\boldsymbol{r})$ corresponds to the scalar product $\langle \boldsymbol{\alpha}, \boldsymbol{f} \rangle$ in Definition 2.11. Note that in the present chapter, LnSIC cost functions are always considered as increasing, i.e. with $\boldsymbol{\alpha} \geq 0$ and λ increasing. The atomic congestion game studied in this chapter is then entirely defined by $\mathbb{G} = \{\mathcal{N}, \mathcal{R}, (c_a)_{a \in \mathcal{R}}\}$.

Remark 3.2. *Game $\mathbb{G}$ is symmetric (between the players), meaning that the cost function of a player i only depends on her choice, and not on the player herself. However, the following study in this chapter can be extended to the non-symmetric case where player i gets the cost $c_{i,r_i} = \alpha_{i,r_i} \lambda \left(\sum_{j=1}^{N} \alpha_{j,r_j} \right)$, which is the same as (3.2) when $\alpha_{i,a} = \alpha_a$ for all i, a. A symmetric game is not to be mistaken with the symmetry property 2.7 of cost functions' derivatives.*

The solution concept of atomic games is called a Nash Equilibrium (while for non-atomic games, it is called Wardrop Equilibrium, see Section 2.4.1).

Definition 3.3 (Nash Equilibrium (NE)). *A pure strategy Nash Equilibrium of atomic game $\mathbb{G} = \{\mathcal{N}, \mathcal{R}, (c_a)_{a \in \mathcal{R}}\}$ is a vector of strategies $\boldsymbol{r}^* \in \mathcal{R}^N$ which verifies:*

$$\forall i \in \mathcal{N}, \forall a \in \mathcal{R}, \quad c_{r_i^*}\left(r_i^*, \boldsymbol{r}_{-i}^*\right) \leq c_a\left(a, \boldsymbol{r}_{-i}^*\right) . \tag{3.4}$$

In other words, a NE is a strategy vector such that no player can reduce her cost by changing her strategy unilaterally.

Remark 3.4. *The convergence of NE towards a Wardrop Equilibrium as the number of players tends to infinity is proved for aggregative[1] games [Paccagnan et al., 2018] and in particular cases of congestion games [Haurie and Marcotte, 1985], where the global cost function vector is strictly monotone at least. For a general driving-and-charging cost (taking into account both traffic congestion and the Charging Unit Price), the global cost function vector is at best monotone (see Remark 2.24) and therefore there might exist several equilibria. However, in the particular case of the present chapter where game $\mathbb{G}$ is only composed of a unique LnSIC cost function, the NE is unique (see Proposition 3.10), and therefore it converges towards the unique WE (see Remark 2.25) of the non-atomic version of game $\mathbb{G}$, which links the present chapter to the previous Chapter 2.*

Mixed strategies are probability distributions over pure strategies. Let $\pi_{i,a}$ denote the probability with which player i chooses pure strategy $a \in \mathcal{R}$, $\boldsymbol{\pi}_i \in \Delta_i$ the mixed strategy vector of player i in simplex Δ_i of $\mathbb{R}^M$, $\boldsymbol{\pi_{-i}}$ the mixed strategies of players other than i and $\boldsymbol{\pi} = (\boldsymbol{\pi}_i, \boldsymbol{\pi_{-i}}) \in \Delta = \prod_i \Delta_i$ the mixed strategies of all players. The mixed strategy notation of player i playing pure strategy a is $\boldsymbol{\pi}_i = \boldsymbol{e}_a$, with $\boldsymbol{e}_a$ the null vector except for the a-th component, equal to 1. The expected cost $\overline{c}_{i,a}$ for player i playing pure strategy a is:

$$\overline{c}_{i,a}(\boldsymbol{\pi_{-i}}) = \mathbb{E}_{\boldsymbol{\pi}}\left[c_a | \pi_i = \boldsymbol{e}_a\right] = \sum_{\boldsymbol{r}_{-i}} \left(c_a(a, \boldsymbol{r}_{-i}) \prod_{j \neq i} \pi_{j,r_j} \right), \tag{3.5}$$

with c_a the LnSIC cost function (3.2). Note that unlike c_a, the expected cost depends on the player due to the mixed strategies terms.

At Nash Equilibrium, the strategies of some players can be mixed, and the NE is then called a mixed NE, defined as follows. When mixed strategies are actually pure, the following definition is tantamount to Definition 3.3 of a pure NE.

[1] In aggregative games, the cost function of a player depends on its strategy and averaged strategy of all players.

Definition 3.5 (Mixed Nash Equilibrium). *A mixed strategy Nash Equilibrium of atomic game* $\mathbb{G} = \{\mathcal{N}, \mathcal{R}, (c_a)_{a\in\mathcal{R}}\}$ *is a vector of mixed strategies* $\boldsymbol{\pi}^* \in \Delta$ *which verifies:*

$$\forall i \in \mathcal{N}, \forall \boldsymbol{\pi}_i \in \Delta_i, \quad c\left(\boldsymbol{\pi}_i^*, \boldsymbol{\pi}_{-i}^*\right) \leq c\left(\boldsymbol{\pi}_i, \boldsymbol{\pi}_{-i}^*\right), \tag{3.6}$$

with:

$$c(\boldsymbol{\pi}) = \sum_{a\in\mathcal{R}} \pi_{i,a}\bar{c}_{i,a}(\boldsymbol{\pi}_{-\boldsymbol{i}}). \tag{3.7}$$

The two remaining sections introduce two different RLAs using this atomic game framework. Section 3.2 focuses on the basic principle of RLA and gives theoretical results of convergence of the learning algorithms, illustrated on a smart charging game. Section 3.3 adds a refined component to this basic RLA – the players perception and rationality parameter – and illustrates it on the same smart charging game.

3.2 Standard reinforcement learning algorithm

This section is mostly inspired by our conference paper [Sohet et al., 2020b]. Learning techniques in atomic congestion games are not very studied: they mainly consider non-atomic games. In [Barth et al., 2009], the authors adapt the Reinforcement Learning Algorithm (RLA) described in [Sastry et al., 1994] to atomic congestion games. In their adaptation of the RLA, cost functions are separable. In this section, this assumption is relaxed and non-separable cost functions are considered, such as the Charging Unit Price defined in Chapter 5. More precisely, in this section, only games with a unique[20] LnSIC cost function (3.2) are considered. In other words, the theoretical results of this section can be applied for example to games considering only the traffic congestion, or only the Charging Unit Price (which is the example taken in Section 3.2.3), but not to games with both costs. Even though it could not be proved, the RLA introduced in Section 3.2.1 appears to converge numerically for such games with several cost functions, as well as the stochastic RLA introduced in next Section 3.3.

The EV smart charging (see Section 1.2.2) is a particularly interesting environment to implement learning algorithms to deal with different degrees of uncertainty and randomness of future knowledge. Most papers related to smart charging consider machine learning techniques from a centralized point of view [Tang et al., 2016]. Deep learning techniques are suggested in [Qian et al., 2019] to minimize the total travel time and the charging cost at Charging Stations, with also a centralized point of view. In [Wang et al., 2016a], the NE of the constrained energy trading game among players with incomplete information is found using a RLA. This game however does not consider a smart charging context, i.e. EV charging profiles are fixed. In this section, we adapt RLA techniques to an atomic smart charging game where an operator use a smart Charging Unit Price to incentivize EV users to charge at the right EVCS, and show convergence to a pure NE.

The standard RLA is introduced in Section 3.2.1 and its convergence towards the NE is proved in Section 3.2.2. The non-separable smart charging game is illustrated in Section 3.2.3.

3.2.1 Principle of the reinforcement learning process

This first section introduces the basic principles of reinforcement learning. In this chapter, players possess incomplete information: their only knowledge is the observation of their cost after taking an action. Best response algorithms can also be applied to game $\mathbb{G}$, but players require additional information (the exact formulation of their own cost function). Here, game $\mathbb{G}$ will be repeated

so that players learn what their best strategy is. More precisely, every iteration k is split into two phases. In the first phase, each player i chooses an action $r_i^{(k)}$ in accordance with her mixed strategy vector $\boldsymbol{\pi}_i^{(k)}$. Thus, a vector of actions $\boldsymbol{r}^{(k)}$ is induced by the decisions of all players, which in turn implies a cost for each player based on the LnSIC cost function (3.2). Then, in the second phase of the iteration, each player updates her strategy probability vector based on her cost[2]. This update mechanism is a reinforcement mechanism [Sutton and Barto, 2018]. This type of RLA is a linear reward-inaction scheme and is also used in stochastic games [Sastry et al., 1994]. Each player i updates her mixed strategy vector $\boldsymbol{\pi}_i$ as follows (for any iteration k):

$$\boldsymbol{\pi}_i^{(k+1)} = \boldsymbol{\pi}_i^{(k)} + \delta \times \left(1 - \frac{c_{i,a}(\boldsymbol{r}^{(k)})}{c_{\max}^{+}}\right) \times \left(\boldsymbol{e}_a - \boldsymbol{\pi}_i^{(k)}\right) , \tag{3.8}$$

with:

- $0 < \delta < 1$ the learning parameter, fixed;
- $a = r_i^{(k)}$ the action taken by player i at iteration[3] k;
- $c_{\max}^{+} = (1+\varepsilon)\max_{i,a,\boldsymbol{r}} c_{i,a}(\boldsymbol{r})$, with $\varepsilon > 0$ an arbitrarily small parameter.

The cost terms "$c_{i,a}(\boldsymbol{r})$" corresponds to the *observed* cost and not the cost function or the expected cost function in the case of mixed strategies, which are not known by players. In this term, the player index i is displayed for a better understanding, although game $\mathbb{G}$ is assumed symmetric (see 3.2) and cost functions are the same for all players.

Remark 3.6. *In this section, the normalized payoff of paper [Sastry et al., 1994] is replaced by* $1 - \frac{c_{i,a}(\boldsymbol{r}^{(k)})}{c_{\max}^{+}}$*, following the idea of [Barth et al., 2009], in order to consider general costs instead of normalized payoffs. However, the difference with [Barth et al., 2009] is that the* ε *introduced in the expression of* $c_{\max}^{+}$ *guarantees that if the learning process* (3.8) *converges towards a limit* $\boldsymbol{\pi}^{\infty}$*, which therefore verifies* (3.8) *(by replacing the* $\boldsymbol{\pi}_i$ *terms by* $\boldsymbol{\pi}^{\infty}$*), then* $\boldsymbol{\pi}^{\infty}$ *is necessarily a pure strategy, as* $1 - \frac{c_{i,a}(\boldsymbol{r}^{(k)})}{c_{\max}^{+}}$ *cannot be equal to zero.*

The basic idea of the updating rule expressed by equation (3.8) is to ensure that actions prompting small or high costs are respectively promoted or not. This update scheme is decentralized: each player makes her decision autonomously. The RLA based on this updating rule is given in Algorithm 3.1. It is assumed that updates are synchronous, meaning that players update their strategy simultaneously at each iteration of the RLA 3.1. At each iteration, Algorithm 3.1 is fully distributed and can be executed in parallel. This is an important property in order to deploy it in large scale complex systems, typically atomic congestion games with a large number of players. The algorithm works as follows:

[2] This second phase is different in the RLA studied in Section 3.3.
[3] Notation a is used for a better readability.

Algorithm 3.1: RLA with synchronous updates

Input: $\boldsymbol{\pi}^{(0)}$, $k = 0$
while *not all players have a pure strategy* **do**
  Take actions $\boldsymbol{r}^{(k)}$ according to mixed strategies $\boldsymbol{\pi}^{(k)}$;
  for *all players* i **do**
    Observe cost $c_{i,a}\left(\boldsymbol{r}^{(k)}\right)$ given by (3.2) (with $a = r_i^{(k)}$);
    Update mixed strategy of i with (3.8);
  end
  $k \leftarrow k + 1$;
end

Remark 3.7. *If at some iteration of the learning process (3.8), a player obtains a pure strategy, then her strategy will never change again in the following iterations. Therefore, it is important that the initial strategy in Algorithm 3.1 is mixed for all players. Moreover, as Proposition 3.14 below states that the learning process (3.8) converges towards a pure strategy for the game under consideration, then the convergence criterion of Algorithm 3.1 can be defined as the iteration when all players have a pure strategy.*

The convergence of Algorithm 3.1 depends on the existence of a potential (i.e. a function from which all cost functions can be retrieved) of game $\mathbb{G}$, which are extended from common payoff games[4] to LnSIC games in the following section.

3.2.2 Theoretical results: existence of potentials and learning convergence

In this particular context of atomic congestion games with a unique LnSIC cost function, we are able to find potentials for game $\mathbb{G}$, which is a powerful tool for the study of NE in pure strategy and convergence of learning procedures [Bournez and Cohen, 2013].

3.2.2.1 Potential function of pure strategies

Following Definition 3.1 of LnSIC cost functions $(c_a)_{a\in\mathcal{R}}$, it is possible to extend the ordinal potential property of separable congestion games [Milchtaich, 1996] to the non-separable game $\mathbb{G} = (\mathcal{N}, \mathcal{R}, (c_a))$.

Definition 3.8 (Ordinal potential)**.** *An ordinal potential for game $\mathbb{G}$ is a function $P : \mathcal{R}^N \to \mathbb{R}$ verifying $\forall i \in \mathcal{N}, \forall \boldsymbol{r}_{-i} \in \mathcal{R}^{N-1}, \forall a, b \in \mathcal{R}$,*

$$c_a\left(a, \boldsymbol{r}_{-i}\right) < c_b\left(b, \boldsymbol{r}_{-i}\right) \Leftrightarrow P\left(a, \boldsymbol{r}_{-i}\right) < P\left(b, \boldsymbol{r}_{-i}\right) . \tag{3.9}$$

This definition follows the idea that an ordinal potential function bears the sign of the difference of cost for any player that changes her action unilaterally. Even if our game $\mathbb{G}$ is not a standard congestion game due to the non-separability of costs functions, it is possible to show the existence of an ordinal potential function.

[4] In common payoff games, also called team games, all players share the same cost function, no matter their action.

Proposition 3.9. *The atomic congestion game $\mathbb{G}$ with a unique LnSIC cost function (3.2) has the following ordinal potential function:*

$$\forall \boldsymbol{r} \in \mathcal{R}^N\,, \quad P(\boldsymbol{r}) = \lambda\left(L\left(\boldsymbol{r}\right)\right)\,. \tag{3.10}$$

Proof. Let $i \in \mathcal{N}$ be any player and $a, b \in \mathcal{R}, \boldsymbol{r}_{-i} \in \mathcal{R}^{N-1}$ any actions.

Firstly, note that $L\left(a, \boldsymbol{r}_{-i}\right) = L\left(b, \boldsymbol{r}_{-i}\right) + \alpha_a - \alpha_b$, by definition. Then, as function λ is increasing:

$$\begin{aligned} \lambda\big(L\left(a, \boldsymbol{r}_{-i}\right)\big) < \lambda\big(L\left(b, \boldsymbol{r}_{-i}\right)\big) &\iff \alpha_a - \alpha_b < 0\,, \\ \text{i.e.} \quad P\left(a, \boldsymbol{r}_{-i}\right) < P\left(b, \boldsymbol{r}_{-i}\right) &\iff \alpha_a < \alpha_b\,, \end{aligned} \tag{3.11}$$

by definition of $P = \lambda \circ L$.

Secondly, function $C_{\boldsymbol{r}_{-i}} : \alpha \mapsto \alpha \times \lambda\big(\alpha + \sum_{j \neq i} \alpha_{r_j}\big)$ is increasing on $\mathbb{R}_+$ as a product of positive increasing functions, meaning that:

$$\begin{aligned} \alpha_a \lambda\Big(\alpha_a + \sum_{j \neq i} \alpha_{r_j}\Big) < \alpha_b \lambda\Big(\alpha_b + \sum_{j \neq i} \alpha_{r_j}\Big) &\iff \alpha_a < \alpha_b\,, \\ \text{i.e.} \quad c_a\left(a, \boldsymbol{r}_{-i}\right) < c_b\left(b, \boldsymbol{r}_{-i}\right) &\iff \alpha_a < \alpha_b\,. \end{aligned} \tag{3.12}$$

□

The existence of a potential implies the existence of a pure NE in such non-cooperative games. The existence of pure NE is not a standard result, but it is true for games with an ordinal potential function. Indeed, as the sets of actions are compact, the minimum of the potential exists and corresponds to a pure NE of the game [Monderer and Shapley, 1996]. In this particular atomic game with a unique LnSIC cost function, pure NE can be fully characterized. Let us define the set $\mathcal{R}^+ = \{a \in \mathcal{R} \mid \alpha_a > \min_{s \in \mathcal{R}}\left(\alpha_s\right)\}$ of resources except the ones associated with the lowest α_a.

Proposition 3.10. *The pure Nash Equilibria of $\mathbb{G}$ are the pure strategies $\boldsymbol{r}^* \in \mathcal{R}^N$ such that:*

$$\forall a \in \mathcal{R}^+\,, \quad n_a\left(\boldsymbol{r}^*\right) = 0\,. \tag{3.13}$$

Proof. First, let $\boldsymbol{r}^* \in \mathcal{R}^N$ verify (3.13). Then, for any player $i \in \mathcal{N}$ and any resource $a \in \mathcal{R}$, $\alpha_{r_i^*} = \min_{s \in \mathcal{R}}\left(\alpha_s\right)$, by definition of $\boldsymbol{r}^*$. Thus, $\alpha_{r_i^*} \leq \alpha_a$ and $C_{\boldsymbol{r}^*_{-i}}\left(\alpha_{r_i^*}\right) \leq C_{\boldsymbol{r}^*_{-i}}\left(\alpha_a\right)$, with increasing function $C_{\boldsymbol{r}^*_{-i}} : \alpha \mapsto \alpha \times \lambda\left(\alpha + \sum_{j \neq i} \alpha_{r_j^*}\right)$ defined in proof of Proposition 3.9. This is equivalent to $c_{r_i^*}\left(r_i^*, \boldsymbol{r}^*_{-i}\right) \leq c_a\left(a, \boldsymbol{r}^*_{-i}\right)$.

Secondly, let $\boldsymbol{r}^* \in \mathcal{R}^N$ be such that there exists $a \in \mathcal{R}^+$ with $n_a(\boldsymbol{r}^*) \geq 1$. Let i be one of the players having chosen resource a. Let $b \in \mathcal{R}$ be such that $\alpha_b = \min_{s \in \mathcal{R}}(\alpha_s)$. Then, $\alpha_a > \alpha_b$ by definition of $\mathcal{R}^+$, and $c_{r_i^*}\left(r_i^*, \boldsymbol{r}^*_{-i}\right) > c_b\left(b, \boldsymbol{r}^*_{-i}\right)$ using again function $C_{\boldsymbol{r}^*_{-i}}$, which contradicts the NE Definition 3.3.

□

This proposition shows that in atomic LnSIC games, pure NE correspond to situations where all players choose the resources a with the lowest coefficient α_a. There might be several NE in such games, in the case where several resources a are associated with the lowest α_a (and therefore at NE, players choose indistinctly between these resources).

This parameter may not be known by players in advance, hence the need of learning algorithms for players in order to optimally adapt their actions. Such RLA are fully decentralized and are based on updates, for each player, of mixed strategies. It is shown in [Sastry et al., 1994] that there is a link between the potential function in pure strategies and the one in mixed strategies for common payoff games. This result is extended in this thesis to more general games and is fundamental in order to prove the convergence of RLA to pure NE.

3.2.2.2 Action-dependent continuous potential

Considering mixed strategies, the strategy sets are topological spaces and the expected cost functions given in (3.5) are continuously differentiable. In such continuous games, there may exist continuous potential functions, defined in [Monderer and Shapley, 1996]: the gradient of these functions correspond to the expected costs. This type of potential is widely considered in population games [Sandholm, 2001], as it serves as a Lyapunov function for strategies' dynamics, or in games with non-atomic players [Cheung and Lahkar, 2018]. In our particular setting of atomic LnSIC game $\mathbb{G}$, a generalization of these potential functions is needed, and defined as follows:

Definition 3.11 (Action-dependent continuous potential)**.** *An action-dependent continuous potential of game $\mathbb{G}$ is a $\mathcal{C}^1$ function F over mixed strategies such that, for all resources $a \in \mathcal{R}$, there exists a constant γ_a verifying:*

$$\forall i, \quad \frac{\partial F}{\partial \pi_{i,a}}(\boldsymbol{\pi}) = \gamma_a \bar{c}_{i,a}(\boldsymbol{\pi}_{-\boldsymbol{i}}) \,. \tag{3.14}$$

Note that as expected cost are $\mathcal{C}^1$ functions, such potentials F are then $\mathcal{C}^2$ functions. Continuous potential functions verify (3.14) with $\gamma_a = 1$ for all resources a. Considering continuous strategy sets of mixed strategies, atomic game $\mathbb{G}$ has an action-dependent continuous potential function. In fact, this function is the conditional expectation (according to the mixed strategy vector $\boldsymbol{\pi}$) of the ordinal potential function P when players choose pure strategies.

Proposition 3.12. *Atomic game $\mathbb{G}$ with a unique LnSIC cost function has the following action-dependent continuous potential function (associated with $\gamma_a = \frac{1}{\alpha_a}, \forall a$):*

$$F(\boldsymbol{\pi}) = \mathbb{E}_{\boldsymbol{\pi}}\left[P\right] \,, \tag{3.15}$$

with P the ordinal potential of $\mathbb{G}$.

Proof. For any player $i \in \mathcal{N}$, the linearity of the expected value $\mathbb{E}_{\boldsymbol{\pi}}\left[P\right]$ gives:

$$\begin{aligned} F(\boldsymbol{\pi}) &= \sum_a \pi_{i,a} \mathbb{E}_{\boldsymbol{\pi}}\left[P \mid \boldsymbol{\pi}_i = \boldsymbol{e}_a\right] \\ &= \sum_{i,a} \pi_a \frac{1}{\alpha_a} \mathbb{E}_{\boldsymbol{\pi}}\left[c_a \mid \pi_i = \boldsymbol{e}_a\right] \,, \end{aligned} \tag{3.16}$$

using $c_a(\cdot) = \alpha_a \lambda(L(\cdot)) = \alpha_a P(\cdot)$. Then, (3.14) is found by differentiating by $\pi_{i,a}$ for any $a \in \mathcal{R}$, with $\gamma_a = \frac{1}{\alpha_a}$. □

The previous proposition generalizes the particular case studied in [Sastry et al., 1994] for games with common payoff, while a similar result is obtained in [Bournez and Cohen, 2013] for continuous potential games. The following proposition gives a more precise result and shows that only games with particular cost functions admit an action-dependent continuous potential function.

Proposition 3.13. *Atomic congestion games that admit a $\mathcal{C}^2$ action-dependent continuous potential function correspond to atomic congestion games with cost functions defined as:*

$$\forall i, a, \quad c_{i,a}(\boldsymbol{r}) = \beta_a \mu(\boldsymbol{r}) \,, \tag{3.17}$$

with β_a any constant which depends on the action a, and μ any function of pure strategies (not necessarily increasing or linearly non-separable).

Proof. Let F be a $\mathcal{C}^2$ action-dependent continuous potential function, associated with constants γ_a and cost functions $c_{i,a}$ $(\forall i, a)$. Then, by Definition (3.14) of F and according to Clairaut-Schwarz theorem (symmetry of second derivatives):

$$\forall i, j, a, b, \quad \gamma_a \frac{\partial \overline{c}_{i,a}}{\partial \pi_{j,b}} = \gamma_b \frac{\partial \overline{c}_{j,b}}{\partial \pi_{i,a}} \,, \tag{3.18}$$

which, using (3.5), leads to (for all vectors of mixed strategies $\boldsymbol{\pi}$):

$$\sum_{\boldsymbol{r}_{-ij}} \Big(\prod_{k \neq i,j} \pi_{k,r_k} \big[\gamma_a c_{i,a} - \gamma_b c_{j,b}\big](a, b, \boldsymbol{r}_{-ij}) \Big) = 0 \,, \tag{3.19}$$

with $\boldsymbol{r}_{-ij}$ the vector of actions of players other than i and j. For all pure strategies $\boldsymbol{r}_{-ij} \in \mathcal{R}^{N-2}$, last equation considered with $\boldsymbol{\pi}_k = \boldsymbol{e}_{r_k}$ $(\forall k \neq i, j)$ becomes:

$$\gamma_a c_{i,a}(a, b, \boldsymbol{r}_{-ij}) = \gamma_b c_{j,b}(a, b, \boldsymbol{r}_{-ij}) \,. \tag{3.20}$$

Therefore, cost functions $(c_{i,a})$ verify (3.17) by defining for example $\mu = c_{i,a}$ for any a and $\beta_b = \frac{\gamma_a}{\gamma_b}$ $(\forall b)$.

Conversely, suppose a game with cost functions verifying (3.17). Then, $\overline{c}_{i,a} = \beta_a \mathbb{E}_{\boldsymbol{\pi}} \left[\mu \mid \pi_i = \boldsymbol{e}_a\right]$, as seen in (3.5). Let $F(\boldsymbol{\pi}) = \mathbb{E}_{\boldsymbol{\pi}} \left[\mu\right]$. By linearity of the expected value, $F = \sum_{i,a} \pi_{i,a} . \mathbb{E}_{\boldsymbol{\pi}} \left[\mu \mid \boldsymbol{\pi}_i = \boldsymbol{e}_a\right]$. Therefore, (3.14) is verified, with $\gamma_a = \beta_a$ $(\forall a)$.

□

This type of games is a generalization of common payoff games, with a unique action-dependent cost function.

The property of having an action-dependent continuous potential leads to convergence of simple RLA, as shown in next Proposition 3.14, for which only local information is accessible for each player (basically her own perceived cost) in order to update her mixed strategy vector and find her best action. In fact, in most cases, players are not even aware that they are involved in a game with other players and interact through their actions. That is why the framework of learning in which players make repeated decisions with a priori unknown rules and outcomes is suitable. The convergence of the simple RLA introduced in Algorithm 3.1 has already been proved when the game has a continuous potential function. In the next section, we prove that there is still convergence for games with an action-dependent continuous potential, such as game $\mathbb{G}$.

3.2.2.3 Convergence of the reinforcement learning algorithm towards the Nash equilibrium

Proposition 3.14 shows that Algorithm 3.1 converges for games having an action-dependent continuous potential function towards the corresponding NE. The updating mechanism (3.8) can be written in an aggregate manner as:

$$\boldsymbol{\pi}^{(k+1)} = \boldsymbol{\pi}^{(k)} + \delta G\left(\boldsymbol{\pi}^{(k)}, \boldsymbol{r}^{(k)}\right), \tag{3.21}$$

with $G = [(1 - \frac{c_{i,r_i}(\boldsymbol{r})}{c^{+}_{\max}}) \times (\boldsymbol{e}_{r_i} - \boldsymbol{\pi}_i)]_i$ the updating function. Let us define function $f(\boldsymbol{\pi}) = \mathbb{E}_{\boldsymbol{\pi}}[G]$ and for any δ the function $\Pi_\delta : \mathbb{R}_+ \to \mathbb{R}$ as the piecewise-constant interpolation of sequence $\left(\boldsymbol{\pi}^{(k)}\right)_k$ of mixed strategies of all players. A direct application of Theorem 3.1 in [Sastry et al., 1994] demonstrates that RLA 3.1 converges weakly, as δ tends to 0, to the solution Π of the following Ordinary Differential Equation (ODE):

$$\frac{\mathrm{d}X}{\mathrm{d}t} = f(X), \quad X(0) = \boldsymbol{\pi}^{(0)}. \tag{3.22}$$

Considering $\Pi = (\pi_{i,a})$ and $f(\Pi) = (f_{i,a})$, the ODE (3.22) can be written element-wise as:

$$\begin{aligned} \forall i, a, \quad \frac{\mathrm{d}\pi_{i,a}}{\mathrm{d}t} = f_{i,a} = \; & \pi_{i,a}(1-\pi_{i,a})(1-\bar{c}_{i,a}/c_{\max}) \\ & + \sum_{b \neq a} \pi_{i,b}(-\pi_{i,a})(1-\bar{c}_{i,b}/c_{\max}) \\ = -\pi_{i,a} \; & \sum_{b \neq a} \pi_b \left(\bar{c}_{i,a} - \bar{c}_{i,b}\right)/c_{\max}. \end{aligned} \tag{3.23}$$

Thus, for sufficiently small learning parameters δ, the convergence points of RLA 3.1 are related to the solutions of a particular ODE, which must be characterized in order to prove that the convergence points are NE of the considered game. In fact, next proposition proves that having an action-dependent continuous potential implies convergence to pure NE of RLA 3.1, for sufficiently small learning parameters δ.

Proposition 3.14. *If an atomic congestion game has an action-dependent continuous potential then, for any initial non-pure strategies $\boldsymbol{\pi}^{(0)}$, function $\Pi = \lim_{\delta \to 0} \Pi_\delta$ converges to a pure NE of the game.*

Proof. This proof is inspired by the one of Theorem 3.3 of [Sastry et al., 1994]. Here, the continuous potential F of the game is action-dependent and associated with constants γ_a:

$$\frac{\mathrm{d}F}{\mathrm{d}t}(\Pi) = -\sum_{i \in \mathcal{N}} \sum_{k=1}^{M} \sum_{l>k} \gamma_{a_k} \pi_{i,a_k} \pi_{i,a_l} \frac{\left(\bar{c}_{i,a_k} - \bar{c}_{i,a_l}\right)^2}{c_{\max}} < 0, \tag{3.24}$$

with $\mathcal{R} = \{a_1, \ldots, a_M\}$ the set of resources. Then, $t \mapsto F(\Pi(t))$ is non-increasing. Therefore, the RLA always converges to a NE, which is pure (see Remark 3.6). □

Note that Algorithm 3.1 works with synchronous updates, meaning that all players update their strategy simultaneously at each iteration. An asynchronous version of Algorithm 3.1 can be considered, where only one player updates her strategy at each iteration. A player i is chosen at iteration k with uniform probability $p_i = \frac{1}{N}$. The convergence of such an asynchronous

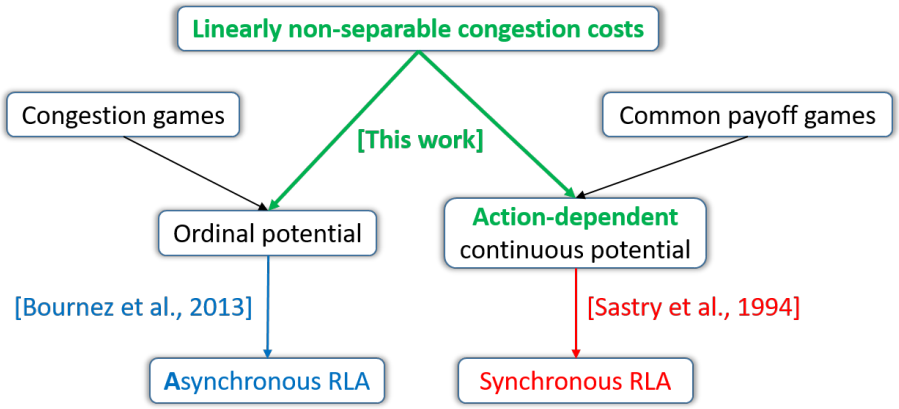

Figure 3.2: Summary of contributions (in green) of paper [Sohet et al., 2020b] compared to papers [Bournez and Cohen, 2013] (in blue) and [Sastry et al., 1994] (in red).

algorithm towards a pure ε-NE[5] has been proved in [Bournez and Cohen, 2013] for games having an ordinal potential function. This result can be applied directly to our framework of atomic congestion games with a unique LnSIC cost function, as an ordinal potential function exists (see Proposition 3.9). The theoretical results added to the literature by our paper [Sohet et al., 2020b] are summarized in Figure 3.2. In next Section, we illustrate the convergence of both synchronous and asynchronous RLA in a atomic smart charging congestion game problem with a unique LnSIC cost function.

3.2.3 Application to a non-separable smart charging game

3.2.3.1 Choice of charging station in function of charging cost

In this section, the synchronous Reinforcement Learning Algorithm (RLA) 3.1 and its asynchronous version are illustrated on a real example of an atomic congestion game $\mathbb{G}$ with a unique LnSIC cost function. The players of $\mathbb{G}$ are Electric Vehicle (EV) users who choose at which Charging Station (EVCS) they charge their vehicle. It is assumed that there are enough charge points to welcome all EVs at each EVCS. These EVCSs are part of an electrical grid network[6] shown in Figure 3.3. In game $\mathbb{G}$, the resources are the EVCSs. Each EVCS r is associated with a bus bar r, representing in power engineering an electrical substation. At each bus r, there is some fixed electricity consumption L_r^0 corresponding to other usages than EV charging. Strategies of EV users in game $\mathbb{G}$ only depend on the observed cost c_r of their charging operation at EVCS r, proportional to the Charging Unit Price (CUP) p_r. All users are supposed to have the same charging need ρ (in kWh) to simplify notations, but this assumption (symmetric game) can be relaxed, in line with Remark 3.2. The charging cost for any EV user at EVCS r is then $c_r = \rho \times p_r$. The CUP function p_r at EVCS r depends on the total power demand L_s at *all* EVCSs s, defined by

$$L_s = L_s^0 + n_s(\boldsymbol{r})\rho\,, \tag{3.25}$$

with $\boldsymbol{r}$ the strategy vector of all EV users and $n_s(\boldsymbol{r})\rho$ the charging need at EVCS s aggregated over all users choosing this EVCS. The CUP functions are detailed in the following.

[5]For any $\varepsilon \geq 0$, a pure strategy vector $\boldsymbol{r}^*$ is an ε-Nash Equilibrium if $\forall i, a,\ c_{r_i^*}(\boldsymbol{r}^*) \leq c_a\left(a, \boldsymbol{r}_{-i}^*\right) + \varepsilon$.

[6]Note that the learning algorithm of previous section can be applied to more general grid topologies.

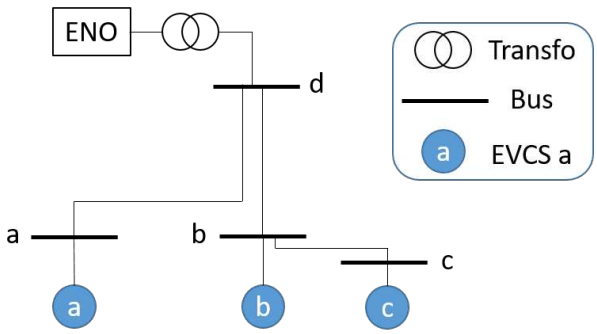

Figure 3.3: Electrical grid containing three EVCS a, b, c, all managed by the Electrical Network Operator (ENO). *EVCS c is connected to the same power line as EVCS b, and the power line of EVCS a is twice as long as the one of EVCS b.*

Remark 3.15. *Unlike in other chapters, here the temporal load profiles are not considered, in order to lighten notations (but the following study can be extended). All electricity needs are fulfilled at constant power, and without loss of generality the charging operation is supposed to last exactly one hour, so that energy needs (in MWh) and corresponding power loads (in MW) have the same values, and therefore share the same notation (ρ and L_r^0, respectively for charging and other usages).*

All the EVCSs and the grid are supposed to be managed by the same Electric Network Operator (ENO)[7]. The ENO chooses CUP functions p_r as incentives to reduce the grid cost $\mathcal{G}$ caused by the total power loads L_r and defined in Section 4.4.1. More precisely, the CUPs correspond to the marginal grid costs: $p_r = \frac{\partial \mathcal{G}}{\partial L_r}(L_a, L_b, L_c)$. Such a pricing mechanism is called Locational Marginal Pricing (LMP) and is detailed in Chapter 5. Unfortunately, these CUPs are general non-separable congestion cost functions and do not verify the Definition 3.1 of LnSIC cost functions, because the derivatives of $\mathcal{G}$ are not necessarily proportional, and in addition are general functions of the three quantities $n_r(\boldsymbol{r})$ $(r = a, b, c)$. The idea is then to transform this LMP into a pricing scheme verifying the LnSIC property[8].

To this end, the power flow in this grid is approximated as if the total power load L_r at each bus r came from bus d (see Figure 3.3). More precisely, as EVCSs have different impacts on the grid, the total power load L_r at EVCS r is replaced by an augmented power load $\tilde{\alpha}_r L_r$ at bus d. with constant $\tilde{\alpha}_r > 1$ modeling the specific impact of EVCS r. This linear load approximation is summarized as follows:

$$(L_a\,, L_b\,, L_c\,, 0) \quad \longrightarrow \quad (0\,, 0\,, 0\,, \sum_r \tilde{\alpha}_r L_r)\,. \tag{3.26}$$

In this linear approximation, the CUP function at EVCS r is equal to:

$$p_r = \frac{\partial \mathcal{G}}{\partial L_r}(0\,, 0\,, 0\,, \sum_r \tilde{\alpha}_r L_r) = \tilde{\alpha}_r \frac{\partial \mathcal{G}}{\partial L_d}(0\,, 0\,, 0\,, \sum_r \tilde{\alpha}_r L_r)\,. \tag{3.27}$$

Then, by defining $\alpha_r = \rho \tilde{\alpha}_r$ and $\lambda : L \mapsto \frac{\partial \mathcal{G}}{\partial L_d}(0, 0, 0, L + \sum_r \tilde{\alpha}_r L_r^0)$, the charging cost function at EVCS r verifies $c_r(\boldsymbol{r}) = \alpha_r \lambda(\sum_s \alpha_s n_s(\boldsymbol{r}))$, i.e. the LnSIC Definition 3.1.

[7] This simplifying assumption is relaxed in the other chapters of this thesis.

[8] Note that non-atomic games with this LMP pricing can be solved by the same Beckmann's method as for LnSIC cost functions (see Proposition 2.19), without any modification in the CUPs (see Remark 5.9).

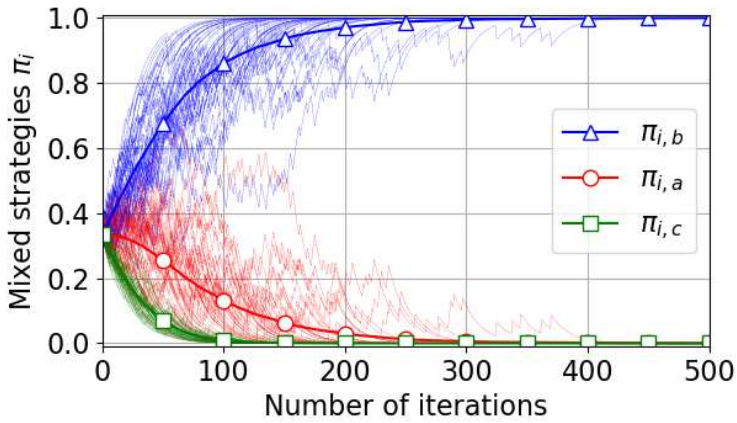

Figure 3.4: Evolution of mixed strategies $\boldsymbol{\pi}_i$ (of only 50 users) throughout iterations of Algorithm 3.1. Thicker lines represent the average (over all users) mixed strategy.

According to Proposition 3.10, the unique NE of game $\mathbb{G}$ is not sensitive[9] to the exact values of parameters $\tilde{\alpha}_r$, but only to their relative values, and more precisely to which EVCSs have the smallest $\tilde{\alpha}_r$. EVCSs a and c should have a greater impact on the grid cost (i.e., a higher $\tilde{\alpha}_r$) than EVCS b because they are further away from the transformer and in turn generate more power losses (see Figure 3.3). The values taken here for parameters $\tilde{\alpha}_r$ are from section IV.A of our paper [Sohet et al., 2020b] and are equal to $\tilde{\alpha}_a = 1.12$, $\tilde{\alpha}_b = 1.07$ and $\tilde{\alpha}_c = 1.18$. Then, according to Proposition 3.10, all EV users choose EVCS b at NE. A method to defined parameters $\tilde{\alpha}_r$ is given in Section 5.4.1.1.

3.2.3.2 Numerical illustration of convergence

The parameters of the smart charging game are set as follows: the distribution grid considered has around 1500 customers, with a standard 6 kVA contract power, for a total of 9 MW if all customers reach their contract limit at the same time. The electricity consumption other than EV charging is the same at each EVCS r: $L_r^0 = 3$ MWh. The total number of EV users is set to $N = 1500$. The energy need is $\rho = 3$ kWh, half of the daily mean individual EV consumption in France[10], assuming a constant electricity consumption of $m_e = 0.2$ kWh/km [De Cauwer et al., 2015]. The values of the grid parameters are given in Section 4.4.4.1. Regarding learning characteristics, the learning parameter is set to $\delta = 0.5$ and the initial mixed strategies are equally distributed among resources: $\pi_{i,r} = 1/3$ for all users i and EVCS $r = a, b, c$. For the asynchronous version of Algorithm 3.1, each player i is chosen with a probability $p_i = 1/N$ for the update phase.

Figures 3.4 and 3.5 show the evolution of mixed strategies $\boldsymbol{\pi}_i$ (of only 50 users, for readability) throughout iterations, respectively for the synchronous Algorithm 3.1 and for the asynchronous version. As mentioned in Section 3.2.2.1, although the pure NE of this game (all users choosing the EVCS with the lowest impact on grid costs) may seem trivial, EV users need hundreds of iterations to learn it (see Figure 3.4), as they have no information on the grid topology. Observing thicker lines (average mixed strategy over all users), it can be seen that, while the synchronous algorithm converges in less than 500 iterations (Figure 3.4), it takes more than a thousand times as many iterations for the asynchronous one (Figure 3.5). This is understandable since in the

[9] The exact values only impact the convergence speed of RLA 3.1: the further away $\tilde{\alpha}_r$ are from one another, the faster the convergence.

[10] The daily mean driving distance is 30 km [CGDD, 2010]

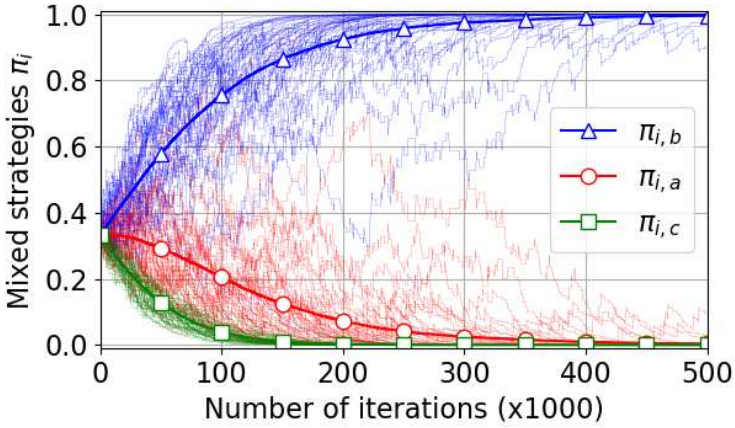

Figure 3.5: Evolution of mixed strategies $\boldsymbol{\pi}_i$ (of only 50 users) throughout iterations of asynchronous version of Algorithm 3.1.

asynchronous version, only one player updates her strategy at each iteration, instead of all the 1500 players like in the original Algorithm 3.1. This also explains why larger number of players lead to slower convergence for the asynchronous version, while it has no effect on the original Algorithm 3.1. Note that the asynchronous version of RLA 3.1 converges towards the $\varepsilon-$NE of game $\mathbb{G}$ with $\varepsilon = 0$, i.e. the exact pure NE given in Proposition 3.10.

Proposition 3.14 states that the RLA 3.1 converges towards the NE found in Proposition 3.10 for sufficiently small learning parameters δ. It has been observed that for this specific smart charging game, there is always convergence for approximately $\delta \leq 0.5$ (in the case of uniform initial mixed strategies). Smaller δ values may be required for other initial mixed strategies. The number of iterations until convergence decreases with the learning parameter δ, hence the choice $\delta = 0.5$ in this section. Even for $\delta > 0.5$, the RLA 3.1 may converge, faster than for $\delta \leq 0.5$, but the limit does not corresponds exactly to the NE of game $\mathbb{G}$. Note that the exact number of iterations until convergence may slightly vary from one execution to another (of either algorithm), due to actions randomly chosen from mixed strategies.

The same case study is used to illustrate the stochastic RLA introduced in next Section 3.3.

3.3 Stochastic reinforcement learning algorithm

In this section, the basic RLA introduced in previous Section 3.2 is refined by considering the vehicle users' perception and a rationality parameter. This stochastic RLA was first introduced in paper [Cominetti et al., 2010] and is described in Section 3.3.1, as well as the theoretical results found in this paper (Section 3.3.2). The contribution of this thesis is to apply in Section 3.3.3 this particular RLA to the smart charging game defined previously in Section 3.2.3, which has the specificity to have LnSIC cost functions.

3.3.1 Principle of the stochastic reinforcement learning process

The learning algorithm considered in this section is the one introduced in [Cominetti et al., 2010]. Instead of updating directly her strategy after observing her personal costs as in the standard learning Algorithm 3.1, player i updates her *perceptions* $z_{i,r}$ of the costs on resource r as follows. For all resources $r \in \mathcal{R}$, the perceptions $z_{i,r}^{(k+1)}$ by player i of the associated costs at iteration

$k+1$ ($k \in \mathbb{N}$) of this RLA are given by:

$$z_{i,r}^{(k+1)} = \begin{cases} (1-\delta_k) \times z_{i,r}^{(k)} + \delta_k \times c_{i,r}^{(k)}\left(\boldsymbol{r}^{(k)}\right), & \text{if } r = r_i^{(k)}, \\ z_{i,r}^{(k)}, & \text{otherwise,} \end{cases} \tag{3.28}$$

with:

- $\delta_k > 0$ the averaging factor such that $\sum_{k=0}^{N} \delta_k \xrightarrow[N \to +\infty]{} +\infty$ and $\sum_{k=0}^{+\infty} \delta_k^2 < +\infty$ (e.g., $\delta_k = \frac{1}{(k+1)^\gamma}$ with $0.5 < \gamma \leq 1$);
- $r_i^{(k)}$ the resource chosen by player i at iteration k.
- $c_{i,r}^{(k)}(\boldsymbol{r}^{(k)})$ the total costs observed by vehicle user i having chosen resource r at iteration k, which depends on the resources chosen by the other players $\boldsymbol{r}^{(k)}$.

Remark 3.16. *Note that if the averaging factor is $\delta_k = \frac{1}{(k+1)^\gamma}$ with $\gamma = 1$, and player i chooses the same action $r \in \mathcal{R}$ for the first k iterations, then her perception of r is the mean value of the corresponding costs over all iterations: $z_{i,r}^{(k+1)} = \frac{1}{k+1} \sum_{k=0}^{k} c_{i,r}^{(k)}(\boldsymbol{r}^{(k)})$. If $\gamma < 1$, more weight is put on recent iterations than old ones.*

If player i chooses several resources throughout iterations, the perceptions associated with these resources do not correspond to the mean of the observed costs. However, it is the case when using the sophisticated learning rate presented in Remark (3.30).

Then, each player i chooses her mixed strategy vector $\boldsymbol{\pi}_i$ in function of all her perceptions, using for example the Logit rule [McFadden et al., 1973]:

$$\pi_{i,r} = \frac{e^{-\beta_i \times z_{i,r}}}{\sum_{r' \in \mathcal{R}} e^{-\beta_i \times z_{i,r'}}}, \tag{3.29}$$

with $\beta_i \geq 0$ the rationality of player i:

- If $\beta_i = 0$, player i chooses all resources uniformly, i.e. with the same probability. This is the lowest level of (economical) rationality, as player i does not choose more often the resources with lower perceptions;
- If $\beta_i \to +\infty$, then player i always (i.e. with probability 1) chooses the resource with the minimal perception.

Assumption 3.17. *In the following, all β_i are assumed equal: $\forall i$, $\beta_i = \beta$, but the following study can be extended to the case of heterogenous players with different rationalities.*

Remark 3.18. *Note that having a too high rationality level is not necessarily optimal for the player, as she might stick to a non-optimal resource and never try again the others because they were too expensive at first. For example, if all players choose the same resource a at the first iteration and therefore associate it to a high perception (due to the congestion phenomenon), they will never choose it again and therefore this resource a will become cheaper (without any congestion). A better rationality parameter β would allow the trial and error mechanism.*

Remark 3.19. *Under the Logit mapping $\boldsymbol{z} \mapsto \boldsymbol{\pi}$ defined in (3.29), players do not choose exactly the mixed strategies $\boldsymbol{\pi}$ minimizing their perceptions $\boldsymbol{z}$, due to the finite rationality parameters β. Actually, this mapping is the same as the one obtained when players choose the mixed strategies effectively minimizing their perceptions, while knowing their perceptions are associated with a random error term (following Gumbel distribution with shape parameter β, in the case of the Logit rule) [Cominetti et al., 2010].*

The stochastic RLA is summarized in Algorithm 3.2. The notation $\overline{\boldsymbol{\pi}}_k$ at iteration k stems for the mixed strategy vector averaged over the last ten iterations[11] and all players.

Algorithm 3.2: Discrete-time stochastic learning process

Input: $\boldsymbol{z}^{(0)}$ the initial perceptions, $k = 0$ the iteration number

while $\|\overline{\boldsymbol{\pi}}_k - \overline{\boldsymbol{\pi}}_{k-1}\|_2 > \varepsilon$ **do**

  All players **simultaneously** take action and update their perceptions and mixed strategies: $\boldsymbol{z}^{(k)} \xrightarrow{(3.29)} \boldsymbol{\pi}^{(k)} \longrightarrow \boldsymbol{r}^{(k)} \xrightarrow{(3.2)} \boldsymbol{c}^{(k)} \xrightarrow{(3.28)} \boldsymbol{z}^{(k+1)}$;

  $k \leftarrow k + 1$

end

Note that the stochastic learning Algorithm 3.2 is chosen as synchronous, like the standard learning Algorithm 3.1.

Remark 3.20. *The theoretical results obtained by [Cominetti et al., 2010] (described in next section) were extended to the following altered version of (3.28) by [Bravo, 2016]:*

$$z_{i,r}^{(k+1)} = \begin{cases} \left(1 - \frac{1}{\theta_{i,r}^{(k)}}\right) \times z_{i,r}^{(k)} \quad + \quad \frac{1}{\theta_{i,r}^{(k)}} \times c_{i,r}^{(k)}\,, & \text{if } r = r_i^{(k)}\,, \\ z_{i,r}^{(k)}\,, & \text{otherwise,} \end{cases} \tag{3.30}$$

with $\theta_{i,r}^{(k)}$ the number of times when player i chose resource r among the first k iterations:

$$\theta_{i,r}^{(k)} = \sum_{k=0}^{k} \mathbb{1}_{r_i^{(k)}=r}\,. \tag{3.31}$$

Here, the perception by player i of r is the mean value of the costs associated with r observed throughout all iterations. We observed in the smart charging game studied in Section 3.2.3 that this learning version may be numerically faster.

3.3.2 Theoretical results from literature

This section is entirely based on paper [Cominetti et al., 2010]: it rephrases a part of the theoretical results found in this paper (with costs instead of payoffs).

3.3.2.1 Adaptive dynamics and perturbed Nash equilibrium

In [Benaim and Hirsch, 1999], close connections are established between the asymptotics of the discrete time random process (3.28) for $k \to \infty$ and the behavior as $t \to \infty$ of the continuous time deterministic averaged dynamics, defined in Proposition 3.21.

Proposition 3.21 (Proposition 1 of [Cominetti et al., 2010]). *The continuous dynamics may be expressed as:*

$$\forall i, r, \quad \frac{\mathrm{d}z_{i,r}}{\mathrm{d}t} = \pi_{i,r}\left(\boldsymbol{z_i}\right) \times \left(\overline{c}_{i,r}\left(\boldsymbol{\pi_{-i}}(\boldsymbol{z})\right) - z_{i,r}\right). \tag{3.32}$$

Next Proposition 3.22 clarifies the link between these dynamics (3.32) and learning process (3.28): in particular cases, the latter converges towards the rest points of the former.

[11] Without the moving average, the Euclidean norm is too noisy and the convergence threshold may be reached arbitrarily early.

Proposition 3.22 (Theorem 4 of [Cominetti et al., 2010]). *If* $C = \left(\boldsymbol{z} \mapsto \bar{c}_{i,r}\left(\boldsymbol{\pi}_{-\boldsymbol{i}}(\boldsymbol{z})\right)\right)_{i,r}$ *is a* $||\cdot||_\infty$*-contraction then its unique fixed point* $\tilde{\boldsymbol{z}}$ *is a global attractor for the adaptive dynamics* (3.32)*, and the learning process* (3.28) *converges almost surely towards* $\tilde{\boldsymbol{z}}$*.*

Following the expression of (3.32), rest points of (3.32) and fixed points of C are equivalent. Let $\mathcal{E}$ denote the set of rest points of (3.32) and Σ its image by $\boldsymbol{\pi}$. Proposition 3.23 shows that these rest points are related to the atomic game under consideration.

Proposition 3.23 (Proposition 3 of [Cominetti et al., 2010]). *Under the Logit rule* (3.29)*,* Σ *is equal to the set of Nash Equilibria of the perturbed game* $\mathbb{G}^*$ *defined by the following cost functions:*

$$\forall i\,, \quad c_i(\boldsymbol{\pi}) = \sum_r \pi_{i,r}\ \bar{c}_{i,r}(\boldsymbol{\pi}_{-\boldsymbol{i}}) \quad + \quad \frac{1}{\beta_i}\sum_r \pi_{i,r} \ln\left(\pi_{i,r}\right)\,. \tag{3.33}$$

In the case where C of Proposition 3.22 is a $||\cdot||_\infty$-contraction, the set $\mathcal{E}$ of its fixed points is reduced to a singleton (Proposition 3.22) and therefore the set of NE of $\mathbb{G}^*$ too (Proposition 3.23). Thus, for games such that C is a contraction, the stochastic learning Algorithm 3.2 converges towards the unique NE of the perturbed versions of the games. Sufficient conditions on games to ensure that C is a contraction are given in the following section.

3.3.2.2 Sufficient conditions for the convergence of the stochastic learning algorithm

In [Cominetti et al., 2010], the authors link the property "C is a $||\cdot||_\infty$-contraction" with parameters of the game for general atomic games (Proposition 3.24). Next proposition requires two definitions:

- $\omega = \max_i \sum_{j\neq i} \beta_j \quad \Big(= (N-1)\beta \ \text{ in the case of symmetric players}\Big)\,,$
- $\Delta_{\max}$ an upper bound for the absolute impact over a player's costs when another single player changes her choice.

Proposition 3.24 (Proposition 5 of [Cominetti et al., 2010]). *Under the Logit rule* (3.29)*, if* $\omega\Delta_{\max} < \frac{1}{2}$ *then* C *is a* $||\cdot||_\infty$*-contraction.*

Note that because ω is almost proportional to the total number of players N, the rationality parameter β needs to be relatively small for the condition $\omega\Delta_{\max} < \frac{1}{2}$ to be satisfied. Unfortunately, for such small values of β, the entropic term in (3.33) is preponderant, such that the strategies of the players depend only slightly on the characteristics of the game considered and are almost uniform. In [Cominetti et al., 2010], sufficient conditions weaker than $\omega\Delta_{\max} < \frac{1}{2}$ were given for specific classes of games, such as separable congestion games ($\omega\Delta_{\max} < 2$). Furthermore, if the players of a separable congestion game are symmetric, the even weaker condition $\beta\Delta_{\max} < 2$ guarantees that the unique NE of the perturbed game is a local attractor for the continuous dynamics (3.32). There is no proof yet that it is also a global attractor (and that therefore the learning process (3.28) converges almost surely towards it), but no numerical counterexample has been found [Cominetti et al., 2010].

In any case, the proofs presented in [Cominetti et al., 2010] for congestion games cannot be directly extended to non-separable games, as they use the separable property. However, next section shows that the learning process (3.28) converges numerically on the example of the non-separable smart charging game of Section 3.2.3.

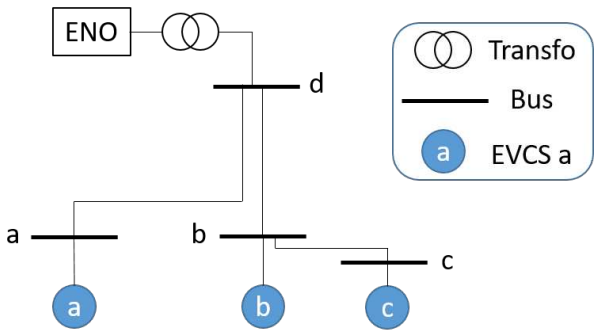

Figure 3.6: Electrical grid containing three EVCS a, b, c, all managed by the Electrical Network Operator (ENO). *EVCS c is connected to the same power line as EVCS b, and the power line of EVCS a is twice as long as the one of EVCS b.*

3.3.3 Application to a non-separable smart charging game

3.3.3.1 Illustration of the stochastic reinforcement learning algorithm

The stochastic RLA presented in Section 3.3.1 is illustrated on the same smart charging game as for the standard RLA (see Section 3.2.3). The players are Electric Vehicle (EV) users who choose at which Charging Station (EVCS) they charge their EV battery. These EVCS are part of an electrical grid network shown in Figure 3.6. The averaging factor is defined as $\delta_k = \frac{1}{(k+1)^\gamma}$. The number of iterations until convergence of the stochastic RLA on this specific smart charging game decreases with parameter γ up to $\gamma = 0.7$, which is chosen as the value of γ in this section. The convergence threshold of Algorithm 3.2 is set to $\varepsilon = 5 \times 10^{-6}$.

First, Figure 3.7 illustrates the mechanism of the stochastic RLA, which is different from the standard RLA of previous section. As mentioned earlier, instead of directly updating her mixed strategy in function of the observed cost, a player in a stochastic RLA updates her perceptions associated with each EVCS, and updates her strategy in a second phase. Figure 3.7 shows the perceptions of a given player[12] associated with each EVCS throughout the iterations of the stochastic RLA, and for different values of the rationality parameter β.

Note that during the first three iterations, players try all EVCSs once in order to have a starting perception for each one. For example, the perception of EVCS a for $\beta = 500$ (in red) starts at the third iteration, when the player tries EVCS a for the first time, and terminates at iteration 23 when the stochastic RLA has reached convergence. Figure 3.7 shows that the higher β is, the faster the stochastic RLA converges. Indeed, a player with a higher rationality parameter β chooses the EVCS with the lowest perception more systematically, so that the actions, the perceptions and therefore the mixed strategies (see Algorithm 3.2) vary less. Note that as the final perceptions associated with $\beta = 500$ and $\beta = 1000$ are the same, the limit of the corresponding mixed strategies are the same (see Figure 3.8).

Remark 3.25. *In this section, the convergence criterion is applied to the mixed strategies averaged over all players rather than the set of all mixed strategies in order to obtain the convergence sooner. If the individual strategy vectors have not converged yet when the average strategy vector did, the individual mixed strategy vectors can be replaced by the converged average. Indeed, the convergence of the individual mixed strategies is equivalent to the convergence of the individual perceptions. The limit $\boldsymbol{z}_i^\infty$ of the perceptions of player i should verify (3.28) (with $\boldsymbol{z}^\infty$ in place*

[12]The choice of the player does not change the nature of the results presented in Figure 3.7.

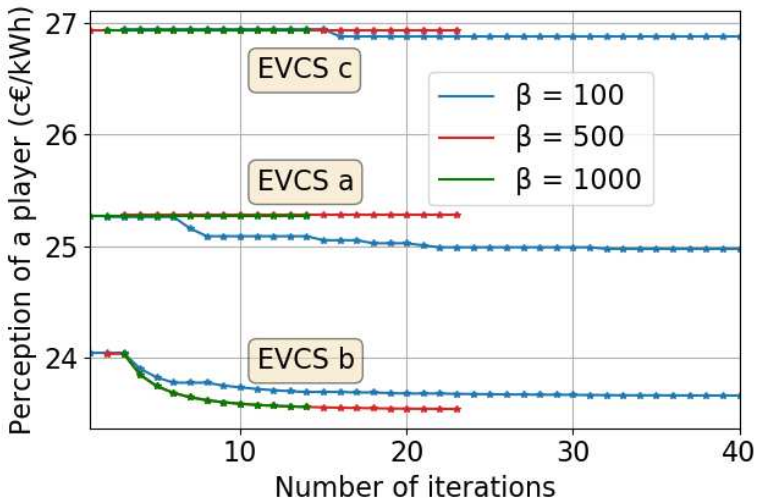

Figure 3.7: Perceptions of a given player associated with the three EVCSs, throughout the iterations of the stochastic RLA and for different rationality values β. *For the low rationality* $\beta = 100$*, players regularly try EVCSs a and c even if the associated perceptions are higher than for EVCS b, and therefore the stochastic RLA converges slower than for higher rationalities.*

of the perception terms), and therefore should be equal to the observed costs. These costs do not depend on the player i, therefore all limits $\boldsymbol{z}_i^\infty$ *are equal and consequently, all players share the same mixed strategy vector (which is then equal to the average strategy vector).*

Given that the perception value corresponding to an EVCS is updated only when the player chooses this EVCS at one iteration, Figure 3.7 shows that EVCS b is visited more often than the others (because players learn that it is cheaper than the other EVCSs), and even more so when the rationality parameter β is high and the player is more likely to effectively minimize her costs (see Remark 3.18). Note that all perceptions decrease as the stochastic RLA progresses, because more and more EV users choose the cheapest EVCS for the grid and therefore reduce the Charging Unit Price for all EVs at all EVCSs (see Section 5.4.1.1).

Figure 3.8 shows, for $\beta = 100$, how the mixed strategies and the corresponding mean (in thick) over all players converge throughout the iterations of the stochastic RLA. As mentioned earlier, the players try all the EVCSs during the first iterations, which explains the corresponding erratic behavior that can be observed on Figure 3.8 (although the average mixed strategy is steady and equal to a third). During the following iterations, note how similar the mixed strategies of all players are, compared to the standard RLA (see Figure 3.4 and 3.5). Indeed, in the stochastic RLA, once a player has tried all EVCSs, her perceptions are already more or less accurate. For the standard RLA, the update at each iteration of the mixed strategies is small because of the term "$\delta(1 - \frac{c_{i,a}}{c^+_{\max}})$" (see (3.8)). However, for $\beta < 400$ approximately, the convergence of the mean mixed strategy is slightly slower for the stochastic RLA (in the case of Figure 3.8, the convergence criterion is actually verified only after 1000 iterations) than for the standard one (500 iterations, see Figure 3.4). Moreover, the individual mixed strategies have not converged yet towards the mixed strategy averaged over all players (see Remark 3.25). In the case of $\beta > 400$, players are rational enough to systematically choose the cheapest EVCS and the stochastic RLA converges in only a dozen iterations (see Figure 3.7).

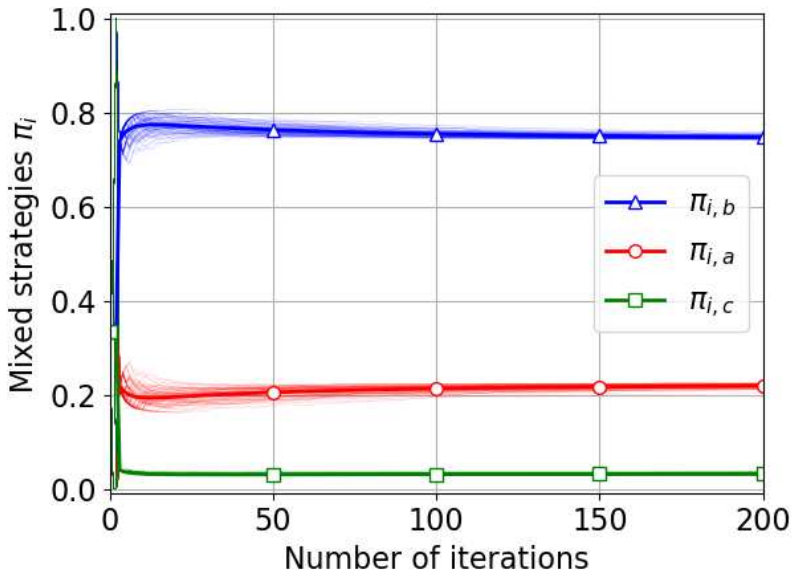

Figure 3.8: Evolution of mixed strategies of all players (thin lines) and the corresponding mean (thick marked line) throughout the iterations of the stochastic RLA (for $\beta = 100$). *Soon after the first iterations, the players have similar mixed strategies, contrary to the standard RLA (see Figure 3.4*

3.3.3.2 Learning the perturbed Nash equilibrium

Figure 3.8 shows the convergence speed of the stochastic RLA, but does not explain the nature of the limit obtained. At the limit, EV users do not choose the cheapest EVCS b as a pure strategy like for the standard RLA (see Figure 3.4), but they tend to a mixed strategy (for $\beta = 100$). This is due to Proposition 3.24, which states that in certain conditions, the stochastic RLA converges towards the unique NE of the atomic game under consideration, with an added entropy term due to the finite rationality of players.

This perturbed NE is computed using the following cycling averaged best response Algorithm 3.3. The standard best response algorithm is here accelerated by approximating the mixed strategy vector of each player by the mixed strategies averaged over all players. The mixed strategies are updated cycling over the set of players until convergence [Gilboa and Matsui, 1991]. Although these best response dynamics seem to converge for this particular smart charging game, it is not proved yet for general atomic non-separable congestion games with any number of players [Jacquot et al., 2018].

The limit of the cycling average best response Algorithm 3.3 is shown in Figure 3.9 in function of the rationality parameter β (continuous lines). As mentioned before, if players have a low rationality β, their mixed strategy is uniform at equilibrium ($\pi_{i,r} = \frac{1}{3}$), while if their rationality is high ($\beta > 400$), they systematically choose the cheapest EVCS b at equilibrium, like the limit of the standard RLA (see Figure 3.4). Figure 3.9 also shows that the stochastic RLA (dashed lines) seems to converge towards the perturbed NE even beyond the sufficient condition given in Proposition 3.24 for general atomic games. For this smart charging game, the maximal individual impact on a player's cost (found numerically) is $\Delta_{\max} = c_c(\boldsymbol{r}_1) - c_c(\boldsymbol{r}_2)$ with $\boldsymbol{r}_1$ (respectively $\boldsymbol{r}_2$) the action vector corresponding to all players choosing EVCS c (respectively all players but

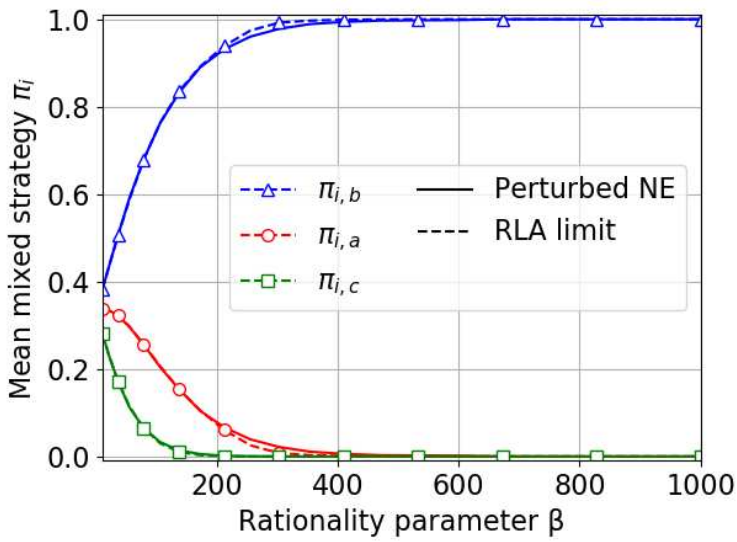

Figure 3.9: Comparison of the perturbed NE obtained with Algorithm 3.3 (in continuous lines) and the limit of the stochastic learning Algorithm 3.2 (in dashed and marked lines), in function of the rationality parameter β. *For this particular non-separable game, the stochastic RLA seems to converge to the perturbed NE beyond the sufficient condition given in Proposition 3.24. This perturbed NE goes from a uniformly mixed strategy for low rationality values, to a pure strategy for* $\beta \geq 400$.

one which chooses EVCS b). In this case, $\omega \times \Delta_{\max} = \frac{1}{2}$ when $\beta \simeq 40$ ($\omega = (N-1)\beta$), while Figure 3.9 indicates that Algorithm 3.2 converges towards the perturbed NE at least up to $\beta = 160$, which is the refined sufficient condition for *separable* congestion games. Therefore, the weaker condition $\omega \times \Delta_{\max} = 2$ seems to be sufficient to obtain convergence of the stochastic RLA towards the perturbed NE for this particular *non-separable* congestion game. For $\beta \geq 400$, both Algorithms 3.2 and 3.3 deliver a pure strategy limit (i.e., $\pi_{i,r} = 0$ or 1). However, for $200 < \beta < 400$, the stochastic RLA does not exactly converge towards the perturbed NE.

3.4 Conclusion

In this chapter, vehicle users do not have common knowledge, unlike the rest of this thesis. They follow a standard reinforcement learning process: they observe their costs of the day and then update their strategy for the following day. It is shown that by doing so, they reach the stationary behavior (or equilibrium) obtained in previous Chapter 2.

To prove this, the existence of an ordinal potential function for the atomic congestion game between vehicles, as well as a continuous potential function, has been extended to Linearly non-Separable Increasing Congestion (LnSIC) cost functions, such as the Charging Unit Price. Consequently, the Reinforcement Learning Algorithm 3.1 and its asynchronous version (where players do not update their strategies simultaneously) both converge towards the unique Nash Equilibrium of the LnSIC game. This convergence is illustrated on a smart charging game where Electric Vehicle users choose their charging station in function of the corresponding CUPs, which are LnSIC cost functions.

The convergence of another RLA is also shown on this example, in the absence of any new

Algorithm 3.3: Cycling averaged best response dynamics

Input: random initial mixed strategy vector $\boldsymbol{\pi}^{(0)}$, iteration index $k = 0$

while $|\overline{\boldsymbol{\pi}}^{(k)} - \overline{\boldsymbol{\pi}}^{(k-1)}| > 10^{-3}$ **do**

  $k \leftarrow k + 1$;

  for *all players* i **do**

    Player i maximizes her expected cost c_i assuming all the other players play the average mixed strategy $\overline{\boldsymbol{\pi}}_{-i}$:

$$\boldsymbol{\pi}_i^{(k)} \leftarrow \underset{\boldsymbol{\pi}_i}{\operatorname{argmin}} \;\; c_i(\boldsymbol{\pi}_i, \overline{\boldsymbol{\pi}}_{-i}) \tag{3.34}$$

  end

end

theoretical proof. In this stochastic RLA, vehicle users are not hyper-rational, unlike the rest of this thesis: they do not systematically choose the cheapest strategy, due to a finite rationality parameter. This RLA appears not to converge towards the NE of the atomic smart charging game (when there is convergence), but the NE of a perturbed version of the game with an additional entropy term.

A natural extension of this work would be to extend the sufficient condition for the convergence of this stochastic RLA for atomic LnSIC games. The convergence proof of the standard RLA 3.1 and its asynchronous version also needs to be extended to the case where there are several LnSIC cost functions. Finally, a future work could study theoretically the covnergence speed of all these RLAs in the case of atomic LnSIC games.

Part II

Smart charging and pricing mechanisms

Chapter 4

Smart charging scheduling at charging stations

The EV user behavior models of previous Part I result in charging need values at each charging station. This chapter focuses on how the operators of these stations schedule the charging of these EV user needs. The water-filling solution is chosen to schedule the aggregated *charging profile of the EVs. Several extensions of this method are then considered: for time-dependent operator's cost functions, for self-consumption of local electricity generation, for asynchronous EV arrival and departure times and in the case of several charging stations. The optimal operator's cost obtained with these algorithms is then used in next chapter to design the EV charging unit prices per kWh.*

This chapter is in part inspired from the following papers, among others:

[Sohet et al., 2020a] **Sohet, B.**, Hayel, Y., Beaude, O., and Jeandin, A. (2020). Impact of strategic electric vehicles driving behavior on the grid. *In 2020 IEEE PES Innovative Smart Grid Technologies Europe (ISGT-Europe)*, pages 454-458.

[Sohet et al., 2021a] **Sohet, B.**, Hayel, Y., Beaude, O., Breal, J., and Jeandin, A. (2021). Online smart charging algorithm with asynchronous electric vehicles demand. *In 2021 IEEE PES Innovative Smart Grid Technologies Europe (ISGT-Europe).*

Contents

4.1 Introduction **62**

4.2 Smart charging of aggregated charging need at a charging station **64**

4.2.1 Basic water-filling scheduling 64

4.2.1.1 Formulation of the aggregated charging scheduling problem 64

4.2.1.2 Water-filling resolution 65

4.2.2 Extensions of the water-filling scheduling 69

4.2.2.1 Time-dependent load cost function 69

4.2.2.2 Self-consumption of local electricity generated at charging station 70

4.3 Online smart charging of asynchronous charging needs **73**

4.3.1 Asynchronous charging scheduling framework 73

4.3.2 Offline charging scheduling 74
4.3.3 Online charging scheduling 74
4.3.3.1 Description of the online procedure 75
4.3.3.2 Analysis of online procedure and proof of optimality . . . 75
4.3.3.3 Illustration of online charging scheduling on a simple example 77
4.3.4 Illustration and comparison of online and offline schedulings on asynchronous commuting. 78
4.3.4.1 Commuting framework with real data 78
4.3.4.2 Comparison of online and offline charging schedulings . . 79
4.4 Smart charging at several charging stations of a grid 81
4.4.1 Model of grid costs related to EV charging 81
4.4.2 Three different possible operators for the charging scheduling . . . 82
4.4.3 Three charging scheduling methods depending on available information 83
4.4.4 Numerical comparison between the three charging schedulings . . . 85
4.4.4.1 Illustration of the scheduling methods on a simplified distribution grid 85
4.4.4.2 Comparison of grid costs and execution times between the three methods 86
4.5 Conclusion 87

4.1 Introduction

The ultimate goal of this thesis is to efficiently design incentives of operators of the coupled electrical-transportation system (see Figure 1.5 for a schematic view of these operators). As mentioned in Section 1.4, the typical use case corresponding to this coupled system is commuting. In this case, the vehicle users choose their path to go to their workplace, the EV Charging Station (EVCS) where they leave their vehicle charging during the working hours, their charging need, etc. These choices are modeled in previous Part I, and they result among others in charging need values at each EVCS at the beginning of the working day. The present Part II focuses on two incentives of the EVCSs' operators (charging scheduling and pricing), which are evaluated using the vehicle user behavior model in the last Part III.

The present chapter focuses on how the operators of the EVCSs, called Charging Service Operators (CSOs, see Section 1.2.2), schedule the EV charging in time throughout the working day in order to fulfill the EV charging needs while optimizing some objective function. Charging scheduling, also called smart charging, is one of the many possible Demand-Side Management (DSM) mechanisms, implemented to control energy consumption [Palensky and Dietrich, 2011]. In the case of EV charging, DSM uses the flexibility, both in terms of compatibility with EV users mobility needs, and technical capabilities. Charging scheduling can be done using Demand Response (DR) mechanisms, a subset of DSM, with the particularity of sending incentives to EV users to change their charging profile [Vardakas et al., 2014]. For example, the charging pricing schemes studied in next Chapter 5 are DR mechanisms. Note that in this thesis, these price incentives are used to affect the EV users' choice of the EVCS where they charge.

Concerning the charging scheduling (in time), a Direct Load Control (DLC) mechanism [Ruiz et al., 2009] is considered instead in the present chapter. The choice of the EV charging

profile at the EVCS is supposed to be centralized at the level of the CSO of the chosen EVCS and not driven by price signals. However, this centralized control is based on an agreement between the CSO and EV users, which can receive incentive payments in advance, which is common in the residential sector in the USA [Samad and Kiliccote, 2012] for example. Note that the pricing schemes in next Chapter 5 are actually based on the CSO's objective function obtained with the DLC mechanism of the present chapter. In order to integrate this charging scheduling problem into the multilevel problem introduced in Chapter 7, and to keep a reasonable computation speed, the CSO only chooses the charging profile *aggregated* over all EVs at a given EVCS (see Section 4.2.1 for more details). A natural example of DLC scheduling is the Water-Filling (WF) scheduling [Shinwari et al., 2012, Mohsenian-Rad et al., 2010], which reduces the variance in time of the total load at the EVCS in an efficient manner. This method is described in Section 4.2.1 on a simple case and then extended in the following Sections 4.3 and 4.4 respectively to asynchronous EV arrival (at the EVCS) and departure times, and to several EVCSs.

4.2 Smart charging of aggregated charging need at a charging station

Table 4.1: Notations of Section 4.2

Symbols	Signification
L	Charging need aggregated over all EVs at the EVCS
$\mathcal{T} = \{1, \dots, T\}$	Set of time slots t of equal duration δ
$\ell_t^{\text{tot}} = \ell_t^0 + \ell_t$	Sum of the charging and non-flexible (i.e cannot be scheduled) loads at t
$f_t = \eta_t \ell^2$	Time-dependent load cost function at t
$\bar{t}(L)$	Number of time slots used for the optimal charging profile for need L
L_t^0	Cumulative non-flexible load up to time t
$\overline{L}_t$	Energy threshold below which $\bar{t}(L) \leq t$
G^*	Optimal CSO's cost
E	Total PV generation during $\mathcal{T}$

4.2.1 Basic water-filling scheduling

4.2.1.1 Formulation of the aggregated charging scheduling problem

For the moment, there is only one EVCS considered, managed by a Charging Service Operator (CSO). The case where there are several EVCSs is mentioned in Section 4.4. The charging time period is discretized into several time slots. Here, the following assumption is made:

Assumption 4.1. *All EVs arrive at the EVCS at the same time slot and leave at the same time slot.*

This simplifying assumption is legitimate in the commuting use case, where the arrival time distribution is relatively peaky (variance of 22 minutes, see Figure 4.8). This assumption is relaxed in Section 4.3, where EVs may arrive at the EVCS and leave at different time slots.

Then, instead of determining the charging profile of each EV, the CSO only optimizes the *aggregated* charging profile, corresponding to the charging need L aggregated over all EVs at the EVCS. The numbers of variables and constraints are thus divided by the number of EVs, and an explicit solution is available (see for example Proposition 4.2). The disaggregation of the aggregated charging profile is assumed possible here: thanks to the potentially large number of EVs charging, and the compatible temporal constraints (synchronous arrivals and departures), the aggregated charging profile can be decomposed into charging profiles for every EV [Jacquot et al., 2019]. In practice, the underlying assumption is that at the EVCS, there are enough charging points for all EVs at any moment (no reservation or queuing effect here).

The scheduling problem is written in discrete time: the CSO schedules this aggregated charging need L among a finite number $T \geq 2$ of time slots $t \in \mathcal{T} \triangleq \{1, \dots, T\}$ of equal duration δ, representing the time period where EVs are all at the EVCS (see Assumption 4.1). More precisely, the CSO chooses the aggregated charging power ℓ_t during each time slot t in order to minimize a cost function, while fulfilling the aggregated charging need, i.e. $\sum_{t=1}^{T} \ell_t = L/\delta$. The cost function G of the CSO is assumed to be aligned with the costs/impact of the charging operation on the electrical grid (introduced later in Section 4.4.3). In practice, a specific electricity

contract would be signed between the CSO and the grid operator, determining the remuneration of the CSO for the effort made when flexibly scheduling EV load to minimize the impact of EV charging on the grid[1] (see Section 7.2.3). The grid costs associated with EV charging are mainly transformer aging [Hilshey et al., 2012], thermal overloading of cables [Hu et al., 2013], power losses due to Joule heating [Sortomme et al., 2010], impact on grid voltage [Geth et al., 2012] and impact on power quality [Gómez and Morcos, 2003]. In this thesis, the CSO's costs associated with an EVCS are reduced to a function of the total power load at this EVCS. Then, the CSO schedules EV charging in order to smooth the total power load at the EVCS throughout the working hours. To this end, the load cost function f_t associated with the total power load ℓ_t^{tot} at time slot t is assumed quadratic: $f_t(\ell_t^{\text{tot}}) = f(\ell_t^{\text{tot}}) = (\ell_t^{\text{tot}})^2$. Such a "proxy"[2] is widely used in the literature to model the local impact of electricity consumption on the electrical system [Mohsenian-Rad et al., 2010]. Note that the quadratic load cost function is extended to time-dependent monomials ($f_t(\ell_t^{\text{tot}}) = \eta_t(\ell_t^{\text{tot}})^n$) in Section 4.2.2.1.

This scheduling is not trivial since the CSO's costs may depend inherently on the time slot t via a time-dependent load function (e.g., solar panels generate electricity only during the day) and are increasing with the total electricity load ℓ_t^{tot} during that time slot [Wood and Wollenberg, 2012]. At each time slot t, the total electricity load ℓ_t^{tot} is made of two components: the aggregated charging power ℓ_t which is scheduled at t, and a *non-flexible (fixed) consumption* ℓ_t^0 which includes electrical usages that are present in charging locations where EVs are plugged (e.g., household appliances when charging at home, tertiary ones at professional sites, etc.). While non-flexible consumption ℓ_t^0 is a parameter of the charging problem, ℓ_t is the control variable. As modeled in [Mohsenian-Rad et al., 2010] (and in many other papers about EV smart charging), EV consumption has to be scheduled depending on other electrical usages, the impact on the grid being dependent on the total consumption (obtained as the sum of flexible and non-flexible profiles). The CSO is assumed to know in advance (before the first charging time slot) the non-flexible consumption ℓ_t^0 for all $t \in \mathcal{T}$. For the moment, the non-flexible terms ℓ_t^0 are assumed non-negative (only consumption), but the scheduling problem is extended to local electricity generation ($\ell_t^0 < 0$) in Section 4.2.2.2.

Formally, the charging problem solved by the CSO is stated as follows:

$$\min_{(\ell_t)_t} G(\boldsymbol{\ell}) \ , \quad \text{such that} \quad \begin{cases} \ell_t \geq 0 \ \ \forall t \in \mathcal{T} \, , \\ \sum_{t=1}^{T} \ell_t = L/\delta \, , \end{cases} \qquad \text{with} \ \ G(\boldsymbol{\ell}) = \sum_{t=1}^{T} f_t\left(\ell_t^0 + \ell_t\right) \ , \qquad (\mathcal{S})$$

where $G(\boldsymbol{\ell})$ is the objective of the CSO in function of the aggregated charging profile $\boldsymbol{\ell}$. Note that G depends implicitly on the non-flexible profile $\boldsymbol{\ell}^0$. For a global charging need L issued from the driving problem (second constraint in ($\mathcal{S}$)), the CSO has to determine the aggregated charging profile $\boldsymbol{\ell} = (\ell_1, \ldots, \ell_T)$ which minimizes the total charging cost. This problem is parametrized by both the global charging need L (from the driving problem, so endogenous in the coupled charging-driving model) and the non-flexible load profile $\boldsymbol{\ell}^0$ (exogenous). The explicit solution of the minimization problem ($\mathcal{S}$) introduced in the present section is given in the following.

4.2.1.2 Water-filling resolution

The minimization problem ($\mathcal{S}$) has a strictly convex objective function (as f is quadratic) and linear constraints, so that the optimal value and aggregated charging profile solutions of ($\mathcal{S}$) are

[1] In France see the "Offres de Raccordement Intelligentes" by Enedis for an example of such a remuneration scheme.

[2] It does not include dynamic or location effects.

unique. As ($\mathcal{S}$) is more precisely a quadratic optimization problem (QP), its unique solution is easily found, for example by built-in Python function *minimize* (in SciPy package), which relies on a sequential least squares programming method [Boggs and Tolle, 1995]. However, it is important to ensure fast numerical computations in order to integrate this smart charging problem into the multilevel problem described in Chapter 7, considering ($\mathcal{S}$) may have a high number of variables[3]. Thus, the rest of the present chapter focuses on explicit formulations of the solution of ($\mathcal{S}$) and its extensions (in the following sections). Moreover, the following explicit formulations help for the analysis of Charging Unit Prices based on water-filling charging profiles (see Section 5.2.2 and 5.3.2). Suppose without loss of generality (because there are no dynamical effect taken into account here) that the non-flexible part of the load is ordered such that $\ell_1^0 \leq \cdots \leq \ell_T^0 \leq \ell_{T+1}^0 = +\infty$, where fictive time slot $T+1$ is added to unify notations. Considering the following auxiliary parameter $L_t^0 = \delta \sum_{s=1}^{t} \ell_s^0$, representing the cumulative non-flexible load up to time t, the solution of problem ($\mathcal{S}$) is given by the following proposition, and illustrated in Figure 4.2.

Proposition 4.2. *Given an aggregated charging need L and a non-negative non-flexible vector ℓ^0, the optimal aggregated charging profile $\boldsymbol{\ell}^*$ solution of the charging scheduling problem ($\mathcal{S}$) with a quadratic load function $f_t : \ell \mapsto \ell^2$ is:*

$$\ell_t^* = \begin{cases} \dfrac{L + L_{\bar{t}}^0}{\bar{t}(L) \times \delta} - \ell_t^0 & if \quad t \in \{0, \ldots, \bar{t}(L)\}\,, \\ 0 & if \quad t > \bar{t}(L)\,, \end{cases} \tag{4.1}$$

and the optimal value G^* is given by:

$$G^*(L) = \frac{\left(L + L_{\bar{t}}^0\right)^2}{\bar{t}(L) \times \delta^2} + \sum_{t=\bar{t}+1}^{T} \left(\ell_t^0\right)^2\,, \tag{4.2}$$

with $\bar{t}(L)$ such that $L \in \left]\overline{L}_{\bar{t}-1}, \overline{L}_{\bar{t}}\right]$ and $\overline{L}_{\bar{t}}$ the energy threshold defined as:

$$\forall t \in \{0, \ldots, T\},\ \overline{L}_t = t\delta \times \ell_{t+1}^0 - L_t^0 = \delta \sum_{s=1}^{t} \left(\ell_{t+1}^0 - \ell_s^0\right)\,. \tag{4.3}$$

Proof. The proof of Proposition 4.2 is given here in the case of a general differentiable and strictly convex function f (instead of only quadratic) and is inspired from [Boyd et al., 2004]. In this case, as the constraints constitute a convex set, this problem has a unique solution $(\ell_t)_t$. This solution verifies the Karush-Kuhn-Tucker necessary conditions corresponding to ($\mathcal{S}$):

$$\begin{cases} \forall t,\ \frac{\partial \mathcal{L}}{\partial \ell_t} = 0, \quad \frac{\partial \mathcal{L}}{\partial \mu} = 0\,, \\ \forall t,\ \nu_t \ell_t = 0\,, \\ \forall t,\ \nu_t, \ell_t \geq 0\,, \end{cases} \quad \text{with} \quad \begin{aligned} \mathcal{L} \quad = \quad & \sum_{t=1}^{T} \left(f\left(\ell_t^0 + \ell_t\right) - \nu_t \ell_t\right) \\ & - \mu \left(\sum_{t=1}^{T} \ell_t - L/\delta\right)\,. \end{aligned} \tag{4.4}$$

The first order condition with respect to ℓ_t for any t gives:

$$f'\left(\ell_t^0 + \ell_t\right) - \mu - \nu_t = 0, \tag{4.5}$$

[3]The variables are the aggregated charging power for each time slot, each EVCS (see Section 4.4) and each EV class (see Section 4.3).

which in turn implies:

$$\begin{cases} f'\left(\ell_t^0 + \ell_t\right) - \mu \geq 0 & \textit{since} \quad \nu_t \geq 0, \\ \ell_t\Big(f'\left(\ell_t^0 + \ell_t\right) - \mu\Big) = 0 & \textit{since} \quad \ell_t \times \nu_t = 0. \end{cases} \tag{4.6}$$

As f is strictly convex, f' is increasing so all ℓ such that $f'(\ell) = \mu$ are equal (injectivity) to $M = (f')^{-1}(\mu)$. Using respectively each relation of the previous system:

1. either $\ell_t = 0$ and $\ell_t^0 \geq M$, with M independent in time;
2. or $0 < \ell_t = M - \ell_t^0$, so $\ell_t^0 < M$.

Assuming $L \neq 0$, there must exist t such that $\ell_t^0 < M$: let $\bar{t}$ be the maximum of these t. Because $\left(\ell_t^0\right)_t$ is non-decreasing, $\ell_t^0 < M$ is verified for all $t \leq \bar{t}$ so $\ell_t = M - \ell_t^0$ for such t. For $t > \bar{t}$, $\ell_t = 0$. Then, the first order condition with respect to μ gives:

$$M = \frac{L/\delta + \sum_{t=1}^{\bar{t}} \ell_t^0}{\bar{t}} \,. \tag{4.7}$$

Thanks to this last relation, we can deduce (4.1) and (4.2). Last, by definition of $\bar{t}$, we have $\ell_{\bar{t}}^0 < M$ and $\ell_{\bar{t}+1}^0 \geq M$, which gives respectively:

$$0 < \ell_{\bar{t}} = \frac{L - \overline{L}_{\bar{t}-1}}{\bar{t} \times \delta} \quad \textit{and} \quad 0 \geq M - \ell_{\bar{t}+1}^0 = \frac{L - \overline{L}_{\bar{t}}}{\bar{t} \times \delta}, \tag{4.8}$$

meaning that $L \in \left]\overline{L}_{\bar{t}-1}, \overline{L}_{\bar{t}}\right]$. □

Notation. *Note the difference between functions G and G^*. The CSO's objective G is a function of the aggregated charging profile. The optimal value $G^* = G(\boldsymbol{\ell}^*)$ of CSO's objective function obtained with the water-filling charging profile $\boldsymbol{\ell}^*(L)$ is a function of the aggregated charging need L. It can be written as:*

$$G^*(L) = G\big(\boldsymbol{\ell}^*(L)\big) \,. \tag{4.9}$$

The proof of Proposition 4.2 actually shows that any increasing and convex function f leads to the same optimal charging profile $\boldsymbol{\ell}^*$ (but not the same optimal value G^*). The valley-filling structure (see Figure 4.2) of the optimal solution is directly observable in (4.2): while the first $\bar{t}$ ordered time slots contribute equally to the total cost at optimum (they share the same water level, sum of non-flexible plus EV consumption), the next ones ($t \geq \bar{t} + 1$) provide different contributions corresponding only to the non-flexible part of consumption, as they are not used for charging. Figure 4.2 illustrates this on a simple example of a non-flexible ordered vector for $T = 4$ time slots (orange bars). The first two energy thresholds $\overline{L}_1 < \overline{L}_2$ are shown (respectively dotted and tight dashed bars). As the aggregated charging need L (loose dashed bars) is higher than $\overline{L}_2$ but lower than $\overline{L}_3$ (delimited by black horizontal dashed line at level ℓ_4^0), the optimal aggregated charging profile only uses the first $\bar{t}(L) = 3$ time slots.

Remark 4.3. *The energy thresholds are initially defined recursively, by*

$$\begin{cases} \overline{L}_0 = 0 \,, \\ \overline{L}_t = \overline{L}_{t-1} + t\delta\left(\ell_{0,t+1} - \ell_{0,t}\right) \,. \end{cases} \tag{4.10}$$

The meaning of $\overline{L}_t$ is that this is the energy threshold from which the CSO starts using time slot $t+1$ to charge part of the aggregated charging need $L \geq \overline{L}_t$.

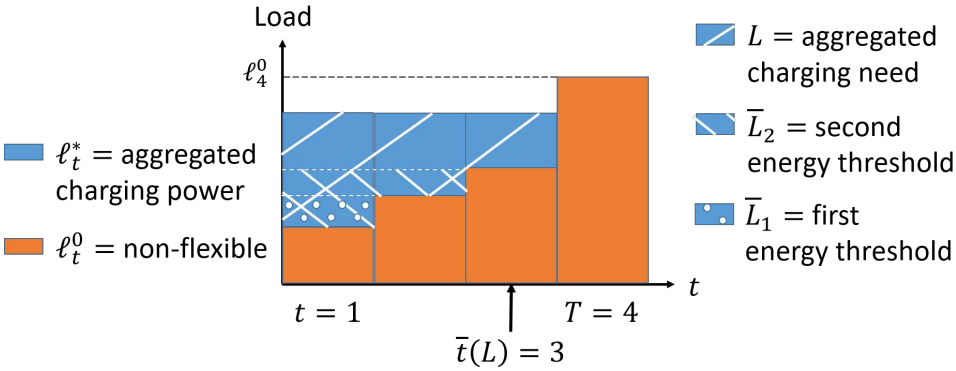

Figure 4.2: Illustration of the water-filling charging profile solution (blue bars) of the charging scheduling problem ($\mathcal{S}$), given in Proposition 4.2. *The aggregated charging need L (loose dashed bars) verifies $\overline{L}_2 < L < \overline{L}_3$, with the energy thresholds $\overline{L}_2, \overline{L}_3$ respectively represented by tight dashed bars, and delimited by dotted line ℓ_4^0. Therefore, L is charged during the first $\overline{t}(L) = 3$ time slots.*

Remark 4.4. *Concerning the Vehicle to Grid (V2G) functionality, mathematically, it extends the set of charging decisions, and can thus in general decrease the grid cost*[4] *G^*. In practice, the technology is not massively implemented yet. For example in France, except for some experimental test-beds, injected electricity is not compensated financially; "reverse flows" in the distribution network may be potentially harmful for the local distribution grid [Habib et al., 2015], etc. Where V2G is available, the reinjection functionality is mainly operated at a given consumption node ("V2Home"). On this basis, we chose not to consider the V2G for the sake of realism, but also to focus on other key - and complex - methodological aspects, starting with a multilevel framework (see Part III) combined with smart charging.*

However, integrating the V2G technology in the smart charging problem ($\mathcal{S}$) is somehow straightforward. Function f_t of ($\mathcal{S}$) should represent both the load cost when $\ell_t + \ell_t^0 > 0$, and a financial compensation when $\ell_t + \ell_t^0 < 0$. Convexity of f_t would be appreciated to conduct a theoretical study (existence and uniqueness of a solution of this new scheduling problem). In addition, there would be additional constraints:

$$\forall t, \quad S_{\min} \leq \overbrace{S_0 + \sum_{s \leq t} \ell_{i,s}}^{\triangleq S_t} \leq S_{\max}\,, \tag{4.11}$$

with S_0 the "aggregated State of Charge[5] *(SoC)" over all EVs' batteries at the beginning of the day (i.e., the sum of the individual SoC of all the EVs connecting to the station). $S_{\min}$ and $S_{\max}$ are respectively the minimal and maximal SoC aggregated over all EVs. We did not find any analytical nor algorithmic solution for this new scheduling problem yet, in part because the new constraints couple the different time slots.*

The results obtained in Proposition 4.2 are extended in next section, respectively for time-dependent load cost functions f_t and local electricity generation $\boldsymbol{\ell}^0 \leq 0$ at the EVCS.

[4]Note however that there can be negative effects induced by battery cycling, mainly battery aging [Zhou et al., 2011].

[5]The State of Charge of an EV is the level of charge of its battery relative to its capacity.

4.2.2 Extensions of the water-filling scheduling

4.2.2.1 Time-dependent load cost function

Compared to the basic case covered by Proposition 4.2 in previous section, the cost associated with the total power load ℓ_t^{tot} during time slot t depends on the time slot itself in this section. These results are part of our paper [Sohet et al., 2021b]. The load cost functions f_t are extended to any monomial cost function (instead of only quadratic ones):

$$\forall t \in \mathcal{T}\,, \quad f_t(\ell_t^{\text{tot}}) = \eta_t(\ell_t^{\text{tot}})^n \qquad (n \geq 2) \tag{4.12}$$

with parameters $\eta_t > 0$. Thanks to these parameters, it is possible to put more or less weight on some time slots for the charging scheduling optimization. For example, these parameters may be chosen by the grid operator as an incentive for the CSO.

Proposition 4.5. *Let the load cost functions $f_t : \ell \mapsto \eta_t \ell^n$ be monomials as in (4.12). Given a non-flexible vector $\boldsymbol{\ell}^0$ and a global charging need L, let $\bar{t}(L)$ be such that $L \in \left]\overline{L}_{\bar{t}-1}, \overline{L}_{\bar{t}}\right]$, where $\overline{L}_t = \delta\left[\sum_{s=1}^{t}(\eta_{t+1}/\eta_s)^{1/(n-1)}\right]\ell_{t+1}^0 - L_t^0$ for $t \in \mathcal{T}$ are the energy thresholds. Then the aggregated charging profile solution of the charging scheduling problem ($\mathcal{S}$) is:*

$$\ell_t^* = \begin{cases} \dfrac{\eta_t^{-\frac{1}{n-1}}}{\delta\sum_{s=1}^{\bar{t}}\eta_s^{-\frac{1}{n-1}}}\left(L + L_{\bar{t}}^0\right) - \ell_t^0 & \text{if} \quad t \in \{0, \ldots, \bar{t}(L)\}\,, \\ 0 & \text{if} \quad t > \bar{t}(L)\,, \end{cases} \tag{4.13}$$

and yields the optimal value:

$$G^*(L) = \Big(\sum_{s=1}^{\bar{t}}\eta_s^{-\frac{1}{n-1}}\Big)^{-(n-1)} \times \left(\frac{L + L_{\bar{t}}^0}{\delta}\right)^n + \sum_{t=\bar{t}+1}^{T} f_t\left(\ell_t^0\right)\,. \tag{4.14}$$

Proof. As in previous section, without loss of generality, time slots are assumed to be ordered by marginal cost $f_t'(\ell_t^0)$, i.e. $f_1'(\ell_1^0) \leq f_2'(\ell_2^0) \leq \ldots \leq f_T'(\ell_T^0)$. At the optimal scheduling of a given charging need L, time slots used share the same marginal cost, lower than the marginal costs of the unused time slots. This way, the CSO schedules L in the order of time slot indices ($t = 1$, then $t = 2$, etc.).

As a consequence, energy thresholds $\overline{L}_t$ are defined as the charging need from which the CSO starts using time slot $t+1$ ($0 \leq t < T$). If the charging need is equal to the energy threshold $\overline{L}_t$ (for any t), it is scheduled (solution written $\boldsymbol{\ell}^{(t)}$) among the time slots already used ($s \leq t$) and so that the resulting marginal costs are all equal to the one of the empty time slot $t+1$: $f_s'\left(\ell_s^0 + \ell_s^{(t)}\right) = f_{t+1}'\left(\ell_{t+1}^0\right)$, i.e. $(n-1)\eta_s\left(\ell_s^0 + \ell_s^{(t)}\right)^{n-1} = (n-1)\eta_{t+1}\left(\ell_{t+1}^0\right)^{n-1}$. As cost functions f_t are convex, this method ensures that the marginal cost associated with each infinitesimal portion of $\overline{L}_t$ was lower than $f_{t+1}'\left(\ell_{t+1}^0\right)$. Mathematically, $\overline{L}_t = \sum_{s=1}^{t}\ell_s^{(t)}$ with:

$$\begin{cases} \ell_s^{(t)} = \left(\frac{\eta_{t+1}}{\eta_s}\right)^{\frac{1}{n-1}}\ell_{t+1}^0 - \ell_s^0 & \text{for } s \leq t\,, \\ \ell_s^{(t)} = 0 & \text{for } s > t\,, \end{cases} \tag{4.15}$$

using the marginal costs equality, which yields the energy thresholds formula.

Thus, if $\bar{t}(L)$ is such that the charging need L is in $]\overline{L}_{\bar{t}-1}, \overline{L}_{\bar{t}}]$, then the optimal charging profile $\boldsymbol{\ell}$ is such that for $t > \bar{t}(L)$, $\ell_t = 0$ and for $t \leq \bar{t}(L)$, $f_t'\left(\ell_t^0 + \ell_t\right) = f_1'\left(\ell_1^0 + \ell_1\right)$, so that $\ell_t^0 + \ell_t = \left(\frac{\eta_1}{\eta_t}\right)^{\frac{1}{n-1}} \left(\ell_1^0 + \ell_1\right)$ and:

$$\begin{aligned} G^*(L) &= \sum_{t=1}^{\bar{t}} \eta_t \left(\frac{\eta_1}{\eta_t}\right)^{\frac{n}{n-1}} \left(\ell_1^0 + \ell_1\right)^n + \sum_{t=\bar{t}+1}^{T} f_t(\ell_t^0)\,, \\ &= \eta_1 \sum_{t=1}^{\bar{t}} \left(\frac{\eta_1}{\eta_t}\right)^{\frac{1}{n-1}} \left(\ell_1^0 + \ell_1\right)^n + \sum_{t=\bar{t}+1}^{T} f_t(\ell_t^0)\,. \end{aligned} \tag{4.16}$$

Finally, ℓ_1 is deduced using constraint $L = \delta \sum_{t=1}^{T} \ell_t = \delta \sum_{t=1}^{\bar{t}} \ell_t$, which gives:

$$\ell_1^0 + \ell_1 = \left(\sum_{t=1}^{\bar{t}} \left(\frac{\eta_1}{\eta_t}\right)^{\frac{1}{n-1}}\right)^{-1} \frac{L + L_{\bar{t}}^0}{\delta}\,, \tag{4.17}$$

and both formulas for G^* and $\boldsymbol{\ell}^*$ follow. □

Remark 4.6. *When the load cost functions f_t are time-dependent as in (4.12), the corresponding optimal aggregated charging profile is likely to differ from a water-filling structure, due to the differences between parameters η_t.*

Note that some properties (like convexity) of the solution G^* of time-dependent ($\mathcal{S}$) given in Proposition 4.5 are studied in Section 5.2.2 in order to define the smart Charging Unit Prices studied in this thesis.

4.2.2.2 Self-consumption of local electricity generated at charging station

This section extends the charging scheduling to the case where an EVCS owns PhotoVoltaïc (PV) solar panels and can self-consume the electricity generated from it, for the non-flexible electricity usages or for EV charging. This way, the CSO needs to buy less electricity from the grid and therefore reduces its costs. Local electricity storage for PV generation is not considered here. Its presence could decrease the net load during some time slots and, in turn, the impact on the grid.

In the present section, load cost functions are assumed quadratic and time-independent, as in Section 4.2.1. In the corresponding Proposition 4.2, the non-flexible energy vector $\boldsymbol{\ell}^0$ is assumed non-negative, meaning that only non-flexible consumption is considered, or that there can be local electricity generation at the EVCS but it is negligible compared to the non-flexible consumption terms and entirely self-consumed by them. The case when there is more non-flexible generation than consumption – and therefore some locally generated electricity available for EV charging – can be treated in two different manners, depending on the remuneration associated with unused PV generation.

No remuneration for unused PV.
If there is no remuneration associated with unused PV electricity, the load cost function, represented in Figure 4.3, can be written:

$$f\left(\ell_t^{\text{tot}}\right) = \begin{cases} 0 & \text{if } \ell_t^{\text{tot}} \leq 0\,, \\ \left(\ell_t^{\text{tot}}\right)^2 & \text{if } \ell_t^{\text{tot}} > 0\,. \end{cases} \tag{4.18}$$

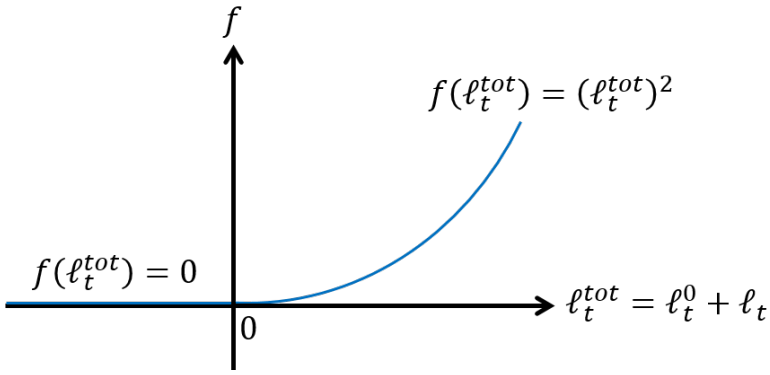

Figure 4.3: Load cost f at time slot t in function of EV charging ℓ_t and PV generation ℓ_t^0 (through the net total load ℓ_t^{tot}), in the case of no remuneration for unused PV. *If PV generation is higher (resp. smaller) than EV charging load, there is no (resp. a quadratic) impact.*

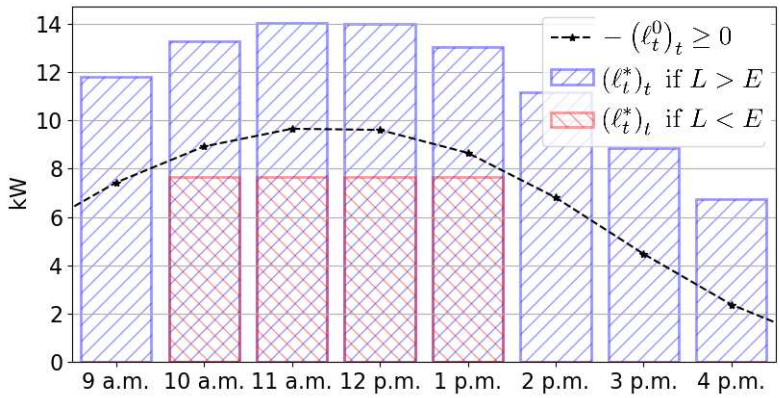

Figure 4.4: Water-filling optimal scheduling of the charging operation considering PV electricity generation (in black), for two different aggregated charging needs L (in blue and red). *For the red bars, any scheduling using only PV generation is optimal, while for blue bars, the only optimal scheduling uses the whole PV generation plus the same amount (blue bars minus black line is constant) from the electrical grid at each time slot.*

This load cost function is quadratic when the net load is positive and zero if not. This is the assumption made in our paper [Sohet et al., 2019b]. Then, the CSO maximizes the self-consumption of its PV generation.

In the particular case where $\ell_t^0 \leq 0$ for all t, the solution of problem ($\mathcal{S}$) with load functions defined in (4.18) only depends (relatively to L) on the total PV energy $E = \delta \sum_{t=1}^{T} \ell_t^0$ generated during working hours $\mathcal{T}$, and not on the profile $\boldsymbol{\ell}^0$ shape. To illustrate that, the PV profile in Figure 4.4 is considered, and corresponds to a total generation of $E = 57.9$ kWh (between 9 a.m. and 5 p.m.).

- If the aggregated charging need L verifies $L < E$, any charging profile below the PV generation is optimal, since the associated cost is zero. In such cases, the optimal charging profile does not have necessarily a water-filling shape.

- If $L = E$, the optimal scheduling has to perfectly match the generation.

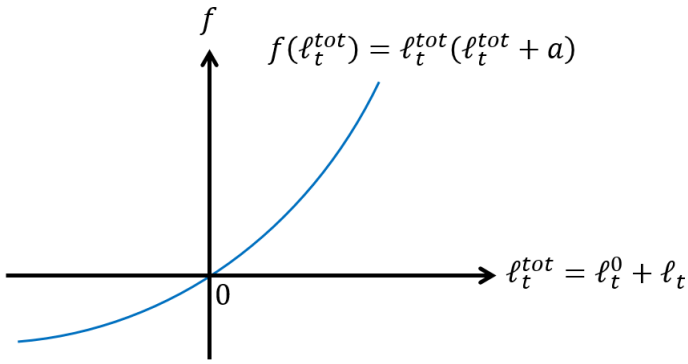

Figure 4.5: Load cost f at time slot t in function of EV charging ℓ_t and PV generation ℓ_t^0 (through the net total load ℓ_t^{tot}) in case of convex remuneration. *In this case, the CSO is remunerated when re-injecting PV generation into the grid, with the remuneration per energy unit decreasing with the total energy re-injected. This is due to parameter a which translates the original quadratic function.*

- If $L > E$, all PV generation is consumed and the remaining charging need has to be equally shared between all time slots, and the net load taken from the grid is constant.

The corresponding optimal CSO's cost G^* is equal to:

$$G^*(L) = \begin{cases} 0 & \text{if } \; L \leq E\,, \\ \frac{1}{T}\left(-E + L\right)^2 & \text{if } \; L > E\,. \end{cases} \tag{4.19}$$

Note that the optimal charging profile would be the same if the remuneration associated with unused PV electricity was linear: $f(\ell_t^{\text{tot}}) = \eta^- \ell_t^{\text{tot}}$ for $\ell_t^{\text{tot}} \leq 0$ with $\eta^- \geq 0$. Similarly, there would be no priority to charge EVs during time slots with high PV generation first, as long as as much PV generation as possible is used for EV charging during the working hours in general.

The coupling between this smart charging problem and EV users behavior can be found in Section 6.2.

Convex remuneration for unused PV.
In the case when there is more PV generation than EV charging, the CSO could be remunerated when re-injecting what is left of the PV generation into the grid. However, as too much electricity re-injected may be potentially harmful for the local distribution grid, this remuneration decreases with the quantity re-injected[6]. Therefore, the increasing and quadratic function f, initially used to model during a time slot the load cost when the total load is positive, can be extended to negative total loads (see Figure 4.5). In such a case, the optimal charging profile is the same as the one obtained in Proposition 4.2, meaning that EVs are charged in priority during time slots with the highest PV generation, unlike in Figure 4.4, in red, where EVs can be charged randomly during all the time slots when there is PV generation. This is the assumption made in our conference paper [Sohet et al., 2021a].

[6]See taxes on network companies: https://bofip.impots.gouv.fr/bofip/797-PGP.html/identifiant=BOI-TFP-IFER-30-20210210 (in French).

4.3 Online smart charging of asynchronous charging needs

Table 4.6: Notations of Section 4.3

Symbols	Signification
$\mathcal{R}$	Set of couples (a, d) of arrival $a \in \mathcal{T}$ and departure $d \in \mathcal{T}$ times
$L^{(a,d)}$	Charging need aggregated over EVs arriving at a and leaving at d (class (a, d))
a^-	Last EV arrival time considered
L_a^d	Charging need left to charge from a of EVs leaving at d
$\mathcal{D}_a$	Departure times' set of *charging* EVs at a
$\ell_t^{(a,d)}$	Charging load at t aggregated over EV class (a, d)
$\boldsymbol{\ell}^{\mathrm{WF}}$	Charging load solution of basic water-filling
$\tilde{G}^a, \left(\tilde{\ell}_{a,t}^d\right)_t$	Optimal CSO's cost and charging profile for charging need L_a^d

Notation. *Note that in this Section 4.3 compared to the rest of this chapter, the optimal charging profiles and CSO's cost are denoted with a $\sim$ instead of a $*$. For example, the optimal CSO's cost corresponding to the online charging scheduling at arrival time a is denoted $\tilde{G}^a$ instead of $(G^a)^*$, to avoid multiple exponents.*

In this section, the charging scheduling results of Proposition 4.2 – with time-independent load cost function f – are extended to the case where EVs may arrive at the EVCS and leave at different time slots. The CSO does not necessarily have this information in advance. There exist papers such as [He et al., 2012, Chen et al., 2014] which deal with this asynchronous charging need using an online charging scheduling, where the CSO solves an optimization problem at each time slot using the newly available EV information, but no simple explicit solution is given. The following is largely inspired from our conference paper [Sohet et al., 2021a]. The smart Charging Unit Prices based on the following charging schedulings can be found in Section 5.3.3. Note that the optimal charging profiles found in the present section are the same[7] for all increasing and convex time-independent load cost functions f.

4.3.1 Asynchronous charging scheduling framework

The EVs are divided into different classes (a, d), depending on their arrival a and departure d time slots at the EVCS. More precisely, EVs of class (a, d) arrive at the EVCS at the beginning of time slot $a \in \mathcal{T}$ and leave at the end of time slot $d \in \mathcal{T}$, and therefore may only charge during time slots $\{a, \dots, d\}$. For example if $d = a$, the corresponding EV class only charges during time slot a. The set of times' pairs (a, d) is written $\mathcal{R} \subseteq \mathcal{T} \times \mathcal{T}$. The charging need aggregated over all EVs of class (a, d) is written $L^{(a,d)}$.

For each class (a, d), the CSO wants to determine the charging power $\ell_t^{(a,d)}$ at each time slot $t \in \{a, \dots, d\}$ aggregated over all EVs of class (a, d), so that the corresponding aggregated charging need $L^{(a,d)}$ is fulfilled at departure time slot d, i.e. $\sum_{t=a}^{d} \ell_t^{(a,d)} = L^{(a,d)}/\delta$. For all t, $\ell_t^{(a,d)} \geq 0$ but, as mentioned in Remark 4.4, vehicle to grid could constitute a direct extension of this work by relaxing this constraint.

[7] This is not the case for the optimal CSO's costs $\tilde{G}$ and $\tilde{G}^a$, respectively defined in the offline and online Sections 4.3.2 and 4.3.3.

The per-class aggregated charging profile selected by the CSO (vector written $\tilde{\boldsymbol{\ell}}$) is the one minimizing some charging cost function (whose minimum value is written $\tilde{G}$), which also depends on non-flexible electrical usages $\boldsymbol{\ell}^0$ at the EVCS. Even if this term can include both electricity generation and consumption, it will be simply called "consumption" in the following to get a generic terminology. At a given time slot t, the charging cost is represented by an increasing and convex function f of the total power load $\ell_t^0 + \sum_{(a,d)} \ell_t^{(a,d)}$, and f does not depend on the time slot t, as in Section 4.2.1.

The next two sections introduce two different charging scheduling problems, depending on the information available to the CSO. Keep in mind however that in both problems, the CSO is assumed to know in advance (before the first charging time slot) the non-flexible consumption $\boldsymbol{\ell}^0$ over all time slots. For example, the local electricity generation of the day can be accurately predicted the day before by using weather models, and the non-flexible consumption using statistical data collected at the EVCS.

4.3.2 Offline charging scheduling

In this section, the CSO is assumed to know in advance all arrival a and departure d time slots and the corresponding charging needs $L^{(a,d)}$ before the beginning of the whole time period $\mathcal{T}$. In practice, all EV users could declare this information through the connected dashboard of the vehicle before the first charging time slot, or the CSO could base the values $L^{(a,d)}$ on statistical data. Therefore, the CSO can compute the optimal charging profiles *offline*, i.e. before the first charging time slot, by solving the following charging scheduling problem ($\mathcal{P}$):

$$\min_{(\ell_t^{(a,d)})_{a\le t\le d}^{(a,d)\in\mathcal{R}}} \sum_{t=1}^{T} f\Big(\ell_t^0 + \sum_{(a,d)\in\mathcal{R}} \ell_t^{(a,d)}\Big), \quad \text{s.t. } \forall (a,d)\in\mathcal{R}, \begin{cases} \sum_{t=a}^{d} \ell_t^{(a,d)} = L^{(a,d)}/\delta\,, \\ \ell_t^{(a,d)} \ge 0\,,\ \forall t\in\{a,\dots,d\}\,. \end{cases} \tag{$\mathcal{P}$}$$

It is difficult to find an explicit charging scheduling solution of ($\mathcal{P}$) compared to ($\mathcal{S}$) due to the interdependence of the aggregated charging needs $L^{(a,d)}$ of all EV classes. However, the objective function to minimize in ($\mathcal{P}$) is still convex (because f is). Then, this convex optimization problem can be easily solved using a sequential least squares programming method [Boggs and Tolle, 1995]. Moreover, there is a unique minimal value $\tilde{G}$, even if several possible optimal charging profiles $\tilde{\boldsymbol{\ell}} = (\ell_t^{(a,d)})_{a\le t\le d}^{(a,d)\in\mathcal{R}}$ may exist.

In practice, such a scheduling may suffer from forecast errors made on arrival and departure time slots "seen from" time slot 0 (i.e. the time when the problem is solved), due to unexpected events on the transportation network for example. However, this ideal offline problem where all EV classes' demands are supposed to be known in advance can provide an upper bound for the performance of a more realistic method presented below, in order to measure its efficiency.

4.3.3 Online charging scheduling

In this section, a more realistic assumption on the CSO's access to information is considered. Here, the CSO does not know all the arrival and departure times in advance: the CSO knows the arrival/departure time slots of an EV and its charging need only when the EV arrives at the EVCS (and communicates this information to the CSO). Therefore, for the whole time period $\mathcal{T}$, the CSO waits for the next EV arrival to update charging scheduling decisions.

4.3.3.1 Description of the online procedure

At each EV arrival time slot $a \in \{1, \dots, T\}$ at the EVCS, the CSO does the following procedure:

1. Update the quantities L_a^d left to charge from this arrival time slot a to all possible departure times $d \in \{a, \dots, T\}$. For each $d \geq a$, L_a^d is made of the charging need $L^{(a,d)}$ aggregated over EVs which arrived at a and leave at d, plus the charging need left to charge of EVs which arrived earlier (and leave also at d). This charging need corresponds to the quantity $L_{a^-}^d$ which was left to charge from the previous EV arrival[8] time slot a^- (up to departure time d), minus the amount $\delta \times \sum_{t=a^-}^{a-1} \tilde{\ell}_{a^-,t}^d$ (with $\tilde{\ell}_{a^-,t}^d$ defined in step 2) that has already been charged since a^-:

$$\forall d \in \{a, \dots, T\}, \quad L_a^d = L_{a^-}^d - \delta \sum_{t=a^-}^{a-1} \tilde{\ell}_{a^-,t}^d + L^{(a,d)} . \tag{4.20}$$

   Note that at the first EV arrival time slot a, the quantity L_a^d is simply equal to $L^{(a,d)}$. The (increasingly) ordered set of departure times $d \in \{a, \dots, T\}$ where $L_a^d > 0$ is denoted $\mathcal{D}_a$. Seen from instant a, it corresponds to all the (future) departure times for which a non-zero charging need has to be satisfied;

2. Use Algorithm 4.1 to compute the optimal value $\tilde{G}^a$ and per-class aggregated charging profile $\left(\tilde{\ell}_{a,t}^d\right)$ $(d \in \mathcal{D}_a,\ a \leq t \leq d)$, solutions of the following problem $(\mathcal{P}(\boldsymbol{L}_a))$. This problem corresponds to the charging scheduling of the per-class remaining energy needs $\boldsymbol{L}_a = \{L_a^d,\ \forall d \in \mathcal{D}_a\}$ left to charge at arrival time a:

$$\min_{(\ell_{a,t}^d)_{a \leq t \leq d}^{d \in \mathcal{D}_a}} \sum_{t=a}^{T} f\left(\ell_t^0 + \sum_{d \in \mathcal{D}_a} \ell_{a,t}^d\right) \quad \text{s.t. } \forall d \in \mathcal{D}_a, \begin{cases} \sum_{t=a}^{d} \ell_{a,t}^d = L_a^d/\delta\,, \\ \ell_{a,t}^d \geq 0,\ \forall t \in \{a, \dots, d\}\,. \end{cases} \tag{$\mathcal{P}(\boldsymbol{L}_a)$}$$

   Note that $\ell_{a,t}^d$ is the charging power *programmed* for time slot t and aggregated over all EVs which arrived at the EVCS at a or before and leave at d: $\ell_{a,t}^d = \sum_{b=1}^{a} \ell_t^{(b,d)}$. The charging power of these EVs at time t may be updated later due to future EV arrivals.

4.3.3.2 Analysis of online procedure and proof of optimality

By following this two-step procedure for the whole time period $\mathcal{T}$, the CSO minimizes at each arrival time slot a the corresponding charging costs $\tilde{G}^a$ (objective function of $(\mathcal{P}(\boldsymbol{L}_a))$). This procedure only gives, at each time slot t and for all departure time slots $d \geq t$, the optimal charging power aggregated over *all* EVs leaving at d and which arrived at t *or before*. This power is given by the last update $\tilde{\ell}_{\underline{t},t}^d$ done by Algorithm 4.1 at $\underline{t}$, the last EV arrival time slot before *or at*[9] t. Then, there are infinite ways to dispatch this power among the different EV classes (a, d) arriving at $a \leq \underline{t}$ and leaving at d, so that $\sum_{a=1}^{\underline{t}} \tilde{\ell}_t^{(a,d)} = \tilde{\ell}_{\underline{t},t}^d$. The fact that at each arrival time slot a, Algorithm 4.1 provides an optimal solution to problem $(\mathcal{P}(\boldsymbol{L}_a))$ relies on the basic water-filling solution given in Proposition 4.2, which is written $\boldsymbol{\ell}^{\mathrm{WF}}(L, \boldsymbol{\ell}^0)$ in the present section[10]. Unlike the offline problem for which an optimization solver is needed, the solution has

[8] For example, if some EVs arrived at the EVCS at the previous time slot, $a^- = a - 1$. If some EVs arrived at the first time slot and no EV arrived at the EVCS since, then $a^- = 1$, etc.

[9] Note the difference between notations a^- and $\underline{t}$. a^- is the last arrival time slot before *arrival* time slot a, and it is used in the two-step procedure. $\underline{t}$ is the last arrival time slot before *or at* time slot t (with t not necessarily an arrival time slot, except if $\underline{t} = t$), and it is used only to explain the two-step procedure.

[10] Note that between arrival and departure time slots a and d, the basic water-filling solution is completely characterized by the aggregated charging need and the non-flexible consumption profile during time period $[a, d]$.

Algorithm 4.1: (run at time a) Solution of $(\mathcal{P}(\boldsymbol{L}_a))$

Available information: departure times $\mathcal{D}_a$ and charging needs L_a^d, $\forall d \in \mathcal{D}_a$

1 **for** *each departure time* $d \in \mathcal{D}_a$ **do**

2 Optimal charging profile of EVs leaving at d using Water-Filling solution $\boldsymbol{\ell}^{\mathrm{WF}}$ (see Proposition 4.2):

$$(\tilde{\ell}_{a,t}^d)_{a \le t \le d} = \boldsymbol{\ell}^{\mathrm{WF}} \left(L_a^d \,, \left(\ell_t^0 + \sum_{u \in \mathcal{D}_a}^{u<d} \tilde{\ell}_{a,t}^u \right)_{a \le t \le d} \right) \tag{4.21}$$

end

3 Minimal CSO cost $\tilde{G}^a = \sum_{t=a}^{T} f\left(\ell_t^0 + \sum_{d \in \mathcal{D}_a} \tilde{\ell}_{a,t}^d\right)$ (with $\tilde{\ell}_{a,t}^d = 0$ for $t > d$)

Output: Charging profiles $(\tilde{\ell}_{a,t}^d)_{a \le t \le d}^{d \in \mathcal{D}_a}$ and cost $\tilde{G}^a$

here an explicit form; it is obtained without delay.

The core idea of Algorithm 4.1 is to first solve (solution written $\tilde{\boldsymbol{\ell}}_a^{d_1} = (\tilde{\ell}_{a,t}^{d_1})_{a \le t \le d_1}$) the standard charging scheduling problem $(\mathcal{S})$ introduced in Proposition 4.2 for EVs leaving the EVCS at the first departure time slot $d_1 \in \mathcal{D}_a$, in function of the per-class aggregated charging need $L_a^{d_1}$ and the non-flexible vector $\boldsymbol{\ell}^0$. Then, to solve this standard optimization problem $(\mathcal{S})$ for EVs leaving the EVCS at the second departure time slot d_2, in function of $L_a^{d_2}$ and a fictitious non-flexible vector $\boldsymbol{\ell}^0 + \tilde{\boldsymbol{\ell}}_a^{d_1}$ which includes the charging profile of EVs which will have left earlier at $d_1 < d_2$, and so on...

The following Proposition 4.7 proves that Algorithm 4.1 gives an optimal solution of $(\mathcal{P}(\boldsymbol{L}_a))$ at each EV arrival time slot a.

Proposition 4.7. *The output* $\tilde{\boldsymbol{\ell}}_a^d$ $(\forall d \in \mathcal{D}_a)$ *of Algorithm 4.1 is a solution of optimization problem* $(\mathcal{P}(\boldsymbol{L}_a))$*, for any EV arrival time slot* $a \in \mathcal{T}$*.*

Proof. This can be shown by recurrence according to the departure time slots, using Proposition 4.2 and the Karush-Kuhn-Tucker conditions, given that f is convex and differentiable. Let $(\tilde{\ell}_{a,t}^d)_{a \le t \le d}^{d \in \mathcal{D}_a}$ be the output of Algorithm 4.1. The sorted departure times set can be written $\mathcal{D}_a = \{d_1, \dots, d_H\}$ with H the set's cardinal. Let $\mathcal{D}_a^n = \{d_1, \dots, d_n\}$ and $\boldsymbol{L}_{a,n} = \{L_a^d,\ \forall d \in \mathcal{D}_a^n\}$. We are going to show that $P(n) =$ "$(\tilde{\ell}_{a,t}^d)_{a \le t \le d}^{d \in \mathcal{D}_a^n}$ is solution of $(\mathcal{P}(\boldsymbol{L}_{a,n}))$" for all $n \in \{1, \dots, H\}$ by recurrence, which will prove Proposition 4.7 because problems $(\mathcal{P}(\boldsymbol{L}_a))$ and $(\mathcal{P}(\boldsymbol{L}_{a,H}))$ are equivalent.

Initialization: By definition, problems $(\mathcal{P}(\boldsymbol{L}_{a,1}))$ and $(\mathcal{S})$ are equivalent, therefore $(\tilde{\ell}_{a,t}^{d_1})_{a \le t \le d} = \boldsymbol{\ell}^{\mathrm{WF}}\left(L_a^{d_1}, (\ell_t^0)_{a \le t \le d_1}\right)$ is solution of $(\mathcal{P}(\boldsymbol{L}_{a,1}))$.

Recurrence: For any $n \in \{1, \dots, H-1\}$ we show $P(n+1)$, assuming $P(n)$. Problem $(\mathcal{P}(\boldsymbol{L}_{a,n+1}))$ is convex and differentiable because function f is, so that it is equivalent to its Karush-Kuhn-Tucker (KKT) conditions:

$$\forall d \in \mathcal{D}_a^{n+1}, \forall t,\ \ell_{a,t}^d \times \left(\overbrace{f'\left(\ell_t^0 + \ell_{a,t}^{d_{n+1}} + \sum_{d \in \mathcal{D}_a^n} \ell_{a,t}^d\right) - \mu^d}^{\ge 0} \right) = 0, \tag{4.22}$$

with μ^d the (charging need) equality constraints Lagrange multipliers. We show that $(\tilde{\ell}_{a,t}^d)_{a \le t \le d}^{d \in \mathcal{D}_a^{n+1}}$ is solution of (4.22).

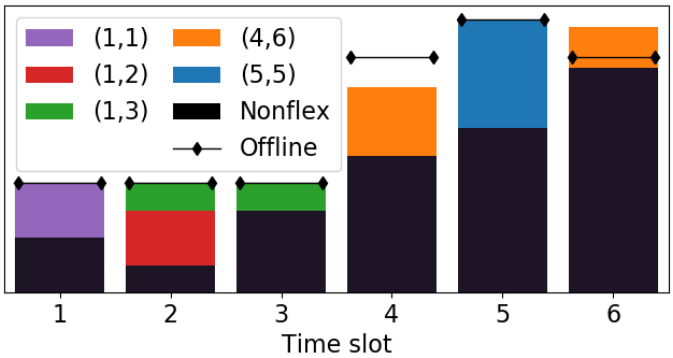

Figure 4.7: Example of the optimal charging profiles for five EV classes (a, d) (colored bars), computed with the online scheduling charging problem of Section 4.3.3 in function of a non-flexible consumption profile (black bars). *The resulting total power load is less smooth than the one obtained by solving the offline scheduling problem* $(\mathcal{P})$ *(diamond line), due to unexpected EV arrivals in the online procedure.*

By definition of $(\tilde{\ell}_{a,t}^{d_{n+1}})_{a \leq t \leq d}$ and the KKT conditions of $(\mathcal{S})$, (4.22) is verified for $d = d_{n+1}$ and all $t \in \{a, \ldots, d\}$, with $\mu^{d_{n+1}} = \mu_{n+1}$ the Lagrange multiplier of $(\mathcal{S})$.

Let $\mu_1, \ldots, \mu_n$ be the Lagrange multipliers of $(\mathcal{P}(\boldsymbol{L}_{a,n}))$. For $d_k \in \mathcal{D}_a^n$, there are two cases. For t such that $\ell_{a,t}^{d_{n+1}} = 0$, (4.22) is verified with $\mu^{d_k} = \mu_k$. Otherwise, (4.22) is verified with $\mu^{d_k} = \mu_{n+1}$. □

Note that the optimal charging profile $\tilde{\boldsymbol{\ell}}$ suggested in Algorithm 4.1 and solution of $(\mathcal{P}(\boldsymbol{L}_a))$ is not the only profile to give the unique minimal value $\tilde{G}^a$ of the corresponding charging cost function. For example, the algorithmic solution with some charging power "exchanged" between two EV classes and two time slots is also solution of $(\mathcal{P}(\boldsymbol{L}_a))$. The unique optimal value $\tilde{G}^a = \sum_{t=a}^{T} f(\ell_t^0 + \sum_{d \in \mathcal{D}_a} \tilde{\ell}_{a,t}^d)$ is used to define a Charging Unit Price for EV class (a, d) arriving at a and leaving at any $d \geq a$ (see Section 5.3.3). Note that this value $\tilde{G}^a$ may be different from the CSO's cost when these EVs leave the EVCS at some $d > a$. Indeed, if additional EVs arrive between a and d, the CSO updates the charging profiles and its costs with the online Algorithm 4.1.

Remark 4.8. *Algorithm 4.1 can actually be extended to problems with EV classes with presence time slots at the EVCS embedded in one another. For example, one EV class arrives at* $a_1 = 2$ *and leaves at* $d_1 = 3$*, and for another class,* $a_2 = 1$ *and* $d_2 = 4$*. However, if* $a_1 = 1$*,* $d_1 = 3$*,* $a_2 = 2$ *and* $d_2 = 4$*, this "embedded property" is not verified. Note that it is verified in the case of problem* $(\mathcal{P}(\boldsymbol{L}_a))$*, where all EV classes considered have the same arrival time slot* a*.*

4.3.3.3 Illustration of online charging scheduling on a simple example

The global online charging scheduling procedure is illustrated in Figure 4.7 with an example on a time period of $T = 6$ time slots (e.g., the working hours from 8 am to 8 pm with $\delta = 2$ h) and five EV classes. The CSO starts by scheduling the charging profile of the EV classes which arrive for the first charging time slot: $(1, 1)$, $(1, 2)$, $(1, 3)$. Following Algorithm 4.1, the CSO starts with EV class $(1, 1)$, which has no choice but to charge only during the first time slot. Then, the CSO charges EV class $(1, 2)$ only during the second time slot because of the high total power load in the first slot, due to EV class $(1, 1)$. Finally, the charging need of EV class $(1, 3)$ is

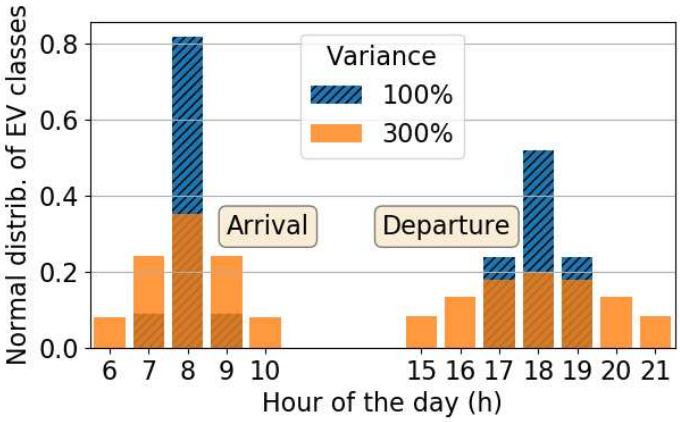

Figure 4.8: Arrival and departure discretized distributions, both with ENTD data and in the case where both variances were multiplied by three. *The arrival distribution is more peaky than the departure one.*

adequately split between the first three time slots in order to smooth the total power load over the first three time slots. When other EVs arrive at the fourth time slot, the charging needs of EV classes which arrived before have already been fulfilled. The CSO plans to charge EV class $(4, 6)$ during the fourth and fifth time slots. Unfortunately, at time slot $t = 5$, the CSO must charge EV class $(5, 5)$ which just arrived and has to postpone the charge of EV class $(4, 6)$ to the sixth and last time slot. If the CSO knew in advance that EVs would arrive at the fifth time slot, it could have charged more charging need of EV class $(4, 6)$ during the fourth time slot, as in the offline charging problem (diamond line).

4.3.4 Illustration and comparison of online and offline schedulings on asynchronous commuting.

4.3.4.1 Commuting framework with real data

The offline and online charging problems are illustrated on the use case of commuting, where workers leave their EVs plugged in at an EVCS during working hours. As in Section 4.2.2.2, the EVCS is assumed to own PhotoVoltaic (PV) solar panels and use its PV generation to charge EVs and re-inject the remainder into the grid. This PV generation is the only non-flexible term at the EVCS, and thus the vector $\boldsymbol{\ell}^0$ is non-positive. The data[11] used for the PV generation comes from [Pfenninger and Staffell, 2016a] and represents the hourly generation of a 560 kilowatt peak panel during a random[12] day (January 15, 2014) in Paris (see green piecewise constant curve in Figure 4.9). The load cost function $f : \ell \mapsto \ell^2$ is supposed quadratic. The CSO wants to minimize its costs by scheduling the EV charging during this day.

The distribution of EVs in the different (a, d) classes is given by the data from the French mobility survey [CGDD, 2010]. The arrival and departure time slots are both modeled by independent normal distributions, respectively with means 8 am and 6 pm and variances 22 and 45 minutes (the arrival distribution is more peaky, as is the morning peak in France). These distributions are discretized into time slots of one hour (following the PV generation data discretization) and shown in Figure 4.8, with ENTD data and in the case where both variances

[11] Available at https://www.renewables.ninja/.
[12] The choice of the day does not affect the nature of the numerical results.

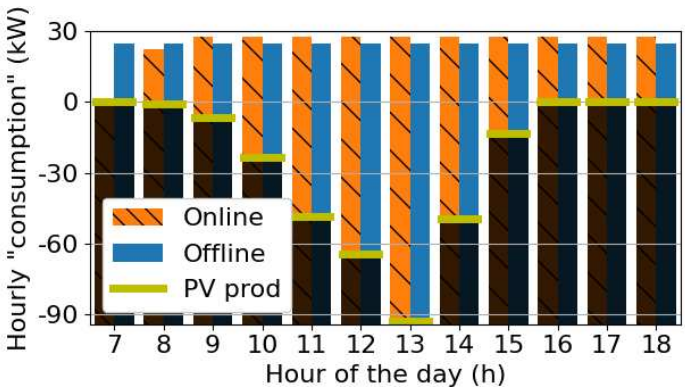

Figure 4.9: Comparison of optimal per-class aggregated charging profiles obtained with online and offline charging problems. *In the online charging problem, the CSO waits for a higher PV generation before charging the EVs which arrived at 7 am, while in the offline charging problem, the CSO starts charging them right away because it knows at lot of EVs arrive at 8 am.*

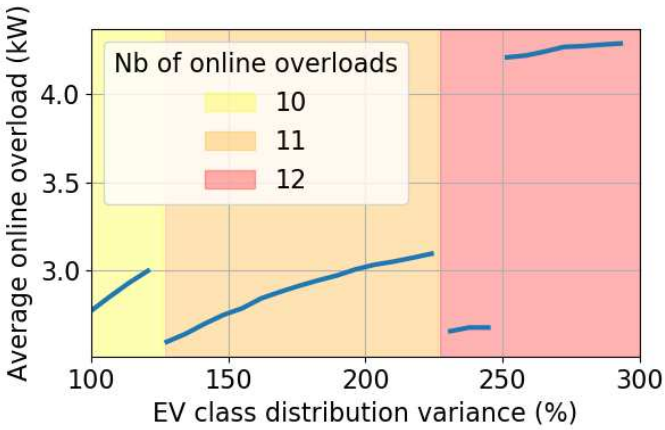

Figure 4.10: Average power overload of the online charging profile over the offline one and number of overload time slots in a day, in function of the EVs distribution variance. *As the number of EVs arriving early increases with the variance, the overload increases too (see Figure 4.9), but may be divided into more time slots (when a new departure time is considered).*

were multiplied by three. The latter scenario with higher variance could be realized with the remote working of nowadays. We consider $N = 100$ EVs, and the number $N^{(a,d)}$ of EVs in class (a, d) is the product of N with the distribution values of a and $d + 1$ (according to the convention that EV class (a, d) can charge between the a-th and d-th time slots included, and leave at the beginning of time slot $d + 1$). EV users are assumed to have the same charging need, equivalent to their daily driving consumption: 6 kWh, due to the 30 km daily driving distance according to ENTD survey [CGDD, 2010], at a 0.2 kWh/km average consumption per distance unit [De Cauwer et al., 2015]. The charging need aggregated over class (a, d) is therefore $L^{(a,d)} = 6 \times N^{(a,d)}$ kWh.

4.3.4.2 Comparison of online and offline charging schedulings

Figure 4.9 shows the optimal per-class aggregated charging profiles obtained with the online and offline charging problems and corresponding to the charging needs associated with ENTD data.

We can see that considering the online charging problem, the CSO does not charge the few EVs which arrived at the EVCS at 7 am right away, but wait for time slots with higher PV generation. In the offline charging problem, the CSO knows that many EVs arrive at 8 am and will need a lot of PV generation, and therefore starts to charge the EVs arriving at 7 am as soon as possible.

Figure 4.10 studies the power overload of the online charging profile with respect to the offline one. More precisely, Figure 4.10 shows the number of time slots when the online charging power is greater than the offline one, and the average overload value during these time slots (blue line). The time slots where the online charging is lower than the offline one (e.g., the first two time slots of Figure 4.9) are not considered. From 125 % of EVs arrival and departure distributions variance, some EVs start to leave at 8 pm from the EVCS (see Figure 4.8) and thus the online overload (see Figure 4.9) can be divided into 11 time slots instead of 10, which mechanically reduces the average overload. The same goes from 225 % of the variance, where some EVs start to leave at 9 pm. However from 250 %, some EVs start to arrive at 6 am at the EVCS which allows the offline charging scheduling to start one hour earlier while the online one still waits for the PV generation peak (see Fig 4.9), hence the average overload increases. Except from these discontinuities, the average overload increases with the variance for the same reasons: the higher the variance, the higher the number of EVs arriving early. Generally, the online scheduling may lead to peak load problems, which needs to be investigated in more details.

Finally, note that the explicit computations of the online charging profile are approximately a thousand times faster than the QP solver used for the offline optimization problem ($\mathcal{P}$).

4.4 Smart charging at several charging stations of a grid

Table 4.11: Notations of Section 4.4

Symbols	Signification
L_i	Charging need aggregated over all EVs at EVCS i
$\ell^{\text{tot}}_{i,t} = \ell^0_{i,t} + \ell_{i,t}$	Sum of the charging and non-flexible loads at t and EVCS i
$m = l, g, a$	Respectively local, global and grid aware methods
$\mathcal{G}_m$	Grid cost caused by charging profile of method m
$\tilde{\mathcal{G}}_m$	Normalized grid cost of method m
T_m	Execution time of method m

In this section, the charging scheduling problem ($\mathcal{S}$) is studied in the case where there are several EVCSs, all connected to the same distribution grid. For example, in the numerical study in Section 4.4.4, EV users have the choice to charge at three different EVCSs belonging to the distribution grid of Figure 4.12. Yet, the different charging schedulings introduced in this section can be applied to grids with any number of EVCSs. As already mentioned in Section 4.2.1.1, the objective functions on which the charging scheduling problems are based are aligned as much as possible with the grid cost, defined in next Section 4.4.1. Note that in this section, the load cost function f is assumed increasing, convex and time-independent, as in Section 4.2.1. Though, all of the following results can be extended to time-dependent load functions f_t. The following work is largely inspired from our conference paper [Sohet et al., 2020a].

Depending on whether the charging scheduling at EVCSs is managed by the same operator or not, and on which information this operator has, the present section defines three different charging scheduling problems in Section 4.4.2, whose corresponding optimal charging profiles are given in the subsequent Section 4.4.2. These three methods are then compared on the example of grid of Figure 4.12. First, Section 4.4.1 details the concept of grid cost, which is often used in the present section.

4.4.1 Model of grid costs related to EV charging

In this thesis, the term "grid cost" refers to a simple model of the impact EV charging has on the distribution grid. The key variable of this model is the apparent power[13] required at the "head" of the grid in order to meet the charging and non-flexible loads at all EVCSs of this grid. By "head of the grid" is typically meant in the commuting use case the corresponding MV/LV (Medium and Low Voltages) transformer. This head power can relate to transformer aging and power losses due to Joule heating, among other grid costs caused by EV charging and identified in Section 4.2.1.1.

Like for CSO's costs in the present chapter, the grid costs at time slot t are defined using the increasing and convex load function f_t, evaluated with the apparent power value S_t at the transformer at time slot t. In this Section 4.4, $f : \ell \mapsto \ell^2$ is assumed time-independent, and the total grid cost is then defined as:

$$\mathcal{G} = \sum_t \mathcal{G}_t = \sum_t f(S_t)\,. \tag{4.23}$$

[13]The apparent power is the magnitude of the complex power, the vector sum of active and reactive powers.

The apparent power S_t at time slot t is obtained by solving the power flow equations from the Bus Injection Model [Zhu, 2015] (*runpp* function in *pandapower* Python library). This model corresponds to the power balance at each bus, between the given power generation/load $S_{0,k}$ at bus k and power flows S_k from/to the bus:

$$\begin{aligned} S_{0,k} &= S_k \\ &= U_k \sum_{m \in X_k} \overline{Y_{k,m} U_m}\,, \end{aligned} \tag{4.24}$$

with U_k the complex voltage at bus k, X_k the set of buses connected to bus k and $Y_{k,m}$ the admittance of the line between buses k and m.

Following numerical observations, for each time slot t, the corresponding grid cost function $\mathcal{G}_t$ is assumed differentiable with respect to load at each bus, and strictly convex.

4.4.2 Three different possible operators for the charging scheduling

Given the charging need L_i at each EVCS i of the grid, the charging operation of EVs during working hours at all EVCSs is scheduled by one or several operators (depending on the scenario considered, as explained later in this section). Each EVCS i has its own non-flexible consumption $\ell^0_{i,t}$ for each time slot t. Then, for each EVCS i, an operator has to determine the quantity $\ell_{i,t}$ to charge at each time slot t in order to minimize its cost function, and satisfying the aggregated charging need L_i at this EVCS.

Several operators are part of the electrical system considered, as shown in Figure 4.12. Each EVCS i is under the supervision of a Charging Service Operator (CSO). Several CSOs may be managed together by what is called a Flexibility Operator (FO). The electrical grid, from the transformer to the EVCSs, is managed by an Electric Network Operator (ENO). Depending on which of these three operators controls the charging operation scheduling, three scenarios are considered. The algorithms solution of these scenarios are detailed in next Section 4.4.3.

CSO (local scheduling method)
The charging scheduling at each EVCS is done by the corresponding CSO. Each CSO has no knowledge about non-flexible loads at other EVCSs, charging profiles chosen by the other CSOs, and about the characteristics of the grid. Thus, each CSO i solves the standard charging scheduling problem ($\mathcal{S}$):

$$\min_{(\ell_{i,t})_t} \sum_{t=1}^{T} f\left(\ell^0_{i,t} + \ell_{i,t}\right)\,, \quad \text{s.t.} \quad \begin{cases} \ell_{i,t} \geq 0 \quad \forall t \in \mathcal{T}\,, \\ \sum_{t=1}^{T} \ell_{i,t} = L_i/\delta\,. \end{cases} \tag{$\mathcal{S}$}$$

FO (global scheduling method)
The charging scheduling of all EVCSs is done by the FO. This FO has complete information on all EVCSs, but not on the grid. The FO does not minimize the sum of all CSO's cost functions in ($\mathcal{S}$), which would give the same optimal charging profiles (4.1). Indeed, this is not a judicious use of the whole information the FO has. For example, if the FO uses the local method introduced in previous paragraph, it may charge EVs at one EVCS during a time slot when there is a tremendous non-flexible load at another EVCS, which may be detrimental to the grid (see Section 4.4.4).

Instead, the FO solves the standard charging scheduling problem ($\mathcal{S}$) defined on the charging needs and non-flexible profiles *aggregated* over all EVCSs:

$$\min_{(\ell_{i,t})_{i,t}} \sum_t f\left(\sum_i \left(\ell^0_{i,t} + \ell_{i,t}\right)\right) \quad \text{s.t.} \quad \forall i\,, \begin{cases} \ell_{i,t} \geq 0 \quad \forall t \in \mathcal{T}\,, \\ \sum_t \ell_{i,t} = L_i/\delta\,. \end{cases} \tag{4.25}$$

Note that there are an infinite number of charging profiles $(\ell_{i,t})_{i,t}$ solution of the aggregated problem (4.25). The chosen disaggregation is detailed in next section.

In the last two scenarios, the operators considered solve optimization problems ($\mathcal{S}$) and (4.25) regardless of the grid topology, unlike the ENO in next scenario.

ENO (grid aware scheduling method)
The charging scheduling of all EVCSs is done by the ENO, which has complete information on the EVCSs and the grid. The objective function of the ENO is the grid cost $\mathcal{G} = \sum_t \mathcal{G}_t$ defined in Section 4.4.1, and the resulting charging scheduling problem is:

$$\min_{(\ell_{i,t})_{i,t}} \sum_t f\left(S_t\right) \quad \text{s.t.} \quad \forall i\,, \begin{cases} \ell_{i,t} \geq 0 \quad \forall t \in \mathcal{T}\,, \\ \sum_t \ell_{i,t} = L_i/\delta\,. \end{cases} \tag{4.26}$$

Note that the apparent power S_t at the transformer at time slot t is a function all total loads $\ell^{\text{tot}}_{i,t} = \ell^0_{i,t} + \ell_{i,t}$ at the EVCSs.

Note that in all three scenarios, the various operators all minimize the sum over time of the load function applied to different powers: the active powers of each EVCS in the local scenario, the sum of these powers in the global one and the apparent power at the "head" of the grid for the grid aware one. The scheduling algorithms of the three scenarios are detailed in next section.

4.4.3 Three charging scheduling methods depending on available information

Local scheduling method (CSO)
At each EVCS i, the corresponding CSO uses the water-filling charging scheduling, whose explicit expression is given in Proposition 4.2 and is already denoted $\boldsymbol{\ell}^{\text{WF}}(L_i\,, \boldsymbol{\ell}^0_i)$:

$$\ell^*_{i,t} = \ell^{\text{WF}}_{i,t} = \begin{cases} \dfrac{L_i + L^0_{i,\bar{t}}}{\bar{t}(L_i) \times \delta} - \ell^0_{i,t} & if \quad t \in \{0, \ldots, \bar{t}(L_i)\}\,, \\ 0 & if \quad t > \bar{t}(L_i)\,. \end{cases} \tag{4.1}$$

Global scheduling method (FO)
The FO objective function in (4.25) is minimized by solving a basic scheduling problem ($\mathcal{S}$), with $L = \sum_i L_i$ and $\ell^0_t = \sum_i \ell^0_{i,t}$ respectively the charging need and non-flexible consumption profile, both aggregated over all EVCSs. Proposition 4.2 then gives an optimal aggregated profile $(\ell^*_t)_t = \boldsymbol{\ell}^{\text{WF}}(L\,, (\ell^0_t)_t)$ which minimizes $\sum_t f(\ell^0_t + \ell_t)$. However, an infinite number of profiles $(\ell_{i,t})_{i,t}$ verify the disaggregation property:

$$\forall t \in \mathcal{T}\,, \quad \sum_i \ell_{i,t} = \ell^*_t\,, \tag{4.27}$$

i.e., are solution of (4.25). For example, the pro-rata profile defined by $\ell_{i,t} = \frac{L_i}{L}\ell^*_t$ (for all i, t) verifies property (4.27).

Algorithm 4.2: Disaggregation algorithm of global scheduling

Input: Charging needs $(L_i)_i$, non-flexible profiles $\left(\ell^0_{i,t}\right)_{i,t}$ and aggregated optimal profile $(\ell^*_t)_t = \boldsymbol{\ell}^{\mathrm{WF}}\left(\sum_i L_i\,, \left(\sum_i \ell^0_{i,t}\right)_t\right)$

1 $\left(\ell^*_{i,t}\right)_t \xleftarrow{\forall i} \boldsymbol{\ell}^{\mathrm{WF}}\left(L_i\,, \left(\ell^0_{i,t}\right)_t\right)$, local optimal profile at EVCS i

2 $\ell_{i,t} \xleftarrow{\forall i,t} \ell^*_{i,t} + \frac{1}{T}\left(\ell^*_t - \sum_i \ell^*_{i,t}\right)$, so that $\sum_i \ell_{i,t} = \ell^*_t \quad (\forall t)$

3 **for** i, t such that $\ell_{i,t} < 0$ **do**

4 $\quad Z \longleftarrow -\ell_{i,t} \quad (> 0)$

5 $\quad \ell_{i,t} \longleftarrow 0$, so that $\ell_{i,t} \geq 0$

6 $\quad \ell_{j,t} \xleftarrow{\forall j} \ell_{j,t} - x_j$, with $(x_j)_j$ given by Algo. 4.3 $(Z, (\ell_{j,t})_j)$, so that $\sum_j \ell_{j,t} = \ell^*_t$

7 $\quad \ell_{i,s} \xleftarrow{\forall s} \ell_{i,s} - y_s$, with $(y_s)_s$ given by Algo. 4.3 $(Z, (\ell_{i,s})_s)$, so that $\sum_s \ell_{i,s} = L_i$

8 $\quad \ell_{j,s} \xleftarrow{\forall j \neq i, s \neq t} \ell_{j,s} + \frac{x_j y_s}{Z}$, so that $\sum_j \ell_{j,s} = \ell^*_s$ and $\sum_s \ell_{j,s} = L_j \quad (\forall j \neq i, s \neq t)$

end

Output: Valid disaggregated profile $(\ell_{i,t})_{i,t}$

The disaggregation $((\ell^*_t)_t \to (\ell_{i,t})_{i,t})$ defined in this thesis is presented in Algorithm 4.2, and has the following ambition. By definition, the aggregated solution of (4.25) makes sure that the aggregated total load vector $(\sum_i \ell^{\mathrm{tot}}_{i,t})_t$ is as much smoothed as possible. The goal is to find a disaggregated (i.e. which verifies property (4.27)) profile $(\ell_{i,t})_{i,t}$ for which the total load vector $(\ell^{\mathrm{tot}}_{i,t})_t$ is as much smoothed as possible for all EVCSs i.

The idea of Algorithm 4.2 is to first compute the optimal local[14] charging profile $(\ell^*_{i,t})_t$ for each EVCS i using Proposition 4.2 (line 1 of Algorithm 4.2). Combined together, these local profiles are not a solution of the global scheduling problem (4.25). To this end, these profiles $(\ell^*_{i,t})_{i,t}$ are adjusted using the optimal aggregated profile $(\ell^*_t)_t$ (line 2), so that the newly formed profiles $(\ell_{i,t})_{i,t}$ are a disaggregation (i.e., verify (4.27)) of solution $(\ell^*_t)_t$ of (4.25). However, this disaggregation is not valid yet, in the sense that $\ell_{i,t} < 0$ for some i, t, which violates[15] the constraints of (4.25). The purpose of the "for" loop (line 3) is to modify $(\ell_{i,t})_{i,t}$ so that these constraints are verified, while keeping the disaggregation property (4.27). While setting their value to 0 (line 5), the negative loads $\ell_{i,t} < 0$ are distributed – using Algorithm 4.3 – on the one hand among the other loads at EVCS i (line 6), and on the other hand among the other loads at time slot t (line 7), so that respectively the charging need constraint at EVCS i and the disaggregation property (4.27) at t remain verified. The other loads $\ell_{j,s}$ (for all $j \neq i, s \neq t$) are then adjusted with the same purpose (line 8).

Both lines 6 and 7 in Algorithm 4.2, which dispatch a negative load $-Z$ within a vector $(\ell_k)_{1 \leq k \leq K}$, use the same Algorithm 4.3. In the increasing order of elements ℓ_k (line 1 of Algorithm 4.3), the dispatched quantity $-z_k$ verifies (line 2):

- if $\ell_k < 0$, $z_k = 0$ because the k-th load is already negative;
- $z_k = \frac{Z}{K}$ if $\ell_k - \frac{Z}{K} \geq 0$ (the k-th load remains non-negative);
- $z_k = \ell_k$ otherwise.

[14] The FO has the necessary information to solve each local scheduling.

[15] In the case where the V2G technology is considered, $\ell_{i,t} < 0$ is not necessarily a violation and Algorithm 4.2 may be terminated.

Algorithm 4.3:

Input: Positive number Z and real vector $(\ell_k)_{1\leq k\leq K}$

1 **for** k in argsort($\boldsymbol{\ell}$) **do**

2 $\quad z_k \longleftarrow \max\left[0\,,\min\left(\ell_k\,,\frac{Z}{K}\right)\right]$

3 $\quad Z \longleftarrow Z - z_k$

4 $\quad K \longleftarrow K - 1$

end

Output: Positive vector $(z_k)_k$ such that $\sum_k z_k = Z$ and $\ell_k + z_k \geq \min(0\,,\ell_k) \quad (\forall k)$

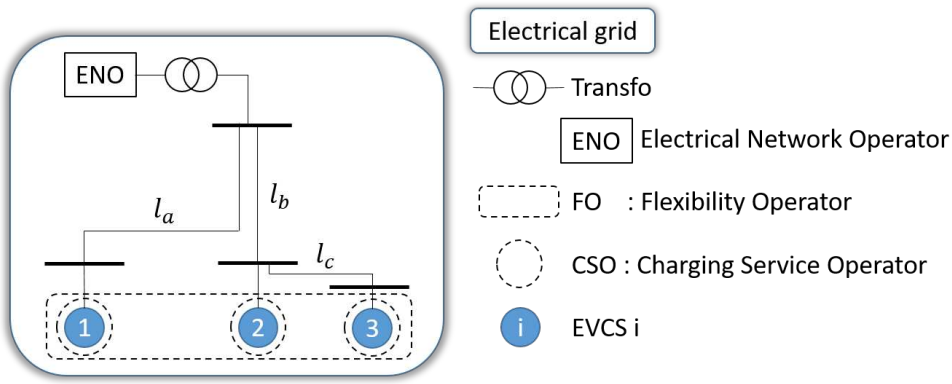

Figure 4.12: Electrical network considered in this work. ENO, FO and CSO respectively stand for Electrical Network, Flexibility and Charging Service Operators.

Then, the remaining quantity $-(Z - z_k)$ (line 3) is dispatched amid the $K - 1$ other loads (line 4), and so on.

Grid aware scheduling method (ENO)

Because of the implicit nature of $\mathcal{G}$, iterative water-filling algorithms applied to problem (4.26) do not result in an explicit solution, as in the local and global scenarios. Instead, (4.26) is seen as a convex optimization problem, solved by built-in Python function *minimize*, relying on a sequential least squares programming method.

4.4.4 Numerical comparison between the three charging schedulings

4.4.4.1 Illustration of the scheduling methods on a simplified distribution grid

An example of the three scheduling methods introduced in sections 4.4.2 and 4.4.3 is given in Figure 4.13. The parameters of the scheduling problem are set as follows. The data set used for the non-flexible loads are hourly electric consumption throughout a year of Texan households[16] (see Section 5.2.3). More precisely, the non-flexible load of each EVCS (in grey in Figure 4.13) is taken proportional to the consumption of one Texan household (from 9 a.m. to 5 p.m., averaged over a year), so that the global demand over the working hours is $\delta \sum_i \sum_{t=1}^{T} \ell_{i,t}^0 = 30$ MWh. The aggregated charging needs L_i for EVCSs 1, 2 and 3 are respectively 3.94, 2.91 and 0.46 MWh. Note that these charging needs are the one obtained at the Wardrop Equilibrium (see Definition 2.14) of the driving-and-charging game described in Section 5.4.2.1. The number

[16] Data available at http://www.pecanstreet.org/.

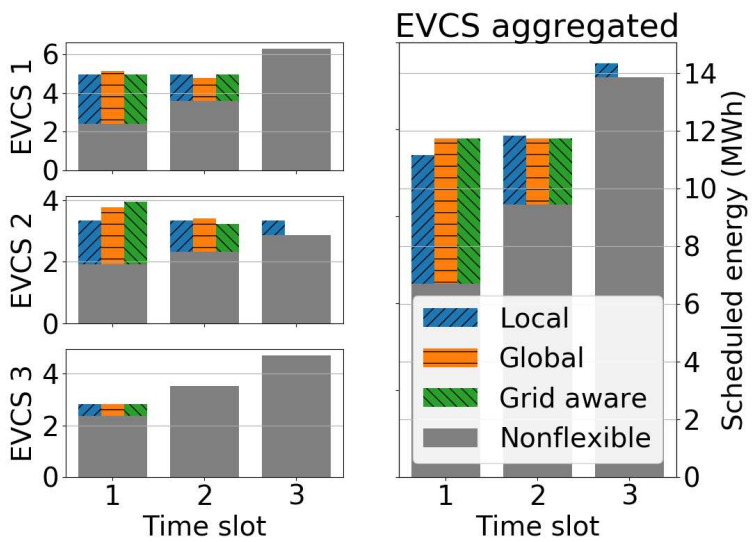

Figure 4.13: Example of the three scheduling algorithms.

of time slots for the scheduling is $T = 3$ and the load cost function $f : \ell \mapsto \ell^2$ used in scheduling problems ($\mathcal{S}$), (4.25) and (4.26) is assumed to be quadratic. Concerning the distribution grid, standard types[17] were used for the transformer (63 MVA 110/20 kV) and the lines (1x240 RM/25 12/20 kV). This grid covers an urban area and the lengths of these lines are $l_a = 10$ km and $l_b = l_c = 5$ km.

The local method smooths each EVCS i load profile $(\ell^{\text{tot}}_{i,t})_t$ (upward diagonal hatch in Figure 4.13). Unfortunately, in some scenarios like here, the corresponding aggregated load profile can be far from smoothed (right figure). This is the reason why the local method may result in higher grid costs (see Table 4.14). For example, charging vehicles at EVCS 2 during time slot $t = 3$ while there is already a high non-flexible consumption (possibly at other EVCSs) can be costly. The global method smooths the aggregated load profile of the three EVCSs (see the horizontal hatches on right figure). The corresponding disaggregated local profiles at each EVCS are as smoothed as possible thanks to disaggregation Algorithm 4.2 (see left figure). The Grid aware method, minimizing the grid cost by definition, has almost smoothed aggregated and EVCS 1 profiles as EVCS 1 is farther away from the transformer than EVCS 2 (10 km instead of 5), charging there is more expensive for the grid.

4.4.4.2 Comparison of grid costs and execution times between the three methods

Then, a comparison between the three methods is given in Table 4.14. For this, a thousand non-flexible profiles with $T = 8$ time slots are randomly generated for each EVCS, such that for each generation, $\delta \sum_i \sum_{t=1}^{T} \ell^0_{i,t} = 30$ MWh. Each generated profile has also a 2 and a 4 time slots version. This table shows for each method m ($m = l, g, a$ resp. for local, global and grid aware) the mean over these random profiles of the execution time T_m and the normalized grid cost $\tilde{\mathcal{G}}_m$ defined as[18]:

$$\tilde{\mathcal{G}}_m = \frac{\mathcal{G}_m - \mathcal{G}_a}{\mathcal{G}_a}, \tag{4.28}$$

[17] https://pandapower.readthedocs.io/en/v2.2.0/std_types.html.

[18] Note that in this Section 4.4, the notation $\tilde{\mathcal{G}}$ does not refer to the minimal value of $\mathcal{G}$ (as in Section 4.3), but to a relative difference between two grid costs.

Table 4.14: Depending on the number of time slots into which working hours are divided, mean over 1000 randomly generated non-flexible profiles, of normalized grid cost $\tilde{\mathcal{G}}_m$ and execution time T_m of method m.

Nb time slots	$\tilde{\mathcal{G}}_l$ (%)	$\tilde{\mathcal{G}}_g$ (%)	T_l (s)	T_g (s)	T_a (s)
2	0.4	8e-03	5e-05	9e-05	0.8
4	1.0	2e-02	6e-05	3e-04	4.3
8	2.2	3e-02	6e-05	1e-03	20.9

with $\mathcal{G}_m$ the grid cost defined in equation (4.23) associated with each scheduling method m. The normalized grid costs of the three methods are illustrated in our paper [Sohet et al., 2020a]. This table confirms that the grid aware method is optimal with respect to the grid cost ($\tilde{\mathcal{G}}_l, \tilde{\mathcal{G}}_g > 0$) and shows that the global one remains very close, while the local method difference is of the order of the percent. In terms of execution times obtained with an Intel Core i7-6820HQ 2.70GHz, the local and global methods are negligible compared to the grid aware method.

The execution time depends on the number of variables of the optimization problems ($\mathcal{S}$), (4.25) and (4.26): the number of EVCSs multiplied by the number of time slots. A comparison between 2, 4 and 8 time slots shows that the execution time of the grid aware method goes from 1 s ($T = 2$) to approximately 21 s ($T = 8$), over the set of random scenarios. However, the normalized grid costs of the other two methods increase too (nearly proportional to the number of time slots). Thus, the choice of the method is a trade-off between execution time and optimal grid cost. The global method seems to be the best choice as it is fast and near-optimal, even if it does not take into account the network topology. This is thanks to the simple grid topology of Figure 4.12, in which the potential impacts of each EVCS on the grid (e.g., such as power losses) are similar.

4.5 Conclusion

This chapter focuses on how the operators of the EV Charging Stations (EVCSs) manage the charging scheduling of EVs. The result of this charging scheduling is then integrated in the charging pricing schemes in next Chapter 5. Therefore, the basic Water-Filling (WF) scheduling [Shinwari et al., 2012] is used to schedules the charging need aggregated over all EVs. This method is a Direct Load Control mechanism, in which the choice of the charging profile is centralized at the operator level, which schedules it in order to smooth the total load profile, which includes EV charging together with other electricity usages which cannot be scheduled (and thus called non-flexible). Several adaptations of the WF scheduling as well as the corresponding explicit solutions are given in this chapter.

First, WF is extended to the case of time-dependent load cost functions, in addition to the fluctuations in time of the non-flexible load. Second, local electricity generation and self-consumption is considered, and two different charging scheduling methods are given, depending on whether the unused electricity generated is remunerated. Another direct extension of the WF scheduling could be the consideration of power limits. In the case of different limits for each time slot, no explicit solution has been found. Explicit WF charging profiles also remain to be found if the vehicle to grid technology is considered, which couple the different time slots due to the boundary constraints on the aggregated State of Charge.

So far, EVs arrive at the EVCS, and then leave, at the same time slot. Another contribution of this chapter is to give an EVCS operator a simple procedure to follow in the case additional

EVs may arrive at each time slot, without knowing it in advance. This could be further extended to a stochastic version of WF considering general uncertainty with respect to non-flexible loads and charging needs.

Finally, the WF is adapted to a distribution grid supplying several EVCSs. Three different charging schedulings are provided, depending on whether the charging scheduling at the different EVCSs is managed by the same operator or not, and on which information this operator has on the grid metrics. The main contribution is an algorithm destined to an operator of several EVCSs without any information on the grid. This algorithm disaggregates an optimal charging profile corresponding to the charging need aggregated over all EVCSs, into a charging profile for each EVCS. Compared to an implicit minimization of the grid cost by a potential operator of both the grid and the EVCSs, the disaggregation method seems to be a good compromise between execution time and reduction of the grid cost.

Chapter 5

Smart charging pricing methods at charging stations

The present chapter deals with the charging pricing of EV users chosen by the operators of the Charging Stations. The goal of pricing mechanisms is to influence EV users in their choices (which charging station, which charging quantity, etc.). Note that the choice of the charging profile is assumed to be done in a centralized manner by the operator of the EVCS which uses the Water-Filling charging scheduling (see previous Chapter 4). The two pricing methods used in this thesis are introduced. The corresponding Charging Unit Prices are defined as functions of the WF scheduling cost. They are compared to an enhanced version of the iterative Locational Marginal Pricing method used in the related literature. A simplified version of this LMP method – which does not require full information on the grid – is also introduced. It is shown that Beckmann's method (Proposition 2.19) can be used for all four pricing methods. Numerical illustrations show that the three pricing methods introduced in this chapter have similar impacts on the grid as the LMP method found in the literature.

This chapter is in part inspired from the following papers:

[Sohet et al., 2021b] **Sohet, B.**, Hayel, Y., Beaude, O., and Jeandin, A. (2021). Coupled charging-and-driving incentives design for electric vehicles in urban networks. *IEEE Transactions on Intelligent Transportation Systems*, 22(10):6342-6352.

[Sohet et al., 2021c] **Sohet, B.**, Hayel, Y., Beaude, O., and Jeandin, A. (2021). Hierarchical coupled routing-charging model of electric vehicles, stations and grid operators. *IEEE Transactions on Smart Grid*, 12(6):5146-5157.

Contents

5.1 Introduction **90**

5.1.1 State of the art 90

5.1.2 Iterative locational marginal pricing method 92

5.2 Average water-filling pricing method **93**

5.2.1 Definition based on the water-filling scheduling cost 93

5.2.2 Properties of the charging unit price functions 94

5.2.3 Illustration of the increasing property with real data 96

5.3 Locational marginal pricing method based on water-filling charging scheduling . . . 99
5.3.1 Definition based on the marginal water-filling scheduling cost . . . 99
5.3.2 Properties of the charging unit price functions . . . 99
5.3.3 Online and offline pricing methods for asynchronous charging needs 100
5.3.3.1 Definitions . . . 100
5.3.3.2 Numerical comparison . . . 101
5.4 Numerical comparisons of the pricing methods . . . 102
5.4.1 Illustration of the pricing methods . . . 102
5.4.1.1 Definition of the α-locational marginal pricing method . . . 103
5.4.1.2 Illustration of the effect of charging needs on the pricing methods . . . 104
5.4.2 Impact of the pricing methods on a transportation-electrical system 106
5.4.2.1 Driving-and-charging game setting . . . 107
5.4.2.2 Comparison of the pricing methods in function of a traffic toll . . . 108
5.5 Conclusion . . . 111

Table 5.1: Notations of Chapter 5

Symbols	Signification
m	Pricing method index: cst, avg, wf, ga and α
λ_i^m	Charging Unit Price function at EVCS i for pricing method m
G_i^*	Optimal Water-Filling objective function at EVCS i
$\mathcal{G}_t$	Grid cost function at time slot t
η^m	Conversion parameter associated with pricing m
$\mathcal{B}_{\lambda_i^m}$	Beckmann term associated with CUP λ_i^m
α_i	Impact coefficient EVCS i on the grid
$\tilde{\mathcal{G}}_m$	Grid cost of pricing m normalized by GA pricing

5.1 Introduction

5.1.1 State of the art

This chapter deals with the charging price incentives that mobility service providers (referred to as Charging Service Operators in this thesis, or CSOs) can use at public EV Charging Stations (EVCSs) to induce specific EV users charging behaviors. These charging behaviors include the choice of the EVCS, the arrival and departure times, the charging quantity, the charging profile, etc. This chapter focuses on the impact pricing incentives have on the choice of the EVCS, but the impact study can be extended to the other choices by adding the pricing incentives considered to EV driving-and-charging games other than game $\mathbb{G}$ described in Section 5.4.2.1. Concerning the choice of the charging profile specifically, in this thesis it is assumed to be centralized at the level of the CSO, the EVCS operator (and not driven by price signals), and is detailed in

previous Chapter 4: EV users let the CSO decide their charging profiles which guarantee them a given State of Charge (SoC) when they leave the EVCS.

Charging pricing is a type of Demand Response (DR) mechanism. [Vardakas et al., 2014] gives in details three different classifications of DR mechanisms, respectively based on the control mechanism, the incentives offered to consumers and the DR decision variables. The most relevant classification in our case is the one based on offered motivations, which distinguishes price-based (or time-based) and incentive-based DR mechanisms. Incentive-based DR mechanisms, such as Direct Load Control [Ruiz et al., 2009], curtailable load [Aalami et al., 2010] or Demand Bidding [Oh and Thomas, 2008], offer payments to consumers which reduce their electricity usage when needed. Price-based DR mechanisms are dynamic pricing schemes which depend on the cost of electricity, and are more suited than incentive-based mechanisms for the commuting use case modeled in this thesis. The main price-based mechanisms are listed below. Real application of these DR mechanisms is presented in the more recent review [Paterakis et al., 2017].

- Flat pricing consists in a constant price: the only way for EV users to reduce their electricity bill is to charge less.

- Time-Of-Use (TOU) pricing defines different periods of time and a constant price for each period. In France for example, EDF proposes to residential customers the *Heures Creuses* option, with a 8-hour off-peak window where the price is lower[1]. These different constant prices for each time period reflect long term grid costs. Refinements of TOU pricing scheme exist, like Critical Peak Pricing [Herter, 2007], where some periods' prices can be modified the day ahead, reflecting short term fluctuations in electricity costs.

- Real-time pricing [Chen et al., 2011] determines the price of a time slot and announces it to the consumers right before the start of the time slot. However, this pricing method requires a continuous real-time communication between EV users and the CSO. This assumption can be relaxed using for example the day-ahead real-time pricing as in the paper [Doostizadeh and Ghasemi, 2012], where the charging price is fixed the day before.

In the first place, the goal of these pricing mechanisms is to incentivize consumers to postpone electricity usages to the benefit of the grid operator, or in our case to incentivize EV users to choose a charging profile adequate to the objective of the CSO. In this thesis the charging profile's choice is centralized at the level of the CSO[2] (see Chapter 4), and the focus of the present chapter is put on the choice of the EVCS. In this case, time-based DR mechanisms can still be used by considering several EVCSs instead of several time slots: for example, the TOU pricing scheme consists in the case of the EVCS's choice to assign to each EVCS a constant price. The main pricing method used in papers which focus on the coupling of EV users' driving-and-charging decisions (see review [Wei et al., 2019]) is the Locational Marginal Pricing [Li et al., 2013] (LMP), where EV users pay the charging quantity multiplied by the marginal CSO's cost associated with an additional marginal charging quantity. The LMP can be seen as a real-time pricing, where EV users indicate to the CSO their charging need and the CSO determines and communicates the constant charging prices at each EVCS and time slot before the charging time period. The LMP method employed in these papers is described in next section. The pricing methods considered in this thesis are inspired from this LMP and detailed in Sections 5.2 and 5.3.

[1] Note that the "peak price" is higher than the price in the flat pricing contract (https://particulier.edf.fr/en/home/contract-and-consumption/options/off-peak-times.html).

[2] In practice, the vehicle users may receive incentive payments in advance (like in incentive-based DR mechanisms) to agree with this centralized charging scheduling.

5.1.2 Iterative locational marginal pricing method

In this section the most commonly used model of EV charging incentives in coupled electrical-transportation systems [Alizadeh et al., 2016, Wei et al., 2017] is introduced briefly. In this reference model, a unique System Operator (SO) is in charge both of all EVCSs of the electrical grid considered, and of the grid itself. Note that this SO has the same control and access to information as the Electrical Network Operator (ENO) in the Grid Aware (GA) method introduced in Section 4.4.2. Having a complete knowledge of the grid, the SO chooses the Locational Marginal Pricing (LMP) scheme: the corresponding Charging Unit Price (CUP) function at EVCS i is defined as the differential of the grid cost function $\mathcal{G}$ defined in Section 4.4.1, with respect to the aggregated charging need at this EVCS.

Remark 5.1. *Note that in the numerical Section 5.4, the increasing and convex load cost function f (in part used in the definition of the grid cost function $\mathcal{G}$) is assumed time-independent. For example, the grid cost function $\mathcal{G}$ corresponding to the charging time period $\{1, \ldots, T\}$ is:*

$$\mathcal{G} = \sum_{t=1}^{T} \mathcal{G}_t = \sum_{t=1}^{T} f(S_t)\,, \tag{5.1}$$

with S_t the power at the transformer of the considered distribution grid (see Section 4.4.1). However, all the results of the present chapter are valid for time-dependent load cost functions f_t.

Remark 5.2. *In this chapter, the term "Charging Unit Price" (CUP) λ_i refers to the charging cost function of EV users charging at EVCS i (per charged energy unit) in the game framework introduced in Chapter 2. The term "(charging) pricing scheme/method/mechanism" relates to the conceptual incentive mechanism corresponding to this CUP function.*

The LMP is proved to be the most efficient pricing scheme to incentivize EV users to reduce $\mathcal{G}$ (see [Alizadeh et al., 2016] or Remark 5.9), in the case where EV users have no other costs. The corresponding CUP function λ_i at EVCS i is defined as the marginal cost corresponding to $\mathcal{G}$ with respect to aggregated charging need L_i:

$$\lambda_i(\boldsymbol{\ell}) = \eta \times \frac{\partial \mathcal{G}}{\partial L_i}(\boldsymbol{\ell}) = \eta \sum_{t=1}^{T} \frac{\partial \mathcal{G}}{\partial L_i}(\boldsymbol{\ell}_t)\ , \tag{5.2}$$

where parameter η converts the marginal grid cost into a standard charging price, and $\boldsymbol{\ell}$ is the aggregated charging profiles at every EVCS. No method to fix η is available in the literature: it is therefore chosen empirically in numerical Section 5.4.

Remark 5.3. *This parameter η can be seen as the parameter used in the power load cost function f when defined as a monomial: $f : \ell \mapsto \eta \ell^n$ ($n \geq 2$). As this parameter is expressed outside of this load cost function, the load cost functions used in the present chapter are only $f : \ell \mapsto \ell^n$.*

The grid cost function $\mathcal{G}$ depends, among other things, on the EV charging scheduling $\boldsymbol{\ell}$ at all EVCSs of the grid. Papers using LMP scheme (5.2) do not consider any charging scheduling algorithm. Thus, in this chapter a first pricing method assumes that the whole EV charging need is charged during the first time slot: $\boldsymbol{\ell}_1^{\mathrm{pc}} = \boldsymbol{L}$. This method is referred to as PC-GA thereafter, for Plug-and-Charge regarding the charging scheduling, and Grid Aware regarding the cost function on which the CUP function is based, which is the grid cost function $\mathcal{G}$ used in GA method in

Section 4.4. However, it is possible to consider an improved method (referred to as GA-GA) by solving the Grid Aware charging scheduling problem (4.26) defined in Section 4.4.2 in order to obtain $\boldsymbol{\ell}^{\mathrm{ga}}$:

$$\min_{(\ell_{i,t})_{i,t}} \sum_{t=1}^{T} f\Big(S_t(\boldsymbol{\ell}_t)\Big) \quad \text{s.t.} \quad \forall i\,, \begin{cases} \ell_{i,t} \geq 0 \quad \forall t \in \mathcal{T}\,, \\ \sum_{t=1}^{T} \ell_{i,t} = L_i/\delta\,. \end{cases} \tag{4.26}$$

See previous Chapter 4 for more details on the notations. Method GA-GA takes full advantage of the knowledge of the SO, but the corresponding CUPs $\boldsymbol{\lambda}$ are not a Linearly non-Separable Congestion cost functions as in Definition 2.11, in part due to the implicit nature of the solution of scheduling problem (4.26). For the numerical Section 5.4, a third method is considered (referred to as WF-GA, for Water-Filling), where the SO solves the scheduling problem ($\mathcal{S}$) instead, for each EVCS i:

$$\min_{(\ell_{i,t})_t} \sum_{t=1}^{T} f\left(\ell^0_{i,t} + \ell_{i,t}\right)\,, \quad \text{s.t.} \quad \begin{cases} \ell_{i,t} \geq 0 \quad \forall t \in \mathcal{T}\,, \\ \sum_{t=1}^{T} \ell_{i,t} = L_i/\delta\,, \end{cases} \tag{$\mathcal{S}$}$$

whose solution is the WF scheduling $\boldsymbol{\ell}^{\mathrm{wf}}$ (see Proposition 4.2). This WF-GA method is the one chosen for the comparison Section 5.4, while the two other methods PC-GA and GA-GA are studied in another chapter, in Section 7.5.3. Together, these three methods are referred to as "iterative LMP" due to the computation process of (5.2) (compared to the LMP method defined in Section 5.3, whose CUP function is the marginal cost associated with ($\mathcal{S}$)).

In order to determine the CUP functions via (5.2), it is necessary to know the grid cost function $\mathcal{G}$, which depends on the aggregated charging needs $\boldsymbol{L}$ for the three iterative methods PC-GA, GA-GA and WF-GA, which in turn depend on CUP functions $\boldsymbol{\lambda}$. Therefore, in the literature, an iterative process is followed: the aggregated charging needs $\boldsymbol{L}^{(0)}$ at Wardrop Equilibrium (WE) corresponding to CUP constant functions $\boldsymbol{\lambda}^{(0)}$ is computed. Then $\boldsymbol{\lambda}^{(1)}$ is computed using (5.2), and the charging needs are updated ($\boldsymbol{L}^{(1)}$), and so on. This iterative process is executed "offline", before EV users make their decisions based on their different cost functions, including the CUP. Note that at each iteration, the CUPs at all EVCSs are not congestion cost functions but constant cost functions and therefore, the WE and the corresponding aggregated charging needs are not necessarily unique in the driving-and-charging game $\mathbb{G}$ considered in this thesis (see Section 2.4.3). This complicates the concept of convergence of this iterative process. In such cases, the WE verifying the pro-rata condition (2.21) is selected. This shortcoming is overcome in Section 5.4.1.1 by replacing this iterative process by the Beckmann method, presented in Section 2.4.2.

5.2 Average water-filling pricing method

5.2.1 Definition based on the water-filling scheduling cost

The first charging pricing mechanism elaborated during this thesis is an average Water-Filling pricing, studied in our papers [Sohet et al., 2019a] and [Sohet et al., 2021b], and referred to as AVG[3] (for average) pricing method. The main difference with the iterative LMP method used in the literature is that the CSO, the operator of an EVCS, does not have any knowledge on the electrical grid its EVCS is connected to. In other words, the CSO is distinct from the Electrical Network Operator (ENO)[4]. However, as detailed in Section 7.2.3, it is still in the interest of the

[3]The corresponding superscripts is in lowercase: "avg", as in λ_i^{avg} the Charging Unit Price function of AVG pricing method at EVCS i.

[4]In previous Section 5.1.2, the SO groups together the ENO and the CSOs.

CSO to incentivize EV users to reduce the grid cost because in practice, an electricity contract is signed between the CSO and the ENO. The definition of the CUP functions is therefore adapted accordingly. In previous Section 5.1.2, the CUP is a function of grid cost function $\mathcal{G}$, defined in Section 4.4.1 as the load cost function f of the power load profile at the head of the grid. As the CSO of EVCS i cannot deduce this head power, the CUP λ_i^{avg} is defined as a function of the load profile at the level of EVCS i. More precisely, it is a function of the optimal objective value $G_i^*(L_i)$ (defined in (4.2)) of charging scheduling problem ($\mathcal{S}$) at EVCS i, solved by the WF scheduling in Proposition 4.2:

$$\lambda_i^{\text{avg}}(L_i) = \eta^{\text{avg}} \frac{G_i^*(L_i)}{L_i + L_i^0} = \eta^{\text{avg}} \frac{\bar{t}(L_i) \times f\left(\frac{L_i + L_{i,t}^0}{\bar{t}(L_i)\times\delta}\right) + \sum_{s=\bar{t}+1}^{T} f\left(\ell_{i,t}^0\right)}{L_i + L_i^0}, \tag{5.3}$$

with η^{avg} a conversion parameter to be fixed and $(\ell_{i,t}^0)_t$ the *sorted* non-flexible load profile at EVCS i. The other notations relative to the corresponding WF solution are defined in Section 4.2 and summarized in Table 4.1. Note that the same conversion parameter is chosen for each EVCS i and its CUP function λ_i^{avg}. Contrary to the iterative LMP scheme presented in last section, this CUP function is defined locally, meaning that λ_i^{avg} does not depend on L_j or $\boldsymbol{\ell}_j^0$ at EVCS $j \neq i$. For the rest of Section 5.2, i denotes any EVCS i.

With the AVG pricing scheme, the CSO makes EV users and consumers of non-flexible appliances pay equally (per energy unit) for the total grid cost caused by their aggregated electricity consumption, hence the name of "average" method. This means that for consumers, electricity usages during peak hours are as much expensive as during off-peak hours. This also means that households may have a smaller electricity bill thanks to the efforts made by the EV community. An additive constant term can be added to CUP function λ_i^{avg}, as in our paper [Sohet et al., 2019b], without changing the results in this section.

5.2.2 Properties of the charging unit price functions

As the aggregated charging need L_i at EVCS i is a linear positive combination of the vehicle flow vector $\boldsymbol{f}$ (see its definition in (5.22)), the CUP λ_i^{avg} is a Linearly non-Separable Congestion cost function, and Beckmann's method can be used (see Proposition 2.19). Tn the Beckmann function $\mathcal{B}$ of game $\mathbb{G}_{\text{avg}}$ with the AVG pricing mechanism, the term associated with the λ_i^{avg} at EVCS i is:

$$\mathcal{B}_{\lambda_i^{\text{avg}}} = \eta^{\text{avg}} \int_0^{L_i} \lambda_i^{\text{avg}}(L)\mathrm{d}L\,, \tag{5.4}$$

which is well defined because function λ_i^{avg} is continuous (see Lemma 5.4). Moreover, Proposition 2.22 (uniqueness of charging needs at Wardrop Equilibrium) can be applied when $L_i \mapsto \lambda_i^{\text{avg}}(L_i)$ is increasing ($\forall i$). Next Proposition 5.6 gives a necessary and sufficient condition – on non-flexible load $\boldsymbol{\ell}_i^0$ – to have an increasing λ_i^{avg}. The proof of this proposition requires the two following properties on λ_i^{avg}. The results of the present section are valid for time-dependent load cost functions f_t.

Lemma 5.4. *Function G_i^* and therefore λ_i^{avg} are C^1 on $\mathbb{R}_+$.*

Proof. Because G_i^* is easily C^∞ on $\left]\overline{L}_{i,t-1}, \overline{L}_{i,t}\right[$ for $t = 1, \cdots, T$, the proof only consists in checking the continuity at points $\left(\overline{L}_{i,t}\right)_{t=1,\cdots,T-1}$. Let $t \in \{1, \ldots, T-1\}$. Function G_i^* evaluated

in $\overline{L}_{i,t}^{-}$ gives, using definition $\overline{L}_{i,t} = t\delta\ell_{i,t+1}^{0} - L_t^0$:

$$G_i^*(\overline{L}_{i,t}^{-}) = tf\left(\frac{\overline{L}_{i,t}^{-} + L_{i,t}^0}{t\delta}\right) + \sum_{s=t+1}^{T} f(\ell_{i,s}^0) = tf\left(\ell_{i,t+1}^0\right) + \sum_{s=t+2}^{T} f(\ell_{i,s}^0) + \left(\ell_{i,t+1}^0\right) . \tag{5.5}$$

Using the same definition for $\overline{L}_{i,t}^{+}$:

$$G_i^*(\overline{L}_{i,t}^{+}) = (t+1)f\left(\frac{\overline{L}_{i,t}^{+} + L_{i,t+1}^0}{(t+1)\delta}\right) + \sum_{s=t+2}^{T} f(\ell_{i,s}^0) = (t+1)f\left(\ell_{i,t+1}^0\right) + \sum_{s=t+2}^{T} f(\ell_{i,s}^0) = G_i^*(\overline{L}_{i,t}^{-}) . \tag{5.6}$$

The continuity of the derivative $(G_i^*)'(L) = f'\left(\frac{L+L_{\bar{t}}^0}{\bar{t}(L)\times\delta}\right)$ is shown in the same way, and the C^1 property of λ_i^{avg} follows immediately as a well-defined polynomial of C^1 functions. This proof can easily be extended to the case where $f_t : \ell \mapsto \eta_t \ell^n$. □

Lemma 5.5. *Function λ_i^{avg} is strictly convex on $[0, \overline{L}_{i,T-1}[$ and linear increasing on $[\overline{L}_{i,T-1}, +\infty[$.*

Proof. In this proof, the duration of the time slots δ is set to 1 in order to simplify notations. It is assumed that $f_t : \ell \mapsto \eta_t \ell^n$ and the following quantity is defined: $H_t = (\sum_{s=1}^{t} \eta_s^{-\frac{1}{n-1}})^{-(n-1)}$ for all $t \in \mathcal{T}$. According to Lemma 5.4, function λ_i^{avg} is C^1. Moreover, $(\lambda_i^{\text{avg}})'$ is piecewise differentiable and for all $\bar{t} \in \mathcal{T}$ and $L_i \in \left]\overline{L}_{i,\bar{t}-1}, \overline{L}_{i,\bar{t}}\right[$:

$$\begin{aligned}\frac{1}{\eta^{\text{avg}}}\left(\lambda_i^{\text{avg}}\right)''(L_i) = \frac{2\sum_{t=\bar{t}+1}^{T} f_t(\ell_{i,t}^0 + \ell_{i,t}^*(L_i))}{(L_i + L_T^0)^3} + H_{\bar{t}}\frac{(L_i + L_{\bar{t}}^0)^{n-1}}{(L_i + L_T^0)^4}\Big[(n-1)(n-2)L_i^2 \\ +2(n-2)\left(nL_T^0 - L_{\bar{t}}^0\right)L_i + \left(2\varepsilon^2 - 2n\varepsilon + n^2 - n\right)\left(L_T^0\right)^2\Big] ,\end{aligned} \tag{5.7}$$

where $\varepsilon = \frac{L_{\bar{t}}^0}{L_T^0}$. The second term is non-negative since the three polynomial coefficients are non-negative for $n \geq 2$. The first term is also non-negative, and even positive for $\bar{t} \leq T-1$. The proof is completed using the continuity of $(\lambda_i^{\text{avg}})'$. □

Proposition 5.6. *For time-dependent load cost functions $f_t(\ell) = \eta_t \ell^n$ $(n \geq 2, \forall t)$, the average Water-Filling Charging Unit Price function λ_i^{avg} at EVCS i is increasing on $\mathbb{R}_+^*$ if and only if:*

$$\frac{\sum_{t=1}^{T} \tilde{\eta}_t \left(\tilde{\ell}_{i,t}^0\right)^n}{\sum_{t=1}^{T} \tilde{\ell}_{i,t}^0} \leq n , \quad \textit{with} \begin{cases} \tilde{\ell}_{i,t}^0 = \frac{\ell_{i,t}^0}{\ell_{i,1}^0} , \\ \tilde{\eta}_t = \frac{\eta_t}{\eta_1} . \end{cases} \tag{5.8}$$

Proof. The case without non-flexible consumption ($\boldsymbol{\ell}^0 = 0$) is ruled out, as $\lambda_i^{\text{avg}}(L_i) = \eta^{\text{avg}} L_i^{n-1}$ would be unconditionally increasing. According to lemma 5.5, $(\lambda_i^{\text{avg}})'$ is strictly increasing on $[0, \overline{L}_{i,T-1}[$ and constant thereafter. In that case, $(\lambda_i^{\text{avg}})' > 0$ on $\mathbb{R}_+^*$ (which is equivalent to λ_i^{avg} always increasing) if and only if $(\lambda_i^{\text{avg}})'(0) \geq 0$, which is equivalent to condition (5.8). □

Remark 5.7. *A sufficient condition on non-flexible consumption $\boldsymbol{\ell}_i^0$ for an increasing λ_i^{avg} is used in our conference paper [Sohet et al., 2019a], which can be deduced from equivalent condition (5.8), which is equivalent to:*

$$\sum_{t=1}^{T} \tilde{\ell}_{i,t}^0 \left(\tilde{\eta}_t \left(\tilde{\ell}_{i,t}^0 \right)^{n-1} - n \right) \leq 0 \,. \tag{5.9}$$

Then, replacing $\tilde{\ell}_{i,t}^0$ for all t by $\tilde{\ell}_{i,T}^0 \geq \tilde{\ell}_{i,t}^0$ (the non-flexible profile is assumed sorted), the inequality $\tilde{\eta}_t (\tilde{\ell}_{i,t}^0)^{n-1} \leq n$ is a sufficient condition for an increasing λ_i^{avg}. For example, for a time-independent quadratic load cost function ($\tilde{\eta}_t = 1$ $\forall t$ and $n = 2$), this sufficient condition is:

$$\max \left(\boldsymbol{\ell}_i^0 \right) \leq 2 \times \min \left(\boldsymbol{\ell}_i^0 \right) \,. \tag{5.10}$$

Observe that a smooth non-flexible profile ($\forall t$, $|\ell_{i,t}^0 / \ell_{i,1}^0 - 1|$ small) leads to a low ratio in (5.8), which induces an increasing λ_i^{avg}. This, and more generally Proposition 5.6, is illustrated on real datasets in next section.

Remark 5.8. *The derivative of function λ_i^{avg} (which is C^1 on $\mathbb{R}_+$ according to Lemma 5.4) with respect to the aggregated charging need L_i verifies the following:*

$$(\lambda_i^{avg})' (L_i) = \eta^{avg} \frac{(G_i^*)'(L_i) - \lambda_i^{avg}(L_i)}{L_i} \,. \tag{5.11}$$

In other words, the average Water-Filling CUP function λ_i^{avg} is increasing in L_i if and only if $\lambda_i^{avg}(L_i)$ is smaller than the marginal CSO's cost $(G_i^*)'(L_i)$, which is exactly the CUP function defined in Section 5.3 (up to a multiplicative constant η^{wf}).

5.2.3 Illustration of the increasing property with real data

This section focuses on two different sets of real data (respectively from France and Texas, USA) of hourly household electricity consumption throughout a year. This consumption is taken as the non-flexible load $\boldsymbol{\ell}_i^0$ of some EVCS i, assuming this EVCS is a public charging station in a residential neighborhood for example. The subscript i is ignored in this numerical section. As discussed previously, properties of the scheduling of ($\mathcal{S}$) such as condition (5.8) depend on $\boldsymbol{\ell}^0$. The present numerical section studies the sensitivity of these properties to the discretization level of $\boldsymbol{\ell}^0$, i.e. the number of time slots T (or equivalently their common duration δ, which verifies $T \times \delta = 24$ h). The load cost function $f_t : \ell \mapsto \ell^2$ is assumed to be a timed-independent quadratic function.

The first dataset, "Recoflux", is from Enedis (the main French distribution network operator) and is a statistical representation of a typical French household consumption profile, taking into account electrical heating, water heating and all the other usages[5]. Figure 5.2.a shows samples of each type of days in this dataset. The winter consumption looks like an "upward shifted" version of the summer one due to constant heating in winter.

In the raw data, the non-flexible consumption $(\ell_t^0(d))_{1 \leq t \leq 24}$ of each day d is split into 24 hourly time slots. Figure 5.3.a gives for each month of a year the proportion of days d where $\boldsymbol{\ell}^0(d)$ verifies the equivalent condition (5.8) to an increasing λ^{avg}. This figure shows that with $T = 24$ time slots (star markers), condition (5.8) is not verified during the whole summer (see

[5] Available at https://www.enedis.fr/coefficients-des-profils (RES1_BASE).

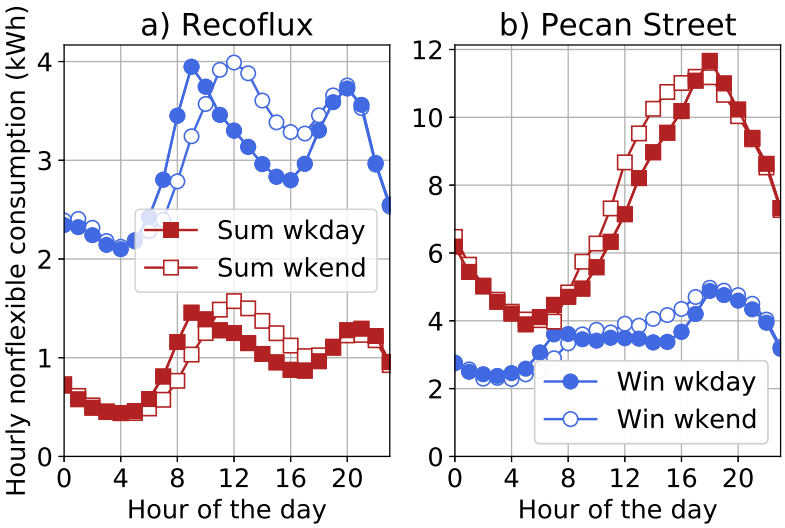

Figure 5.2: Household electricity consumption during sum(mer) and win(ter), w(ee)kday and w(ee)kend, in France (a) and Texas (b).

below for more details on this figure). Therefore, the CUP function λ^{avg} is not increasing and the aggregated charging needs at WE may be not unique (see Section 2.4.3), which makes it difficult to predict actual vehicle users' behavior with the game theory model defined in Chapter 2. Condition (5.8) is thus tested on the Recoflux consumption profiles aggregated into fewer time slots.

In the following, the non-flexible daily profiles are first increasingly sorted before being aggregated into $T < 24$ time slots. For example for $T = 2$, for each day d the non-flexible profile $\boldsymbol{\ell}^0(d)$ is divided in two: the twelve lowest hourly consumption values of $\boldsymbol{\ell}^0(d)$ are summed into the term $\overline{\ell}_1^0(d)$ and the others into $\overline{\ell}_2^0(d)$. Note that consecutive hourly consumptions $\ell_t^0(d)$ might not be in the same $\overline{\ell}_t^0(d)$, as it is the case for the off-peak hours in France, corresponding to night hours and some of the afternoon hours (from 11pm to 9am and from 3pm to 5pm). This modeling choice leads to an underestimation of the number of days for which λ^{avg} is increasing, compared to any other aggregation of non-flexible profiles. Indeed, for example for $T = 2$, any sum $\underline{\ell}_1^0$ of twelve non-flexible hourly consumption values verifies $\underline{\ell}_1^0 \geq \overline{\ell}_1^0$, by definition of the aggregated profile $\overline{\boldsymbol{\ell}}^0$. Similarly, $\underline{\ell}_2^0 \leq \overline{\ell}_2^0$. Thus, $\sum_{t=1,2} \underline{\ell}_t^0 = \sum_{t=1,2} \overline{\ell}_t^0$, but $\sum_{t=1,2} (\underline{\ell}_t^0)^2 < \sum_{t=1,2} (\overline{\ell}_t^0)^2$ because the quadratic function is convex. Therefore, the aggregated profile $\underline{\boldsymbol{\ell}}^0$ is more likely to verify the condition (5.8) than aggregated profile $\overline{\boldsymbol{\ell}}^0$ chosen here. For example in Figure 5.3.a, in May and for $T = 4$, there are *at least* 60 % of the days where λ^{avg} is increasing.

The same argument explains why an aggregated profile $\overline{\boldsymbol{\ell}}^0$ in T_1 time slots is associated with more days with λ^{avg} increasing than for $T_2 > T_1$. For $T > 2$ time slots, summer months (from May to October) include days when λ^{avg} is not increasing. This is likely to be caused by the absence of heating during these months. This phenomenon is worse with a higher T. In winter, nearly constant heating makes up a substantial part of consumption, lowering the impact of other electrical appliances consumption variations. The maximal hourly consumption is a little less than 4 kWh while the minimal a little more than 2 kWh, so that the sufficient condition (5.10) is verified. In conclusion, the *lower* the number T of time slots, the higher the proportion of days with an increasing CUP function λ^{avg}. This means that, considering the AVG pricing scheme,

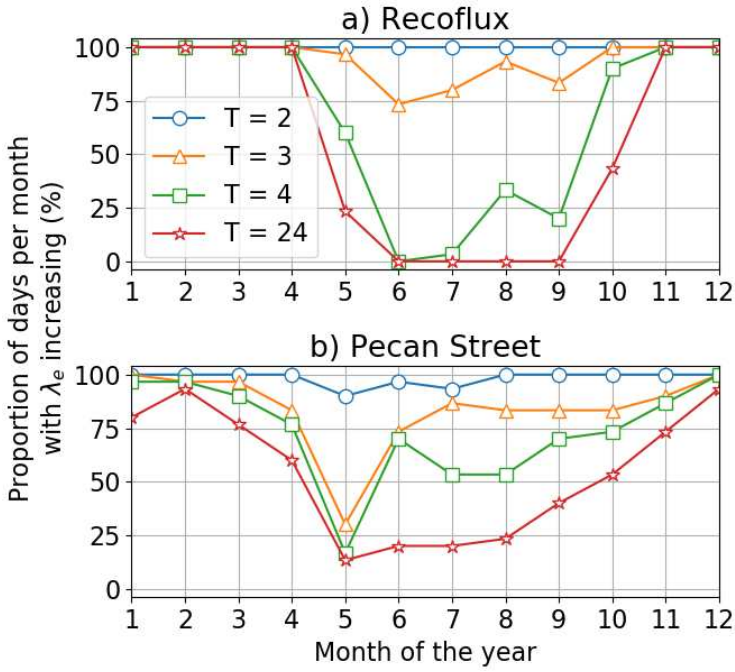

Figure 5.3: Proportion of days per month when λ_i is increasing (using Proposition 5.6 with $\eta_t = \eta$ and $n = 2$), for different number T of time slots (top: Recoflux; bottom: Pecan Street). *A lower T ensures a higher proportion of days where WE is unique.*

the CSO does not need refined non-flexible consumption profiles to model the behavior of vehicle users. For such refined profiles, the CSO should aggregate them into the highest number T of time slots which leads to an increasing CUP function λ^{avg} everyday of the year. This way, the CSO schedules EV charging in the highest number of time slots guaranteeing uniqueness Proposition 2.22. In the case no such T exists, another pricing scheme is defined in next section, with always increasing CUP functions.

The second dataset is a residential hourly electric consumption throughout year 2018, given by the company Pecan Street. More precisely, the original data contains 25 Texan households, whose consumptions are averaged into a unique hourly consumption (corresponding to a fictitious household). Compared to the previous dataset, consumption here is higher during summer because of the intensive use of air conditioning in Texas (see Figure 5.2). The use of air conditioning is such that the consumption peak observed at 7 a.m. in winter is negligible compared to summer consumption. In a year, the total number of days where λ^{avg} is increasing is roughly the same between Recoflux and Pecan Street datasets, for each number of time slots T (see Figure 5.3). The drop of this number in May (Figure 5.3.b) is due to heterogenous use of air conditioning throughout each day of the first month of the year where temperatures become high enough.

5.3 Locational marginal pricing method based on water-filling charging scheduling

5.3.1 Definition based on the marginal water-filling scheduling cost

The second charging pricing scheme elaborated during this thesis is the LMP based on Water-Filling charging scheduling, studied in our papers [Sohet et al., 2021c] and [Sohet et al., 2021a]. This method is called WF-WF – the first WF designating the charging scheduling method and the second, the WF objective which is differentiated to obtain the Charging Unit Price functions[6] –, and the corresponding subscript is "wf". The WF-WF pricing scheme follows the idea of the average WF pricing scheme of last section: the corresponding CUP λ_i^{wf} at EVCS i is also a function of the CSO's cost function G_i^* obtained with the WF scheduling of Proposition 4.2 and expressed by (4.2). Therefore, λ_i^{wf} is also a local CUP function and does not depend on loads L_j at other EVCSs $j \neq i$. For the rest of Section 5.3, i denotes any EVCS i. Like for the AVG pricing method, the CSO does not need information or control over the electrical grid. The difference between λ_i^{wf} and λ_i^{avg} is that, instead of being CSO's cost function G_i^* divided by the total aggregated load $L_i + L_i^0$ at EVCS i, it is the derivative of G_i^* with respect to the aggregated charging need L_i, in line with the iterative LMP method presented in Section 5.1.2. Function λ_i^{wf} also has an explicit formulation depending on L_i:

$$\lambda_i^{\mathrm{wf}}(L_i) = \eta^{\mathrm{wf}} \frac{\partial G_i^*}{\partial L_i} = \frac{\eta^{\mathrm{wf}}}{\delta} f' \left(\frac{L_i + L_{i,\bar{t}}^0}{\bar{t}(L_i) \times \delta} \right) , \tag{5.12}$$

with η^{wf} a conversion parameter to be fixed.

5.3.2 Properties of the charging unit price functions

Like λ_i^{avg}, λ_i^{wf} is a function of the aggregated charging need L_i at EVCS i, which makes it a Linearly non-Separable Congestion cost function, and Beckmann's method can be used to find the Wardrop Equilibrium (see Proposition 2.19). Note that for marginal cost functions such as λ_i^{wf}, defined as the derivative of another function $\eta^{\mathrm{wf}} G_i^*$, there always exists a corresponding potential, which is $\eta^{\mathrm{wf}} G_i^*$, even for general non-separable congestion cost functions. If the functions G_i^* are *strictly* convex and $\eta^{\mathrm{wf}} > 0$ on top of that, then Proposition 2.22 is true for game $\mathbb{G}_{\mathrm{wf}}$ with the WF-WF pricing mechanism. Therefore, in the Beckmann function $\mathcal{B}$ of game $\mathbb{G}_{\mathrm{wf}}$, the term associated with the CUP function λ_i^{wf} at EVCS i and given by (2.11) is simply:

$$\mathcal{B}_{\lambda_i^{\mathrm{wf}}}(\boldsymbol{f}) = \eta^{\mathrm{wf}} G_i^*\big(L_i(\boldsymbol{f})\big) , \tag{5.13}$$

with $L_i(\boldsymbol{f})$ a linear combination of vehicle flow vector $\boldsymbol{f}$ by definition (5.22).

Remark 5.9. *In this remark, the index i of the EVCS is dropped. The well-known result [Alizadeh et al., 2016] that LMP method is optimal, in the sense that for example CUP function λ^{wf} incentivizes EV users to minimize the objective function G^* (when EV users face no other costs in game $\mathbb{G}_{wf}$), comes from the particular form of its potential $\mathcal{B} = \eta^{wf} G^*$. If $\mathcal{B}$ is convex and η^{wf} is positive, the Wardrop Equilibrium of game $\mathbb{G}_{wf}$ correspond to the global minima of $\mathcal{B}$ (under constraints (2.1)), as explained in Remark 2.24. Thus, at WE of game $\mathbb{G}_{wf}$,*

[6] In Section 5.1.2, the three different iterative LMP schemes use different charging scheduling methods (PC, WF and GA), but the corresponding CUP functions are defined as the differentials of the same objective function, obtained with the Grid Aware charging scheduling.

function G^* is minimized ($\eta^{wf} > 0$). In the case where EV users have others costs in addition to the charging cost (e.g., the traffic congestion cost, like in the comparison made in Section 5.4), function G^* is not necessarily minimized at WE.

On top of that, contrary to λ_i^{avg}, λ_i^{wf} is unconditionally increasing:

Proposition 5.10. *In the WF-WF pricing method, the Charging Unit Price function λ_i^{wf} is increasing.*

Proof. This is shown for time-independent load function $f : \ell \mapsto \ell^n$ ($n \geq 2$) but can be extended to time-dependent load functions. Function $\lambda_i^{\text{wf}} : L_i \mapsto \frac{n\eta^{\text{wf}}}{\delta}\left(\frac{L_i+L_{i,\bar{t}}^0}{\bar{t}(L_i)\times\delta}\right)^{n-1}$ is piecewise differentiable, with derivative $\frac{n(n-1)\eta^{\text{wf}}}{\bar{t}\delta^2}\left(\frac{L_i+L_{i,\bar{t}}^0}{\bar{t}(L_i)\times\delta}\right)^{n-2} > 0$. We can conclude that λ_i^{wf} is increasing by showing that it is continuous, which is done in the same way as for Lemma 5.4. Let $t \in \{1, \ldots, T-1\}$. As $\bar{t}(\overline{L}_{i,t}^-) = t$, we have $\overline{L}_{i,t}^- + L_{i,\bar{t}}^0 = t\delta \times \ell_{i,t+1}^0$ and:

$$\lambda_i^{\text{wf}}(\overline{L}_{i,t}^-) = \frac{n(n-1)\eta^{\text{wf}}}{\bar{t}\delta^2}\left(\ell_{i,t+1}^0\right)^{n-2} . \tag{5.14}$$

As $\bar{t}(\overline{L}_{i,t}^+) = t+1$, the same value is obtained for $\lambda_i^{\text{wf}}(\overline{L}_{i,t}^+)$. □

Therefore, Proposition 2.22 applies and the aggregated charging needs at WE are unique, no matter the value of the non-flexible loads $\boldsymbol{\ell}_i^0$.

The following section shows how λ^{wf} is adapted to the case of asynchronous departures and arrivals of EVs at EVCSs. In this section, the subscript i relative to an EVCS i is omitted.

5.3.3 Online and offline pricing methods for asynchronous charging needs

5.3.3.1 Definitions

This work is inspired from our paper [Sohet et al., 2021a]. The notations of this section are defined in Section 4.3 and summarized in Table 4.6. In the case of asynchronous EV arrivals a and departures d at the EVCS, we suggest a CUP function $\lambda^{(a,d)}$ for each EV class (a, d), based on CSO' cost functions minimized by adequately choosing[7] the per-class aggregated charging profiles of all EV classes. More precisely, we define $\lambda^{(a,d)}$ as the marginal CSO's costs corresponding to the charging need $L^{(a,d)}$ of EV class (a, d), following the LMP scheme. Therefore, by definition, different EV classes may have different CUP functions. An interesting property of such a pricing scheme is that the EV class staying at the EVCS the whole time period $\mathcal{T}$ has a smaller CUP than an EV class staying only one time slot, because the former charging profile is more flexible than the latter (i.e. can be scheduled over a larger temporal period). Therefore, such a pricing mechanism can be used as an incentive for EV users to become more flexible for their charging operations, in the commuting context or for example in a shopping mall.

In the offline charging scheduling problem introduced in Section 4.3.2, the CSO's charging cost function[8] $\tilde{G}$ is the one obtained by solving problem ($\mathcal{P}$), which gives the following CUP functions:

$$\lambda^{(a,d)} = \frac{\partial \tilde{G}}{\partial L^{(a,d)}}\left(\boldsymbol{\ell}^0, \boldsymbol{L}\right) . \tag{5.15}$$

[7] The determination of the charging profiles and the CUP functions is done before the charging time period $\mathcal{T}$ or at each EV arrival, respectively for the offline or online methods.

[8] Note that in this Section 5.3.3 compared to the rest of this chapter, the optimal charging profiles and CSO's cost are denoted with a $\sim$ instead of a $*$.

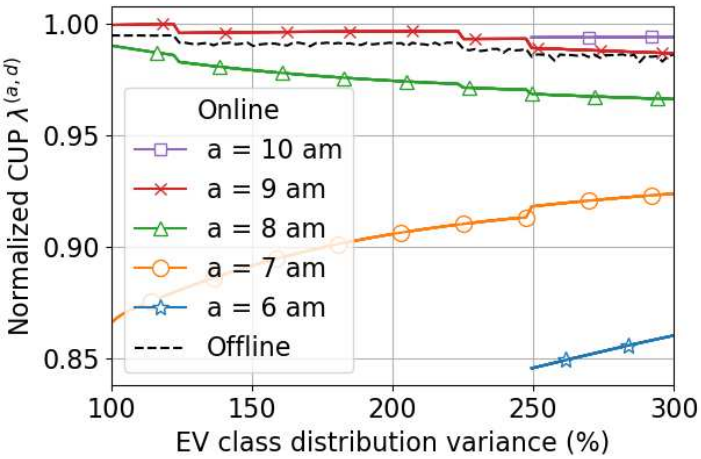

Figure 5.4: CUPs (vertical axis normalized) in function of the variance of EV classes' distribution, for each EV class (a, d) and both online and offline scheduling problems. *The offline CUP function does not depend on the EV class due to the smoothed total load (see Figure 4.7). For the same reason, the online CUP function does not depend on the EV departure time. However, because this CUP function is given at the EV arrival, it is cheaper for EV users arriving earlier because the charging load of future EVs is not taken into account.*

By definition of the offline charging scheduling problem, the CSO knows in advance all arrival and departure time slots and the corresponding per-class aggregated charging needs. Therefore the CSO can compute the minimal charging cost $\tilde{G}$ by solving problem $(\mathcal{P})$ and directly transmits the CUP functions to EV users offline, before the whole time period $\mathcal{T}$.

In the online charging scheduling problem introduced in Section 4.3.3, the CSO's charging cost function considered to establish the CUP function of EV class (a, d) is $\tilde{G}^a$, the one computed at the arrival time slot a of these EVs:

$$\lambda^{(a,d)} = \frac{\partial \tilde{G}^a}{\partial L^{(a,d)}} \left(\boldsymbol{\ell}^0 \,, \left(L^d_{a^-} \right)^{d \in \mathcal{D}_{a^-}}_{a^- \leq a} \right) . \tag{5.16}$$

Note that this cost function $\tilde{G}^a$ may be different from the one when these EVs leave the EVCS, or from the one at the end of the whole charging operation at $t = T$: if additional EVs arrive between a and d, the CSO updates the charging profiles and its costs with the online Algorithm 4.1. The chosen pricing mechanism defined in (5.16) has the advantage of providing a fixed price to EV users at their arrival, thus answering one of the main current EV users' expectations.

5.3.3.2 Numerical comparison

Figure 5.4 compares the CUP functions obtained with the online and offline methods. To better illustrate the differences, the prices are plotted for different variances of EV arrival and departure distributions. More precisely, we suppose that the variances of both the arrival and departure distributions can go up to 300 % of the ENTD values (see Figure 4.8). The vertical axis of Figure 5.4 is normalized so that the highest point is equal to one.

First, Figure 5.4 shows that from 250 % of variance values, the discretized EV classes distribution starts to consider EVs arriving at the EVCS at 6 am or 10 am (see the corresponding online CUP functions respectively with star and square markers), which also explains the discontinuities in the CUP functions. Note that by definition, the online CUP function $\lambda^{(a,d)}$ reflects

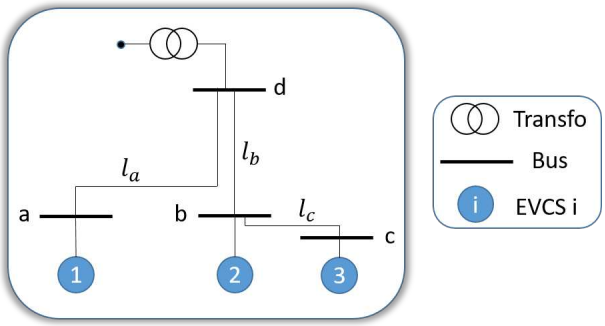

Figure 5.5: Electrical network containing the three EVCS.

the marginal cost of the CSO computed at the arrival a of the EV class (a, d), and not the effective marginal cost (calculable at the departure d of the EV class). Therefore, in the online charging problem, EV users arriving at some time a_1 are likely to pay a CUP cheaper than users arriving at $a_2 > a_1$, because the prices of the former only take into account the charging of EVs arriving at a_1, while the latter take both EV classes into account (see Figure 5.4).

This systematic characteristic of the online CUP function ($\lambda^{a_1,d_1} < \lambda^{a_2,d_2}$ with $a_1 < a_2$) may be unfair in the case EV class (a_2, d_2) might offer more flexibility ($d_2 - a_2 > d_1 - a_1$). This fairness aspect seems not addressed in the literature and could constitute a future work. Similarly, most part of the increasing and decreasing features of the CUP functions are also caused by this issue. For example, for a higher variance of arrival distribution, there is a lower proportion of EVs arriving before or at 8 am, which explains why the CUP function associated with $a = 8$ decreases. Aside from that, Figure 5.4 shows that the online CUP functions do not depend on the departure time and the offline CUP function is the same for all EV classes. The reason is that, in this use case of commuting and PV generation, any small change in the charging need of an EV class can be compensated by the charging profiles of the other EV classes in order to keep a smooth total load (this is not true in the example given in Figure 4.7). Overall, CUP functions vary by 5% at most, which is more likely to be accepted by EV users.

5.4 Numerical comparisons of the pricing methods

In this section, the different pricing schemes introduced in this chapter are compared, as well as their impact on the coupling of EV driving-and-charging decisions. For this, the coupled setting of our paper [Sohet et al., 2020a] is used in Section 5.4.2. Before that, the pricing schemes are illustrated in Section 5.4.1 by only considering the electrical grid of this setting, which is the grid studied in Sections 3.2.3 and 4.4. This grid contains three EVCSs, as shown in Figure 5.5. Its parameters are given in Section 4.4.4.1, as well as the non-flexible load profiles.

5.4.1 Illustration of the pricing methods

Before comparing the different pricing schemes of this chapter using the grid of Figure 5.5, a few specifications are needed concerning the iterative LMP method described in Section 5.1.2. Following Remark 5.9, the iterative process can be replaced by Beckmann method, thanks to the LMP structure, and Proposition 2.22 is true, assuming the grid cost function $\mathcal{G}$ is strictly convex. Thus, the problem of uniqueness at Wardrop Equilibrium mentioned in Section 5.1.2 is sorted out. Note however that numerical tests show that the iterative process converges towards the

WE obtained with the Beckmann method in very few iterations, although no theoretical proof has been obtained yet. The iterative LMP scheme chosen is WF-GA, based on the same WF charging scheduling as the AVG and WF-WF pricing schemes defined respectively in Sections 5.2 and 5.3, in order to conduct a fair comparison. The impact of different charging schedulings is already studied in Section 4.4.4. As WF-GA, AVG and WF-WF methods are all associated with a WF charging scheduling, their names are simplified into respectively GA, AVG and WF. The subscript associated with method GA is "ga", and the potential function corresponding the Charging Unit Price function λ_i^{ga} at EVCS i is:

$$\mathcal{B}_{\lambda_i^{\mathrm{ga}}} = \eta^{\mathrm{ga}} \mathcal{G}(\boldsymbol{\ell}^{\mathrm{wf}}) \,, \tag{5.17}$$

with $\boldsymbol{\ell}^{\mathrm{wf}}$ the optimal WF charging load profile at all EVCSs.

5.4.1.1 Definition of the α-locational marginal pricing method

An additional LMP scheme is considered for the comparative study. In the WF method, the operator defining the CUP functions (the CSO) is distinct from the grid operator (the ENO) and has no information on the grid. Thus, the CUP functions λ_i^{wf} are defined as differentials of the WF objective functions G_i. On the contrary, in the GA method, the CSO and the ENO are the same operator (the SO), which has access to all the information on the grid and which defines the CUP functions λ_i^{ga} as differentials of the grid cost function $\mathcal{G}$. The idea is to define an LMP method in which the CSO is distinct from the ENO, but still has some information on the grid, information which is provided by the ENO. More precisely, the ENO communicates to the CSO all the parameters needed to compute the approximated marginal grid cost $\frac{\partial \mathcal{G}}{\partial \ell_d}(0,0,0,\sum_i \alpha_i \ell_i^{\mathrm{tot}})$ introduced in Section 3.2.3.1. This set of parameters includes the constants $\alpha_i > 1$ reflecting the different impact of each EVCS i on the grid.

For each EVCS i, the ENO defines parameter α_i such that the augmented total load $\alpha_i \ell_i^{\mathrm{tot}}$ at bus d of the grid shown in Figure 5.5 yields similar marginal grid costs as a total load ℓ_i^{tot} at EVCS i. The total load ℓ_i^{tot} at an EVCS i is made of the the aggregated EV charging load ℓ_i and of the non-flexible load ℓ_i^0 at some time slot (whose index is omitted in the following). To be more precise, the parameters α_i are adjusted *simultaneously*, so that replacing the total loads ℓ_i^{tot} at all EVCSs i by a unique augmented total load $\sum_i \alpha_i \ell_i^{\mathrm{tot}}$ at bus d, gives similar marginal grid costs on some *intervals* of aggregated charging load ℓ_i values (while non-flexible loads are fixed to non-zero values). This is expressed as the following minimization problem:

$$\boldsymbol{\alpha} = \underset{\boldsymbol{\alpha}>0}{\operatorname{argmin}} \int_0^{\bar{\ell}} \left(\int_0^{\bar{\ell}-\ell_1} H\left(\ell_1, \ell_2\right) \mathrm{d}\ell_2 \right) \mathrm{d}\ell_1 \,, \quad \text{with} \tag{5.18}$$

$$H\left(\ell_1, \ell_2\right) = \sum_i \left[\frac{\partial \mathcal{G}}{\partial \ell_i} \left(\ell_1^0 + \ell_1 \,, \ell_2^0 + \ell_2 \,, \ell_3^0 + \overbrace{\bar{\ell} - \ell_1 - \ell_2}^{=:\ell_3} \,, 0 \right) - \alpha_i \frac{\partial \mathcal{G}}{\partial \ell_d} \left(0, 0, 0, \sum_i \alpha_i \ell_i^{\mathrm{tot}} \right) \right]^2 ,$$

where $\bar{\ell} = \sum_i \ell_i$ is the *fixed* sum value of all charging power loads (by definition of ℓ_3 in (5.18)).

For the design of constants α_r, the other parameters are set as follows. The total charging need $\overline{L} = 9$ MWh is aggregated over 1500 EVs (typical for such a distribution grid, see Section 3.2.3.2), each with the same charging need of 6 kWh (see Section 4.3.4.1). The non-flexible consumption is assumed uniformly distributed among the three EVCSs: $L_i^0 = 10$ MWh. The time period

$\mathcal{T}$ considered is divided into $T = 8$ time slots, and the power is assumed constant at each EVCS throughout period $\mathcal{T}$. As (5.18) is defined on a single time slot, the load values are then $\overline{\ell} = \overline{L}/T = 2.125$ MW and $\ell_i^0 = 2.5$ MW for all EVCSs i. The resulting parameters α_i are: $\alpha_1 = 1.026$, $\alpha_2 = 1.027$ and $\alpha_3 = 1.046$.

The parameter α_3 associated with EVCS 3 is naturally higher than the others, because its distance from the transformer is the same as EVCS 1, but its power line is also congested by EVCS 2. Nonetheless, $\alpha_1 < \alpha_2$ even though EVCS 2 is closer to the transformer than EVCS 1. The reason is that these parameters are designed considering all EV distributions among the three EVCSs[9]. For example, if almost all EV users charge at EVCS 3, charging the remaining EVs at EVCS 2 leads to a higher grid cost than charging them at EVCS 3. Observe that $\alpha_i > 1$ for all EVCSs i, because a given load at an EVCS causes a higher marginal grid cost than the same load (i.e. $\alpha_i = 1$) at bus d (e.g., due to power losses). Also note that the values of α_i are sensitive to $\overline{\ell}$ and ℓ_i^0, so that different use cases may require to each solve (5.18). However, these values are not very sensitive to the numerical method used the integrals, and solving (5.18) can be done rapidly by evaluating $H(\ell_1, \ell_2)$ only a few times.

The corresponding LMP scheme is referred to as the α method (with α the corresponding subscript). Like in the other pricing schemes, a conversion parameter η^α is needed for the expression of the CUP function λ_i^α at EVCS i, and the charging scheduling chosen is the Water-Filling one $\boldsymbol{\ell}_i^{\mathrm{wf}}(L_i)$. Therefore, λ_i^α is a function of every aggregated charging need L_i via $\boldsymbol{\ell}_i^{\mathrm{tot}} = \boldsymbol{\ell}_i^0 + \boldsymbol{\ell}_i^{\mathrm{wf}}(L_i)$:

$$\lambda_i^\alpha(\boldsymbol{L}) = \eta^\alpha \alpha_i \sum_{t=1}^{T} \frac{\partial \mathcal{G}_t}{\partial L_i}\left(0, 0, 0, \sum_i \alpha_i \ell_{i,t}^{\mathrm{tot}}\right) = \eta^\alpha \alpha_i \frac{\partial \mathcal{G}}{\partial L_i}\left(0, 0, 0, \left(\sum_i \alpha_i \ell_{i,t}^{\mathrm{tot}}\right)_t\right). \tag{5.19}$$

As the α pricing is an LMP scheme, λ_i^α has the following natural potential:

$$\mathcal{B}_{\boldsymbol{\lambda}_i^\alpha} = \eta^\alpha \mathcal{G}\left(0, 0, 0, \left(\sum_i \alpha_i \ell_{i,t}^{\mathrm{tot}}\right)_t\right). \tag{5.20}$$

Like for the GA method, $\mathcal{B}_{\boldsymbol{\lambda}_i^\alpha}$ are strictly convex and Proposition 2.22 is true[10].

5.4.1.2 Illustration of the effect of charging needs on the pricing methods

Four different pricing methods are illustrated in Figure 5.6. More precisely, the corresponding Charging Unit Prices at EVCS $i = 3$ are shown in function of the aggregated charging need L_3 there, considering the non-flexible vector $\boldsymbol{\ell}^0$ defined in Section 4.4.4.1 and the time period made of $T = 4$ time slots. The charging needs at the other EVCSs are assumed constant and equal to zero in order to isolate the effect of L_3 on these CUP functions: $L_1 = L_2 = 0$.

The choice of the conversion – from the grid cost expressed as squared powers, to financial costs – parameter value η is not detailed in the related literature [Alizadeh et al., 2016, Wei et al., 2017]. A method to design this parameter is given in Chapter 7. For the moment, for each pricing method m, its conversion parameter η^m is set so that its highest CUP value is equal to 125 % of the flat rate of 0.20 €/kWh considered in next section, i.e. 0.25 €/kWh.

[9] Note that in Section 3.2.3.1, the EVCS the closest to the transformer is associated with the lowest parameter α. This is due to the slightly different design employed in our paper [Sohet et al., 2020b] for these parameters, which considers that all EV users charge at the same EVCS, because of Proposition 3.10.

[10] Note that if instead of the *local* WF scheduling, the global one was used with a pro-rata disaggregation (see Section 4.4.3), then the CUPs λ_i^α would be linearly non-separable increasing congestion cost functions.

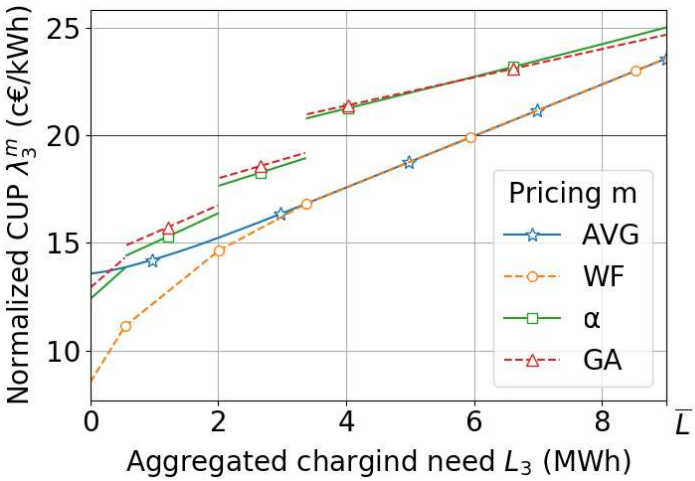

Figure 5.6: Comparison of the CUPs of AVG, WF, GA and α pricing methods at EVCS $i = 3$ in function of the aggregated charging need L_3, with $L_1 = L_2 = 0$. The CUP functions come from the average WF pricing method (AVG) and several Locational Marginal Pricing schemes, differentiated from different cost functions: the Water-Filling costs (WF), the grid aware costs (GA) and the approximated grid aware costs (α). *All CUP functions are increasing (see Propositions 5.6 and 5.10). In addition, for the GA and α pricing methods they are piecewise strictly convex, and for the AVG and WF methods, they are linear on* $[3.37, \overline{L}]$.

Notation. *A euro cent is denoted 1 c€* $= 0.01$ €.

The conversion parameter values of the AVG, WF, GA and α methods are respectively (in 10^{-5} €/kW^2) 4.79, 2.40, 4.50 and 4.50. For GA and α methods, the same η-value is kept to better compare them and visualize the approximation of the power flow in the grid suggested in previous section. Using Figure 5.6, different observations can be made on the CUP function of each pricing method:

[AVG] The CUP function λ_3^{avg} is always increasing because the non-flexible vector $\boldsymbol{\ell}_3^0$ verifies condition (5.8) $\sum_t (\tilde{\ell}_{3,t}^0)^2 / \sum_t \tilde{\ell}_{3,t}^0 = 1.59 \leq 2$. Figure 5.6 also illustrates Lemma 5.5: this CUP function is strictly convex up to $\overline{L}_{3,T-1} = 3.37$ MWh and then equal to linear increasing function $L_3 \mapsto \eta^{\text{avg}} \frac{L_3 + L_3^0}{T}$.

[WF] As expressed by (5.12), Figure 5.6 shows that the CUP function λ_3^{wf} is piecewise linear increasing and concave. Moreover, on $[\overline{L}_{3,T-1}, \overline{L}]$, λ_3^{wf} is equal to the linear function $L_3 \mapsto 2\eta^{\text{wf}} \frac{L_3 + L_3^0}{T}$ (proportional to λ_3^{avg} on this domain). As the conversion parameter value chosen in this pricing method is half the value for the AVG scheme ($\eta^{\text{wf}} = \frac{1}{2}\eta^{\text{avg}}$), it is therefore normal that $\lambda_3^{\text{avg}} = \lambda_3^{\text{wf}}$ on $[\overline{L}_{3,T-1}, \overline{L}] = [3.37, \overline{L}]$. For different η values, these two CUP functions would be different on $[3.37, \overline{L}]$. Finally, the CUP function associated with WF method has the largest range, due to its low value $\lambda_3^{\text{wf}} \simeq 8.5$ c€/kWh for low charging needs $L_3 \simeq 0$.

[GA] The CUP function λ_3^{ga} looks piecewise linear increasing (with decreasing slops), like λ_3^{wf}, but is not continuous at the energy thresholds $\overline{L}_{3,t}$ ($t = 1, 2, 3$) of the WF scheduling. The reason is that, at an energy threshold, an additional time slot t is used to charge EVs at EVCS 3. Then, at energy threshold $\overline{L}_{3,t}$, the grid cost $\mathcal{G}_t$ "appears" in the expression

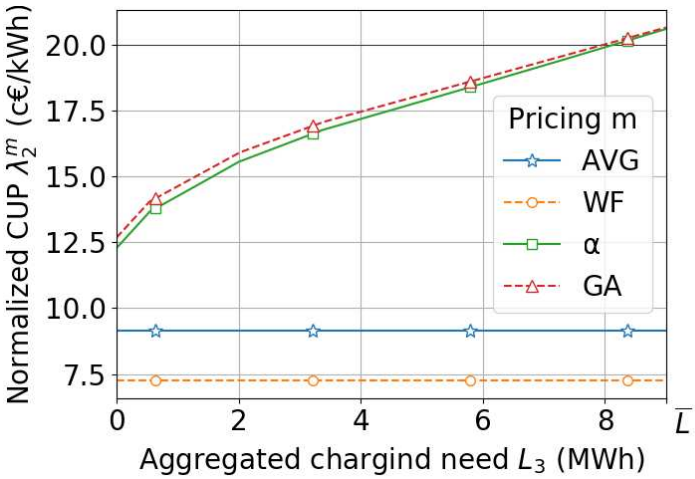

Figure 5.7: Comparison of the CUPs of AVG, WF, GA and α pricing methods at EVCS 2, in function of the aggregated charging need L_3 at EVCS 3, with $L_1 = L_2 = 0$. *The CUP functions* λ_2^{avg} *and* λ_2^{wf} *are constant because they are computed locally and only depend on* L_2*, unlike for GA and* α *methods.*

of the marginal (with respect to L_3) grid cost, which is proportional to λ_3^{ga}. Thus, the discontinuities in λ_3^{ga} comes from the consideration, at energy thresholds, of the impact of additional loads at all EVCSs, corresponding to a time slot not considered so far. Note that between two consecutive energy thresholds, λ_3^{ga} is actually strictly convex and not linear.

[α] The CUP function λ_3^{α} has the same properties as λ_3^{ga}. Moreover, the relative error of λ_3^{α} compared to λ_3^{ga} is of only 2 %.

Note that for *all* EVCS i, λ_i^{ga} and λ_i^{α} depend on the aggregated charging need L_3 at EVCS 3. Figure 5.7 compares the CUP functions of four pricing methods at EVCS 2, in function of L_3. This figure shows that λ_2^{ga} and λ_2^{α} are increasing, because the grid cost function $\mathcal{G}$ on which these CUP functions are based depend on *all* charging needs. These two CUP functions are continuous, unlike λ_3^{ga} and λ_3^{α} shown in Figure 5.6. Indeed here, the time slots considered in the expression of the marginal (with respect to L_2, which is constant) grid cost do not change, even when L_3 reaches an energy threshold $\overline{L}_{3,t}$, because the WF scheduling is local. On the contrary, λ_i^{avg} and λ_i^{wf} do not depend on the charging need at EVCS 3 because both their charging scheduling and CUP functions are based on the *local* objective G_2 defined in ($\mathcal{S}$) which is only function of L_2.

5.4.2 Impact of the pricing methods on a transportation-electrical system

In this section, the pricing methods illustrated in Figure 5.6 are compared in a coupled driving-and-charging framework. Compared to last Section 5.4.1, the aggregated charging needs are not exogenous parameters, but result from vehicle users' choices. Note that the GA and α pricing methods were found to yield almost identical results, so only the AVG, WF and GA methods are studied in the present section, for more clarity. They are compared to a flat pricing scheme (denoted CST, for "constant") associated with a constant CUP function $\lambda_i^{\text{cst}} = 20$ c€/kWh for every EVCS i, and also associated with the Water-Filling charging scheduling in order to conduct a fair comparison. In this setting are studied the different effects of these pricing methods on the users' choices.

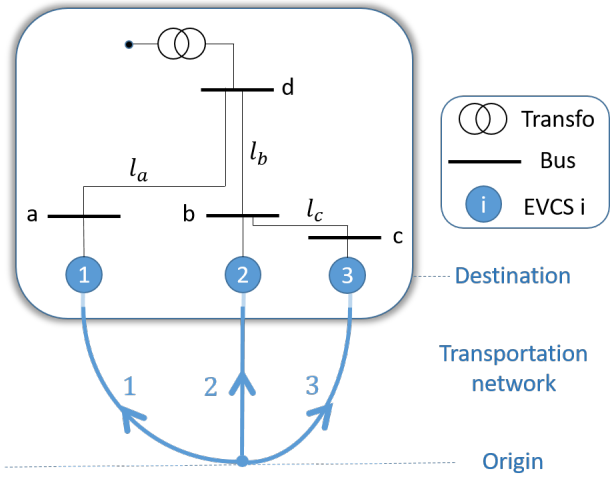

Figure 5.8: Extension of the electrical network of Figure 5.5 by a transportation network.

5.4.2.1 Driving-and-charging game setting

The use case considered here is the same as in our paper [Sohet et al., 2020a]: to commute from home to work, vehicle users choose between three driving arcs, each one leading to a different EVCS (see Figure 5.8, which is an extension of the electrical grid of Figure 5.5). A more general transportation network and/or electrical grid topology can be considered without changing the main messages and results of this study (see for example Section 7.5). In the routing game $\mathbb{G}$ modeling this commuting use case, there are two types of vehicles: EVs (subscript e) and Gasoline Vehicles (GVs, g). The total number of vehicles is $N = 3000$ and the EV penetration level is[11] $X_e = 50$ %.

The vehicle users make their choices considering the total cost function associated with each path $i = 1, 2, 3$, which is made of a traffic congestion cost defined in (2.5), a traffic toll t_i and the charging cost at the terminal EVCS i. In game $\mathbb{G}$, the total cost function $c_{s,i}$ for a vehicle user of class $s = e, g$ on path i has a similar expression as (2.6):

$$c_{s,i} = \tau \frac{l_i}{v_i} \left[1 + 2\left(x_i/C_i\right)^4\right] + t_i + l_i m_s \lambda_{s,i}\,, \tag{5.21}$$

with $\tau = 10$ €/h the average value of time while driving according to a French government report[12], l_i (resp. 30, 20 and 20.06 km for arcs 1, 2 and 3), v_i (resp. 50, 50 and 70 km/h) and $C_i = 1$ respectively the length[13], speed limit and capacity of transportation arc i, x_i the total vehicle flow on path i, m_s the energy consumption of vehicle class s per distance unit ($m_g = 6$ L/100km and $m_e = 0.2$ kWh/km [De Cauwer et al., 2015]) and $\lambda_{s,i}$ the energy unit cost ($\lambda_g = 1.5$ €/L and λ_i^m for EVs). The CUP function λ_i^m corresponds to one of the pricing methods m of Figure 5.6, and can either be constant (in the case of the CST method, $\lambda_i^{\text{cst}} = 20$ c€/kWh), depends on the aggregated charging need L_i at EVCS i (AVG and WF methods) or even depends on all charging needs (GA method). The charging need L_i at EVCS i is defined by:

$$L_i = l_i m_e \times x_{e,i} X_e N\,. \tag{5.22}$$

[11] This penetration level is highly prospective, as the current EV penetration level is around 1 % of the vehicle stock, and the level expected by 2030 ranges from 7 to 12 % [IEA, 2021].

[12] http://www.strategie.gouv.fr/sites/strategie.gouv.fr/files/archives/Valeur-du-temps.pdf.

[13] Note that the length l_1 of the transportation arc 1 is expressed with the same notation as l_a, the length of power line a.

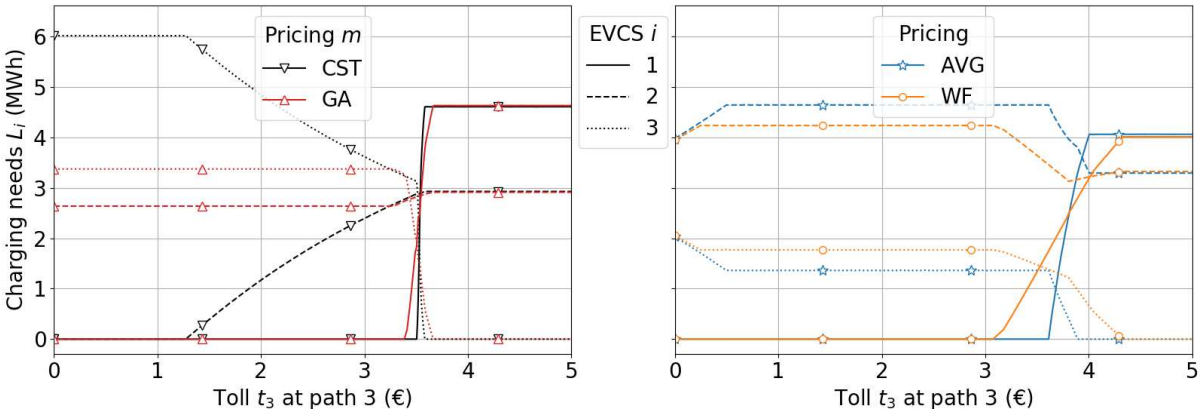

Figure 5.9: Aggregated charging needs at EVCSs 1 (solid line), 2 (dashed) and 3 (dotted) in function of path toll t_3, for the pricing methods CST, GA (respectively downward and upward triangles markers on left figure), AVG and WF (respectively stars and circles on right figure). *For all methods, the charging need L_3 at EVCS 3 drops to 0 around the toll threshold $t_3 = 3.50$ €. More EV users choose EVCS 2 for AVG and WF compared to the CST and GA methods because the non-flexible load is lower at EVCS 2 than at EVCS 3 and that the AVG and WF offer a local incentive.*

The parameters of the electrical grid are the ones defined in Section 5.4.1.

The choices of vehicle users are modeled by a Wardrop Equilibrium of game $\mathbb{G}$ and denoted $\boldsymbol{x}^*$ (see Section 2.4.1). In the case of the pricing methods considered, a WE is also a minimum of the following Beckmann function under the travel demand constraints (see (2.1)) $\sum_r x_{s,r} = X_s$ and $x_{s,r} \geq 0$ (for all s, r):

$$\mathcal{B} = \sum_i \left(l_i m_g \lambda_g x_{g,i} + t_i x_i + \int_0^{x_i} \tau \frac{l_i}{v_i} \left[1 + 2\left(x/C_i\right)^4 \right] \mathrm{d}x \right) + \sum_i \mathcal{B}_{\lambda_i^m} , \tag{5.23}$$

with $\mathcal{B}_{\lambda_i^m}$ the term corresponding to the CUP function of pricing method m at EVCS i. For the CST method, $\mathcal{B}_{\lambda_i^{\text{cst}}} = l_i m_e \lambda_e x_{e,i}$. The Beckmann's term of the methods AVG, WF and GA is respectively given in (5.4), (5.13) and (5.17). This convex optimization problem is easily solved by built-in Python function *minimize* (in SciPy package), relying on a sequential least squares programming method [Kraft, 1988]. Except for the CST pricing scheme, the aggregated charging needs at equilibrium are unique and therefore are the focus of the numerical study in next Section 5.4.2.2, as well as functions of these variables, such as the grid cost function $\mathcal{G}$. As already mentioned, in the case of non-uniqueness of the charging needs for the CST scheme, the WE verifying the pro-rata condition (2.21) is selected. Note however that in the particular setting introduced in this section, no case of non-uniqueness was encountered.

5.4.2.2 Comparison of the pricing methods in function of a traffic toll

In order to observe the differences of EV users behavior at Wardrop Equilibrium between the different pricing methods, a sensitivity analysis is conducted. Figure 5.9 shows the aggregated charging needs at WE for all pricing schemes, in function of a parameter of the driving-and-charging vehicle game $\mathbb{G}$ defined in last section. The chosen parameter is the traffic toll t_3 on path 3, like for the sensitivity analysis of the different charging schedulings (with a flat pricing scheme) done in our paper [Sohet et al., 2020a]. The conversion parameters η^m of the pricing

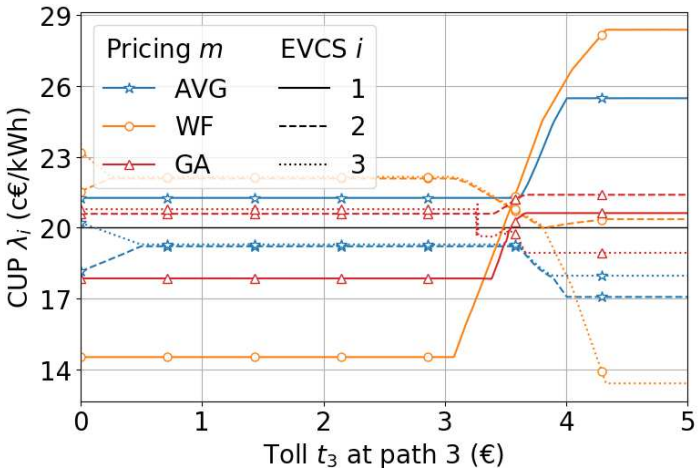

Figure 5.10: Charging Unit Prices at EVCSs 1 (solid line), 2 (dashed) and 3 (dotted) in function of path toll t_3, for GA, AVG and WF pricing methods (respectively upward triangles markers, stars and circles). *The AVG and WF methods offer a higher CUP variability (the difference between CUP values of different EVCSs) than the GA one.*

methods m are set differently than in Section 5.4.1.2, so that for each method, at $t_3 = 0$, the average of the CUP values λ_i^m at all EVCSs i is equal to the flat rate value 20 c€/kWh. The values of conversion parameters η of methods AVG, WF[14] and GA are respectively 6.3, 3.8 and 4.2×10^{-5} €/kW^2.

Figure 5.9 is separated in two for a better visibility, with the CST (downward triangles as markers) and the GA (upward triangles) pricing schemes on the left, and the AVG (stars) and WF (circles) pricings on the right. It shows that all schemes lead to the same global sensitivity: around the threshold value $t_3 = 3.50$ €, the charging needs L_3 at EVCS 3 (dotted lines) dramatically drop to 0, due to a too expensive toll on path 3. Below this threshold, EV users only go to EVCSs 2 and 3, as indicated by the aggregated charging needs L_2 (dashed lines) and L_3, because the driving path 1 is quite longer. When the CUPs are the same at all EVCSs (CST pricing method), drivers favor the fastest path 3 ($l_3 \simeq l_2$ but $v_3 > v_2$). For the three other methods, less drivers choose path 3 because of a higher CUP at the corresponding EVCS: for the AVG and WF methods, this is due to a higher non-flexible load at EVCS 3. For the GA method where λ_3 depends on all non-flexible loads, this is due to the higher power losses associated with charging at EVCS 3. Above the toll threshold, drivers use both EVCSs 1 (solid lines) and 2. Note that due to the higher electricity consumption of EV users choosing the longest path 1, a higher aggregated charging need at EVCS 1 than at EVCS 2 does not necessarily mean that more drivers choose EVCS 1 than EVCS 2.

In general, more EV users choose EVCS 2 in AVG and WF pricing schemes than in CST and GA pricings. The reason is that the AVG and WF schemes offer lower CUPs at EVCS 2 due to the lower non-flexible load there. Regarding the GA scheme, even if EVCS 2 is also associated with the lowest power losses, the corresponding CUP is not lower enough than the ones at the other EVCSs, because in this pricing scheme all CUP functions depend on the whole grid topology. Therefore, EV users are not incentivized to choose EVCS 2 as much as in AVG and WF pricing methods, which can even lead to the same drivers' choices as in the CST method

[14] In this section, the conversion parameter of AVG pricing scheme is not the double of the one of the WF scheme and therefore the associated CUP functions are not equal on $[\overline{L}_{3,T-1}, \overline{L}]$ like in Figure 5.6.

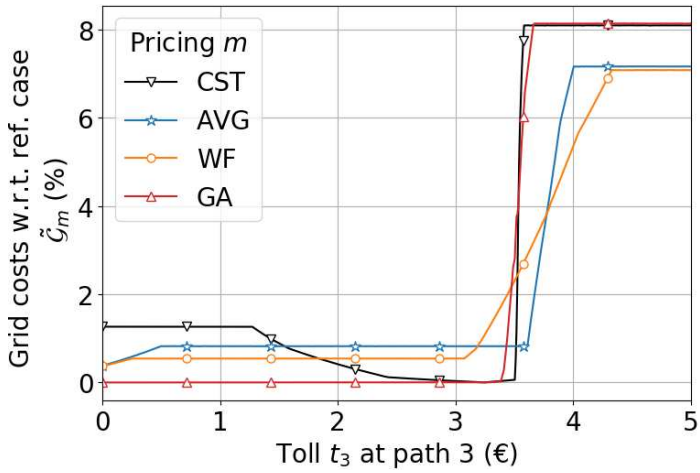

Figure 5.11: Normalized grid cost $\tilde{\mathcal{G}}_m$ in function of path toll t_3, for CST, GA, AVG and WF pricing methods m (respectively downward and upward triangles markers, stars and circles). *For all methods, the associated grid cost functions increase substantially around toll threshold $t_3 = 3.50$ € because EV users start to choose the electricity-consuming transportation arc 1.*

(see above the toll threshold in Figure 5.9). Figure 5.10 shows that for each pricing method, the variability between the CUP functions at each EVCS is different. Above the toll threshold $t_3 = 3.50$ €, the largest difference between the CUP values of a same pricing scheme at different EVCSs is only 2 c€/kWh for the GA scheme, 5.5 c€/kWh for the AVG scheme and 14 c€/kWh for the WF scheme (for which $\lambda_1 \simeq 2 * \lambda_2$).

Remark 5.11. *Figure 5.10 shows that for the three schemes, $\lambda_2 \simeq \lambda_3$ below the toll threshold. This is due to $l_2 \simeq l_3$: $l_2 = 20$ km and $l_3 = 20.06$ km. More precisely, below this toll threshold, paths 2 and 3 are both chosen by some EV and some GV users at Wardrop Equilibrium. Therefore, by definition of the WE, the costs associated with these two paths are equal, for each vehicle class s: $c_{s,2} = c_{s,3}$. These two equalities lead to $l_2\lambda_2 - l_3\lambda_3 = (l_2 - l_3)\lambda_g$, which is relatively small due to $l_2 \simeq l_3$.*

Figure 5.11 shows the normalized grid costs of the different pricing methods in function of the traffic toll t_3. The normalized grid cost function $\tilde{\mathcal{G}}_m$ of a method m ($m =$ CST, AVG, WF or GA) is defined in Section 4.4.4 by:

$$\tilde{\mathcal{G}}_m(t_3) = \frac{\mathcal{G}_m(t_3) - \mathcal{G}_{\text{ga}}(0)}{\mathcal{G}_{\text{ga}}(0)} . \tag{5.24}$$

The CST method corresponds exactly to the local method described in our paper [Sohet et al., 2020b]. The associated grid cost function decreases between $t_3 = 1.25$ € and the toll threshold $t_3 = 3.50$ € because EV users initially charging at EVCS 3 gradually choose to rather charge at EVCS 2 (see Figure 5.9), associated with lower power losses. At the toll threshold, the normalized grid cost functions of all pricing methods dramatically increase by 8 % because EV drivers start to choose the longest path 1 and therefore increase the total charging need $\sum_i L_i$ in the grid[15]. The GA pricing is as expected the best method to reduce the grid cost function below the toll threshold. This is due to a rather homogenous charging need between EVCSs 2 and 3, compared to the other methods (see Figure 5.9). For example for the CST method, all the

[15]This can be observed in Figure 5.9, where $\sum_i L_i$ increases at the toll threshold for all pricing methods.

charging need is at EVCS 3 below $t_3 = 1.25$ €, so the local WF charging scheduling smooths the total load profile at EVCS 3, but cannot do it for EVCS 2 where there is no charging need to smooth the non-flexible load profile. However, above the toll threshold, the GA pricing scheme leads to grids cost functions similar to the ones obtained with CST scheme. On the contrary, the AVG and WF schemes lead to grid cost functions lower by 1 %. The reason is that for the local pricing methods AVG and WF, the CUP values λ_1 at EVCS 1 is substantially higher than λ_2 (see Figure 5.10), which incentivizes EV users to rather choose the shorter path 2 which is less electricity-consuming. The GA pricing is a global method (i.e., λ_i depends not only on L_i but also on L_j with $j \neq i$), and incentivizes collectively *all* EV users not to choose the longest path 1 when all CUP functions increase at the toll threshold $t_3 = 3.50$ € due to a higher total charging need $\sum_i L_i$. However, this collective incentive is less efficient than the local incentives of AVG and WF pricings. This illustrates the fact that the GA LMP is the optimal pricing method (see Remark 5.9) for grid cost reduction *only* when EV users face no other costs (unlike here where there is traffic congestion and toll).

Note that pricing methods are also compared in other chapters of this thesis. In Section 6.2.2, it is shown numerically that when the operator of an EVCS is sizing the solar panel surface at the EVCS, the AVG method yields a higher optimal payoff than with a CST pricing scheme. Chapter 7 suggests a design method for the conversion parameter η^{wf} of WF pricing mechanism. The numerical case study in Section 7.5.3 illustrates the high sensitivity of the GA method to the conversion parameter value η^{ga}: the grid cost obtained with this pricing scheme is slightly lower than with the WF method only for very specific values of η^{ga}. However, the payoff of the operator of the EVCSs is always higher with the WF pricing scheme, because the GA method is only meant to reduce the grid cost function.

5.5 Conclusion

The present chapter defines the two charging pricing methods used in this thesis. At each EV Charging Station, the Charging Unit Price of these methods is a function of the *local* Water-Filling charging scheduling cost presented in Chapter 4 and does not depend on the other EVCSs. For the average WF pricing method (denoted AVG), the CUP function is this WF scheduling cost averaged over all electricity usages, while the CUP function of the WF-based Locational Marginal Pricing method (denoted WF) is the marginal WF scheduling cost. It is shown that the latter CUP function is increasing, which ensures the uniqueness of the aggregated charging needs at the EVCSs at Wardrop Equilibrium according to Proposition 2.22. For the AVG pricing method, equivalent conditions for the increasing property of the corresponding CUP functions are given and tested on real data. An online and an offline versions of the WF pricing method are suggested in the case where arrival and departure times at the EVCSs are not the same for all EVs. However, for the online pricing method, the CUPs are systematically cheaper for EVs arriving earlier, and a complementary work is needed in order to overcome these fairness issues.

The AVG and WF pricing methods are compared to the most commonly used one in the literature relative to the coupling of the electrical and transportation systems, which is an LMP method (denoted GA) whose CUP functions are the marginal grid costs associated with EV charging. The GA method requires full knowledge of the grid, and is iterative in the literature: in order to find the CUPs, the grid cost is computed in function of the charging needs, which depend on the CUPs, etc. Here, the iterations are replaced by Beckmann's method, and the WF charging scheduling is added to the GA pricing method. Compared to the AVG and WF pricing

schemes, for the GA scheme, the CUP function at an EVCS depends on the other EVCSs via the grid cost function. Therefore, the CUP may be less different from one EVCS to another than for the AVG and WF pricing methods. In some cases, this can lead to a higher grid cost associated with GA pricing scheme than AVG and WF schemes. However, in overall, the grid costs resulting from these three schemes are different by 1 % at most.

A fourth pricing method is introduced, for which full knowledge of the grid is not necessary (unlike GA method). Instead, the operator in charge of this pricing scheme (denoted α) only needs one parameter α_i for each EVCS i, which could be communicated by the grid operator. This parameter α_i is such that the augmented load $\alpha_i \ell$ at the transformer of the grid yields similar marginal grid costs as a load ℓ at EVCS i. In a driving-and-charging game between vehicle users, the impact of this α pricing method is almost identical to the one of GA method.

Note that the four pricing methods AVG, WF, GA and α require a conversion parameter (from the dimension of marginal grid cost to the one of monetary cost), which is adjusted by hand in this chapter. A more thorough rule to fix its value is given in Chapter 7.

Part III

Incentive design in coupled electrical-transportation system

Chapter 6

Use cases for numerical incentive design

Chapters 4 and 5 detail how the EV charging at charging stations is respectively scheduled in time and priced. These two features are integrated into a behavior model of vehicle users, which is studied in Chapters 2 and 3. The sensitivity of the behavior model with respect to various parameters is numerically measured on different metrics. In other words, this chapter gives examples of the ability of this model to provide for operators of the coupled electrical-transportation system a way of designing incentives. In the first section, a transportation operator reduces the local air pollution in a city using traffic tolls. In the second section, a multimodal hub operator optimizes the size of its solar park. The theoretical modeling of incentive design is given in next Chapter 7.

This chapter is inspired from the following papers:

[Sohet et al., 2021b] **Sohet, B.**, Hayel, Y., Beaude, O., and Jeandin, A. (2021). Coupled charging-and-driving incentives design for electric vehicles in urban networks. *IEEE Transactions on Intelligent Transportation Systems*, 22(10):6342-6352.

[Sohet et al., 2019b] **Sohet, B.**, Hayel, Y., Beaude, O., and Jeandin, A. (2019). Optimal incentives for electric vehicles at e-park & ride hub with renewable energy source. *World Electric Vehicle Journal*, 10(4):70.

Contents

6.1 Reducing local air pollution with traffic tolls 116

6.1.1 Introduction of use case and game between vehicle users 116

6.1.1.1 Commuting by crossing or bypassing a city 116

6.1.1.2 The energy consumption cost model 117

6.1.1.3 Expression and resolution of game between vehicle users . 118

6.1.2 Sensitivity of Wardrop equilibrium to fuel price 119

6.1.3 Numerical complexity of Wardrop equilibrium computations 120

6.1.4 Definition and numerical study of local air pollution 120

6.1.4.1 Definitions of the environmental cost and gain 121

6.1.4.2 Numerical sensitivity of optimal toll to EV penetration . . 122

6.2 Solar panel sizing at a multimodal e-Park & Ride hub 123

6.2.1 Introduction of use case and game between vehicle users 124

6.2.1.1 E-Park & Ride hub with solar panels 124
6.2.1.2 Travel duration cost model 125
6.2.1.3 Energy consumption cost model 126
6.2.1.4 Expression and resolution of game between vehicle users . 127
6.2.2 Numerical study of solar panel sizing 128
6.2.2.1 Long-term payoff of the hub operator 128
6.2.2.2 Solar panel generation data 129
6.2.2.3 Case of constant charging unit price at hub 129
6.2.2.4 Case of variable charging unit price at hub 132
6.3 Conclusion 133

6.1 Reducing local air pollution with traffic tolls

Table 6.1: Notations of Chapter 6

Symbols	Signification
X_e	EV penetration level
$d_r(x_r)$	Travel duration on path r in function of vehicle flow x_r
m_s	Constant energy consumption of vehicle class s per distant unit
λ_s	Energy unit price for vehicle class s
$t^*_{s,r}$	Optimal traffic toll for vehicle class s at path r
$\boldsymbol{x}^*$	Vehicle flows at Wardrop Equilibrium
γ_a	Weight of local air pollution associated to path a
${c_{\text{env}}}^{(0)}$	Local air pollution corresponding to $t_{g,a} = 0$
${c_{\text{env}}}^*$	Local air pollution corresponding to $t_{g,a} = t^*_{g,a}$
$\delta(X_e)$	Environmental gain versus no-toll case

6.1.1 Introduction of use case and game between vehicle users

The goal of this first numerical study is to illustrate how the behavior model of vehicle users developed in Chapter 2 can help to design a traffic toll in order to optimize an objective such as local air pollution, caused by Gasoline Vehicles (GVs). The optimal traffic toll could depend on the EV penetration level X_e, hence the need of a detailed model of vehicle users' behavior. The entity concerned by pollution and in charge of the traffic toll is here referred to as the Transportation Network Operator (TNO). This Section is largely inspired from our paper [Sohet et al., 2021b].

6.1.1.1 Commuting by crossing or bypassing a city

The TNO is mainly concerned by the pollution caused by commuting[1] and determines the toll design on an average commuting day. For the numerical study, a simple transportation network

[1]See the French map of the percentage of trips which are part of commuting in 2020: https://www.observatoire-des-territoires.gouv.fr/part-des-deplacements-domicile-travail-en-voiture.

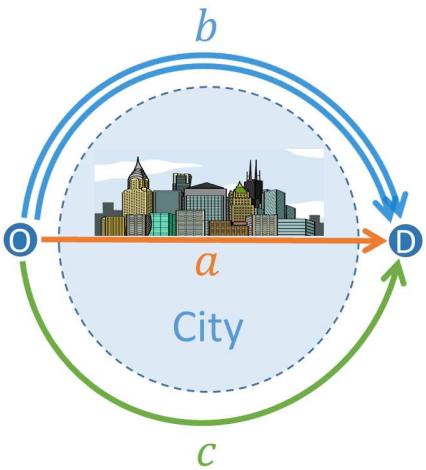

Figure 6.2: Schematic representation of the transportation network considered. *A simple setting allowing a tractable analysis of the proposed coupled charging-and-driving concept, and an evaluation of associated urban externalities. This setting is inspired by the ring road of the city of Paris, France.*

is considered to ensure a good readability of the results, but the method used works on any transportation network. In this use case, vehicle users need to drive from nodes O (for Origin, at home) to D (for Destination, at work) in the morning and have the choice between three different paths a, b and c (see Figure 6.2). Nodes O and D are separated by a city, and path a goes through this city while paths b and c correspond to ring roads, which bypass the city. The length $l_a = 30$ km of arc a is a good approximation of the daily mean individual driving distance in France[2] [CGDD, 2010], and the length of the ring roads verify: $l_b = l_c = \frac{\pi}{2} l_a \simeq 47$ km. For the speed limits on the arcs, the example of Paris[3] was taken: $v_a = 50$ km/h and $v_b = v_c = 70$ km/h. The capacities of the arcs are set to $C_b = 1$ and $C_a = C_c = \frac{1}{2}$, meaning that ring road b contains twice as many lanes as the two other paths. This choice is made in order to differentiate ring road b from c.

In the game $\mathbb{G}$ considered in the present section, there are two types of vehicles, EVs and GVs, whose respective proportions are X_e and $X_g = 1 - X_e$. All vehicle users make their choice considering the total cost function associated to each path $r = a, b, c$, which is made of a traffic congestion cost, a traffic toll $t_{s,r}$ which depends on the vehicle class s (extending the case of Section 5.4.2), and the energy consumption cost. The traffic congestion cost d_r at path r is modeled by the BPR function (2.5), with $\tau = 10$ €/h the value of time according to a French government report[4] and x_r the total vehicle flow on path r.

6.1.1.2 The energy consumption cost model

Concerning the energy consumption cost, GV users may not stop at a gas station the same day as the trip considered, but still take this cost into account for their path choice. In the case of EV

[2] As the daily driving distance also takes into account the return trip, the length l_r actually represents twice the length of path r. The underlying assumption is that vehicle users necessarily take the same path for the return trip.

[3] Note that on the first of September, 2021, the speed limit has been reduced to 30 km/h in most streets in Paris center.

[4] http://www.strategie.gouv.fr/sites/strategie.gouv.fr/files/archives/Valeur-du-temps.pdf.

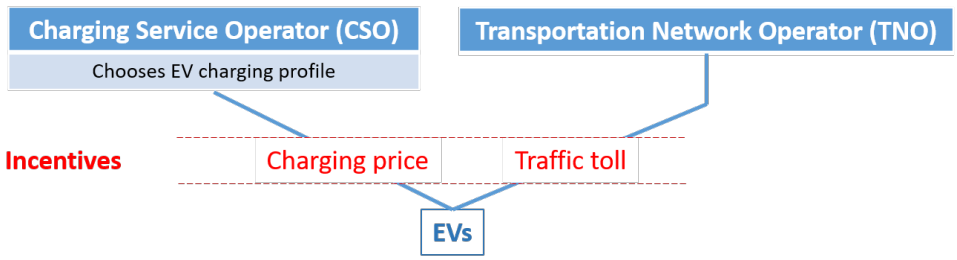

Figure 6.3: Schematic representation of the operators considered in this use case.

users, they charge at a Charging Station (EVCS) located at destination node D. Their charging profile is chosen by a Charging Service Operator (CSO) as in Chapter 4, as well as the Charging Unit Price (CUP) function (see Chapter 5). Figure 6.3 shows a schematic representation of the operators in this use case. Their charging need is equal to the energy consumed during the commuting trip, as if EVs were fully charged at the EVCS and their battery was full before the commuting trip. According to Assumption 2.7, the total energy consumed by an EV user driving on path r is $m_e l_r$, with $m_e = 0.2$ kWh/km the average EV consumption per distance unit [Fontana, 2013]. The total charging need at the EVCS aggregated over all EVs is then:

$$L = m_e \sum_r l_r x_{e,r} N \,, \tag{6.1}$$

with $x_{e,r}$ the EV flow on path r and $N = 3000$ the total number of vehicles. The CUP function $\lambda_e(L)$ considered for the use case of the present Section 6.1 corresponds to λ^{avg}, from the average water-filling pricing method (see Section 5.2) and defined by (5.3).

This pricing method is based on the water-filling charging scheduling (see Proposition 4.2) of the aggregated charging need L during working hours. In the present numerical example, the working hours are divided into $T = 2$ time slots. The non-flexible load $\boldsymbol{\ell}^0$ at the EVCS comes from the Recoflux dataset presented in Section 5.2.3, which is averaged over one year and into $T = 2$ time slots, and factorized so that $\sum_t \ell_t^0 = 30$ MWh: $\ell_1^0 = 11.9$ MWh and $\ell_2^0 = 18.1$ MWh. The load cost function used is $f(\ell) = \eta^{\text{avg}} \ell^2$. In this case, the non-flexible load $\boldsymbol{\ell}^0$ verifies condition (5.8) equivalent to $\lambda_e = \lambda^{\text{avg}}$ increasing (see Figure 5.3). The conversion parameter η^{avg} is chosen so that the CUP $\lambda_e(m_e X_e \sum_r l_r/3)$ corresponding to an average aggregated charging need is equal to 20 c€/kWh, which explicitly depends on the EV penetration level X_e.

6.1.1.3 Expression and resolution of game between vehicle users

Similarly, the energy consumption cost for GV users choosing path r can be written $m_g l_r \lambda_g$, with $m_g = 6$ L/100km the fuel consumption per distance unit and $\lambda_g = 1.50$ €/L the price of a gas unit. Then, in game $\mathbb{G}$, the total cost function $c_{s,r}$ for a vehicle user of class s on path r is:

$$c_{s,r} = d_r(x_r) + t_{s,r} + l_r m_s \lambda_s \,. \tag{6.2}$$

The choice of vehicle users is modeled by the Wardrop Equilibrium (WE) of game $\mathbb{G}$ and denoted $\boldsymbol{x}^*$. By definition (6.1) of the aggregated charging need L as a linear combination of the vehicle flows, the charging cost function $\boldsymbol{x}_e \mapsto m_e \boldsymbol{l} \lambda_e(L(\boldsymbol{x}_e))$ is a Linearly non-Separable Congestion cost function. Then, according to Proposition 2.19, the WE is also a minimum of the following Beckmann function under the travel demand constraints (see (2.1)) $\sum_r x_{s,r} = X_s$ and $x_{s,r} \geq 0$

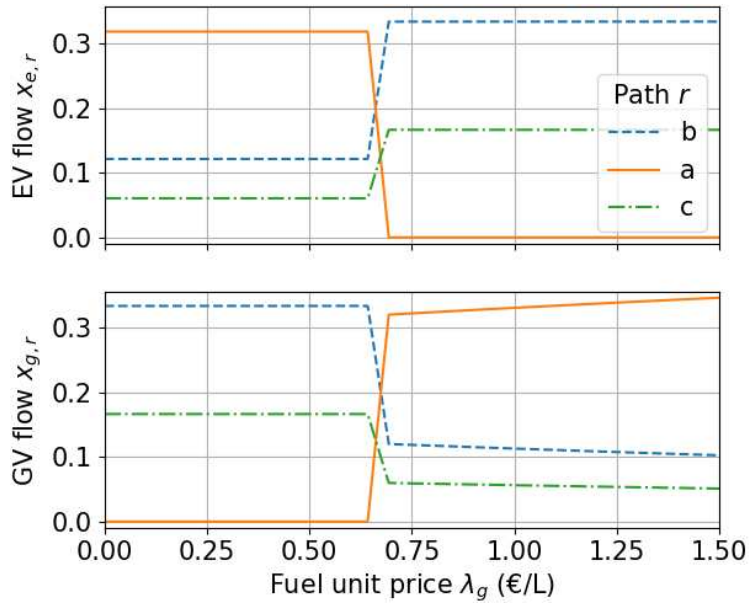

Figure 6.4: Evolution of the vehicle flows $\boldsymbol{x}^*$ at WE with respect to fuel price λ_g, for $X_g = X_e = 0.5$. *There is a threshold around* $\lambda_g = 0.66$ *€/L corresponding to a switch of traffic equilibrium.*

(for all s, r):

$$\mathcal{B} = \sum_r \left(l_r m_g \lambda_g x_{g,r} + \sum_s t_{s,r} x_{s,r} + \int_0^{x_r} d_r(x) \mathrm{d}x \right) + \int_0^L \lambda_e(L) \mathrm{d}L \,. \tag{6.3}$$

Moreover, according to Proposition 2.22, the increasing property of λ_e ensures the uniqueness of the aggregated charging need L at WE, as well as the total vehicle flow x_r^* for every path r. In the case where the per-class vehicle flows $(x_{s,r}^*)_{s,r}$ are not unique at WE, the ones verifying the pro-rata condition (2.21) is selected.

Before studying the impact of a traffic toll on local air pollution, next sections illustrate the Wardrop Equilibrium of the game introduced above, and the numerical complexity associated to computing the WE.

6.1.2 Sensitivity of Wardrop equilibrium to fuel price

In order to illustrate the Wardrop Equilibrium, its sensitivity with respect to the fuel price λ_g is shown in Figure 6.4. The EV penetration level X_e is supposed to be 50 %. Traffic tolls are all set to zero in order to clearly analyze the effect of congestion and energy on the behavior of EV and GV users.

Starting from the actual fuel price (around $\lambda_g = 1.50$ €/L), the cost of energy consumption per distance unit is higher for GV: $m_g \lambda_g > m_e \lambda_e(L(\boldsymbol{x}_e))$ for any EV flows $\boldsymbol{x}_e$. Most GV users then use the shortest arc a, while all EV users choose the ring roads to avoid congestion ($x_{e,a}^* = 0$). As long as $\lambda_g > 0.68$ €/L, the WE obtained remains more or less the same. Then, and down to $\lambda_g > 0.65$ €/L, the proportions of EV and GV flows at WE are inverted. This interval corresponds to a threshold on (exogenous) GV energy cost λ_g, when $m_g \lambda_g$ becomes lower than $m_e \lambda_e(L(\boldsymbol{x}_e))$ for *any* EV flows $\boldsymbol{x}_e$. Then, most EV users choose arc a while all GV users choose the longer ring roads b and c, as they are not that expensive anymore thanks to the low fuel prices.

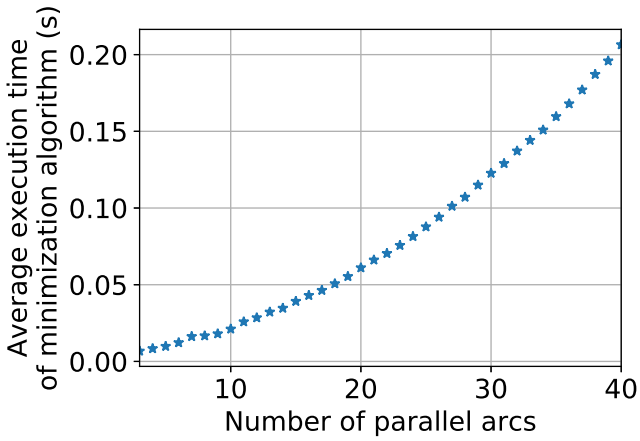

Figure 6.5: Average execution time of minimization algorithm in function of number of parallel arcs.

In terms of decision-making, lowering taxes on fuel (leading to a smaller λ_g) may lower the level of GV traffic inside cities. This effect has a limit, as there still are GVs on arc a even when fuel is free. Note that the two ring roads are used simultaneously, in proportions such that there are twice as many vehicles on the ring road with the larger capacity, so that the travel time is the same for both.

6.1.3 Numerical complexity of Wardrop equilibrium computations

Numerical observations indicate that the complexity (understood here as the execution time on an Intel Core i7-6820HQ 2.70GHz) of the numerical experiments conducted in this Section 6.1 is proportional to the number of WE computations (i.e., Beckmann's function minimizations). The complexity of the minimization algorithm (Sequential Least SQuares Programming, or SLSQP method [Kraft, 1988]) depends on the number of variables in game $\mathbb{G}$, which are the vehicle flows on each arc and for each class. To illustrate that, the minimization algorithm is applied to different transportation networks with various number of parallel arcs (therefore proportional to the number of variables). More precisely, the length of the first arc is 30 km, and each additional arc is 1 km longer than the previous one[5]. The speed limits and capacities are the same for every arc. For each number of arcs, a WE is computed for a thousand different toll values $t_{g,a}$ ranging from -5 €(the GV users get a financial compensation) to 5 €, and the execution times are averaged. Note that in these particular transportation networks, the WE in function of $t_{g,a}$ is the same for all networks[6], and the execution times can be fairly compared. Figure 6.5 shows that this mean execution time depends roughly on the squared number of arcs (and hence, of variables).

6.1.4 Definition and numerical study of local air pollution

[5]For example, for a transportation network made of four parallel arcs, the different lengths are 30, 31, 32 and 33 km.

[6]Only the three shortest arcs are chosen by vehicle users for any $t_{g,a}$ and transportation network.

6.1.4.1 Definitions of the environmental cost and gain

This section focuses on the optimization of an objective function which depends on the vehicle flows $\boldsymbol{x}^*$ at WE, which in turn depend on the exogenous parameters of the problem (traffic toll, EV penetration level, etc.). The objective function considered is the level of pollution, which is optimized by the TNO by changing traffic tolls. Only the polluting substances released by GVs' exhaustion pipes into the air are considered. Therefore the level of pollution depends on the expected number of GVs on each arc. Based on Little's formula of queuing theory [Kleinrock, 1975], this expected number of GVs on arc r is the product of the flow rate $x_{g,r}$ and the expected travel duration $d_r(x_r)$. The TNO only imposes a traffic toll $t_{g,a}$ to GV users choosing arc a, which crosses the city. For all the other arcs, there is no toll applied[7]. This is typically the kind of incentive in large urban cities like London[8].

The purpose of this toll is to limit the number of GVs contributing to the environmental cost function, defined as:

$$c_{\text{env}}(\mathbf{x}) = \gamma_a x_{g,a} d_a(x_a) + x_{g,b} d_b(x_b) + x_{g,c} d_c(x_c)\,, \tag{6.4}$$

with $\gamma_a \geq 1$ the weight of environmental cost on arc a (inside the city): this represents a willingness to diminish (local) pollution in the city center. At WE, the environmental cost function c_{env} depends implicitly on the toll $t_{g,a}$ through the vehicle flows $\boldsymbol{x}^*$ (see Figure 6.4 for the impact of an exogenous parameter on the WE). The TNO can thus control this environmental cost, solving an upper-level optimization problem, written as an MPEC (Mathematical Programming with Equilibrium Constraints) problem:

$$c^*_{\text{env}} = \min_{t_{g,a} \geq 0} \; c_{\text{env}}\big(\mathbf{x}^*(t_{g,a})\big)\,, \tag{6.5}$$

with $\mathbf{x}^*(t_{g,a})$ the vehicle flow at WE considering the toll value $t_{g,a}$. As there is no explicit formulation of $\mathbf{x}^*(t_{g,a})$, it is difficult to determine explicit solutions for this optimization problem, or even to integrate optimality conditions of the lower-level problem (game $\mathbb{G}$ between the vehicles) into the upper one (of the TNO). Thus, an exhaustive search[9] on $t_{g,a}$ with a 1 c€ increment is performed to find the toll $t^*_{g,a}$ solution of (6.5).

The EV penetration level X_e has an important impact on this global minimization problem. Indeed, as the vehicle flows $\boldsymbol{x}^*(t_{g,a}, X_e)$ at WE depend on both X_e and $t_{g,a}$ (among others), the optimal toll $t^*_{g,a}(X_e)$ and the corresponding minimal environmental cost function $c^*_{\text{env}}(X_e) = c_{\text{env}}(t^*_{g,a}(X_e))$ depend on X_e. For the TNO, it is interesting to know the environmental gain $\delta(X_e)$ of taxing optimally with $t_{g,a} = t^*_{g,a}(X_e)$, *relatively* to the reference case $c^{(0)}_{\text{env}}$ obtained when $t_{g,a} = 0$:

$$\delta(X_e) = \frac{c^{(0)}_{\text{env}} - c^*_{\text{env}}(X_e)}{c^{(0)}_{\text{env}}}\,, \quad \text{with } c^*_{\text{env}} \text{ defined in (6.5)}\,. \tag{6.6}$$

The solution of (6.5) also depends on the environmental policy scenario, represented by γ_a, the importance given to local pollution inside the city.

[7] Only the difference of tolls ($t_{g,a} - t_{g,r}$ with $r = b, c$) between two arcs has an impact on vehicle flows at equilibrium, so $t_{g,b} = t_{g,c} = 0$ may be assumed.

[8] In London, vehicles have to pay a toll in order to go across the city downtown: https://tfl.gov.uk/modes/driving/congestion-charge.

[9] Chapter 7 suggests another use case for which a more robust solution algorithm is found.

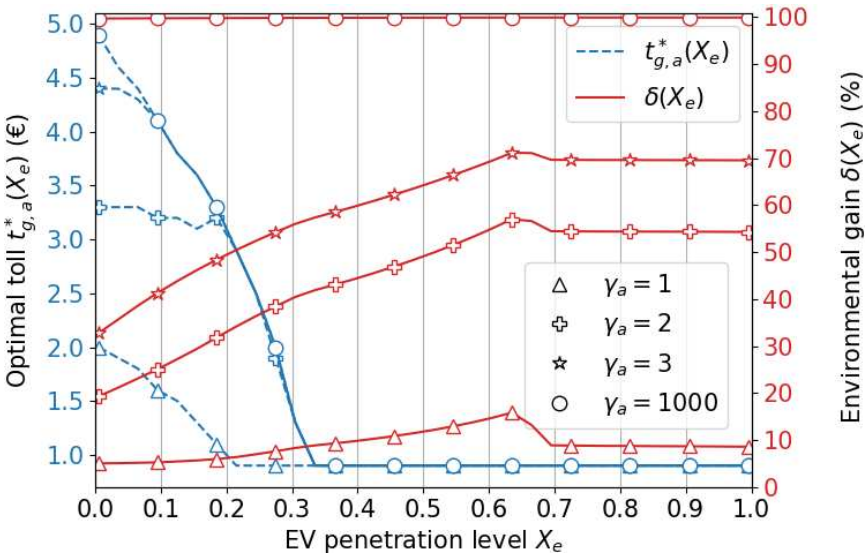

Figure 6.6: Evolution of the optimal toll $t^*_{g,a}(X_e)$ and the environmental gain $\delta(X_e)$ with respect to the EV penetration level X_e, for different local pollution importance levels inside the city (γ_a). *As X_e increases, the TNO induces a bigger impact on pollution if choosing the optimal toll, which decreases.*

6.1.4.2 Numerical sensitivity of optimal toll to EV penetration

In Figure 6.6, the optimal toll value $t^*_{g,a}(X_e)$ and the corresponding environmental gain $\delta(X_e)$ are computed for any EV penetration level X_e, and for different environmental policy scenarios. Figure 6.7 shows, for the $\gamma_a = 2$ scenario, the EV and GV flows at WE in function of the EV penetration level X_e, in the case of optimal toll (Figure 6.7.a) and no toll (Figure 6.7.b). In general in the optimal toll case, for a higher EV penetration level, arc a is more congested, from less than 25 % when $X_e = 0$ to around 40 % of all vehicles when $X_e = 1$ for example (see Figure 6.7.a). Then, a lower toll $t^*_{g,a}$ is sufficient to optimally reduce the number of GV users crossing the city, which explains why the blue dotted curves $t^*_{g,a}(X_e)$ are decreasing. Regarding the different scenarios, the higher γ_a, the higher $t^*_{g,a}$ must be to prevent GV users from crossing the city, and the higher the environmental gain δ. For $\gamma_a = 1000$ (circle markers), the city's environmental cost function is almost equivalent to the environmental cost only on arc a: in the optimal WE, there is no GV user crossing the city, so that our toll mechanism corresponds to a restriction one where GVs would be forbidden to cross the city. For $\gamma_a = 2$ (cross markers), there may be GV users crossing the city at the optimal WE, as shown in Figure 6.7 for EV penetration levels lower than 20 %. In this case of high GV proportions, if all GV users chose only the ring roads there would be too much congestion, i.e., local pollution. For this reason, the optimal toll may be lower than the one deterring all GV users from crossing the city (see the cross and circle markers in Figure 6.6). For EV penetration levels X_e higher than 33 %, the proportion of EV users crossing the city is the same (see Figure 6.7.a), so that the total cost function associated with arc a is constant and the optimal toll $t^*_{g,a}(X_e) = 0.9$ € remains constant (see Figure 6.6).

Finally, Figure 6.6 shows that $\delta(X_e)$ stabilizes from $X_e = 0.7$, no matter the γ_a scenario. The reason is that, from this EV penetration level, the WE keeps the same nature, whether the toll is optimal or zero (see Figure 6.7.b): for increasing $X_e \geq 0.7$, EVs simply replace GVs and total vehicle flow on each arc remains constant. This way, local air pollution decreases proportionally with X_e in both toll cases, hence a constant gain $\delta(X_e)$. For lower EV penetration levels $X_e < 0.7$,

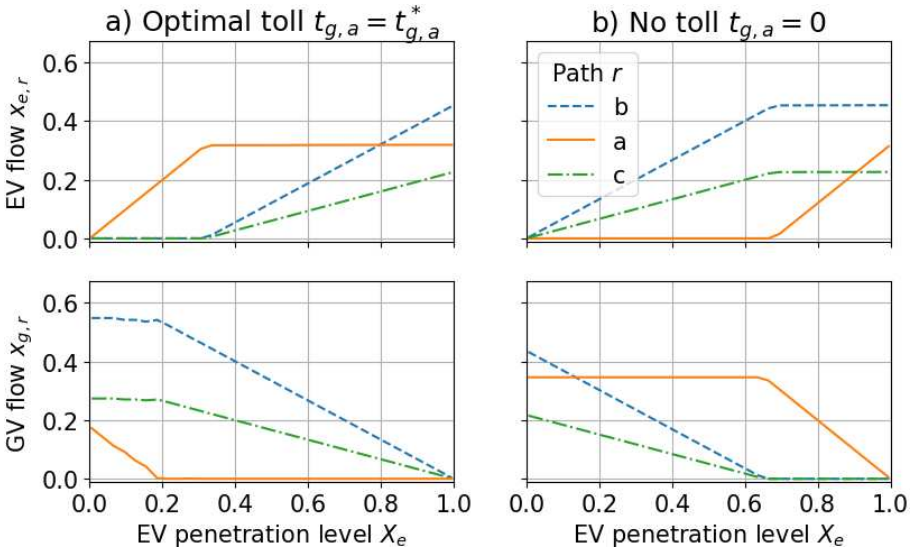

Figure 6.7: Distribution of EVs and GVs at WE corresponding to optimal toll (a) and no toll (b) scenarios, as the proportion of EV grows (for $\gamma_a = 2$). *As X_e grows, EVs replace GVs on arc a, faster in the optimal toll scenario.*

the environmental gain $\delta(X_e)$ increases with X_e, meaning that the toll incentive deters greater proportions of GV users (whose total number decreases with X_e) from crossing the city.

6.2 Solar panel sizing at a multimodal e-Park & Ride hub

Table 6.8: Notations

Symbols	Signification
publ	Public Transport mode (hub + PT)
priv	Private transport mode (driving downtown)
λ_e^0	Constant CUP downtown
λ_e	Smart CUP function at hub
λ_{cst}	Charging fee = constant part of λ_e
λ^{avg}	Variable part of λ_e
L	Charging need aggregated over EVs at hub
E	Total PV energy generated daily during working hours
I	Initial solar panel investment cost
C	Daily electricity supplying cost function
R	Daily EV charging revenue function

The following is largely inspired from our journal paper [Sohet et al., 2019c] based on our conference paper [Sohet et al., 2019b]. This section focuses on the management of an e-Park & Ride hub, where vehicle users can park, charge if their vehicle is electric and take Public Transport (PT) to finish their trip (see Section 6.2.1). Such hubs are built on the outskirts of

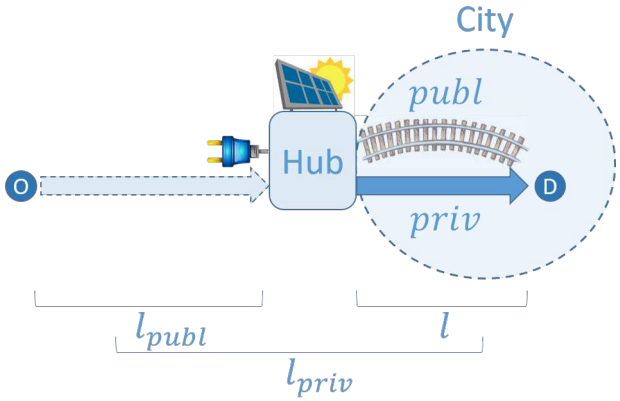

Figure 6.9: Schematic representation of the charging hub scenario: commuters can either choose the public (*publ*) transport mode or the private (*priv*) one. Commuters choosing *priv* drive all the way to their destination D and charge there at a constant Charging Unit Price (CUP). Those choosing *publ* park their vehicle at a hub and take the Public Transport to get to D. At the hub, a smart Charging Unit Price is proposed, thanks to a local source of renewable energy.

the city to limit the number of vehicles downtown and consequently reduce traffic congestion and local pollution[10]. The operator of this hub (called Charging Service Operator, or CSO) wants to know if it is beneficial to install PhotoVoltaic (PV) solar panels and use the generated electricity to charge EVs at the hub (see Section 6.2.2). Note that in the present use case, the electricity generated by PV which is not used for EV charging is *not* remunerated (by reinjecting it into the grid, see Section 4.2.2.2 for more details). The following study then can be seen as a worst-case scenario: in case of a remuneration, the CSO could install more solar panels at the hub than the optimal size found in the present section.

6.2.1 Introduction of use case and game between vehicle users

6.2.1.1 E-Park & Ride hub with solar panels

The CSO only considers daily commuters who want to get to their workplace in the morning: they come from the suburb area (Origin O in Figure 6.9) and head to the city center (Destination D). In this scenario, when commuters arrive at the hub, they can choose between two transport modes. First, they can park and charge (if their vehicle is electric) at the hub and finish their trip by Public Transport (*publ* in Figure 6.9). Commuters choosing this alternative delegate to the CSO the charging profile scheduling during working hours. The CSO chooses the aggregated charging profile in function of the local electricity generated by PV solar panels located nearby (and also managed by the CSO). This CSO also selects a smart CUP function to incentivize EV users to charge at the hub during periods of high PV electricity generation. Second, commuters can drive with their private vehicle (*priv*) all the way across the city center to their destination D, where they can charge at a fixed price. Note that while the private transport mode may be faster, the public one may be cheaper thanks to the charging incentives. Therefore, the CSO needs to model the choice of vehicle users and their reaction with respect to charging prices at the hub, made dependent on the PV generation.

[10]For example in Paris, there are 20500 parking spaces in 73 hubs located nearby a PT station https://www.iledefrance-mobilites.fr/le-reseau/services-de-mobilite/parcs-relais (in French).

The choice made by all commuters between the two transport modes is modeled in a routing game $\mathbb{G}$ and is represented by the two variables $x_{e,publ}$ and $x_{g,publ}$, which are respectively the proportions of EV and GV users choosing the public mode. The proportions of vehicles of type $s = e, g$ choosing the private transport mode may be easily deduced by $x_{s,priv} = X_s - x_{s,publ}$, with X_s the proportion of vehicle class s among all vehicles. In numerical tests, the total number of vehicles is set to $N = 1000$ and the EV penetration level chosen is $X_e = 50$ % (i.e. 500 EVs). The proportion of GVs is then given by $X_g = 1 - X_e$. Vehicle users base their choice on their cost functions, such as travel duration (by private or Public Transport), energy consumption (electricity for EVs and fuel for GVs) and the ticket fare (for PT only). These three types of cost functions in game $\mathbb{G}$ are defined as follows.

6.2.1.2 Travel duration cost model

The delay *from the hub* to the destination is perceived equivalently by EV and GV users:

[*priv*] For the private mode, it corresponds to the driving duration in the city center and is expressed by the BPR function d_{priv} defined in (2.5) and used throughout this thesis. This function depends on the total proportion of vehicles driving downtown $x_{priv} = x_{e,priv} + x_{g,priv}$ due to congestion effects:

$$\tau_{priv} \times \underbrace{\frac{l}{v}\left[1 + 2\left(\frac{x_{priv}}{C}\right)^4\right]}_{d_{priv}(x_{priv})}, \tag{2.5}$$

with $\tau_{priv} = 10$ €/h the value of time *when driving*[11], $l = 5$ km the length of the downtown road (approximately the radius of Paris), $v = 50$ km/h the speed limit (as in French urban areas) and $C = 1$ the capacity of the road, expressed in proportion of the total number of vehicles. For example, if all vehicles choose to drive downtown ($x_{priv} = 1$), the corresponding travel duration $d_{priv}(x_{priv})$ is multiplied by three compared with the empty road situation[12], whose free-flow travel duration is $d^0_{priv} = \frac{l}{v}$.

[*publ*] For the Public Transport mode linking the hub and the destination, the travel cost is assumed constant:

$$\tau_{publ} \times d_{publ}\,, \tag{6.7}$$

with $\tau_{publ} = 12$ €/h the value of time *in Public Transport*[11] – higher than τ_{priv} because PT is perceived by users as less comfortable than personal vehicles – and $d_{publ} = 6$ minutes the constant travel time of PT, which is chosen equal to the free flow travel time d^0_{priv} of the private mode[13]. The duration cost of the public mode is then equal to the fixed value $\tau_{publ}\ d_{publ} = 1.2$ € and is higher than the free flow cost of the private mode. This induces trade-off decisions for vehicles between both transport modes.

[11] The different values of time are based on a French government report http://www.strategie.gouv.fr/sites/strategie.gouv.fr/files/archives/Valeur-du-temps.pdf (in French).

[12] A trip assessment study from Paris city hall (https://cdn.paris.fr/paris/2021/03/03/1ee96c45980515ca57b28bd5da2fd681.pdf, in French) shows that the average speed during morning commuting is 11.9 km/h, which is a little less than the third (16.7 km/h) of the speed limit before the first of September, 2021.

[13] Indeed, there exist reserved pathways for PT in several cities like Paris, so that congestion can be considered as marginal.

6.2.1.3 Energy consumption cost model

It corresponds to the energy consumed by the vehicle *from the origin* to the destination, which is different for EVs and GVs. Following Assumption 2.7, the expression of this cost for vehicles of type $s = e, g$ which have chosen transport mode $r = publ, priv$ is $l_r \times m_s \times \lambda_s$, with l_r the *total* distance driven by the vehicles choosing transport mode r, m_s the energy consumption of vehicle class s per distance unit ($m_g = 6$ L/100km and $m_e = 0.2$ kWh/km) and λ_s the energy unit cost ($\lambda_g = 1.5$ €/L and λ_e defined below). The total driven distances are $l_{publ} = 10$ km between the origin and the hub (see Figure 6.9), and $l_{priv} = l_{publ} + l = 15$ km between the origin and the destination, so that the two-way trip between origin and destination is 30 km. Unlike the fuel unit price λ_g, which is the same for the public and private modes, the CUP function depends on the transport mode chosen:

[*priv*] Downtown, there is a standard constant electricity fare $\lambda_e^0 = 40$ c€/kWh, which corresponds to the electricity unit price in France (15 c€/kWh)[14] with an additional cost (25 c€/kWh) meant for the charging operation.

[*publ*] At the hub, this CUP function λ_e depends on the aggregated charging need $L(x_{e,publ}) = l_{publ} m_e x_{e,publ} N$, proportional to the proportion $x_{e,publ}$ of EVs parked at the hub. Like in previous Section 6.1, the CUP function is inspired from λ^{avg}, from the average water-filling pricing method introduced in Section 5.2, but with an additive fixed charging fee λ_{cst}. In Section 6.2.2, this charging fee[15] is adjusted by the CSO in order to maximize its objective function. The final expression of λ_e is:

$$\lambda_e(L) = \lambda_{\text{cst}} + \lambda^{\text{avg}} = \lambda_{\text{cst}} + \eta^{\text{avg}} \frac{G^*(L)}{L}, \tag{6.8}$$

with G^* the objective function corresponding to the water-filling charging profile scheduling operated by the CSO, *in function of PV electricity generation*, and η^{avg} a conversion parameter.

This objective G^* is detailed in Section 4.2.2.2 and is a function of the aggregated charging need L and the total PV energy E produced during working hours:

$$G^*(L) = \begin{cases} 0 & \text{if } L \leq E, \\ \frac{1}{T}(-E + L)^2 & \text{if } L > E, \end{cases} \tag{4.19}$$

with T the number of time slots representing the working time period. As mentioned in Section 4.2.2.2, the objective G^* does not depend on the specific PV generation profile $\boldsymbol{\ell}^0$ during the working hours, but only on the aggregated amount $E = \sum_{t=1}^{T} \ell_t^0$. Note the threshold role played by the total PV production E during working hours: λ_e depends on the total charging need $L(x_{e,publ})$ only if E is not sufficient to charge L. Otherwise, $G^* = 0$ and the CUP function is constant equal to λ_{cst}. This is illustrated in Figure 6.10, which shows the variable part λ^{avg} of CUP λ_e in function of the EV flow at the hub. For example, when $E = 500$ kWh (star markers), $\lambda^{\text{avg}}(x_{e,publ}) = 0$ up to $x_{e,publ} = 0.5$, the EV flow corresponding to a charging need at the hub of $L = 500$ kWh.

[14] See the prices from EDF, the main electricity supplier https://particulier.edf.fr/content/dam/2-Actifs/Documents/Offres/Grille_prix_Tarif_Bleu.pdf, in French.

[15] The charging fee λ_{cst} is a constant component of the CUP function λ_e, which is different from the CUP function λ^{cst} used in Section 5.4.2, which represents a flat pricing method, as for the private mode in the present use case.

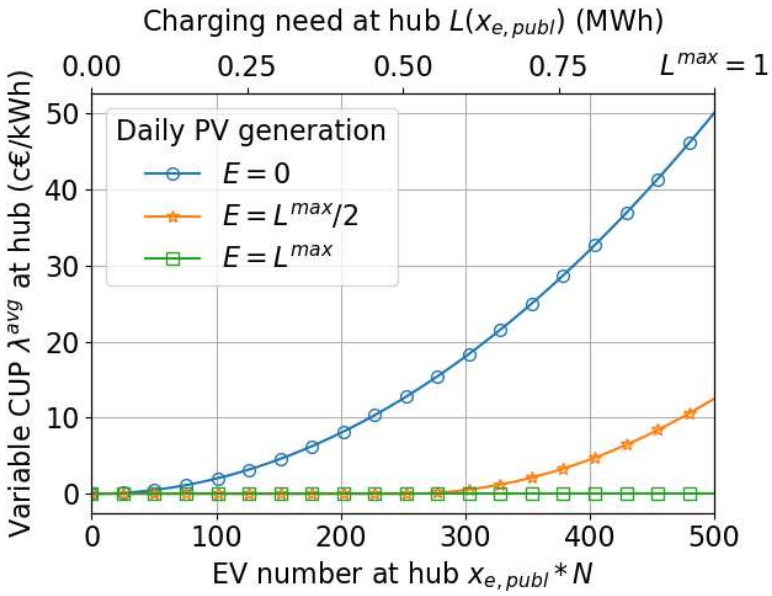

Figure 6.10: Variable part λ^{avg} of Charging Unit Price λ_e at the hub, in function of the EV flow $x_{e,publ}$ at the hub, for different energy amounts PV generated during the working hours of a day. *There is no variable part ($\lambda^{avg} = 0$) as long as there is enough PV generation to charge all EVs at the hub ($E \geq L(x_{e,publ})$).*

The data used to define this daily generation E during working hours is presented in Section 6.2.2.2. The parameter[16] $\eta^{\text{avg}} = 4 \times 10^{-3}$ €/kWh^2 is adjusted so that the value of variable part λ^{avg} of the CUP function λ_e at the hub is equal to $\frac{5}{4}\lambda_e^0 = 50$ c€/kWh when there is no PV production ($E = 0$) and all EV users charge at the hub ($L = l_{publ} m_e X_e$)[17]. This upper bound on λ^{avg} is illustrated in Figure 6.10 when $E = 0$ (circle markers).

6.2.1.4 Expression and resolution of game between vehicle users

The Public Transport ticket fare is the same for EVs and GVs: $t_{publ} = 1$ €. Finally, the total cost function for each type $s = e, g$ of vehicle user which has chosen transport mode $r = publ, priv$ are given in the following table:

Transport mode	Duration cost	Monetary cost	Vehicle class
Public	$\tau_{publ} \times d_{publ}$	$l_{publ}\ m_e\ \lambda_e(L) + t_{publ}$	EV
		$l_{publ}\ m_g\ \lambda_g \quad + t_{publ}$	GV
Private	$\tau_{priv} \times d^0_{priv} \times \left(1 + 2x^4_{priv}\right)$	$l_{priv}\ m_e\ \lambda_e^0$	EV
		$l_{priv}\ m_g\ \lambda_g$	GV

The choice of vehicle users is modeled by a Wardrop Equilibrium of game $\mathbb{G}$, with the corresponding vehicle flows denoted by $\boldsymbol{x}^*$. As the aggregated charging need L is defined as a linear combination of vehicle flows, the CUP λ_e is a Linearly non-Separable Congestion cost function.

[16] Note that the load function associated to this water-filling scheduling (4.19) can be seen as the same as the one of previous Section 6.1: $f : \ell \mapsto \eta^{\text{avg}} \ell^2$.

[17] Note that as there is no PV production, the aggregated charging profile from the water-filling scheduling is perfectly flat: $\ell_t = \frac{L}{T}$ for all time slots $1 \leq t \leq T$.

Then, according to Proposition 2.19, a WE of game $\mathbb{G}$ is also a minimum of the following Beckmann function under the travel demand constraints $\sum_r x_{s,r} = X_s$ and $x_{s,r} \geq 0$ (for all s and r):

$$\mathcal{B} = m_g \lambda_g \sum_r l_r x_{g,r} + (\tau_{publ} d_{publ} + t_{publ}) x_{publ} + m_e \lambda_e^0 l_{priv} x_{priv} + \tau_{priv} \int_0^{x_{priv}} d_{priv}(x) \mathrm{d}x + \int_0^{L(x_{e,publ})} \lambda_e(L) \mathrm{d}L \,. \tag{6.9}$$

6.2.2 Numerical study of solar panel sizing

6.2.2.1 Long-term payoff of the hub operator

In this section, we focus on the financial viability of investing into PV solar panels at the hub, over a period of time $\mathcal{Y}$ of interest for the CSO. Typically, in this section a period of $N_y = 20$ years is considered, in line[18] with the warranties of solar panels [Vázquez and Rey-Stolle, 2008]. The CSO is looking for the optimal size of a solar park in order to maximize an objective function F. Function F corresponds to its payoff obtained N_y years after investing into solar panels, and is made of three different parts:

$$F = -I + N_y \times \sum (R - C) \,, \tag{6.10}$$

with:

- I the initial Investment cost in solar panels, with 750 €/kWp for a solar park[19] of the order of magnitude of 1 MWp. The unit "Watt-peak" is used for *nominal* power values, which corresponds to the installed capacity[20] of a solar park.

The two other parts of objective function F are summed over the days of a typical year:

- $C = \eta^{\text{avg}} G^*$ the daily CSO's Cost, which is function of the objective function G^* minimized by the water-filling charging profile scheduling and defined in (4.19). In other words, the CSO's cost is a simplified model of the grid costs associated with the electricity bought from the grid for the EV charging operation.

- R the daily Revenue function from EV charging at the hub which is, by definition (6.8) of the CUP function λ_e:
$$R = L\left(x^*_{e,publ}\right) \times \lambda_e\left(L\left(x^*_{e,publ}\right)\right) \,, \tag{6.11}$$
with $x^*_{e,publ}$ the EV flow at the hub at a Wardrop Equilibrium of game $\mathbb{G}$, L the corresponding aggregated charging need at the hub. Note that in the present chapter, it is assumed that there is no revenue from reinjecting PV generation into the grid.

Note that the CSO's objective function F depends on the constant part λ_{cst} of the CUP function λ_e at the hub, which is yet to be fixed. As an introduction, the design of both λ_{cst} and the size of the solar park is first illustrated in Section 6.2.2.3 in the case where the CUP function at the hub is only made of its constant part: $\lambda_e = \lambda_{\text{cst}}$. This design is then extended in Section 6.2.2.4 to the complete framework introduced in Section 6.2.1, with $\lambda_e = \lambda_{\text{cst}} + \lambda^{\text{cst}}$. The two Sections 6.2.2.3 and 6.2.2.4 rely on the model of PV generation during time period $\mathcal{Y}$, which is the subject of next section.

[18] More precisely, warranties guarantee that after 10 to 12 years, the output power of the panel is at least 90 % of initial nominal power, and 80 % after 20 to 25 years.

[19] See the report "PV LCOE in Europe 2014-30" of the European PV Technology Platform https://www.qualenergia.it/sites/default/files/articolo-doc/PV_LCOE_Report_July_2015-1.pdf.

[20] The nominal power does not take into account the losses due to solar cells heating or conversion to alternative current.

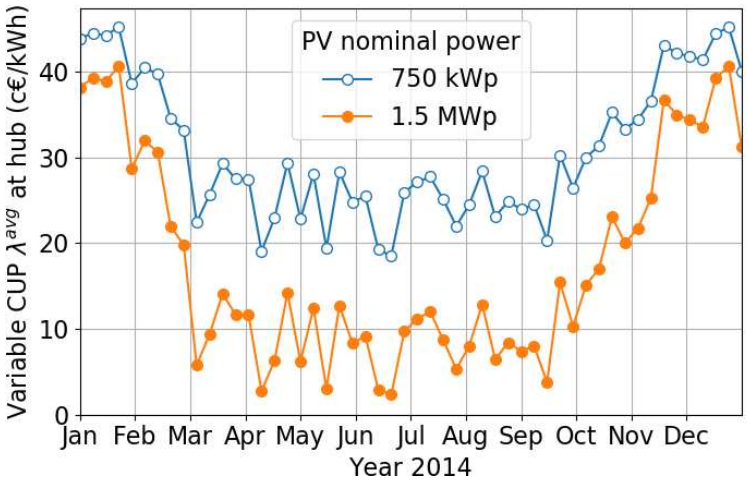

Figure 6.11: Variable part λ^{avg} of Charging Unit Price λ_e at the hub, in function of the PV electricity generation throughout the year 2014 (one point per week), for two different nominal powers. *Charging at the hub in summer is cheaper than in winter thanks to a higher PV generation, even more so with a higher nominal power.*

6.2.2.2 Solar panel generation data

The PV sizing considering a payoff function F over a period of time $\mathcal{Y}$ requires to model the weather during this period. Indeed, for a given nominal power, solar panels do not generate the same amount of electricity E from one day to another due to weather. In the present planning study, the open source data[21] introduced in [Pfenninger and Staffell, 2016b] is used. We extracted from this data the typical generation profile throughout year 2014 of a solar panel located in Paris (per nominal power unit). According to (4.19), the only data which is relevant for the present model is the total electricity E_d generated during working hours of each day d of the year. It is assumed that this yearly profile $(E_d)_d$ is the same for the N_y years[22].

Figure 6.11 shows how the variable part λ^{avg} of the CUP function λ_e responds to the change of daily PV generation $(E_d)_d$ throughout the year 2014, considering two different nominal powers[23] 750 kWp and 1.5 MWp. All EV users are assumed to charge at the hub ($x_{e,publ} = 1$). For both PV nominal powers, the seasonal effect on the CUP function is clearly visible: charging at the hub is cheaper in summer to incentivize EV users to consume the high PV generation levels at the hub. Note that the upper limit 50 c€/kWh (by definition of η^{avg}) of λ^{avg} is not reached because even in winter, the PV generation is not null.

6.2.2.3 Case of constant charging unit price at hub

As a first step, the payoff function F is studied in the framework introduced in Section 6.2.1 except from the CUP function λ_e at the hub, whose variable component λ^{avg} has been omitted. Thus, $\lambda_e = \lambda_{\text{cst}}$ is constant throughout the period of time $\mathcal{Y}$ and does not depend on the number $x_{e,publ}$ of EV users charging at the hub.

[21] The data is available at https://www.renewables.ninja/.

[22] Actually, the PV electricity generation is impacted by climate change. For example, [Jerez et al., 2015] shows that this generation should vary from -14 % to 2 % in European countries by the end of the century, with the largest decreases in Northern countries.

[23] The nominal power 1.5 MWp is the maximal one tested in this planning study (see Figure 6.14 for example).

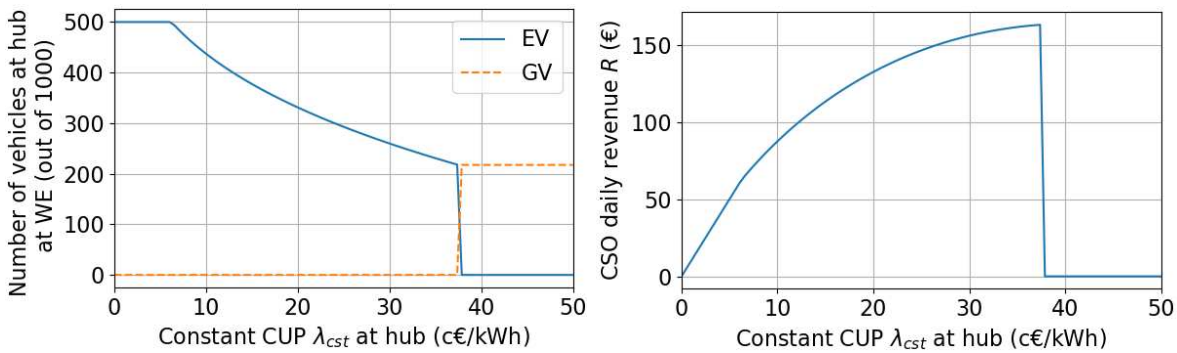

(a) Number of vehicles at the hub at WE in function of λ_{cst}.

(b) CSO's daily revenue R in function of λ_{cst}.

Figure 6.12: Impact of the constant Charging Unit Price $\lambda_e = \lambda_{\text{cst}}$ at the hub on the Wardrop Equilibrium and the CSO revenue function R. *As λ_{cst} increases, fewer EV users choose the hub while R increases, up to a threshold $\lambda^*_{cst} = 37.5$ c€/kWh beyond which all EV users drive downtown.*

Optimization of constant charging fee

In addition to the PV size, the CSO wants to find the optimal constant CUP $\lambda_e = \lambda_{\text{cst}}$ at the hub for the N_y years to come and which maximizes F. Figure 6.12a and 6.12b show how λ_{cst} impacts respectively the number of vehicles $x_{s,publ} \times N$ $(s = e, g)$ at the hub at Wardrop Equilibrium of game $\mathbb{G}$, and the resulting daily revenue R. For each different value of λ_{cst}, the WE is found by minimizing Beckmann's function (6.9) with the sequential least squares programming method [Boggs and Tolle, 1995] (via built-in Python function *minimize* in SciPy package). For $\lambda_{\text{cst}} \leq 7$ c€/kWh, charging at the hub is cheaper enough than $\lambda^0_e = 40$ c€/kWh in the city center, so that all EV users choose to charge at the hub. Meanwhile all GV users prefer to drive through the empty (from all EVs) city center. Naturally, the higher λ_{cst}, the fewer EVs at the hub at WE. However, this decreasing number of EVs is compensated by the increase of λ_{cst}, and the daily revenue function R increases (see Figure 6.12b). Figure 6.12a also shows that there is a threshold[24] $\lambda^*_{\text{cst}} = 37.5$ c€/kWh above which charging at the hub is so expensive that all EV users would rather drive downtown, and therefore some GV users stop at the hub to avoid downtown congestion. This threshold also happens to be the optimal CUP which maximizes the daily revenue function R (see Figure 6.12b). Note that λ^*_{cst} depends on the value of the CUP $\lambda^0_e = 40$ c€/kWh in the city center, and that $\lambda^*_{\text{cst}} < \lambda^0_e$. The value of λ^*_{cst} also is of the same order of magnitude as actual charging prices per energy unit, such as 36 c€/kWh at Tesla superchargers[25] and 50 c€/kWh for regular speed charging at Ionity EVCSs[26] for example.

The equilibrium illustrated in Figure 6.12a is the same for any daily PV energy E produced at the hub, since the CUP $\lambda_e = \lambda_{\text{cst}}$ does not depend on charging demand and PV production (unlike the CUP function defined in (6.8)). While the revenue function R illustrated in Figure 6.12b does not depend on E either, the CSO's cost function C does depend on the amount of electricity taken from the grid, and thus on E. Figure 6.13 shows the daily payoff $R - C$ in function of the constant CUP $\lambda_e = \lambda_{\text{cst}}$ at the hub, for different daily PV productions E. For $E = 1$ MWh, there is enough PV production to charge all EVs so that there are no grid costs and maximizing

[24] The value of this threshold is obtained using a basic exhaustive search method.

[25] https://www.tesla.com/fr_FR/supercharger

[26] For Ionity, the pricing per energy unit only occurs in some countries (in the others, the price is per minute): https://support.ionity.eu/en/general-questions/how-much-does-it-cost-to-charge-at-ionity.

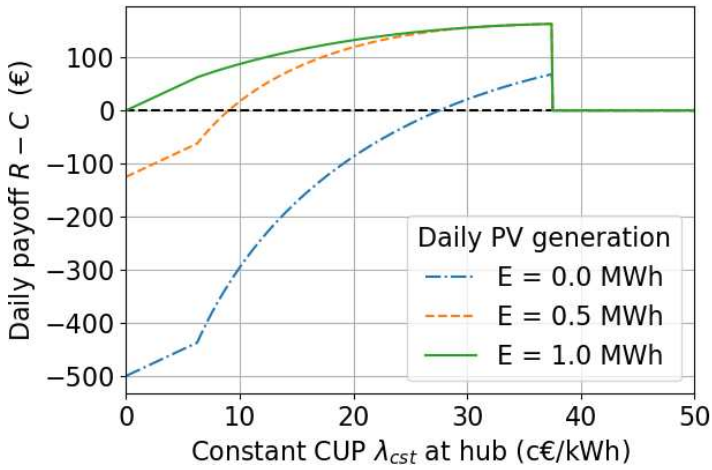

Figure 6.13: Daily CSO's payoff $R-C$ in function of the constant Charging Unit Price $\lambda_e = \lambda_{\text{cst}}$ at the hub, for different daily PV productions E. *No matter E, $\lambda_{cst} = \lambda^*_{cst}$ maximizes $R-C$.*

the payoff is equivalent to maximizing the revenue function R (the top curve in Figure 6.13 is the same as Figure 6.12b).

Figure 6.13 illustrates the fact that the threshold $\lambda^*_{\text{cst}} = 37.5$ c€/kWh maximizes the daily payoff $R - C$, no matter the PV production E (e.g., for all PV sizes and any day of the year). This means that choosing the same constant CUP $\lambda_e = \lambda^*_{\text{cst}}$ at the hub for every day of the year is better than any pricing method made of different (constant) CUPs depending on the day, like for instance seasonal pricing (e.g., one for winter and one for the rest of the year). Naturally, the maximal daily payoff increases with E. Note that this maximal payoff is always positive, even for $E = 0$. This means that even if EVs at the hub may cause grid costs C, the payoff $R - C$ will always be better than when there are no EVs at the hub (i.e., $R - C = 0$).

Optimal sizing of solar panels

In Figure 6.14 the payoff F over $N_y = 20$ years (with $\lambda_e = \lambda^*_{\text{cst}}$) is represented in function of the PV nominal power installed at the hub. Note that as function G^* defined in (4.19) is a quadratic function of the PV nominal power (for low enough daily PV productions), I is linear and R constant, the payoff F is concave with respect to the size of the solar park (see Figure 6.14). Thus, F can be optimized easily, with the SLSQP method [Kraft, 1988] for example. As nominal power increases, the revenue function R remains the same while investments I increase proportionally and CSO's cost function C decreases to zero. Installing solar panels can be profitable if the investments are lower than the grid costs avoided (as it is the case here), but the solar park must not be oversized or the diminution of grid costs will not be significant enough compared to the investments. In order to maximize its payoff F (around 503 k€), the CSO has to install a 236 kWp solar park, corresponding to a surface of 110 parking spots[27]. The different parts of this optimal payoff are as follows: the initial investment is $I = 182$ k€, and the *annual* revenue and cost are respectively 59 k€ and 25 k€, representing over the time period $\mathcal{Y}$ a total of respectively 1.2 M€ and 504 k€. During $\mathcal{Y}$, the Wardrop Equilibrium is the same as the CUP $\lambda_e = \lambda^*_{\text{cst}}$ at the hub does not depend on the weather, and the number of EVs charging at the hub is 220

[27]The conversion from nominal power to PV surface follows https://us.sunpower.com/solar-resources/products/datasheets/, where a PV solar panel with a unit surface of 1 m^2 has a nominal power of 175 Wp. The surface of a parking spot is taken as equal to 12.25 m^2.

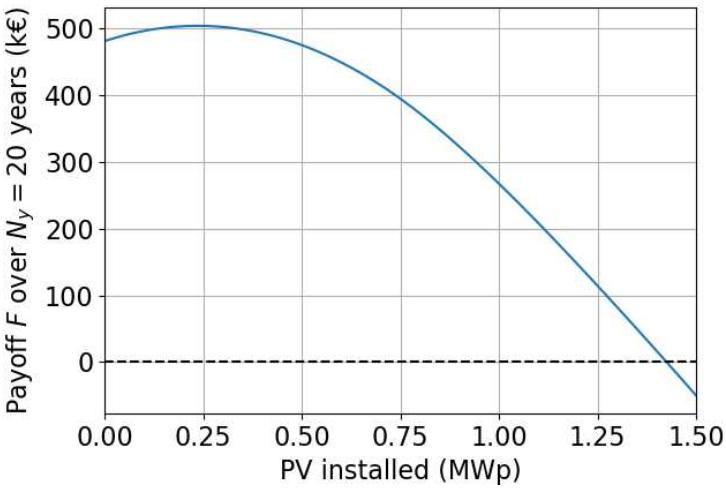

Figure 6.14: CSO's payoff F over $N_y = 20$ years (with $\lambda_e = \lambda^*_{\text{cst}}$) in function of the PV installed at the hub. *The CSO can make more profits by installing the right amount of PV: 236 kWp.*

(everyday), out of a total of 500 in the game $\mathbb{G}$. This means that the optimal PV size is equivalent to covering half of the parking spots used by EVs. The CSO can install up to 1.43 MWp of PV (corresponding to 650 parking spots[28]) until its payoff F becomes negative.

Two key parameters impact the nature of the previous results. First, the period of time $\mathcal{Y}$ over which the CSO's payoff is considered: for small enough N_y, the optimal way to maximize the CSO's payoff is not to install PV at all. The same phenomenon is observed for low enough CUP λ_e^0 inside the city. In these cases, the CUP $\lambda_e = \lambda_{\text{cst}}$ at the hub must be low enough too in order to attract EVs at the hub. However, these λ_{cst} are too low to have sufficient revenue R to pay back the initial investment I in PV.

6.2.2.4 Case of variable charging unit price at hub

The previous study is now applied to the full CUP function (6.8) at the hub: $\lambda_e = \lambda_{\text{cst}} + \lambda^{\text{avg}}$. As in the previous section, the CSO has to choose the optimal constant part λ_{cst} of λ_e for the time period $\mathcal{Y}$ considered. Figure 6.15a shows for each installed PV nominal power value the charging fee λ^*_{cst} which maximizes the CSO's payoff over the N_y years. Note that here, unlike in previous section, this optimal λ^*_{cst} depends on the nominal power: larger PV capacities lead to lower grid costs and thus lower λ_e due to the variable part λ^{avg}, so that the CSO may increase the fixed part λ_{cst} in compensation. The optimal values λ^*_{cst} in this section remain below 37.5 c€/kwh, the optimal value of last section in the case of $\lambda_e = \lambda_{\text{cst}}$, because otherwise the total CUP λ_e would be too expensive compared to the CUP $\lambda_e^0 = 40$ c€/kWh in the city center, due to the variable part λ^{avg}. After $N_y = 20$ years, the payoff F is similar to the one of previous section (see Figure 6.15b compared to Figure 6.14), although the maximal payoff value is 3 % higher with the CUP function λ_e defined in (6.8) instead of the constant CUP case $\lambda_e = 37$ c€/kWh. This means that a feedback mechanism on the impact of the charging operation on the grid for EV owners (i.e., the variable part of λ_e) yields a higher payoff for the CSO. The optimum is reached with a 89 kWp solar park, equivalent to the surface of 40 parking spots, which is more than five times as less than in the constant pricing $\lambda_e = \lambda_{\text{cst}}$ in previous section. In the present section, the WE depends on the PV generation via the variable part λ^{avg} of the CUP function

[28] Note that due to $\lambda_e = \lambda^*_{\text{cst}}$, the number of EVs at the hub at WE is still the same (220).

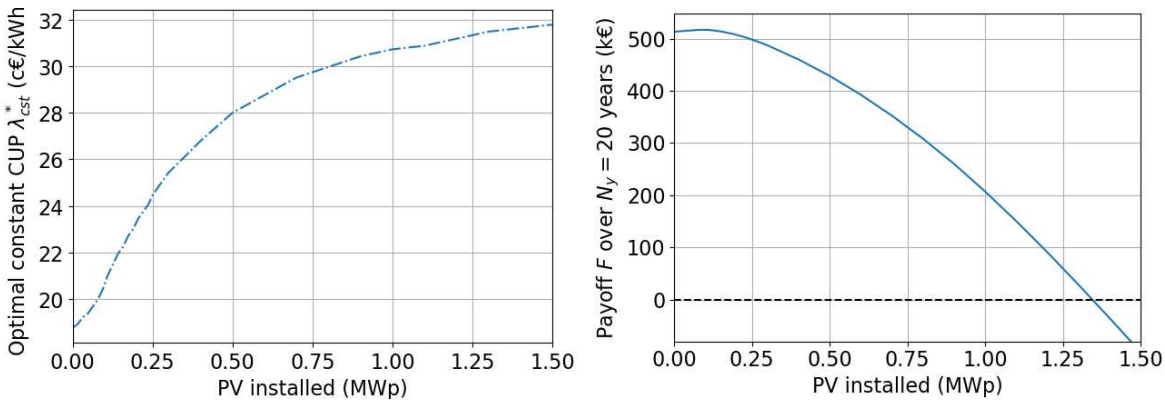

(a) Optimal fixed part λ^*_{cst} in function of nominal power.

(b) Payoff F (with $\lambda_{\text{cst}} = \lambda^*_{\text{cst}}$) in function of nominal power.

Figure 6.15: Optimal CSO's variables to maximize F in function of the PV nominal power installed at the hub. *The variable Charging Unit Price λ_e offers a little more benefits than a fixed one (λ_{cst}, Figure 6.14).*

λ_e. Therefore, the number of EV users charging at the hub depends on the day of the year, and ranges from 175 in winter to 215 in summer.

6.3 Conclusion

This chapter illustrates on two examples the numerical design of incentives, using the vehicle users behavior model given in Chapter 2. In both examples, two mechanisms are already included: the Water-Filling (WF) scheduling of the EV charging profiles, presented in Chapter 4 and centralized at the level of the Charging Service Operator (CSO), and the average WF charging pricing method introduced in Section 5.2.

In the first use case considered, a Transportation Network Operator reduces the local air pollution in a city by taxing Gasoline Vehicle (GV) users driving across the city. This problem is not trivial, as too much congestion on the ring roads of the city would be detrimental to air quality, and because the optimal traffic toll depends on the EV penetration level X_e. Hence the use of the driver's behavior game model to compute their reaction to this traffic toll (via Wardrop Equilibrium) and find the optimal one for each X_e. It is found that for increasing EV penetration levels, the optimal traffic toll decreases: from between 2 and 5 €(depending on the pollution model) when $X_e = 0$, to 90 c€when EVs represent at least a third of the vehicle stock. In the meantime, the toll incentive is more and more efficient and deter greater proportions of GV users (whose total number is decreasing) from crossing the city.

In the second example of this chapter, the CSO manages an e-Park & Ride hub on the outskirt of a city, where commuters can charge their EV with the electricity generated by solar panels at the hub, and go to work in the city by public transport instead of driving there. The goal of this CSO is to maximize its payoff over a long period of time (e.g., 20 years), by choosing the right amount of solar panels, as well as the proper constant charging fee added to the average WF pricing method. In a first step, the Charging Unit Price (CUP) at the hub is considered as only made of the constant charging fee. It is found in this case that a constant 37 c€/kWh CUP is optimal, even compared to a seasonal pricing (e.g., with two constant CUPs: one for summer, which is lower than the one for winter). A natural extension of this work would be to also

compare the acceptability by EV users of these two pricings. In a second step, the full expression – both the constant charging fee and the average WF pricing – of the CUP is considered, and the optimization of both the charging fee and the solar park's size yields an optimal long-term payoff 3 % higher than in the first step.

The optimal toll in the first example and the optimal charging fee in the second are found by exhaustive search, which is not tractable for more complex use cases. The next chapter adapts an iterative optimization method – which is proved to converge towards the optimal solution – to a trilevel framework considering the vehicle users, the CSO and the Electrical Network Operator.

Chapter 7

Hierarchical coupled driving-and-charging model of electric vehicles, stations and grid operators

In this chapter, a theoretical framework of the interactions between different entities of the coupled electrical-transportation system observed in previous Chapter 6 is given. Such a framework is suggested for the electrical system in the context of commuting, which has a typical trilevel structure. Note that the results of this chapter can be extended to other use cases which also include transportation operators. At the lower level of the model, a congestion game between different types of vehicles gives which driving paths and charging stations (or hubs) commuters choose. At the middle level, a Charging Service Operator sets the charging prices at the hubs to maximize the difference between EV charging revenues and electricity supplying costs, following the water-filling locational marginal pricing introduced in Section 5.3. These costs directly depend on the electricity supplying contract, whose structure is chosen by the Electrical Network Operator at the upper level of the model in order to reduce grid costs. This trilevel optimization problem is solved using optimistic iterative and simulated annealing algorithms. The sensitivity of the solution of this trilevel model to exogenous parameters such as the EV penetration level and an incentive from a transportation operator is illustrated on realistic electrical and transportation urban networks. This model is compared to a standard bilevel model in the literature and already introduced in Section 5.1.2, in which the hubs and the grid are operated by the same entity.

This chapter is inspired from the following paper:

[Sohet et al., 2021c] **Sohet, B.**, Hayel, Y., Beaude, O., and Jeandin, A. (2021). Hierarchical coupled routing-charging model of electric vehicles, stations and grid operators. *IEEE Transactions on Smart Grid*, 12(6):5146-5157.

Contents

7.1 Introduction **136**

7.2 A smart coupled driving-and-charging model with three types of actors **138**

7.2.1 Vehicle users: a coupled driving-and-charging decision 138

7.2.2 Charging Service Operator: sets charging price 140

7.2.3 Electrical Network Operator: designs CSO electricity supply contract 141
7.3 The trilevel optimization problem 142
7.3.1 Vehicle users at Wardrop equilibrium 143
7.3.2 The trilevel problem formulation 144
7.4 Resolution of trilevel optimization problem 145
7.4.1 An iterative method for upper and middle levels optimization . . . 145
7.4.2 CSO and ENO optimization problems: a simulated annealing approach 147
7.5 Case studies 148
7.5.1 Sensitivity to electric vehicles penetration level 150
7.5.2 Sensitivity to public transport fare 151
7.5.3 Comparison with the standard bilevel framework 152
7.6 Conclusion 153

Table 7.1: Notations of Chapter 7

i_r	Parking (and charging) hub associated with path r
r_S	Path r and charging at hub
r_H	Path r and charging later (e.g., at home)
$\mathcal{H}_{\text{cso}}$	Set of CSO's hubs
e_1	EV class that can charge at hub or later
e_0	EV class that can only charge at hub
X_e	EV penetration level
t_i	PT fare from hub i to destination
λ_i	Charging Unit Price (7.4) at CSO's hub $i \in \mathcal{H}_{\text{cso}}$
λ_S^0	Constant Charging Unit Price at city's hub $i \in \mathcal{H} \backslash \mathcal{H}_{\text{cso}}$
λ_H^0	Constant Charging Unit Price at home
L_i	Charging need aggregated over all EVs charging at hub i
Π_{mid}	CSO's objective (charging revenues − electricity supply cost)
Π_{up}	ENO's objective (electricity supply revenue − grid costs)
$x_{s,r}$	Flow rate of vehicle class s on path r
$x_{s,a}$	Flow rate of vehicle class s on arc a $(= \sum_{\{r \text{ s.t. } a \in r\}} x_{s,r})$
$\ell_{i,t}$	Aggregated charging power at hub i and time slot t
η	Charging Unit Price magnitude (CSO's decision variable)
P	Elec. supplying contract threshold (ENO's decision variable)

7.1 Introduction

Most of the related literature which studies the coupling between the transportation and electrical systems due to EVs, reviewed in [Wei et al., 2019] or in more recent papers [Shi et al., shed, Qian et al., 2020], consider the following framework. At the lower level, EV users behavior

is modeled as the equilibrium of a driving-and-charging game: EV users choose the resources (driving path, charging station, etc.) with minimal costs – either financial (traffic tolls, charging cost) or temporal (travel duration, queuing and charging times) – which are function of the other EV users' strategies, due to congestion effects. At the upper level, an urban planner from the transportation and/or the electrical system incentivizes these EV users through pricing mechanisms to adopt an "optimal" behavior.

However, the reduction in the literature of the electrical system's management to one type of operator is particularly unrealistic. Concerning electric mobility, the electrical operators carry out two main functions: the Charging Service to EV users (guaranteed by Operators called CSOs) and the management of the Electrical Network (done by the ENO). In this chapter, a CSO brings together both the charging point operator in charge of the station and the mobility service provider which deals with the EV customers, and the ENO is both the grid manager and the electricity provider. In the previously mentioned papers, smart charging pricing is chosen to optimize either the ENO's [Shi et al., shed] or the CSOs' payoff [Tan and Wang, 2017], but the interaction between CSO and ENO is not considered. In this chapter, we use instead a trilevel setting, with the EV users at the lower level, the CSOs at the middle one and the ENO at the upper level. As the decision maker at the upper level of the framework, this trilevel setting is intended for and solved by the ENO[1]. Other works such as [Wu et al., 2015, Vagropoulos et al., 2015] also consider several CSOs, but in a futuristic electricity market environment rather than the current realistic framework of CSOs buying electricity from suppliers (the ENO in the present chapter).

In electrical systems, trilevel frameworks are employed in cyber security [Alguacil et al., 2014], expansion planning [Jin and Ryan, 2013] or demand-side management [Aussel et al., 2020] but to our knowledge, only two papers on electric mobility use a trilevel setting. In the research paper [Shakerighadi et al., 2018], the ENO chooses the wholesale electricity prices for each charging station. Each station charges its EVs, which only choose the charging quantity depending on the local retail electricity price set by the CSO of the corresponding station. Due to the simple formulations of the three levels objective functions (no game between EV users), this trilevel setting is easily solved analytically. In [Alizadeh et al., 2018], EV users choose a driving path, a station and a charging quantity. The CSOs choose the local retail prices in order to minimize their costs (the electricity bought from the ENO) and the time EV users spend on the road. The ENO chooses the local wholesale prices for each station to minimize its costs (related to electrical grid constraints) and also the time EV users spend on the road. Note that the lower level is not a game but simply an optimization problem as there is no interaction between EV users (they do not participate in the congestion on the roads or at charging stations). The trilevel optimization is solved iteratively: the ENO updates the wholesale prices, then the CSO uses an analytic expression to compute the optimal retail prices. The theoretical and algorithmic details are not specified in the paper.

The original contributions of the present chapter are:

1. a realistic model of commuting and charging at work using a trilevel setting, intended for and solved by the ENO, at the upper level. The CSO and ENO maximize their payoffs using realistic pricing mechanisms and EV users interact both while driving and charging in a coupled game;

2. a carefully designed iterative algorithm solving the trilevel model using simulated annealing, Brent's method and convex optimization, with a theoretical proof of the global algorithm's

[1] Note that the truncated bilevel framework made only of the lower and middle levels of this chapter can be seen as intended for and solved by the CSO.

convergence;

3. sensitivity results on a realistic setting and a comparative study of our trilevel model with a bilevel setting (ENO and CSO combined together in a unique operator using Locational Marginal Pricing of Section 5.1.2), standard in the literature [Alizadeh et al., 2016, Wei et al., 2017].

This chapter is organized as follows. The objectives and available strategies of the three types of agents considered (EV users, CSO and ENO) are introduced in Section 7.2. The theoretical trilevel model of the interactions between these agents is given in Section 7.3. An algorithmic solution of this trilevel optimization problem is studied in Section 7.4 and applied in Section 7.5 to examine the sensitivity of our model to exogenous parameters and compare it to a standard model in literature. Finally, conclusions and perspectives are given in last section.

7.2 A smart coupled driving-and-charging model with three types of actors

The smart charging use case considered in this chapter is about commuting: drivers, coming from different places, choose their path to get to their workplace, which are all located in a same city or urban area. In this city, there are Park & Ride hubs where EV users may leave their car charging during working hours, and finish the commuting to their workplace by foot or public transport. In addition to drivers, there are two other types of agents/operators considered in this system:

- The CSOs which are in charge of several hubs and decide the corresponding smart charging fares;
- The ENO which is in charge of the grid[2] of the city considered and which specifies the electricity supply contract with CSOs.

Note that the operators do not control vehicles (in the sense of Vehicle Routing Problems) but only send incentives to influence the decisions of drivers (who interact through congestion effects in the sense of routing games).

7.2.1 Vehicle users: a coupled driving-and-charging decision

The transportation network is modeled by a graph in which each arc represents a street (illustrated in Figure 7.2). Here a path r refers to the successive arcs used to go from an origin O to the hub i_r chosen to park the vehicle, and also includes the public transport arc connecting i_r to the workplace destination D. Vehicle users have to choose one of the paths to go from their origin to their destination, depending on the commuting duration and on the energy consumption costs.

Vehicles are of two distinct types: EVs (index e) and Gasoline Vehicles (GVs, index g) which rely on thermal engines. EVs are split into two classes: EVs in class e_1, when choosing a path r, can either decide to charge at hub i_r during working hours (fictitious path denoted r_S), or only park there and charge later, e.g. at home (path r_H)[3]. EVs in class e_0 do not have enough energy

[2]The grid is assumed to be a medium-voltage one, without loss of mathematical generality.

[3]Note that subscript H refers to charging at Home (and not for "Hub"), and S to charging at Station (which is called a hub in this chapter).

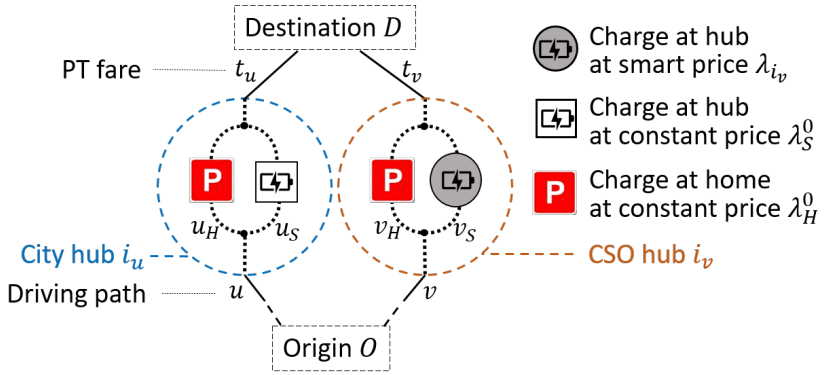

Figure 7.2: Illustration of a transportation network. *Each path $r \in \{u, v\}$ includes the driving path to get to the hub i_r associated with r and the PT fare t_r to go from hub i_r to the workplace. At hub i_r, it is possible to only park there and charge later at constant price λ_H^0 (the corresponding global path is written r_H); or, it is possible to charge at the hub (r_S). Considering the latter decision, the charging price at hub i_r is constant (λ_S^0) if the hub is managed by the City authority (like hub i_u). Otherwise, if the hub is managed by the CSO (like hub i_v) then the charging price λ_{i_v} is smartly designed by the CSO.*

(their State of Charge, or SoC, is low) to go home after work and will automatically choose to charge at the hub (path r_S)[4]. Vehicles of a same class (g, e_0 or e_1) have the same cost functions. More vehicle classes could be considered in order to distinguish for example diesel from gasoline vehicles.

The duration cost of a path r is the same for all vehicle classes and is made of two parts. The first one reflects congestion on each road a composing path r following the Bureau of Public Road (BPR) function [Spiess, 1990], already defined in (2.5). This congestion cost function d_a on road a depends on the drivers path choice through variable $x_a = x_{g,a} + x_{e_0,a} + x_{e_1,a}$, the total flow of vehicles of all classes on arc a The second part of the duration cost is a constant t_i representing, if any, the time (expressed as a cost) to go from the hub i where a vehicle is parked to its workplace. Other constant cost functions can be added to t_i like public transport fares.

The second type of cost for drivers is related to energy consumption. The charging fare at hub i is more precisely a Charging Unit Price (CUP) λ_i, i.e. per unit of energy charged, and is specified in the next section. EV users deciding to charge during working hours will be charged up to full SoC. More precisely, the amount of energy EVs of class e_j charge at the hub is equal to the energy consumed while driving to their workplace, plus the difference s_j between full SoC and the SoC before the morning trip. The former quantity of energy is assumed to depend only on the traveled distance, i.e. the energy m_s consumed by a vehicle of class s per distance unit is constant. Thus, EVs of class e_j charging at the hub i_r of path r have to pay:

$$L_{e_j,r} \times \lambda_{i_r} \,, \quad \text{with} \quad L_{e_j,r} = (l_r m_e + s_j) \,, \tag{7.1}$$

where l_r is the total length of path r. Then, the energy consumed by an EV on path r is approximated by the product $l_r m_e$. It is assumed that EV users which do not charge at the hubs also take into account a consumption cost: $L_{e_j,r}\lambda_H^0$, with λ_H^0 a constant corresponding to the CUP at home for example. Similarly, the consumption cost for GVs is $L_{g,r}\lambda_g$ with $L_{g,r} = l_r m_g$.

[4]Note that in the other chapters of this thesis, there is only one class of EVs: they all have the same initial SoC and charge at the public charging stations.

The total cost function for a vehicle of class s choosing path r is:

$$c_{s,r}(\boldsymbol{x}) = \sum_{a \in r} d_a(x_a) + t_{i_r} + L_{s,r}\lambda\,, \tag{7.2}$$

where λ is equal to λ_g if $s = g$, λ_H^0 if $s = e_1$ and $r = r_H$ or λ_{i_r} if $s = e_j$ and $r = r_S$.

The interaction between drivers through congestion effects constitutes a non-atomic multi-class congestion game [Jiang and Xie, 2014] $\mathbb{G}$ with non-linear cost functions $\boldsymbol{c} = (c_{s,r})$ defined in (7.2). In such frameworks, the concept of Wardrop Equilibrium (WE) denotes a particular distribution of choices of vehicle users between the possible paths, where no user has an interest to change her choice unilaterally (see Definition 2.14). The CUP λ_i at CSO's hub i is a congestion cost function (because it depends on the aggregated charging need at hub i) determined by the CSO and is specified in the next section.

7.2.2 Charging Service Operator: sets charging price

A CSO adapts the Charging Unit Price (CUP) functions at its hubs in order to maximize the difference between its revenues from EV charging and its electricity supplying costs (defined in next section). Here, it is supposed that there is only one CSO in this local urban area. More precisely, this CSO does not own all the hubs of the city, otherwise it could set arbitrarily high prices and EV users of class e_0 would have no choice but to pay these prices. Instead, some hubs belong to the city for example[5] with a constant CUP λ_S^0, supposed higher than λ_H^0, the one available at home[6]. The set of all hubs is denoted $\mathcal{H}$ and the set of the CSO's hubs, $\mathcal{H}_{\text{cso}}$.

At each hub $i \in \mathcal{H}_{\text{cso}}$, the CSO determines the charging load profile $(\ell_{i,t})_{t\in\mathcal{T}}$ over the working time period $\mathcal{T}$ and aggregated over all EVs at hub i, such that their SoC is full at the end of the day. The choice of the aggregated charging profile $\boldsymbol{\ell}_i$ at hub i depends on other electricity usages $(\ell_{i,t}^0)_t$ at this hub, called non-flexible because of their non-shiftable operation. This non-flexible term corresponds for example to the consumption of a shopping mall or a tertiary site attached to the hub[7]. The CSO schedules EV charging in order to smooth the total power loads $\boldsymbol{\ell}_i^{\text{tot}} = \boldsymbol{\ell}_i + \boldsymbol{\ell}_i^0$ at its hubs $i \in \mathcal{H}_{\text{cso}}$ and therefore reduce its electricity supplying costs (see next section for more details). To this end, for each hub $i \in \mathcal{H}_{\text{cso}}$, the CSO chooses the water-filling aggregated charging profile $\boldsymbol{\ell}_i^*(L_i)$ defined in (4.1). This charging profile depends on the charging need L_i aggregated over all EVs at hub i:

$$L_i(\boldsymbol{x_e}) = N \sum_r \delta_{i_r,i} \sum_{j=0,1} x_{e_j,r_S}\; L_{e_j,r}\,, \tag{7.3}$$

with N the total number of vehicles in game $\mathbb{G}$, $\delta_{i_r,i} = 1$ or 0 whether or not the destination hub i_r associated with path r is hub i, and x_{e_j,r_S} the flow of EVs of class e_j choosing path r and charging at hub i at the end of the path. Note that at hubs $j \notin \mathcal{H}_{\text{cso}}$ which do not belong to the CSO, EVs are supposed to apply the plug-and-charge policy: $\ell_{j,1}^* = L_j$ and $\ell_{j,t}^* = 0$ if $t > 1$.

[5] For example Île-de-France Mobilités, the Organising Authority for Mobilities in Paris region, owns 20,500 parking spaces in 73 hubs https://www.iledefrance-mobilites.fr/le-reseau/services-de-mobilite/parcs-relais (in French).

[6] This is actually observed in France for example, where the EDF home contracts are around 15 c€/kWh and 36 c€/kWh at Tesla superchargers for instance

[7] Note that in this chapter the non-flexible term is implicitly considered positive, i.e. is a consumption term. The following results could be extended to negative non-flexible loads (e.g., corresponding to local electricity generation at the hubs) by extending the load cost function used for the charging scheduling (see Figure 4.5) as well as the electricity supplying contract of the CSO (see Figure 7.3).

The CSO chooses a charging pricing mechanism based on this water-filling charging scheduling and uses for each hub $i \in \mathcal{H}_{\text{cso}}$ the CUP function λ_i^{wf} defined in[8] (5.12):

$$\lambda_i(\eta\,, L_i) = \eta \frac{\partial G_i^*}{\partial L_i} = 2\eta \frac{L_i + L_{i,\bar{t}}^0}{\bar{t}(L_i)}\,, \tag{7.4}$$

with G_i^*, $\bar{t}$ and $L_{i,\bar{t}}^0$ defined in the water-filling Proposition 4.2, and η the variable with which the CSO optimizes its payoff. This variable is a conversion parameter (so that λ_i is a monetary price per energy unit, in €/kWh) and is the same for all CSO's hubs i. Note that the CSO does not change the structure (of Locational Marginal Pricing, see Section 5.3) of the CUP functions at its hubs, but only their order of magnitude via η.

According to (7.4), variable η must be non-negative in order to have $\lambda_i \geq 0$. Moreover, it is assumed that some regulator sets an upper-bound $\overline{\eta}$ to the CSO's decision variable. The feasible set of the CSO's strategy is denoted $\mathcal{A} = \{\eta \in \mathbb{R} \mid 0 \leq \eta \leq \overline{\eta}\}$. The CSO wants to optimize its net payoff, the difference between its revenues and its costs. Its revenues are what EV users pay to be charged at CSO's hubs, and its costs come from the electricity supplying contract with the ENO, which are described in next section.

7.2.3 Electrical Network Operator: designs CSO electricity supply contract

In this urban framework, only the medium-voltage distribution grid and the associated Electrical Network Operator are considered, and not the possible interactions with low-voltage distribution and the transmission grids. This ENO specifies the electricity supplying contract with the CSO to engage grid cost reductions. This contract defines $C_{i,t}$, the amount the CSO owes to the ENO for the energy used to charge EVs at CSO's hub i and time slot t. The ENO determines one of the parameters of the contract, a power threshold P, which is the same for all hubs and time slots. Whether the total load at given hub and time slot is above or below this threshold P, the CSO's electricity bill varies.

The total load at CSO's hub i and time slot t is made of the aggregated charging profile given by the water-filling algorithm and the non-flexible part, and is equal to $\ell_{i,t}^{\text{tot}} = \ell_{i,t}^* + \ell_{i,t}^0$. The electricity supplying cost $C(\ell_{i,t}^{\text{tot}}, P)$ associated with this total load follows the idea of increasing block rates used for water consumption [Agthe and Billings, 1987]. It depends on the power threshold P in the following way. If the total load $\ell_{i,t}^{\text{tot}}$ is below P, the price per energy unit is $\mu(P)$, otherwise, the unit price of the exceeding load is $\overline{\mu}(P) > \mu(P)$. In the latter case, the total electricity supplying cost is the sum of the threshold power at a low price rate $(P \times \mu(P))$ and of the exceeding power at the high price rate $((\ell^{\text{tot}} - P) \times \overline{\mu}(P))$. In general, the electricity supplying cost function is defined as:

$$C\left(\ell_{i,t}^{\text{tot}}, P\right) \;=\; \mu(P) \min\left(\ell_{i,t}^{\text{tot}}\,, P\right) + \overline{\mu}(P) \max\left(0\,, \ell_{i,t}^{\text{tot}} - P\right). \tag{7.5}$$

Functions μ and $\overline{\mu}$ are increasing with P: the higher the power threshold P prescribed to the CSO, the higher the price per energy unit. To simplify, linear functions are used: $\mu(P) = qP$ and $\overline{\mu}(P) = \overline{q}P$ with $\overline{q} > q > 0$. Figure 7.3 illustrates function C for two different power thresholds $P_1 < P_2$. The two slopes of function $\ell \mapsto C(\ell, P_2)$ are respectively steeper than for power threshold P_1 (i.e., functions μ and $\overline{\mu}$ are increasing). Note that, in the particular case of Figure 7.3 ($\overline{q} = 3q$, which is the assumption taken in Section 7.5), the electricity supplying cost

[8] In the present chapter, the load function f is assumed quadratic.

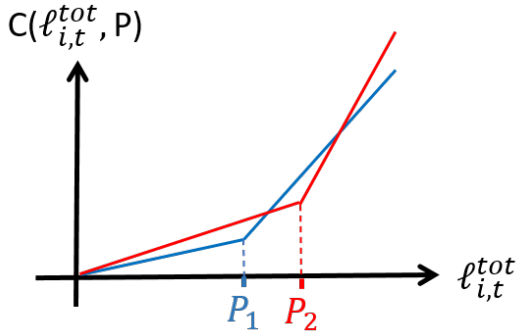

Figure 7.3: Electricity supplying cost C in function of the total load $\ell_{i,t}^{\text{tot}}$ (at hub i and time t), for two values of power threshold $P_1 < P_2$. *In this particular case of $\overline{q} = 3q$, the electricity supplying cost associated with a higher power threshold is not systematically higher.*

associated with a higher power threshold is not systematically higher[9] (see Figure 7.3 around P_2). In other words, increasing the power threshold does not systematically increase the revenue of the ENO. The electricity supplying cost function $C_{i,t}$ only due to EV charging is defined on a pro rata basis[10]:

$$C_{i,t}\left(L_i\,,P\right) = \frac{\ell_{i,t}^{*}(L_i)}{\ell_{i,t}^{\text{tot}}(L_i)} \times C\big(\ell_{i,t}^{\text{tot}}(L_i), P\big)\,. \tag{7.6}$$

Note that even if threshold P is the same for all CSO's hubs, the electricity supplying cost functions $C_{i,t}$ for EV charging are different due to the different non-flexible loads $\ell_{i,t}^{0}$ at each hub i.

For each time slot t, the ENO's cost function is defined as the grid cost associated with the EV charging loads at t at all EVCSs $i \in \mathcal{H}$ of the grid. More precisely, it is the difference between the grid cost $\mathcal{G}_t(\boldsymbol{\ell}_t^{\text{tot}})$ associated with the total power loads $\boldsymbol{\ell}_t^{\text{tot}}$ at t and defined in Section 4.4.1, with the grid cost $\mathcal{G}_t(\boldsymbol{\ell}_t^{0})$ considering only the non-flexible loads $\boldsymbol{\ell}_t^{0}$ at t.

The ENO's objective can then be expressed as:

$$\Pi_{\text{up}}\left(P\,,\boldsymbol{L}\right) = \sum_{t=1}^{T}\Big(\sum_{i\in\mathcal{H}_{\text{cso}}} C_{i,t}\left(L_i\,,P\right) - \beta \times \mathcal{G}_t\left(\boldsymbol{\ell}_t^{*}\right)\Big), \tag{7.7}$$

with $\boldsymbol{L} = (L_i)_i$ and β a parameter which converts $\mathcal{G}_t$ into a monetary cost. The ENO's decision variable, the power threshold $P \geq 0$, is supposed to be bounded by $\overline{P}$ by some regulator, to prevent the ENO from arbitrarily increase its revenue from the CSO's electricity supplying contract. The feasible set of the ENO's strategy is denoted $\mathcal{P} = \{P \in \mathbb{R} \mid 0 \leq P \leq \overline{P}\}$. Note that the ENO's objective depends on $\boldsymbol{L}$, the result of drivers' strategies, which depends itself on ENO's decision variable P, as shown in the next section. The different agents, their decision variables and their interactions are summarized in Figure 7.4.

7.3 The trilevel optimization problem

Last section introduced the three types of agents in our smart charging framework and their interactions. This section focuses on the outcome of such a system. The following multilevel

[9] More precisely, in the case of linear functions μ and $\overline{\mu}$, $C(\ell, P_2) > C(\ell, P_1)$ for all ℓ and $P_2 > P_1$ if and only if $\overline{q} \leq 2q$. Otherwise, $C(\ell, P_2) < C(\ell, P_1)$ for $\frac{P_2}{P_1} \in]1, \frac{\overline{q}}{q} - 1]$.

[10] Other choices could have been made, such as attributing the whole exceeding power cost to EV charging only.

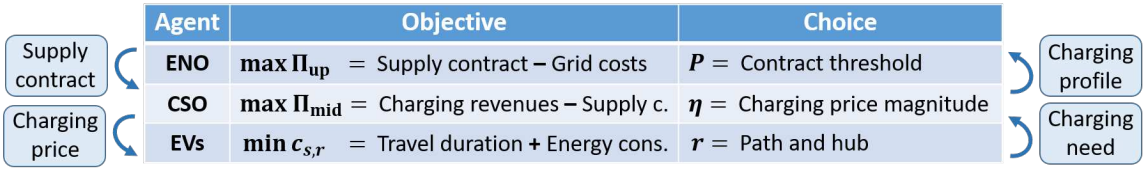

Figure 7.4: Diagram of the different agents, their decision variables and their interactions.

optimization problem is solved by the ENO as the decision maker at the upper level of the decision process. In particular, the ENO aims to maximize its objective function Π_{up} defined in (7.7). The electricity supplying contract between the ENO and CSO, and the CUP functions at CSO's hubs are long-term strategies (resp. of the ENO and CSO). They are assumed to be based on the forecast of drivers' behavior on a specific working day, forecast which is the Wardrop Equilibrium (WE) vehicles naturally reach in the routing game considered in this thesis (see Chapter 3) and which depends on the CUP functions (see next section). For example, the ENO might be pessimistic and optimizes its net payoff on a worst-case-scenario day (e.g., with a high proportion of EVs on the roads).

The information available for each agent is as follows. The drivers know their costs functions on this specific working day: they observe the CUP functions chosen by the CSO. Therefore they can choose the optimal path and place to charge during this working day, corresponding to the WE of this day. The CSO has access to the behavior model of vehicle users and knows the main characteristics of the problem, such as the transportation network properties, the travel demands between origins O and destinations D, etc. Therefore, the CSO can compute the WE for any CUP functions it chooses. However, the CSO has no information on the grid topology and consequently on ENO's cost function, so that it does not know how the ENO chooses the electricity supplying contract. Thus, the CSO must observe its electricity supplying contract only once it is chosen by the ENO. Finally, the ENO has also access to the behavior model of vehicle users and to general information (e.g., travel demands), including the structure of the CUP functions, which is assumed to be publicly disclosed by the CSO. This way, the ENO can compute the WE, the CSO's revenues and then CSO's reaction to its electricity supplying costs (chosen by the ENO). This constitutes a trilevel optimization problem as illustrated on Figure 7.4, with the ENO at the upper level, the CSO at the middle one and the drivers at the lower level.

7.3.1 Vehicle users at Wardrop equilibrium

Before defining the trilevel optimization problem, some details about the lower level are needed. On the working day considered, the city's commuters have to choose how to get to their workplace and whether they charge their vehicle during the working hours. Due to the congestion effects on the road and also on the Charging Unit Prices at CSO's hubs, the decision of a driver depends on the others'. The solution concept used to study this interaction is the Wardrop Equilibrium (see Definition 2.14). In certain conditions, such equilibria correspond to the vehicle flows minimizing a Beckmann function under the travel demand constraints (2.1), following Proposition 2.19. As already mentioned in Section 5.3.2, Proposition 2.19 applies in the particular case of CUP function (7.4). For any CSO's strategy η, the Beckmann minimization problem corresponding

to game $\mathbb{G}$ is:

$$\min_{\boldsymbol{x}\in\mathcal{X}} \mathcal{B}(\boldsymbol{x},\eta)\,, \quad \text{with} \quad \begin{cases} \mathcal{B}(\boldsymbol{x},\eta) = \sum_a \int_0^{x_a} d_a + \sum_{(s,r)\in\mathcal{S}} x_{s,r}\left(t_{i_r} + \ell_{s,r}\lambda_{s,r}\right) + \eta \sum_{i\in\mathcal{H}_{\text{cso}}} G_i^*(\boldsymbol{x}_e)\,, \\ \mathcal{X} \quad = \left\{(x_{s,r})_{s,r} \mid x_{s,r} \geq 0\,,\ \sum_{r\in OD} x_{s,r} = X_s^{OD}\right\}, \end{cases} \tag{7.8}$$

where $x_a = \sum_{\{r \text{ s.t. } a\in r\}} \sum_s x_{s,r}$ is the total vehicle flow on arc a, $\mathcal{S} = \{(e_j, r_S)\ s.t.\ i_r \notin \mathcal{H}_{\text{cso}},\ (g,r),\ (e_1, r_H)\}$ and X_s^{OD} is the portion of class s vehicles with origin O and destination D.

Unfortunately, for some CSO's strategies $\eta \in \mathcal{A}$, there might be several minima of (7.8) and therefore, several WE (see Remark 2.24). However, the Proposition 2.22 shows that even if there are several WE, they all lead to the same congestion $d_a^*(\eta)$ on each road a and the same aggregated charging need $L_i^*(\eta)$ at CSO's hub i. Therefore, for given strategies η and P, the CSO and the ENO obtain a unique drivers' impact on their objective functions. This proposition uses the non-decreasing property of congestion and consumption cost functions, the latter being shown in Proposition 5.10. Note that aggregated charging needs at WE depend on η, CSO's decision variable (see the expression of $\mathcal{B}(\boldsymbol{x},\eta)$ in (7.8)). To summarize this section, any solution of optimization problem (7.8) gives the unique $\boldsymbol{L}^*(\eta) = (L_i^*(\eta))_{i\in\mathcal{H}_{\text{cso}}}$ at WE.

7.3.2 The trilevel problem formulation

As mentioned in Section 7.2.2, the objective Π_{mid} of the CSO is the difference between its charging revenues and its electricity supplying costs. At each CSO's hub i, the revenue R_i is the product between the Charging Unit Price function λ_i and the aggregated charging need L_i at this hub. The CSO knows, for each $\eta \geq 0$, that this need is the unique $L_i^*(\eta)$ when drivers are at equilibrium, so that the revenue from hub i can be written:

$$R_i(\eta\,, L_i^*(\eta)) = L_i^*(\eta) \times \lambda_i\big(\eta\,, L_i^*(\eta)\big)\,. \tag{7.9}$$

The revenue is written $R_i(\eta\,, L_i^*(\eta))$ instead of simply $R_i(\eta)$ in order to better visualize the interdependence between the different entities of the electrical system (here, the CSO and the vehicle users) in the expression (7.11) of the trilevel problem below. In function of ENO's strategy P, the CSO has to maximize over $\eta \in \mathcal{A}$ the following objective:

$$\Pi_{\text{mid}}\left(\eta, P, \boldsymbol{L}^*(\eta)\right) = \sum_{i\in\mathcal{H}_{\text{cso}}} \left(R_i\left(\eta\,, L_i^*(\eta)\right) - \sum_{t=1}^{T} C_{i,t}\big(L_i^*(\eta), P\big)\right). \tag{7.10}$$

For each CSO's strategy $\eta \in \mathcal{A}$, the ENO knows the global charging need $\boldsymbol{L}^*(\eta)$ at WE. However, as the objective function Π_{mid} is not convex with respect to η (in part because $\boldsymbol{L}^*(\eta)$ is an unknown function of η), Π_{mid} might have several global optima.

In this chapter, an optimistic formulation of the multilevel problem is considered. This optimistic assumption states that for any ENO's strategy P, among the η^* maximizing (globally) the CSO's objective function $\eta \mapsto \Pi_{\text{mid}}(\eta, P, \boldsymbol{L}^*(\eta))$, the one giving the highest ENO's objective $\Pi_{\text{up}}(P, \boldsymbol{L}^*(\eta^*))$ is chosen[11]. Finally, the global trilevel optimization problem to solve is:

[11] More precisely, the choice of the η^* which is the most favorable towards the ENO is made by the CSO. As the CSO is not supposed to have any information on the ENO's objective, this requires a minimal cooperation between the two operators (e.g., the CSO lets the ENO choose the η^*).

$$\max_{P\in\mathcal{P},\eta^*\in\mathcal{A}} \ \Pi_{\text{up}}\Big(P\,,\boldsymbol{L}^*(\eta^*)\Big)\,, \tag{7.11a}$$

$$\text{s.t.} \quad \Pi_{\text{mid}}\left(\eta^*\,,P\,,\boldsymbol{L}^*(\eta^*)\right)=\overline{\Pi_{\text{mid}}}\left(P\right)\,, \tag{7.11b}$$

$$\text{s.t.} \quad \boldsymbol{L}^*(\eta^*)=\boldsymbol{L}\left(\underset{\boldsymbol{x}\in\mathcal{X}}{\text{argmin}} \ \mathcal{B}\left(\boldsymbol{x}\,,\eta^*\right)\right)\,, \tag{7.11c}$$

where $\overline{\Pi_{\text{mid}}}\left(P\right)=\max_{\eta\in\mathcal{A}}\Pi_{\text{mid}}\left(\eta\,,P\,,\boldsymbol{L}^*(\eta)\right)$, and function argmin returns the set of global minima of $\mathcal{B}$, which share the same $\boldsymbol{L}^*$ (see Proposition 2.22).

This trilevel problem can be seen as a Stackelberg game (between the upper and middle levels) with equilibrium constraints (lower level) [Ehrenmann, 2004]. Note that depending on the information available to the ENO and CSO, other trilevel frameworks can be considered: if both the CSO and the ENO know the reactions of the other, they play in a simultaneous Nash game, with equilibrium constraints (lower level). However, solving this Nash game with algorithms such as Best Response may not converge due to the equilibrium constraints.

7.4 Resolution of trilevel optimization problem

7.4.1 An iterative method for upper and middle levels optimization

In most multilevel optimization problems, the convex lower level is replaced by the corresponding Karush-Kuhn-Tucker (KKT) conditions [Colson et al., 2007], which would transform the trilevel problem (7.11) into a bilevel (upper-middle) one with equilibrium constraints. However, using KKT conditions introduces integer variables (see for example the coupling constraint "$\mu_{s,r}\times f_{s,r}$" in the proof of Proposition 2.19) and therefore transforms the global optimization problem into a mixed-integer non-linear optimization problem, which increases dramatically the computational complexity [Papadimitriou, 1998]. In our setting we chose to rather keep the initial trilevel structure (7.11) and simply solve the convex lower level using sequential least squares programming [Boggs and Tolle, 1995]. Thus, for the resolution of the global problem, we focus on the upper (ENO) and middle (CSO) levels. The lower level is referred to as an implicit numerical function $\boldsymbol{L}^*(\eta)$ of CSO's price strategy η (see Proposition 2.22), which is the global charging need when vehicle users are at equilibrium. The global trilevel optimization problem is rewritten as:

$$\begin{aligned}\max_{P\in\mathcal{P},\eta^*\in\mathcal{A}} \ & \Pi_{\text{up}}\left(P\,,\boldsymbol{L}^*(\eta^*)\right)\,,\\ \text{s.t.} \quad & \Pi_{\text{mid}}\left(\eta^*\,,P\,,\boldsymbol{L}^*(\eta^*)\right)\geq\overline{\Pi_{\text{mid}}}\left(P\right)-\varepsilon_{\text{mid}}\,,\end{aligned} \tag{7.12}$$

with $\varepsilon_{\text{mid}}>0$ a tolerance level introduced to guarantee the convergence of the algorithm used to solve (7.12). Note that a pessimistic formulation of (7.12) can be used instead, by replacing the expression $\max_{P\in\mathcal{P},\eta^*\in\mathcal{A}}\Pi_{\text{up}}$ by $\max_{P\in\mathcal{P}}(\min_{\eta^*\in\mathcal{A}}\Pi_{\text{up}})$ (i.e., the η^* the least favorable towards the ENO is chosen). To ease notations, $\Pi_{\text{mid}}\left(\eta^*,P,\boldsymbol{L}^*(\eta^*)\right)$ is written $\Pi_{\text{mid}}\left(\eta^*,P\right)$, but both the computation of Π_{mid} and Π_{up} requires $\boldsymbol{L}^*$, i.e. to solve the convex lower level optimization problem.

The global trilevel problem (7.12) is solved using Algorithm 7.1, which is a simplified version of the iterative bounding algorithm introduced in [Mitsos et al., 2008], as there are no constraints at the upper and middle levels other than variable bounds. In Algorithm 7.1, the global optimization problems (7.13) and (7.14) at each iteration are solved by algorithms detailed in next section, but any other suitable algorithms can be applied. By definition of $\overline{\eta}_k$, if the solution of (7.13) at an

Algorithm 7.1: Iterative global algorithm

Input: $P_0\,,\eta_0\,,k=0$

Notation: $\Pi_{\text{mid}}(\eta\,,P)\leftarrow\Pi_{\text{mid}}\big(\eta\,,P\,,\boldsymbol{L}^*(\eta)\big)$

$\overline{\eta}_0=\text{argmax}_{\,\eta}\,\Pi_{\text{mid}}(\eta\,,P_0)$

while $\Pi_{mid}(\eta_k\,,P_k)<\Pi_{mid}(\overline{\eta}_k\,,P_k)-\varepsilon_{mid}$ **do**

$k\leftarrow k+1$

Solving the following problem with simulated annealing Algorithm 7.2:

$$\begin{aligned}&(P_k\,,\eta_k)=\underset{P,\eta}{\text{argmax}}\;\Pi_{\text{up}}(P,\boldsymbol{L}^*(\eta))\,,\\&\text{s.t.}\quad\forall l<k,\;\Pi_{\text{mid}}\,(\eta,P)\geq\Pi_{\text{mid}}\,(\overline{\eta}_l,P)-\varepsilon_{\text{mid}}/3\,,\end{aligned}\tag{7.13}$$

Solving the following problem with Brent's method [Chandram et al., 2008]:

$$\overline{\eta}_k=\underset{\eta}{\text{argmax}}\;\Pi_{\text{mid}}(\eta\,,P_k)\,,\tag{7.14}$$

end

Output: $P_k\,,\eta_k$

iteration k of Algorithm 7.1 verifies the stopping criteria, then it is a solution of the initial trilevel problem (7.12). The convergence of Algorithm 7.1 is guaranteed by the following proposition.

Proposition 7.1. *Algorithm 7.1 stops after a finite number of steps K and delivers an output (P_K,η_K) solution of (7.12).*

Proof. According to the maximum theorem (Beckmann function $\mathcal{B}$ is continuous), the mapping $\boldsymbol{x}^*(\eta)$ solution of (7.8) is upper hemicontinuous. As for a given η, all $\boldsymbol{x}^*(\eta)$ lead to the same $\boldsymbol{L}^*(\eta)$, function $L^*(\eta)$ and therefore Π_{mid} are continuous. The same theorem states that $\overline{\Pi_{\text{mid}}}(P)$ is continuous because Π_{mid} is. As functions Π_{mid} and $\overline{\Pi_{\text{mid}}}$ are continuous respectively on compacts $\mathcal{A}\times\mathcal{P}$ and $\mathcal{P}$, they are uniformly continuous according to Heine–Cantor theorem, which gives δ_ε and $\overline{\delta}_\varepsilon$ verifying respectively:

$$\forall(\eta_0,P_0),(\eta_1,P_1)\in\mathcal{A}\times\mathcal{P}\text{ s.t. }\|(\eta_0,P_0)-(\eta_1,P_1)\|\leq\delta_\varepsilon\,,\tag{7.16}$$

$$\Pi_{\text{mid}}(\eta_1\,,P_1)\geq\Pi_{\text{mid}}(\eta_0\,,P_0)-\frac{\varepsilon_{\text{mid}}}{3}\tag{7.17}$$

$$\forall P_0,P_1\in\mathcal{P}\text{ s.t. }|P_0-P_1|\leq\overline{\delta}_\varepsilon\,,\quad\overline{\Pi_{\text{mid}}}(P_0)\geq\overline{\Pi_{\text{mid}}}(P_1)-\frac{\varepsilon_{\text{mid}}}{3}.\tag{7.18}$$

Let $\delta=\min(\delta_\varepsilon,\overline{\delta}_\varepsilon)$. As $\mathcal{P}$ is compact, the sequence (P_k) built at each iteration of Algorithm 7.1 by (7.13) admits a subsequence $\big(P_{u(n)}\big)$ which converges to P_{lim}. Then, by definition:

$$\exists N_\delta\in\mathbb{N}^*\;\text{ s.t. }\;\forall n\geq N_\delta\,,\quad|P_{u(n)}-P_{\text{lim}}|\leq\frac{\delta}{2}\,.\tag{7.19}$$

Let $k=u(N_\delta),K=u(N_\delta{+}1)$. Then $|P_k{-}P_K|\leq\delta$, so that combining (7.17) with $(\overline{\eta}_k,P_k),(\overline{\eta}_k,P_K)$ gives:

$$\Pi_{\text{mid}}(\overline{\eta}_k,P_K)\geq\Pi_{\text{mid}}(\overline{\eta}_k,P_k)-\frac{\varepsilon_{\text{mid}}}{3}\geq\overline{\Pi_{\text{mid}}}(P_K)-\frac{2}{3}\varepsilon_{\text{mid}},\tag{7.20}$$

Algorithm 7.2: Simulated annealing solving (7.13)

Input: $N_r\,, (\overline{\eta}_l)_l\,, \eta\,, k = 0\,,$ count $= 0$
while count $< N_r$ **do**
  $k \leftarrow k + 1$
  count $\leftarrow$ count $+1$
  P uniformly chosen,
  $\eta_P = \text{argmax}_{\overline{\eta}_l}\, \Pi_{\text{mid}}\,(\overline{\eta}_l\,, P)$
  while $(P\,, \eta)$ *not feasible* **do**
    η randomly chosen from $\mathcal{N}(\eta_P\,, \eta)$
  end
  Acceptation: count $= 0$, with probability $\gamma_{\boldsymbol{z},k}\,(P, \eta)$
end
Output: Accepted $(P\,, \eta)$ giving maximal Π_{up}

with $\overline{\eta}_k$ given by (7.14) at iteration k. Finally, as (P_K, η_K) verifies constraint $l = k$ of (7.13), we have:

$$\Pi_{\text{mid}}(\eta_K, P_K) \geq \Pi_{\text{mid}}(\overline{\eta}_k, P_K) - \frac{\varepsilon_{\text{mid}}}{3}\,, \tag{7.21}$$

$$\text{thus} \quad \Pi_{\text{mid}}(\eta_K, P_K) \geq \overline{\Pi_{\text{mid}}}(P_K) - \varepsilon_{\text{mid}}\,, \tag{7.22}$$

which means that the stopping criteria is reached after iteration K, and Algorithm 7.1 ends with (P_K, η_K) solution of (7.12). □

Note that Algorithm 7.1 can be used to solve any bilevel optimization problem (if constrained, see [Mitsos et al., 2008]). In the context of the coupled electrical-transportation system, this means that other operators could be considered instead of the CSO and ENO.

7.4.2 CSO and ENO optimization problems: a simulated annealing approach

Solving the optimization problems (7.13) and (7.14) of Algorithm 7.1 requires a global optimization method for non-convex and non-differentiable objective functions with continuous constraints. A natural candidate [Dekkers and Aarts, 1991] is the simulated annealing method introduced in [Romeijn and Smith, 1994]. The principle is to explore a sufficient number of random feasible couples $(P\,, \eta)$. The stopping criterion chosen is based on the concept of acceptance, where a potential couple $(P\,, \eta)$ is accepted with probability:

$$\gamma_{\boldsymbol{z},k}\,(P, \eta) = \min\left(1, \exp\left(\frac{\Pi_{\text{up}}(P, \boldsymbol{L}^*(\eta)) - \Pi_{\text{up}}(\boldsymbol{z})}{|\Pi_{\text{up}}(\boldsymbol{z})| \times \mathcal{K}(k)}\right)\right) \tag{7.23}$$

with $\boldsymbol{z}$ the last accepted couple and $\mathcal{K}$ a function of the number of iterations k (of the simulated annealing Algorithm 7.2), here chosen as $\mathcal{K}(k) = 0.99^k$. Note that a couple giving a lower Π_{up} than the last accepted couple may be accepted, although it becomes less likely after many iterations (decreasing $\mathcal{K}$). Following [Wah and Wang, 1999], the algorithm stops when no couple (P, η) has been accepted N_r iterations in a row. This simulated annealing algorithm is shown to converge in probability [Bélisle, 1992].

Solving scalar optimization (7.14) is much faster using scalar algorithms like Brent's method [Chandram et al., 2008] rather than simulated annealing. For problem (7.13), the difficulty with

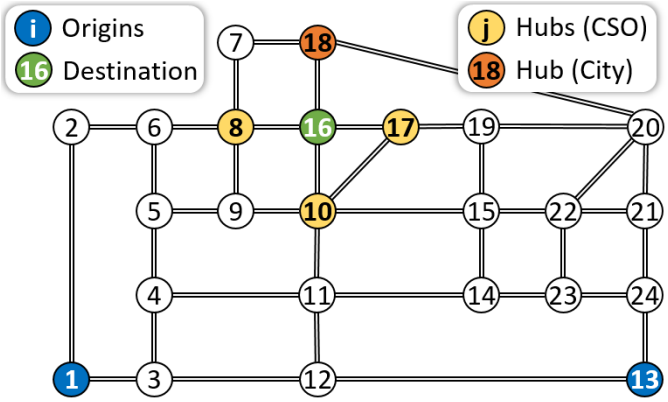

Figure 7.5: Sioux falls transportation network. *Commuters come from two different origins and have the same destination. They choose at which hub to park and the path to get there.*

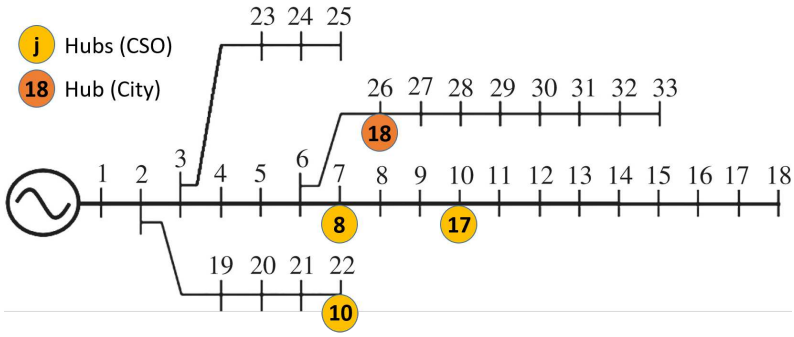

Figure 7.6: IEEE 33-bus medium-voltage distribution network.

simulated annealing is to randomly find feasible couples (P, η), i.e. which verify the constraints in (7.13): $\forall l < k$, $\Pi_{\text{mid}}(\eta, P,) \geq \Pi_{\text{mid}}(\overline{\eta}_l, P) - \frac{\varepsilon_{\text{mid}}}{3}$. However we observed that the $\overline{\eta}$ maximizing $\Pi_{\text{mid}}(\cdot, P)$ depends faintly on P because the variations of the electricity supplying cost functions $C_{i,t}(L_i^*(\eta), P)$ due to P are small. Then for every $P \in \mathcal{P}$, the $\eta \in \mathcal{A}$ such that (P, η) is feasible are in the neighborhood of $\overline{\eta}_P$, with $\overline{\eta}_P = \text{argmax}_{\overline{\eta}_l} \Pi_{\text{mid}}(\overline{\eta}_l, P)$. Consequently, we suggest that P should be uniformly chosen in $\mathcal{P}$ first and then η, drawn from a normal distribution $\mathcal{N}(\overline{\eta}_P, \sigma)$ with mean $\overline{\eta}_P$ and standard deviation some parameter σ to choose. The resulting simulated annealing method is described in Algorithm 7.2.

Our global multilevel problem is solved with Algorithm 7.1, which uses at each iteration global optimization Algorithm 7.2. This numerical resolution is applied in next section to illustrate the design of the charging pricing mechanism and the electricity supplying cost in function of exogenous parameters of the coupled electrical-transportation system.

7.5 Case studies

In this section, Algorithm 7.1 introduced in previous section is applied to our trilevel model to find the optimal strategies for the ENO and the CSO in function of exogenous parameters. The parameters of the problem are set as follows, unless otherwise specified: 1,500 commuters drive from each origin 1 and 13 (N = 3,000 vehicles in total) to destination 16 of Sioux falls (South Dakota, USA) transportation network represented in Figure 7.5 and already introduced in

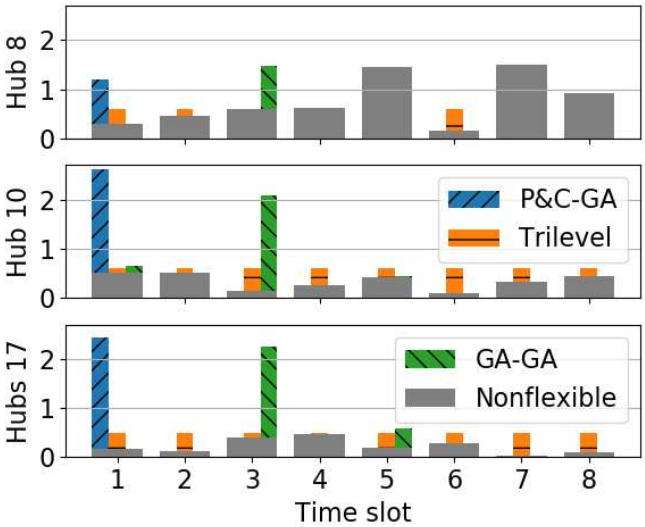

Figure 7.7: Aggregated charging profiles for each CSO's hub, for the water-filling method (4.1) (*Trilevel*), the improved reference method (4.26) (GA-GA) and the PC-GA method. *The plug-and-charge and water-filling structures respectively associated with PC-GA method and Trilevel framework are distinctly observable. The Grid Aware charging profiles are concentrated on the third time slot due to a higher global non-flexible load then (taking into account the other nodes of the electrical network too).*

Section 2.2.2.1. More precisely the drivers have to choose at which of the four hubs (at locations 8, 10, 17 and 18, the latter being owned by the city) they want to park and maybe charge. In Section 7.5.1, hubs are supposed equally distant from destination and $t_i = 0$ without loss of generality. The constant Charging Unit Price at city's hub is $\lambda_S^0 = 25$ c€/kWh, higher than the one at home, $\lambda_H^0 = 20$ c€/kWh. Half of vehicles are electric (except in Section 7.5.1), and the two EV classes e_0 and e_1 are equally represented, with $s_0 = 5$ kWh and $s_1 = 0$ kWh. The length of the road between locations 3 and 4 is 2.5 km and the other lengths can be geometrically deduced from it. For all roads a, the speed limit is $v_a = 50$ km/h and the road capacity is $C_a = 0.2$ (i.e., travel duration triples if 20 % of the 3,000 vehicles take road a). The values of $\tau = 10$ €/h, $m_e = 0.2$ kWh/km, $m_g = 0.06$ L/km and $\lambda_g = 1.50$ €/L are the same as in Section 5.4.2.1. The four hubs belong to the IEEE 33-bus system illustrated in Figure 7.6 and whose parameters are given in [Baran and Wu, 1989]. In particular, the total non-flexible consumption during working hours near each hub is respectively 6.04, 2.62, 1.80 and 1.80 MWh. Each hub's total non-flexible consumption is divided into a random[12] profile over $T = 8$ time slots. The upper bounds for the ENO and the CSO's variables are set high enough to contain the optimal values: $\overline{\eta} = 10^{-3}$ €/kW^2 and $\overline{P} = 4$ MW. The converting parameters are set as follows: $q = 0.1$ €/kW^2, $\overline{q} = 3q$ and $\beta = 10^{-3}$ €/kVA^2. Finally, the simulated annealing parameters $N_r = 15$ and $\mu = 2.5 \times 10^{-6}$ €/kW^2 have been adjusted with the help of brute-force search, to ensure a sufficient exploration of Π_{up} domain[13].

Before studying the global trilevel model in the next sections, the aggregated charging profile (4.1) corresponding to the unique charging need L_i^* at equilibrium at each hub i are illustrated

[12]Except for the charging load profiles in Figure 7.7 (e.g., the grid aware charging profile is not always concentrated on the third time slot), considering different non-flexible load profiles does not change the nature of the numerical results.

[13]For example, above $N_r = 15$, the ratio accepted/explored points is no longer acceptable.

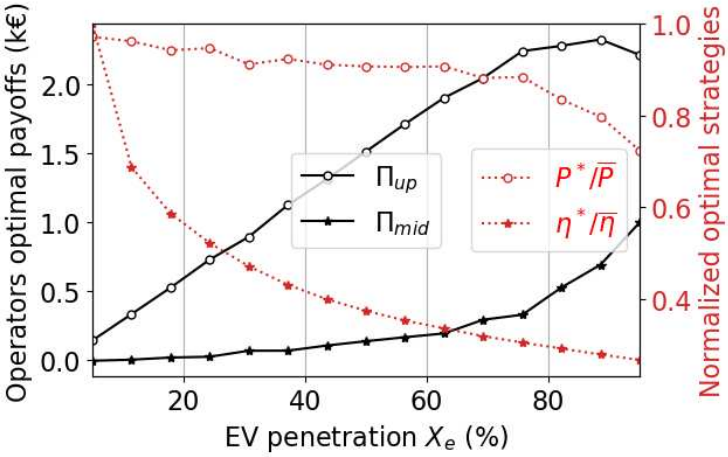

Figure 7.8: Optimal ENO and CSO's payoffs (resp. Π_{up} and Π_{mid}) and normalized strategies (resp. $P^*/\overline{P}$ and $\eta^*/\overline{\eta}$) depending on EV penetration level X_e. *When EV penetration level goes over 75 %, CSO's payoff increases to the detriment of the ENO's because the ENO reduces the power threshold of the CSO's electricity supplying contract.*

in Figure 7.7. This figure shows the local water-filling structure of these profiles (referred to as *Trilevel*) for each CSO's hub. Figure 7.7 also displays the charging profiles obtained solving the Grid Aware (GA) scheduling problem (4.26) (as in the GA-GA method studied in next Section 7.5.3). This profile is exclusively concentrated on the third time slot due to a lower total non-flexible consumption (which depends on the random non-flexible profiles over the whole electrical network) than during the other time slots. These two profiles are also illustrated in Section 4.4.4.1 (where the profiles are respectively called "local" and "grid aware"). For comparison, the Plug & Charge (PC) profile corresponding to $\boldsymbol{L}^*$ is also shown (as in the PC-GA method studied in next Section 7.5.3). It typically leads to significantly larger peak powers compared to the proposed water-filling scheduling and, in turn, higher grid costs.

7.5.1 Sensitivity to electric vehicles penetration level

Solving our trilevel model gives the optimal strategies of the different entities as the proportion X_e of EVs among vehicles grows. More precisely, for each X_e value, Algorithm 7.1 gives the corresponding optimal payoffs and strategies for the ENO and the CSO (see Figure 7.8). This figure shows that in general, both payoffs increase with X_e, as a higher X_e means more EV charging. Furthermore, in order to keep affordable charging prices at its hubs, the CSO has to reduce η as X_e increases and amplifies the price incentive part $\mathrm{d}G_i^*/\mathrm{d}L_i$ (see (7.4)). When the number of EVs is high ($X_e \geq 85$ %), the ENO must lower the CSO's contract threshold P^*, otherwise the CSO would increase the monetary value η of smart charging to reduce its expensive electricity supplying cost by incentivizing EV users to rather charge at city's hub. Thus, the ENO reduces its revenues from CSO's contract so that its payoff stagnates and CSO's payoff considerably increases.

For each EV penetration level X_e, there is a unique charging need at each hub corresponding to vehicles' reaction to optimal strategies of the ENO and the CSO. Note that the uniqueness of the charging need at city's hub is not guaranteed by Proposition 2.22 due to the constant CUP function there. However, it is invalidated only in specific cases where vehicle flows from different vehicle classes and on different paths can be interchanged (e.g., when there are several

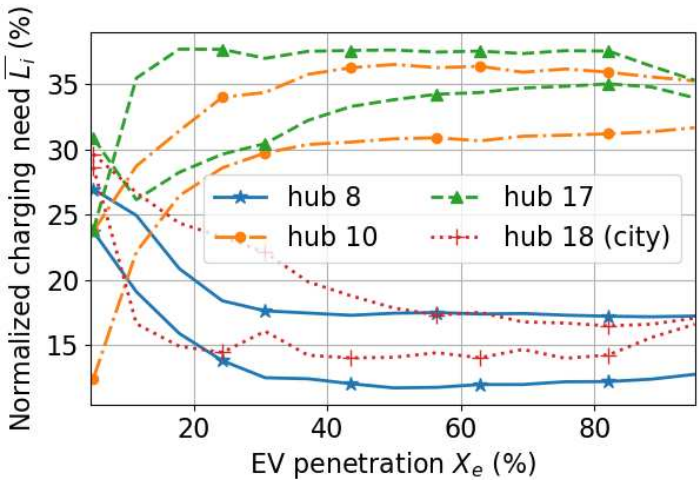

Figure 7.9: Normalized charging needs $\tilde{L}_i = L_i / \sum_j L_j$ at all hubs depending on EV penetration level X_e, for two different non-flexible consumption profiles. *The non-flexible profile considered has a significant impact for low EV penetration levels. For both profiles, $\tilde{L}_8$ and $\tilde{L}_{18}$ decrease with X_e because hub 18 is further away from the origins and hub 8 has a higher non-flexible consumption.*

city's hubs or for specific ratios for roads' lengths and energy prices, etc.). As these charging needs greatly increase with X_e, they are normalized by the total charging need aggregated over all hubs to emphasize their relative variations: $\tilde{L}_i = L_i / \sum_j L_j$ (see Fig 7.9). Different temporal profiles of the same non-flexible consumption (at each hub) lead to similar Figure 7.8, but different normalized charging needs $\tilde{L}_i$. Figure 7.9 shows the $\tilde{L}_i$ for two different non-flexible consumption profiles. This figure reveals that the choice of hub by EV users depends greatly on the non-flexible consumption when the number of EVs is small, but less so as X_e increases. As the EV penetration level increases, GVs are replaced by EVs, which enables more EV users to use closer hubs to the origins (as 10 and 17), to the detriment of city's hub 18. Fewer EV users choose hub 8 rather than hubs 10 and 17 due to the higher non-flexible consumption there (resp. 1.51 compared to 0.68 and 0.45 MWh).

7.5.2 Sensitivity to public transport fare

Last section was dedicated to the long-term EV penetration level. This section focuses on the reaction of the ENO and CSO to an incentive coming from the transportation system. Here, it is supposed that city's hub 18 benefits from a subsidized Public Transport (PT) fare $t_{18} = 1$ €. We consider the PT fare t chosen by a transportation operator and that commuters pay to go from CSO's hubs to the destination: $t = t_8 = t_{10} = t_{17}$. Figure 7.10 shows the evolution of charging needs L_i at all hubs i in function of this PT fare. Note that all EVs of class e_1 charge at home: the CSO is better off with high enough charging prices even if it means fewer EVs charging at its hubs. For PT fares lower than $t = 2$ €, the number of EVs (of class e_0) choosing city's hub increases with t. Between $t = 2$ € and 3 €, this number drops because the PT fare became too expensive for EVs charging at home, which instead all choose paths leading to city's hub 18. Then however, more and more EV users of class e_0 naturally choose the city's hub.

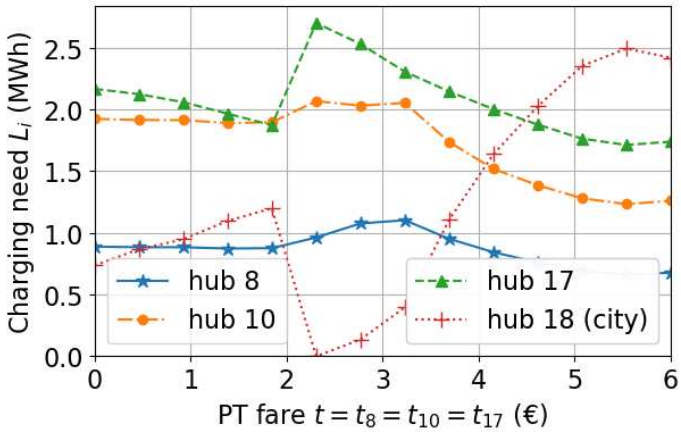

Figure 7.10: Charging needs L_i at all hubs depending on the unique PT fare t. L_{18} *globally increases with* t*, except around* $t = 2$ € *where EVs of class* e_1 *(all charging at home) choose to park at hub 18, forcing the EVs of class* e_0 *(necessarily charging at the hubs) to go to other hubs due to congested driving paths.*

7.5.3 Comparison with the standard bilevel framework

This section compares the trilevel model built in this chapter with the most commonly used model of EV charging incentives in coupled electrical-transportation systems [Alizadeh et al., 2016, Wei et al., 2017] (see Section 5.1.2), on the EV penetration level sensitivity example of Section 7.5.1. The different methods of Section 5.1.2 considered are the PC-GA and GA-GA methods[14], which respectively rely on the Plug & Charge charging profile and the Grid Aware one, which are illustrated in Figure 7.7. Figure 7.11 shows for each EV penetration level X_e the grid cost $\mathcal{G} = \sum_t \mathcal{G}_t$ (filled black markers) and the charging revenues $\mathcal{R} = \sum_{i \in \mathcal{H}_{\text{cso}}} R_i$ (empty red markers) for the trilevel framework (star marker), the improved iterative method (GA-GA) for two values $\eta^{\text{ga}} = 1$ and 3 (in 10^{-5} €/kW^2), and the PC-GA method for $\eta^{\text{pc}} = 1 \times 10^{-5}$ €/kW^2.

Figure 7.11 shows that for the same $\eta^{\text{ga}} = \eta^{\text{pc}} = 1 \times 10^{-5}$ €/kW^2 value, the PC-GA method (diamond marker) gives higher grid costs than the GA-GA one (square), as expected, but also lower charging revenues: as grid costs are higher, the Charging Unit Prices too so that EV users prefer to charge at city's hub (up to $X_e = 60$ %, where they accept these high prices because of the congested paths to access city's hub). The impact of the conversion parameter η^{ga} is also illustrated in Figure 7.11. For example, when η^{ga} is too high (e.g., $\eta^{\text{ga}} = 3 \times 10^{-5}$ €/kW^2), the GA-GA method (triangle marker) gets similar results as the PC-GA one (diamond). Charging revenues are always higher in the trilevel model of this chapter than in the other methods. This seems intuitive given that this metric is explicitly taken into account in the framework of this chapter while the alternative methods focus on grid cost minimization.

Figure 7.11 illustrates that the trilevel model of this chapter (star marker) obtains fairly low grid costs compared to the PC-GA method or the GA-GA one with η^{ga} not carefully designed. This indicates that the electricity supplying contract, the proxy used in the scheduling problem (4.1) and the corresponding LMP (7.4) are good heuristics to reduce the grid cost, as expressed in our paper [Sohet et al., 2020a]. With a particular value $\eta^{\text{ga}} = 1 \times 10^{-5}$ €/kW^2, the

[14] Note that the particular definition of the grid cost in chis chapter (difference between total grid cost and grid cost considering only the non-flexible profiles) does not change the CUP functions of these methods, as only the differentials of the grid cost are relevant.

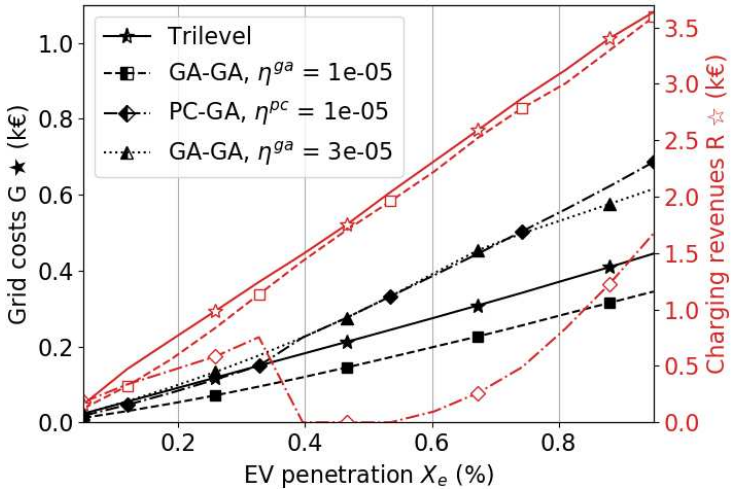

Figure 7.11: ENO grid costs (solid lines) and CSO charging revenues (dashed lines), depending on EV penetration level, obtained with our Trilevel framework (star marker), the PC-GA one (diamond) and GA-GA method for different normalizations η^{ga} (in 10^{-5} €/kW^2) of the LMP (square and triangle). *The literature-based method may lead to minimal grid costs only if smart charging is considered (GA-GA instead of PC-GA method) and if η^{ga} is carefully chosen (square marker). Charging revenues are always higher with the Trilevel framework.*

GA-GA method (square marker) obtains the minimal grid cost. This is made possible because the goal of the operator choosing the charging profiles and prices in this method is to precisely minimize grid cost function. However in practice, the hubs' operator wants to maximize its payoff and may have no information on the electrical grid, as in the trilevel model of the present chapter, which guarantees the highest charging revenues among all methods. Moreover, the results of the GA-GA method are highly sensitive to the choice of parameter η^{ga}, as shown in Figure 7.11.

Finally, note that parallel computations are not practical for the iterative methods. Due to the complexity of solving scheduling problem (4.26), the GA-GA method is actually slower (two times in average) to solve than the trilevel model, which has more optimization layers.

7.6 Conclusion

In this chapter, the impact on the electrical system of EV commuting is modeled by a trilevel optimization problem, compared to the standard bilevel framework in the literature. The lower, middle and upper levels respectively represent the EV users, interacting in a coupled driving-and-charging congestion game, the CSO which can modify the smart charging prices at its hubs and the ENO which designs the electricity supplying contracts with each hub. This trilevel problem is seen as a Stackelberg game (between the upper and middle levels) with equilibrium constraints (lower level), which is solved with an optimistic iterative algorithm combined with simulated annealing. For each ENO and CSO's strategies, there is a unique charging need at each hub when vehicles are at equilibrium (at the lower level, see Proposition 2.22). The behaviors' coupling between the three levels is illustrated on realistic urban networks, in function of the EV penetration level and a transportation incentive. A comparison with a reference model in the coupled electrical-transportation literature shows the efficiency of the incentives (charging price and electricity supplying contract) in our realistic trilevel model.

As for perspectives, several CSOs should interact in a non-cooperative game structure, making the trilevel problem an optimization at the upper level, combined with two games both at the middle and the lower levels. In parallel, a transportation operator (e.g., a public authority responsible for local pollution as in Section 6.1 or dynamic road pricing) will be added to enable a theoretical study of the transportation-electrical coupling.

Conclusion and perspectives

The growing number of Electric Vehicles (EVs) brings challenges to various stakeholders related to the electrical grid as well as the transportation system, and hence couples the two systems. The goal of this thesis is to help operators of this coupled system to design incentives to better face these challenges. This requires a model of the vehicle users' behavior and of the metrics and incentives of the operators. The coupled aspect of the electrical-transportation system is illustrated in this thesis by the commuting use case: vehicle users choose the driving path to go from home to work, and the public Charging Station (EVCS) at which they charge during working hours. The present work focuses on incentives such as the charging pricing mechanism at EVCSs.

Achievements of this thesis

The interactions between vehicle users, as well as the effect of parameters of the electrical and transportation systems on their decisions, are modeled via a game theoretical framework (Chapter 2). In this *routing* game, the choices of the driving path, the EVCS, the charging quantity, etc., are represented in Section 2.2.2 by paths in a graph (which is an extension of the transportation graph). The concept of Linearly non-Separable Congestion (LnSC) cost function is introduced in Definition 2.11 (for the charging pricing mechanism presented in Chapter 5): it is a function of a linear combination, for every path r of the graph, of the number of players choosing r. A Beckmann function is found in Proposition 2.19 for routing games with LnSC cost functions, and can be used to obtain a Wardrop equilibrium of such games. If the LnSC cost functions are increasing, it is proved in Proposition 2.22 that the associated linear combinations are unique at equilibrium. In the case of travel duration and energy consumption costs, the output of Beckmann's method is unique vehicle flows on all roads and unique aggregated charging needs at all EVCSs. Operators of the electrical-transportation system can use such outputs to better understand and anticipate the reaction of vehicle users to various incentives.

The theoretical concept of Wardrop equilibrium of a game is related to the stationary behavior, in a repeated version of this game, of vehicle users who follow a reinforcement learning process (3.8). In this learning game described in Chapter 3, the users have no prior knowledge on their cost functions as in the routing game studied in Chapter 2 (complete information assumption), but only observe their actual costs. Proposition 3.14 extends to increasing LnSC cost functions the proof of convergence of a reinforcement learning process towards the equilibrium of separable congestion games, using potential functions of Definitions 3.8 and 3.11.

The operator of the electrical-transportation system specifically considered in this thesis is the Charging Service Operator (CSO) of an EVCS, along with the particular charging pricing mechanism introduced in Chapter 5. In the commuting use case considered, this pricing method

is used to incentivize EV users to charge at the adequate EVCS.

The pricing mechanism is based on the aggregated EV charging load profiles at the EVCSs, which are scheduled in a centralized manner by the CSO, described in Chapter 4. This chapter presents the Water-Filling (WF) scheduling, whose analytic expression (4.1) is adapted to several cases. First, in the case EVs arrive at the EVCS at different times without the CSO knowing it in advance, an online procedure is suggested in which the CSO computes multiple nested WF schedulings at each EV arrival using Algorithm 4.1. Second, in the case a CSO owns several EVCSs and smooths with the WF scheduling the EV charging profile aggregated over all its EVCSs, the disaggregation Algorithm 4.2 is proposed, with the objective to smooth the charging profiles at all EVCSs.

The charging unit prices (5.3) and (5.12) introduced in Chapter 5 based on the WF load profiles are LnSC cost functions. Propositions 5.6 and 5.10 prove that they are increasing (under certain conditions). Their positive impacts on the grid are similar (1 % of relative difference) to the one of the Locational Marginal Pricing (LMP) method, based on the marginal grid cost associated with EV charging, instead of WF load profiles. Note that in the pricing mechanism used in this thesis, the CSO has no information on the grid whereas for the LMP method, the CSO coincides with the Electrical Network Operator (ENO). Thus, another LMP scheme is defined in-between, in which the ENO only communicates to the CSO one parameter for each EVCS, reflecting its impact (5.18) on the grid. The relative difference of this scheme with the original LMP one is of only 2 %.

Chapter 6 shows two applications of the routing game of Chapter 2 associated with the WF charging scheduling of Chapter 4 and the charging pricing mechanism introduced in Chapter 5, respectively for incentive design and optimal planning. In the first example, a Transportation Network Operator reduces the local air pollution in a city by taxing Gasoline Vehicle users driving across the city, in function of the EV penetration level. In the second example, the CSO manages an e-Park & Ride hub where commuters can charge their EV using the electricity generated by local solar panels, and take public transport instead of driving to work. The goal of this CSO is to maximize its long-term payoff by adequately sizing its solar park.

The theoretical combination of models of both drivers' behavior and charging mechanisms is achieved in Chapter 7. More precisely, a trilevel framework is suggested to model the interactions between different entities of the electrical system in the commuting use case. At the lower level, commuters choose their driving path, the hub at which they park and whether they charge at the hub or later at home. At the middle level, a CSO schedules the EV charging profiles at the hubs and designs the charging pricing mechanism. At the upper level, an ENO designs the electricity supplying contract (7.6) of the CSO. The CSO and the ENO optimize their incentives in a complex system thanks to the provided iterative Algorithm 7.1 using simulated annealing. A numerical sensitivity analysis of these optimal incentives with respect to important parameters of this trilevel framework can then be conducted on any transportation and electrical networks. This trilevel model is also compared to a bilevel one, standard in the literature, in which the CSO and ENO coincide.

Future work perspectives

Regarding the vehicle users' behavior model, a natural follow-up is to find an efficient method (like Beckmann's method presented in Chapter 2) to compute a Wardrop equilibrium of *general* non-separable congestion routing games. Thus, realistic vehicle energy consumption models

and charging pricing schemes taking into account the grid topology could be considered for example. In addition, the proof of convergence of the adjusted reinforcement learning procedure [Bravo, 2016] towards this equilibrium could be proved for such games.

An important line of future research is the robustness study of the models of this thesis with respect to the various sources of uncertainty, such as for example the non-flexible electricity consumption and generation around the EVCSs or the vehicle travel demand. Numerical sensitivity analyses conducted in this thesis show *a posteriori* the impact of some parameters on incentives designs, like the EV penetration in Chapters 6 and 7. Doing these analyses *a priori* would guarantee operators of the electrical-transportation system a level of benefits for example in case the actual values of parameters do not correspond exactly to the outputs of the models of this thesis. These *a priori* analyses could be done using robust optimization with auxiliary variables [Bertsimas and Sim, 2003]. Note that the repeated game associated with the stochastic reinforcement learning process presented in Section 3.3 can be seen as a game where vehicle users perceive their costs with a random error term. In the same line, the game between vehicle users introduced in Chapter 2 could be replaced by a stochastic game [Forouzandehmehr et al., 2014]. Robust and stochastic games could also be used to model the interactions between the operators of the coupled electrical-transportation system.

The charging scheduling and pricing mechanisms emphasized in this thesis may also be enriched. For example, the water-filling charging scheduling of Chapter 4 could incorporate the vehicle-to-grid technology or time-varying power limit constraints at EVCSs. The charging pricing mechanism introduced in Section 5.3.3 in the case of asynchronous arrivals and departures of EVs at the EVCS could be adjusted in order to systematically offer a lower charging unit price to an EV arriving before another one (and leaving at the same time) for example. Other realistic smart charging schemes could be integrated into a multi-level model of the coupled electrical-transportation system, by considering for instance more aspects of the grid costs associated with EV charging [Wang et al., 2016c] (e.g., voltage regulation).

Another interesting follow-up of this thesis would be to take into account theoretical models of other operators' metrics and incentives, like the ones considered in Chapter 6. For example, there is an important research effort [Wei et al., 2019] on the problem of charging infrastructure planning (see Section 6.2), in terms of the number and the location of EVCSs. As for local air pollution reduction (see Section 6.1), a more realistic vehicle energy consumption model could be used, like in [Fontana, 2013] and [Kambly and Bradley, 2014] where the driving speed and the heating system respectively are taken into account. In addition, positive incentives can be envisaged for EVs, such as the permission to use transit lanes or the exemptions of parking fees and car ferry fees like in Norway [Aasness and Odeck, 2015]).

In this thesis, for the operators' metrics and incentives considered, the charging scheduling of Chapter 4 is applied on the charging need aggregated over all EVs at the EVCS. In a future development, this optimally scheduled charging profile could be disaggregated at the level of each EV at the EVCS [Jacquot et al., 2019], in order to better take into consideration the plug-in period and battery constraints, and to propose an individual pricing mechanism. In other use cases than commuting, the waiting time at the EVCSs should be taken into account in the total cost functions of EV users, using queuing models [De Weerdt et al., 2013]. Such short-term studies require real-time models of vehicle users' behavior, as in [Tan and Wang, 2017], in which time is discretized into several time slots and vehicle flows are coupled from one time slot to another.

Another interesting line of research would be to detail the communication processes between the vehicle users and the operators sending incentives in the present work, as in chap-

ter 5 of thesis [Beaude, 2015] or paper [Amini and Karabasoglu, 2018] for example. The price signals could also be defined in order to comply with the current standard communication protocols [Hussain et al., 2018]. Note that an important aspect of such communications is preserving the privacy of vehicle users [Jacquot et al., 2019]. Well-designed and privacy-preserving communication systems are key for the acceptability of incentive mechanisms by vehicle users [Baharlouei and Hashemi, 2014].

The trilevel model introduced in Chapter 7 of the electrical system in the context of commuting EVs is solved by an iterative algorithm (which is proved to converge) using a simulated annealing algorithm (which converges in probability [Wah and Wang, 1999]) at each iteration. A direct extension of this work is to show the strong convergence of this simulated annealing algorithm [Bélisle, 1992]. This stochastic algorithm could also be replaced by a deterministic global optimization method [Horst and Tuy, 2013] to guarantee a certain level of precision after a given computation time. For example, by considering more regular operators' objective functions, an interval branch and bound method algorithm [Kearfott, 1992] could be used.

The asymmetric information between the Charging Service and Electrical Network Operators makes this trilevel structure a Stackelberg game with equilibrium constraints. Other scenarios of information sharing, like the CSO and ENO having access to the same information, could lead to more general equilibrium problems (between the CSO and the ENO) with equilibrium constraints [Su, 2005]. Such bilevel problems could even be extended to problems with games on three levels, for example by considering a game between several CSOs at the middle level, and a game between the ENO and a Transportation Network Operator (TNO) at the upper level. On top of that, the non-cooperative assumption could be relaxed and coalition games considered [Ganjehlou et al., 2020], as in [Alizadeh et al., 2016] where an ENO and a TNO collaborate in order to achieve a higher social welfare.

List of Acronyms

AVG AVeraGe (pricing scheme)
BEV Battery Electric Vehicle
CSO Charging Service Operator
CST ConSTant (pricing scheme)
CUP Charging Unit Price
ENO Electrical Network Operator
EV Electric Vehicle
EVCS Electric Vehicle Charging Station
FO Flexibility Operator
GA Grid Aware
GV Gasoline Vehicle
LMP Locational Marginal Price
LnSC Linearly non-Separable Congestion
LnSIC Linearly non-Separable Increasing Congestion
NE Nash Equilibrium
RLA Reinforcement Learning Algorithm
TSO Transportation System Operator
WE Wardrop Equilibrium
WF Water-Filling

Bibliography

[Aalami et al., 2010] Aalami, H., Moghaddam, M. P., and Yousefi, G. (2010). Demand response modeling considering interruptible/curtailable loads and capacity market programs. *Applied Energy*, 87(1):243–250.

[Aasness and Odeck, 2015] Aasness, M. A. and Odeck, J. (2015). The increase of electric vehicle usage in norway—incentives and adverse effects. *European Transport Research Review*, 7(4):1–8.

[Agthe and Billings, 1987] Agthe, D. E. and Billings, R. B. (1987). Equity, price elasticity, and household income under increasing block rates for water. *American Journal of Economics and Sociology*, 46(3):273–286.

[Alguacil et al., 2014] Alguacil, N., Delgadillo, A., and Arroyo, J. M. (2014). A trilevel programming approach for electric grid defense planning. *Computers & Operations Research*, 41:282–290.

[Alizadeh et al., 2016] Alizadeh, M., Wai, H.-T., Chowdhury, M., Goldsmith, A., Scaglione, A., and Javidi, T. (2016). Optimal pricing to manage electric vehicles in coupled power and transportation networks. *IEEE Transactions on control of network systems*, 4(4):863–875.

[Alizadeh et al., 2018] Alizadeh, M., Wai, H.-T., Goldsmith, A., and Scaglione, A. (2018). Retail and wholesale electricity pricing considering electric vehicle mobility. *IEEE Trans. on Control of Network Systems*, 6(1):249–260.

[Amini and Karabasoglu, 2018] Amini, M. H. and Karabasoglu, O. (2018). Optimal operation of interdependent power systems and electrified transportation networks. *Energies*, 11(1):196.

[Aumann, 1976] Aumann, R. J. (1976). Agreeing to disagree. *The annals of statistics*, pages 1236–1239.

[Aumann and Peleg, 1960] Aumann, R. J. and Peleg, B. (1960). Von neumann-morgenstern solutions to cooperative games without side payments. *Bulletin of the American Mathematical Society*, 66(3):173–179.

[Aumann and Shapley, 2015] Aumann, R. J. and Shapley, L. S. (2015). *Values of non-atomic games*. Princeton University Press.

[Aussel et al., 2020] Aussel, D., Brotcorne, L., Lepaul, S., and von Niederhäusern, L. (2020). A trilevel model for best response in energy demand-side management. *European Journal of Operational Research*, 281(2):299–315.

[Baharlouei and Hashemi, 2014] Baharlouei, Z. and Hashemi, M. (2014). Efficiency-fairness trade-off in privacy-preserving autonomous demand side management. *IEEE Transactions on Smart Grid*, 5(2):799–808.

[Baran and Wu, 1989] Baran, M. E. and Wu, F. F. (1989). Network reconfiguration in distribution systems for loss reduction and load balancing. *IEEE Power Engineering Review*, 9(4):101–102.

[Barth et al., 2009] Barth, D., Cohen, J., Bournez, O., and Boussaton, O. (2009). Distributed learning of equilibria in a routing game. *Parallel Processing Letters*, 19(02):189–204.

[Bauer et al., 2015] Bauer, C., Hofer, J., Althaus, H.-J., Del Duce, A., and Simons, A. (2015). The environmental performance of current and future passenger vehicles: Life cycle assessment based on a novel scenario analysis framework. *Applied energy*, 157:871–883.

[Beaude, 2015] Beaude, O. (2015). *Modélisation et optimisation de l'interaction entre véhicules électriques et réseaux d'électricité : apport de la théorie des jeux*. Theses, Université Paris-Saclay.

[Beaude et al., 2016] Beaude, O., Lasaulce, S., Hennebel, M., and Mohand, I. (2016). Reducing the impact of EV charging operations on the distribution network. *IEEE Transactions on Smart Grid*, 7(6):2666–79.

[Beckmann et al., 1956] Beckmann, M., McGuire, C., and Winsten, C. (1956). *Studies in the economics of transportation*. Research memorandum. Published for the Cowles Commission for Research in Economics by Yale University Press.

[Bélisle, 1992] Bélisle, C. J. (1992). Convergence theorems for a class of simulated annealing algorithms on $\mathbb{R}^d$. *Journal of Applied Probability*, 29(4):885–895.

[Benaım and Hirsch, 1999] Benaım, M. and Hirsch, M. W. (1999). Mixed equilibria and dynamical systems arising from fictitious play in perturbed games. *Games and Economic Behavior*, 29(1-2):36–72.

[Bertsimas and Sim, 2003] Bertsimas, D. and Sim, M. (2003). Robust discrete optimization and network flows. *Mathematical programming*, 98(1):49–71.

[Block et al., 2015] Block, D., Harrison, J., Brooker, P., Center, F., and Dunn, M. D. (2015). Electric vehicle sales for 2014 and future projections. *Electric Vehicle Transportation Center*.

[Boggs and Tolle, 1995] Boggs, P. T. and Tolle, J. W. (1995). Sequential quadratic programming. *Acta numerica*, 4(1):1–51.

[Bournez and Cohen, 2013] Bournez, O. and Cohen, J. (2013). Learning equilibria in games by stochastic distributed algorithms. In *Computer and information sciences III*, pages 31–38. Springer.

[Boyd et al., 2004] Boyd, S., Boyd, S. P., and Vandenberghe, L. (2004). *Convex optimization*. Cambridge university press.

[Bravo, 2016] Bravo, M. (2016). An adjusted payoff-based procedure for normal form games. *Mathematics of Operations Research*, 41(4):1469–1483.

[Brown, 1951] Brown, G. W. (1951). Iterative solution of games by fictitious play. *Activity analysis of production and allocation*, 13(1):374–376.

[Burton, 2013] Burton, N. (2013). *History of electric cars*. Crowood.

[Campello Vicente et al., 2017] Campello Vicente, H., Peral-Orts, R., Campillo-Davo, N., and Velasco-Sanchez, E. (2017). The effect of electric vehicles on urban noise maps. *Applied Acoustics*, 116:59–64.

[CGDD, 2010] CGDD (2010). La mobilité des français - panorama issu de l'enquête nationale transports et déplacements 2008 (in french). , Commissariat général au développement durable.

[Chandram et al., 2008] Chandram, K., Subrahmanyam, N., and Sydulu, M. (2008). Brent method for dynamic economic dispatch with transmission losses. In *IEEE/PES Transmission and Distrib. Conference and Exposition*, pages 1–5.

[Chau and Sim, 2003] Chau, C. and Sim, K. (2003). The price of anarchy for non-atomic congestion games with symmetric cost maps and elastic demands. *Operations Research Letters*, 31.

[Chen et al., 2011] Chen, C., Kishore, S., and Snyder, L. V. (2011). An innovative rtp-based residential power scheduling scheme for smart grids. In *2011 IEEE International Conference on Acoustics, Speech and Signal Processing (ICASSP)*, pages 5956–5959. IEEE.

[Chen et al., 2014] Chen, N., Tan, C. W., and Quek, T. Q. (2014). Electric vehicle charging in smart grid: Optimality and valley-filling algorithms. *IEEE Journal of Selected Topics in Signal Processing*, 8(6):1073–1083.

[Cheung and Lahkar, 2018] Cheung, M.-W. and Lahkar, R. (2018). Nonatomic potential games: the continuous strategy case. *Games and Economic Behavior*, 108:341–362.

[Cohen et al., 2017] Cohen, J., Héliou, A., and Mertikopoulos, P. (2017). Learning with bandit feedback in potential games. In *Proceedings of the 31st International Conference on Neural Information Processing Systems*, pages 6372–6381.

[Colson et al., 2007] Colson, B., Marcotte, P., and Savard, G. (2007). An overview of bilevel optimization. *Annals of operations research*, 153,1:235–56.

[Cominetti et al., 2010] Cominetti, R., Melo, E., and Sorin, S. (2010). A payoff-based learning procedure and its application to traffic games. *Games and Economic Behavior*, 70(1):71–83.

[Correa et al., 2008] Correa, J., Schulz, A., and Stier-Moses, N. (2008). A geometric approach to the price of anarchy in nonatomic congestion games. *Games and Economic Behavior*, 64:457–469.

[Dafermos, 1971] Dafermos, S. C. (1971). An extended traffic assignment model with applications to two-way traffic. *Transportation Science*, 5(4):366–389.

[Dafermos, 1972] Dafermos, S. C. (1972). The traffic assignment problem for multiclass-user transportation networks. *Transportation science*, 6(1):73–87.

[Dalyac et al., 2021] Dalyac, C., Henriet, L., Jeandel, E., Lechner, W., Perdrix, S., Porcheron, M., and Veshchezerova, M. (2021). Qualifying quantum approaches for hard industrial optimization problems. a case study in the field of smart-charging of electric vehicles. *EPJ Quantum Technology*, 8(1):12.

[Davidson, 1966] Davidson, K. (1966). A flow travel time relationship for use in transportation planning. In *Australian Road Research Board (ARRB) Conference, 3rd, 1966, Sydney*, volume 3.

[Davis, 2009] Davis, L. (2009). Realizing wardrop equilibria with real-time traffic information. *Physica A: Statistical Mechanics and its Applications*, 388(20):4459–4474.

[De Cauwer et al., 2015] De Cauwer, C., Maarten, M., Heyvaert, S., Coosemans, T., Van Mierlo, J., et al. (2015). Electric vehicle use and energy consumption based on realworld electric vehicle fleet trip and charge data and its impact on existing ev research models. *World Electric Vehicle Journal*, 7(3):436–446.

[De Weerdt et al., 2013] De Weerdt, M. M., Gerding, E. H., Stein, S., Robu, V., and Jennings, N. R. (2013). Intention-aware routing to minimise delays at electric vehicle charging stations. In *Twenty-Third International Joint Conference on Artificial Intelligence*.

[Dekkers and Aarts, 1991] Dekkers, A. and Aarts, E. (1991). Global optimization and simulated annealing. *Mathematical programming*, 50(1-3):367–393.

[Deng et al., 2015] Deng, R., Yang, Z., Chow, M.-Y., and Chen, J. (2015). A survey on demand response in smart grids: Mathematical models and approaches. *IEEE Transactions on Industrial Informatics*, 11(3):570–582.

[Doostizadeh and Ghasemi, 2012] Doostizadeh, M. and Ghasemi, H. (2012). A day-ahead electricity pricing model based on smart metering and demand-side management. *Energy*, 46(1):221–230.

[EEA, 2018] EEA (2018). Electric vehicles from life cycle and circular economy perspectives. transport and environment reporting mechanism report. , European Environment Agency.

[Ehrenmann, 2004] Ehrenmann, A. (2004). *Equilibrium problems with equilibrium constraints and their application to electricity markets*. PhD thesis, Citeseer.

[Ellingsen et al., 2016] Ellingsen, L. A.-W., Singh, B., and Strømman, A. H. (2016). The size and range effect: lifecycle greenhouse gas emissions of electric vehicles. *Environmental Research Letters*, 11(5):054010.

[Enedis, 2019] Enedis (2019). Report on the integration of electric mobility in the public electricity distribution network. .

[Enedis and RTE, 2019] Enedis and RTE (2019). Les besoins électriques de la mobilité longue distance sur autoroute (french). .

[Erev and Roth, 1998] Erev, I. and Roth, A. E. (1998). Predicting how people play games: Reinforcement learning in experimental games with unique, mixed strategy equilibria. *American economic review*, pages 848–881.

[Florian and Hearn, 1995] Florian, M. and Hearn, D. (1995). Network equilibrium models and algorithms. *Network routing*, pages 485–550.

[Fontana, 2013] Fontana, M. W. (2013). *Optimal routes for electric vehicles facing uncertainty, congestion, and energy constraints.* PhD thesis, Massachusetts Institute of Technology.

[Forouzandehmehr et al., 2014] Forouzandehmehr, N., Esmalifalak, M., Mohsenian-Rad, H., and Han, Z. (2014). Autonomous demand response using stochastic differential games. *IEEE Transactions on Smart Grid*, 6(1):291–300.

[Fréry, 2000] Fréry, F. (2000). Un cas d'amnésie stratégique : l'éternelle émergence de la voiture électrique. In *IXème Conférence Internationale de Management Stratégique*, page Montpellier.

[Fudenberg et al., 1998] Fudenberg, D., Drew, F., Levine, D. K., and Levine, D. K. (1998). *The theory of learning in games*, volume 2. MIT press.

[Fudenberg and Tirole, 1991] Fudenberg, D. and Tirole, J. (1991). Game theory mit press. *Cambridge, MA*, 86.

[Ganjehlou et al., 2020] Ganjehlou, H. G., Niaei, H., Jafari, A., Aroko, D. O., Marzband, M., and Fernando, T. (2020). A novel techno-economic multi-level optimization in home-microgrids with coalition formation capability. *Sustainable Cities and Society*, 60:102241.

[Gaonac'h, 2015] Gaonac'h, T. (2015). *Contribution à l'analyse de l'impact des véhicules électrifiés sur le réseau de distribution d'électricité (in Frenh).* Theses, CentraleSupélec.

[Geth et al., 2012] Geth, F., Leemput, N., Van Roy, J., Büscher, J., Ponnette, R., and Driesen, J. (2012). Voltage droop charging of electric vehicles in a residential distribution feeder. In *2012 3rd IEEE PES Innovative Smart Grid Technologies Europe (ISGT Europe)*, pages 1–8. IEEE.

[Gilboa and Matsui, 1991] Gilboa, I. and Matsui, A. (1991). Social stability and equilibrium. *Econometrica: Journal of the Econometric Society*, pages 859–867.

[Gómez and Morcos, 2003] Gómez, J. C. and Morcos, M. M. (2003). Impact of ev battery chargers on the power quality of distribution systems. *IEEE transactions on power delivery*, 18(3):975–981.

[Habib et al., 2015] Habib, S., Kamran, M., and Rashid, U. (2015). Impact analysis of vehicle-to-grid technology and charging strategies of electric vehicles on distribution networks–a review. *Journal of Power Sources*, 277:205–214.

[Harsanyi et al., 1988] Harsanyi, J. C., Selten, R., et al. (1988). A general theory of equilibrium selection in games. *MIT Press Books*, 1.

[Haurie and Marcotte, 1985] Haurie, A. and Marcotte, P. (1985). On the relationship between nash—cournot and wardrop equilibria. *Networks*, 15(3):295–308.

[Hawkins et al., 2013] Hawkins, T. R., Singh, B., Majeau-Bettez, G., and Strømman, A. H. (2013). Comparative environmental life cycle assessment of conventional and electric vehicles. *Journal of industrial ecology*, 17(1):53–64.

[He et al., 2012] He, Y., Venkatesh, B., and Guan, L. (2012). Optimal scheduling for charging and discharging of electric vehicles. *IEEE transactions on smart grid*, 3(3):1095–1105.

[Herter, 2007] Herter, K. (2007). Residential implementation of critical-peak pricing of electricity. *Energy policy*, 35(4):2121–2130.

[Hilshey et al., 2012] Hilshey, A. D., Hines, P. D., Rezaei, P., and Dowds, J. R. (2012). Estimating the impact of electric vehicle smart charging on distribution transformer aging. *IEEE Transactions on Smart Grid*, 4(2):905–913.

[Horst and Tuy, 2013] Horst, R. and Tuy, H. (2013). *Global optimization: Deterministic approaches*. Springer Science & Business Media.

[Hu et al., 2013] Hu, J., You, S., Lind, M., and Østergaard, J. (2013). Coordinated charging of electric vehicles for congestion prevention in the distribution grid. *IEEE Transactions on Smart Grid*, 5(2):703–711.

[Hussain et al., 2018] Hussain, S. S., Ustun, T. S., Nsonga, P., and Ali, I. (2018). Ieee 1609 wave and iec 61850 standard communication based integrated ev charging management in smart grids. *IEEE Transactions on Vehicular Technology*, 67(8):7690–7697.

[IEA, 2017] IEA (2017). Tracking clean energy progress 2017. , International Energy Agency.

[IEA, 2021] IEA (2021). Global ev outlook 2021. *International Energy Agency, France*.

[Jacquot et al., 2019] Jacquot, P., Beaude, O., Benchimol, P., Gaubert, S., and Oudjane, N. (2019). A privacy-preserving disaggregation algorithm for non-intrusive management of flexible energy. In *2019 IEEE 58th Conference on Decision and Control (CDC)*, pages 890–896. IEEE.

[Jacquot et al., 2018] Jacquot, P., Beaude, O., Gaubert, S., and Oudjane, N. (2018). Analysis and implementation of an hourly billing mechanism for demand response management. *IEEE Transactions on Smart Grid*, 10(4):4265–4278.

[Jacquot and Wan, 2018] Jacquot, P. and Wan, C. (2018). Nonsmooth aggregative games with coupling constraints and infinitely many classes of players. *arXiv preprint arXiv:1806.06230*.

[Jeihani et al., 2006] Jeihani, M., Lawe, S., and Connolly, J. (2006). Improving traffic assignment model using intersection delay function. 47th Annual Transportation Research Forum, New York, New York, March 23-25, 2006 208046.

[Jerez et al., 2015] Jerez, S., Tobin, I., Vautard, R., Montávez, J. P., López-Romero, J. M., Thais, F., Bartok, B., Christensen, O. B., Colette, A., Déqué, M., et al. (2015). The impact of climate change on photovoltaic power generation in europe. *Nature communications*, 6(1):1–8.

[Jiang and Xie, 2014] Jiang, N. and Xie, C. (2014). Computing and analyzing mixed equilibrium network flows with gasoline and electric vehicles. *Computer-Aided Civil and Infrastructure Engineering*, 29(8):626–641.

[Jin and Ryan, 2013] Jin, S. and Ryan, S. M. (2013). A tri-level model of centralized transmission and decentralized generation expansion planning for an electricity market. *IEEE Trans. on Power Systems*, 29(1):132–41.

[Kambly and Bradley, 2014] Kambly, K. R. and Bradley, T. H. (2014). Estimating the hvac energy consumption of plug-in electric vehicles. *Journal of Power Sources*, 259:117–124.

[Kearfott, 1992] Kearfott, R. B. (1992). An interval branch and bound algorithm for bound constrained optimization problems. *Journal of Global Optimization*, 2(3):259–280.

[Kim et al., 2016] Kim, H. C., Wallington, T. J., Arsenault, R., Bae, C., Ahn, S., and Lee, J. (2016). Cradle-to-gate emissions from a commercial electric vehicle li-ion battery: a comparative analysis. *Environmental science & technology*, 50(14):7715–7722.

[Kleinrock, 1975] Kleinrock, L. (1975). Queueing systems. Technical report.

[Knight, 1924] Knight, F. H. (1924). Some fallacies in the interpretation of social cost. *The Quarterly Journal of Economics*, 38(4):582–606.

[Kraft, 1988] Kraft, D. (1988). *A Software Package for Sequential Quadratic Programming.* Deutsche Forschungs- und Versuchsanstalt für Luft- und Raumfahrt Köln: Forschungsbericht. Wiss. Berichtswesen d. DFVLR.

[Lasaulce and Tembine, 2011] Lasaulce, S. and Tembine, H. (2011). *Game theory and learning for wireless networks: fundamentals and applications.* Academic Press.

[Li et al., 2013] Li, R., Wu, Q., and Oren, S. S. (2013). Distribution locational marginal pricing for optimal electric vehicle charging management. *IEEE Transactions on Power Systems*, 29(1):203–211.

[McFadden et al., 1973] McFadden, D. et al. (1973). Conditional logit analysis of qualitative choice behavior.

[Milchtaich, 1996] Milchtaich, I. (1996). Congestion games with player-specific payoff functions. *Games and economic behavior*, 13(1):111–124.

[Mitsos et al., 2008] Mitsos, A., Lemonidis, P., and Barton, P. I. (2008). Global solution of bilevel programs with a nonconvex inner program. *Journal of Global Optimization*, 42(4):475–513.

[Mohsenian-Rad et al., 2010] Mohsenian-Rad, A.-H., Wong, V. W., Jatskevich, J., Schober, R., and Leon-Garcia, A. (2010). Autonomous demand-side management based on game-theoretic energy consumption scheduling for the future smart grid. *IEEE Trans. on Smart Grid*, 1(3):320–331.

[Monderer and Shapley, 1996] Monderer, D. and Shapley, L. S. (1996). Potential games. *Games and economic behavior*, 14(1):124–143.

[Morlok, 1973] Morlok, E. K. (1973). *Development and application of a highway network design model*, volume 1. Federal Highway Administration.

[Nagel, 1995] Nagel, R. (1995). Unraveling in guessing games: An experimental study. *The American Economic Review*, 85(5):1313–1326.

[Nash et al., 1950] Nash, J. F. et al. (1950). Equilibrium points in n-person games. *Proceedings of the national academy of sciences*, 36(1):48–49.

[Nie et al., 2004] Nie, Y., Zhang, H., and Lee, D.-H. (2004). Models and algorithms for the traffic assignment problem with link capacity constraints. *Transportation Research Part B: Methodological*, 38(4):285–312.

[Nimalsiri et al., 2019] Nimalsiri, N. I., Mediwaththe, C. P., Ratnam, E. L., Shaw, M., Smith, D. B., and Halgamuge, S. K. (2019). A survey of algorithms for distributed charging control of electric vehicles in smart grid. *IEEE Trans. on Intelligent Transportation Systems*, 21, 11:4497–4515.

[Nordelöf et al., 2014] Nordelöf, A., Messagie, M., Tillman, A.-M., Söderman, M. L., and Van Mierlo, J. (2014). Environmental impacts of hybrid, plug-in hybrid, and battery electric vehicles—what can we learn from life cycle assessment? *The International Journal of Life Cycle Assessment*, 19(11):1866–1890.

[Oh and Thomas, 2008] Oh, H. and Thomas, R. J. (2008). Demand-side bidding agents: Modeling and simulation. *IEEE Transactions on Power Systems*, 23(3):1050–1056.

[Ortega and Rheinboldt, 2000] Ortega, J. M. and Rheinboldt, W. C. (2000). *Iterative solution of nonlinear equations in several variables.* SIAM.

[Osborne et al., 2004] Osborne, M. J. et al. (2004). *An introduction to game theory*, volume 3. Oxford university press New York.

[Paccagnan et al., 2018] Paccagnan, D., Gentile, B., Parise, F., Kamgarpour, M., and Lygeros, J. (2018). Nash and wardrop equilibria in aggregative games with coupling constraints. *IEEE Transactions on Automatic Control*, 64(4):1373–1388.

[Palensky and Dietrich, 2011] Palensky, P. and Dietrich, D. (2011). Demand side management: Demand response, intelligent energy systems, and smart loads. *IEEE transactions on industrial informatics*, 7(3):381–388.

[Pan et al., 2019] Pan, L., Yao, E., and MacKenzie, D. (2019). Modeling ev charging choice considering risk attitudes and attribute non-attendance. *Transportation Research Part C: Emerging Technologies*, 102:60–72.

[Papadimitriou, 1998] Papadimitriou, C. H.; Steiglitz, K. (1998). *Combinatorial optimization: algorithms and complexity.* Dover Publications.

[Paterakis et al., 2017] Paterakis, N. G., Erdinç, O., and Catalão, J. P. (2017). An overview of demand response: Key-elements and international experience. *Renewable and Sustainable Energy Reviews*, 69:871–891.

[Patriksson, 2015] Patriksson, M. (2015). *The traffic assignment problem: models and methods.* Courier Dover Publications.

[Perakis, 2004] Perakis, G. (2004). The price of anarchy when costs are non-separable and asymmetric. *proccedings of IPCO.*

[Pfenninger and Staffell, 2016a] Pfenninger, S. and Staffell, I. (2016a). Long-term patterns of european pv output using 30 years of validated hourly reanalysis and satellite data. *Energy*, 114:1251–1265.

[Pfenninger and Staffell, 2016b] Pfenninger, S. and Staffell, I. (2016b). Long-term patterns of european pv output using 30 years of validated hourly reanalysis and satellite data. *Energy*, 114:1251–1265.

[Pi et al., 2019] Pi, X., Ma, W., and Qian, Z. S. (2019). A general formulation for multi-modal dynamic traffic assignment considering multi-class vehicles, public transit and parking. *Transportation Research Part C: Emerging Technologies*, 104:369–389.

[Plötz et al., 2020] Plötz, P., Moll, C., Biecker, G., Mock, P., and Li, Y. (2020). Real-world usage of plug-in hybrid electric vehicles: Fuel consumption, electric driving, and co2 emissions.

[Prager, 1954] Prager, W. (1954). *Problems of traffic and transportation.*

[Qian et al., 2020] Qian, T., Shao, C., Li, X., Wang, X., and Shahidehpour, M. (2020). Enhanced coordinated operations of electric power and transportation networks via ev charging services. *IEEE Trans. on Smart Grid*, 11(4):3019–3030.

[Qian et al., 2019] Qian, T., Shao, C., Wang, X., and Shahidehpour, M. (2019). Deep reinforcement learning for ev charging navigation by coordinating smart grid and intelligent transportation system. *IEEE Transactions on Smart Grid*, 11(2):1714–1723.

[Rauh et al., 2015] Rauh, N., Franke, T., and Krems, J. F. (2015). Understanding the impact of electric vehicle driving experience on range anxiety. *Human factors*, 57(1):177–187.

[Romeijn and Smith, 1994] Romeijn, H. E. and Smith, R. L. (5(2), p101-26, 1994). Simulated annealing for constrained global optimization. *Journal of Global Optim.*

[Rosenthal, 1973] Rosenthal, R. W. (1973). A class of games possessing pure-strategy nash equilibria. *International Journal of Game Theory*, 2(1):65–67.

[Roughgarden, 2007] Roughgarden, T. (2007). Routing games. *Algorithmic game theory*, 18:459–484.

[Roughgarden and Tardos, 2000] Roughgarden, T. and Tardos, E. (2000). How bad is selfish routing. *in proceedings of FOCS.*

[RTE, 2019] RTE (2019). Integration of electric vehicles into the power system in france. , Réseau de Transport d'Électricité.

[RTE, 2021] RTE (2021). Bilan prévisionnel de l'équilibre offre-demande d'électricité en france - édition 2021 (in french). , Réseau de Transport d'Électricité.

[Ruiz et al., 2009] Ruiz, N., Cobelo, I., and Oyarzabal, J. (2009). A direct load control model for virtual power plant management. *IEEE Transactions on Power Systems*, 24(2):959–966.

[Samad and Kiliccote, 2012] Samad, T. and Kiliccote, S. (2012). Smart grid technologies and applications for the industrial sector. *Computers & Chemical Engineering*, 47:76–84.

[Samadi et al., 2012] Samadi, P., Mohsenian-Rad, H., Schober, R., and Wong, V. W. (2012). Advanced demand side management for the future smart grid using mechanism design. *IEEE Transactions on Smart Grid*, 3(3):1170–1180.

[Sandholm, 2001] Sandholm, W. H. (2001). Potential games with continuous player sets. *Journal of Economic theory*, 97(1):81–108.

[Sassi and Oulamara, 2017] Sassi, O. and Oulamara, A. (2017). Electric vehicle scheduling and optimal charging problem: complexity, exact and heuristic approaches. *International Journal of Production Research*, 55(2):519–535.

[Sastry et al., 1994] Sastry, P., Phansalkar, V., and Thathachar, M. (1994). Decentralized learning of nash equilibria in multi-person stochastic games with incomplete information. *IEEE Transactions on systems, man, and cybernetics*, 24(5):769–777.

[Sender et al., 1970] Sender, J., Netter, M., and de Recherche des Transports ; Joinville, I. (1970). *Équilibre offre-demande et tarification sur un réseau de transport: modèle ASTARTÉ (Application de Systèmes Tarifaires à un réseau de Transport : trafics et tarifs d'Équilibre).* Rapport de recherche IRT. IRT.

[Shakerighadi et al., 2018] Shakerighadi, B., Anvari-Moghaddam, A., Ebrahimzadeh, E., Blaabjerg, F., and Bak, C. L. (2018). A hierarchical game theoretical approach for energy management of electric vehicles and charging stations in smart grids. *Ieee Access*, 6:67223–67234.

[Sheffi, 1985] Sheffi, Y. (1985). *Urban transportation networks: Equilibrium analysis with mathematical programming methods.* Prentice-Hall, Inc.

[Shi et al., shed] Shi, X., Xu, Y., Guo, Q., Sun, H., and Gu, W. (to be published). A distributed ev navigation strategy considering the interaction between power system and traffic network. *IEEE Trans. on Smart Grid.*

[Shinwari et al., 2012] Shinwari, M., Youssef, A., and Hamouda, W. (2012). A water-filling based scheduling algorithm for the smart grid. *IEEE Transactions on Smart Grid*, 3(2):710–719.

[Simon, 1972] Simon, H. A. (1972). Theories of bounded rationality. *Decision and organization*, 1(1):161–176.

[Smith, 1979] Smith, M. J. (1979). The existence, uniqueness and stability of traffic equilibria. *Transportation Research Part B: Methodological*, 13(4):295–304.

[Sohet et al., 2019a] Sohet, B., Beaude, O., and Hayel, Y. (2019a). Routing game with nonseparable costs for ev driving and charging incentive design. In *Network Games, Control, and Optimization: Proceedings of NETGCOOP 2018, New York, NY*, pages 233–248. Springer.

[Sohet et al., 2019b] Sohet, B., Beaude, O., Hayel, Y., and Jeandin, A. (2019b). Optimal incentives for electric vehicles at e-park & ride hub with renewable energy source. *World Electric Vehicle Journal*, 10(4):70.

[Sohet et al., 2021a] Sohet, B., Hayel, Y., Beaude, O., Bréal, J.-B., and Jeandin, A. (2021a). Online smart charging algorithm with asynchronous electric vehicles demand. In *2021 IEEE PES Innovative Smart Grid Technologies Europe (ISGT-Europe).*

[Sohet et al., 2019c] Sohet, B., Hayel, Y., Beaude, O., and Jeandin, A. (2019c). A model to evaluate coupled driving-and-charging incentives for electric vehicles. In *32nd Electric Vehicle Symposium (EVS32).*

[Sohet et al., 2020a] Sohet, B., Hayel, Y., Beaude, O., and Jeandin, A. (2020a). Impact of strategic electric vehicles driving behavior on the grid. In *2020 IEEE PES Innovative Smart Grid Technologies Europe (ISGT-Europe)*, pages 454–458.

[Sohet et al., 2020b] Sohet, B., Hayel, Y., Beaude, O., and Jeandin, A. (2020b). Learning pure nash equilibrium in smart charging games. In *2020 59th IEEE Conference on Decision and Control (CDC)*, pages 3549–3554.

[Sohet et al., 2021b] Sohet, B., Hayel, Y., Beaude, O., and Jeandin, A. (2021b). Coupled charging-and-driving incentives design for electric vehicles in urban networks. *IEEE Transactions on Intelligent Transportation Systems*, 22(10):6342–6352.

[Sohet et al., 2021c] Sohet, B., Hayel, Y., Beaude, O., and Jeandin, A. (2021c). Hierarchical coupled driving-and-charging model of electric vehicles, stations and grid operators. *IEEE Transactions on Smart Grid*, 12(6):5146–5157.

[Sortomme et al., 2010] Sortomme, E., Hindi, M. M., MacPherson, S. J., and Venkata, S. (2010). Coordinated charging of plug-in hybrid electric vehicles to minimize distribution system losses. *IEEE transactions on smart grid*, 2(1):198–205.

[Spiess, 1990] Spiess, H. (1990). Technical note—conical volume-delay functions. *Transportation Science*, 24(2):153–158.

[Su, 2005] Su, C.-L. (2005). *Equilibrium problems with equilibrium constraints: Stationarities, algorithms, and applications*. Stanford University.

[Sutton and Barto, 2018] Sutton, R. S. and Barto, A. G. (2018). *Reinforcement learning: An introduction*. MIT press.

[Tan and Wang, 2017] Tan, J. and Wang, L. (2017). Real-time charging navigation of electric vehicles to fast charging stations: A hierarchical game approach. *IEEE Trans. on Smart Grid*, 8(2):846–856.

[Tang et al., 2016] Tang, W., Bi, S., and Zhang, Y. J. (2016). Online charging scheduling algorithms of electric vehicles in smart grid: An overview. *IEEE communications Magazine*, 54(12):76–83.

[Turker, 2012] Turker, H. (2012). *Véhicules électriques Hybrides Rechargeables: évaluation des Impacts sur le Réseau électrique et Stratégies Optimales de recharge*. PhD thesis, Université de Grenoble.

[Vagropoulos et al., 2015] Vagropoulos, S. I., Kyriazidis, D. K., and Bakirtzis, A. G. (7(2), p948-57, 2015). Real-time charging management framework for electric vehicle aggregators in a market environment. *IEEE Trans. on Smart Grid*.

[Vardakas et al., 2014] Vardakas, J. S., Zorba, N., and Verikoukis, C. V. (2014). A survey on demand response programs in smart grids: Pricing methods and optimization algorithms. *IEEE Communications Surveys & Tutorials*, 17(1):152–178.

[Vasirani et al., 2013] Vasirani, M., Kota, R., Cavalcante, R. L. G., Ossowski, S., and Jennings, N. R. (2013). An agent-based approach to virtual power plants of wind power generators and electric vehicles. *IEEE Transactions on Smart Grid*, 4(3):1314–1322.

[Vázquez and Rey-Stolle, 2008] Vázquez, M. and Rey-Stolle, I. (2008). Photovoltaic module reliability model based on field degradation studies. *Progress in photovoltaics: Research and Applications*, 16(5):419–433.

[Wah and Wang, 1999] Wah, B. W. and Wang, T. (p461-75, 1999). Simulated annealing with asymptotic convergence for nonlinear constrained global optimization. In *International Conf. on Principles and Practice of Constraint Prog.*

[Wang et al., 2016a] Wang, H., Huang, T., Liao, X., Abu-Rub, H., and Chen, G. (2016a). Reinforcement learning for constrained energy trading games with incomplete information. *IEEE transactions on cybernetics*, 47(10):3404–3416.

[Wang et al., 2019a] Wang, J., Peeta, S., and He, X. (2019a). Multiclass traffic assignment model for mixed traffic flow of human-driven vehicles and connected and autonomous vehicles. *Transportation Research Part B: Methodological*, 126:139–168.

[Wang et al., 2019b] Wang, N., Tang, L., and Pan, H. (2019b). A global comparison and assessment of incentive policy on electric vehicle promotion. *Sustainable Cities and Society*, 44:597–603.

[Wang et al., 2016b] Wang, Q., Liu, X., Du, J., and Kong, F. (2016b). Smart charging for electric vehicles: A survey from the algorithmic perspective. *IEEE Communications Surveys & Tutorials*, 18(2):1500–1517.

[Wang et al., 2016c] Wang, Q., Liu, X., Du, J., and Kong, F. (2016c). Smart charging for electric vehicles: A survey from the algorithmic perspective. *IEEE Communications Surveys & Tutorials*, 18(2):1500–1517.

[Wardrop, 1952] Wardrop, J. G. (1952). Road paper. some theoretical aspects of road traffic research. *Proceedings of the institution of civil engineers*, 1(3):325–362.

[Wei et al., 2019] Wei, W., Danman, W., Qiuwei, W., Shafie-Khah, M., and Catalao, J. P. (2019). Interdependence between transportation system and power distribution system: A comprehensive review on models and applications. *Journal of Modern Power Systems and Clean Energy*, 7(3):433–448.

[Wei et al., 2017] Wei, W., Wu, L., Wang, J., and Mei, S. (2017). Network equilibrium of coupled transportation and power distribution systems. *IEEE Transactions on Smart Grid*, 9(6):6764–6779.

[West et al., 2001] West, D. B. et al. (2001). *Introduction to graph theory*, volume 2. Prentice hall Upper Saddle River.

[Wood and Wollenberg, 2012] Wood, A. and Wollenberg, B. (2012). *Power Generation, Operation, and Control*. Wiley.

[Wu et al., 2015] Wu, H., Shahidehpour, M., Alabdulwahab, A., and Abusorrah, A. (7(1), p374-85, 2015). A game theoretic approach to risk-based optimal bidding strategies for electric vehicle aggregators in electricity markets with variable wind energy resources. *IEEE Trans. on Sustainable Energy*.

[Zamir, 2020] Zamir, S. (2020). *Bayesian games: Games with incomplete information*. Springer.

[Zhou et al., 2011] Zhou, C., Qian, K., Allan, M., and Zhou, W. (2011). Modeling of the cost of ev battery wear due to v2g application in power systems. *IEEE Transactions on Energy Conversion*, 26(4):1041–1050.

[Zhu, 2015] Zhu, J. (2015). *Optimization of power system operation*. John Wiley & Sons.